Structures Research Report No. 922
Final Project Report

June 2004

UF Project No. 4504-922-12
Contract No. BC-354 RPWO #55

CFRP REPAIR OF IMPACT-DAMAGED BRIDGE GIRDERS VOLUME I – STRUCTURAL EVALUATION OF IMPACT DAMAGED PRESTRESSED CONCRETE I GIRDERS REPAIRED WITH FRP MATERIALS

Principal Investigator: Perry S. Green
Co-Principal Investigator: Andrew J. Boyd

Graduate Research Assistant: Kimberly Lammert

Project Manager: Marcus Ansley, P.E.

Department of Civil & Coastal Engineering
College of Engineering
University of Florida
Gainesville, Florida 32611

Engineering and Industrial Experiment Station

UNIVERSITY OF FLORIDA

Civil & Coastal Engineering

Technical Report Documentation Page

1. Report No.	2. Government Accession No.	3. Recipient's Catalog No.
BC354 RPWO #55		

4. Title and Subtitle

CFRP Repair of Impact-Damaged Bridge Girders Volume I – STRUCTURAL EVALUATION OF IMPACT DAMAGED PRESTRESSED CONCRETE I GIRDERS REPAIRED WITH FRP MATERIALS

5. Report Date: June 2004

6. Performing Organization Code:

8. Performing Organization Report No.: 4910 45 04 922

7. Author(s)

Perry S. Green, Andrew J. Boyd, Kimberly Lammert

9. Performing Organization Name and Address

University of Florida
Department of Civil & Coastal Engineering
P.O. Box 116580
Gainesville, FL 32611-6580

10. Work Unit No. (TRAIS):

11. Contract or Grant No.: BC354 RPWO #55

13. Type of Report and Period Covered: Final Report

12. Sponsoring Agency Name and Address

Florida Department of Transportation
Research Management Center
605 Suwannee Street, MS 30
Tallahassee, FL 32301-8064

14. Sponsoring Agency Code:

15. Supplementary Notes

16. Abstract

A research project was recently completed to assist the Florida Department of Transportation in establishing a list of acceptable methods for the repair of impact damaged prestressed concrete bridge girders using fiber reinforced polymer (FRP) materials. Over the last several years numerous bridges throughout the state have been struck by over-height vehicles and successfully repaired by the FDOT using FRP on an experimental basis. One of the main efforts of the project was to standardize the type of repair procedures used in the field for impact damaged prestressed concrete girders. The experimental portion of the research consisted of testing six full-scale, 44'-0" long AASHTO Type II girders. The tests represented an undamaged control specimen, a control specimen with simulated damage, and four specimens with simulated damage that were then repaired with different fiber reinforced polymer systems. The FRP systems varied in material type, laminate properties, application procedures, reinforcing schemes, and repair design procedures and assumptions. The specimens were tested to failure to determine moment and shear capacities, as well as deformation and ductility behavior of the undamaged, damaged, and repaired girders. Through experimental and analytical comparisons of the behavior of the repaired girders to the undamaged girder, the specific fiber reinforced polymer systems were evaluated for acceptance as potential repair techniques to be used by the FDOT. Each FRP system was evaluated structurally on its ability to restore the undamaged moment and shear capacity of the prestressed concrete girder, the type of failure mode that occurred, the cost of repair system including installation and ease of installation.

17. Key Words	18. Distribution Statement
	No restrictions. This document is available to the public through the National Technical Information Service, Springfield, VA, 22161

19. Security Classif. (of this report)	20. Security Classif. (of this page)	21. No. of Pages	22. Price
Unclassified	Unclassified		

Form DOT F 1700.7 (8-72)

TABLE OF CONTENTS

LIST OF TABLES

LIST OF FIGURES

CHAPTER 1
INTRODUCTION

The 1990 edition of the American Association of State Highway and Transportation Officials' *A Policy on Geometric Design of Highways and Streets* states that the minimum vertical clearance for highways is recommended as 14.5 feet and is desired as 16.5 feet (AASHTO 1990). Not all overpass bridges currently meet these standards either due to being constructed before these standards were issued or paving overlays of the underlying roadway (Bridge Engineering Software and Technology [BEST] 2001). Figure 1-1, assembled by the National Bridge Inventory (NBI), shows the clearance heights for 79000 bridges that have service both over and under the structure in the U.S. Figure 1-2 shows the clearance heights of these 79000 bridges in terms of their functional classification either interstates and freeways or other arterials, collectors, and locals.

In Florida, any vehicle over 13 feet 6 inches is defined as an over-height vehicle and requires a permit to travel on any road system in the state (Florida Department of Transportation [FDOT] 1998). By obtaining a permit the driver of an over-height vehicle is provided with knowledge of how to get to the desired destination on roads with sufficient vertical clearance, and the FDOT is provided information about who, where, and when the road system will have an over-height vehicle in case of bridge damage. Low clearance postings are placed in advance of every bridge or structure with a minimum vertical clearance of 14 feet 6 inches or less (FDOT 1999 revised 2002). In

addition, low clearance postings are placed on the structure for every bridge or structure with a minimum clearance of 13 feet 6 inches or less.

Although regulations exist and are enforced does not ensure that collisions with bridge structures due to over-height vehicles will not occur. Impact damage due to over-height vehicles can lead to structure collapse, reinforcement damage, girder misalignment, steel yielding, connection failure, reinforcement exposure, concrete spalling, and concrete cracking. After a collision has occurred in which an emergency repair is required, a fast, inexpensive, effective, and easy repair is preferred. Table 1-1 lists the bridges in Florida that were placed on the FDOT Declaration of Emergency list due to over-height vehicle impacts over the past two years. The table provides for each of the impacted bridges the approximate date of impact, district number, intersecting roads, and if any other impacts due to over-height vehicles have been reported.

Many research projects have been conducted to determine what criteria should be used for the assessment of damaged concrete structures (Shanafelt and Horn 1980, Shanafelt and Horn 1985, Zobel et al. 1996, Arockiasamy and Barbosa 2000). Establishment of these assessments would provide the necessary means to ensure that if the structure is to be repaired that all potential problems are investigated, and a proper and effective repair could be installed.

Numerous experimental studies of laboratory repairs and in field repairs with fiber reinforced polymer (FRP) systems on concrete structures have been conducted (Sen and Liby 1994, Arockiasamy 1995, Tedesco et al. 1998, Klaiber et al. 1999, Mayo et al. 1999, Shahawy and Beitelman 1999, Labossieere et al. 2000, Tumialan et al. 2001, Scheibel et al. 2001, Boyd and Banthia 2001, Spadea et al. 2001). All of the experimental research

has shown a promising future for fiber reinforced polymer systems for the repair of damaged or deteriorated concrete or steel structures.

Objective of Current Study

The impetus for this research is to assist the Florida Department of Transportation in establishing a qualified products list (QPL) of acceptable methods for the repair of impact damaged prestressed concrete bridge girders using fiber reinforced polymer (FRP) materials. It is felt that having a qualified products list will enable qualified companies to be certified by the FDOT to perform emergency repairs to vehicular damaged bridge girders using FRP materials in a timely manner. Table 1-1 lists those bridges in Florida that were damaged by vehicular impacts and required repair during a two-year period 2001-2002.

The Chaffee Road Bridge, built in 1960, carries CR115C over I-10 near Jacksonville, FL. The bridge is comprised of five Type III AASHTO girders with a 7" deck and an original under-clearance of 15'-6" and is one of those listed in Table 1-1. On July 7, 2001 it was struck by two over-height vehicles that caused major damage as shown in Figure 1-3. In addition to concrete cover loss, there were cracks extending into the web in all the girders and severing of prestressing strands in the exterior girders. Due to the extensive damage, a load restriction was placed on the structure until the FDOT could determine how severely the structural integrity of the span was compromised and then design a repair that would return it to full service. An emergency repair was carried out that included the application of carbon fiber reinforced polymer sheets to both the bottom and sides of the girders to restore their original design capacity. Figures 1-4 and 1-5 show more detailed views of the damage where the vehicles exited from under the

bridge overpass and where one vehicle made first contact with the bridge overpass and the resulting damage.

Relevance of Current Study

Full-scale girder tests of six type II AASHTO girders were performed. The six tests represented an undamaged control specimen, a control specimen with simulated damage, and four specimens with simulated damage that were then repaired with different fiber reinforced polymer systems. The FRP systems varied in material type, laminate properties, application procedures, reinforcing schemes, and repair design procedures and assumptions. The specimens were tested to failure to determine moment and shear capacities, as well as deformation and ductility behavior of the undamaged, damaged, and repaired girders. Through experimental and analytical comparisons of the behavior of the repaired girders to the undamaged girder, the specific fiber reinforced polymer systems were evaluated for acceptance to be placed on the FDOT Qualified Products List. The FRP systems were evaluated structurally on their ability to restore the undamaged moment capacity as well as the shear strength of the prestressed concrete girder, the type of failure mode that occurred, the cost of repair system including installation and ease of installation.

Table 1-1: Summary of Bridges in Florida Damaged due to Vehicular Impact

Date	District	Facility Carries	Intersects	Multiple hits
1/15/2002	2	I-95	SR 206	YES
7/6/2001	2	I-10	CR 115C (Chaffee Road)	YES
2/16/2001	4	I-95	Linton Blvd (SW 12th St)	NO
4/24/2002	4	I-95	SR 708 (Blue Heron Blvd)	YES
8/13/2001	7	SR 618 (Crosstown EXPY)	34th St	YES
9/5/2002	8	SR 91 TPK	SR 826 Palmetto EXPY	NO
5/29/2001	8	SR 91 TPK	SR 91 Jupiter Interchange	NO

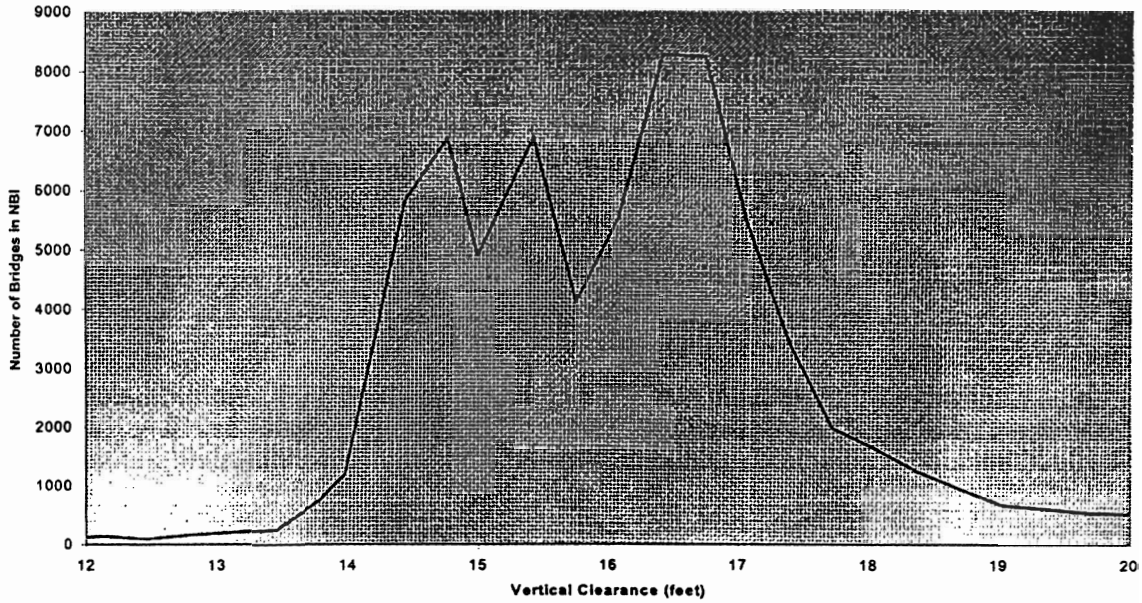

Figure 1-1: Number of Bridges in NBI versus Vertical Clearance of Selected 79000 Bridges (BEST 2001)

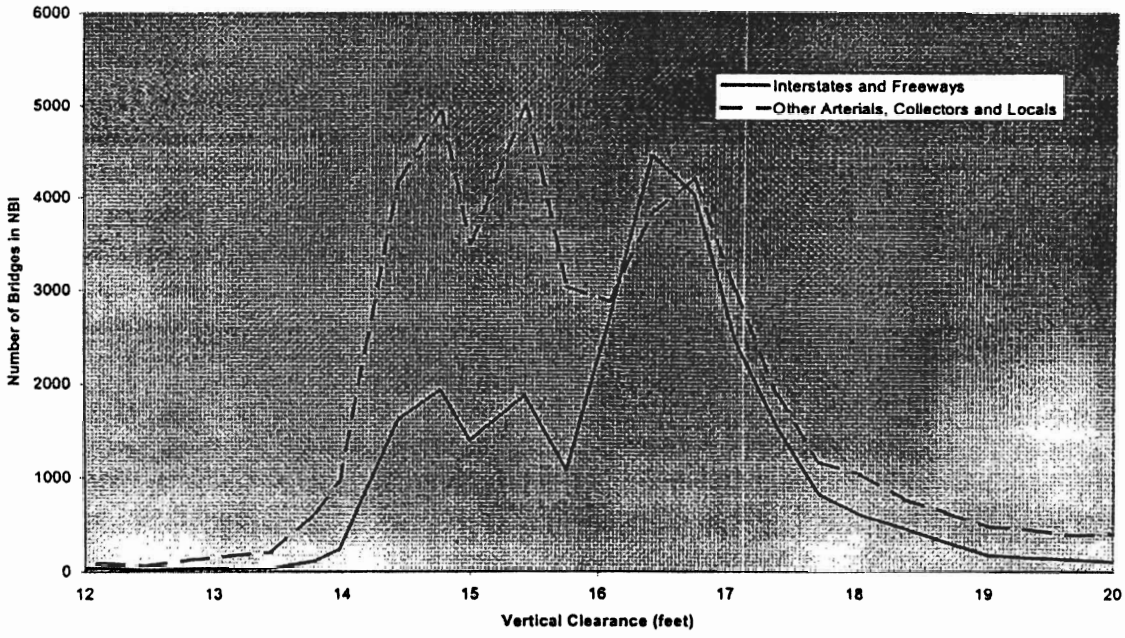

Figure 1-2: Number of Bridges in NBI versus Vertical Clearance of Selected 79000 Bridges by Functional Classification (BEST 2001)

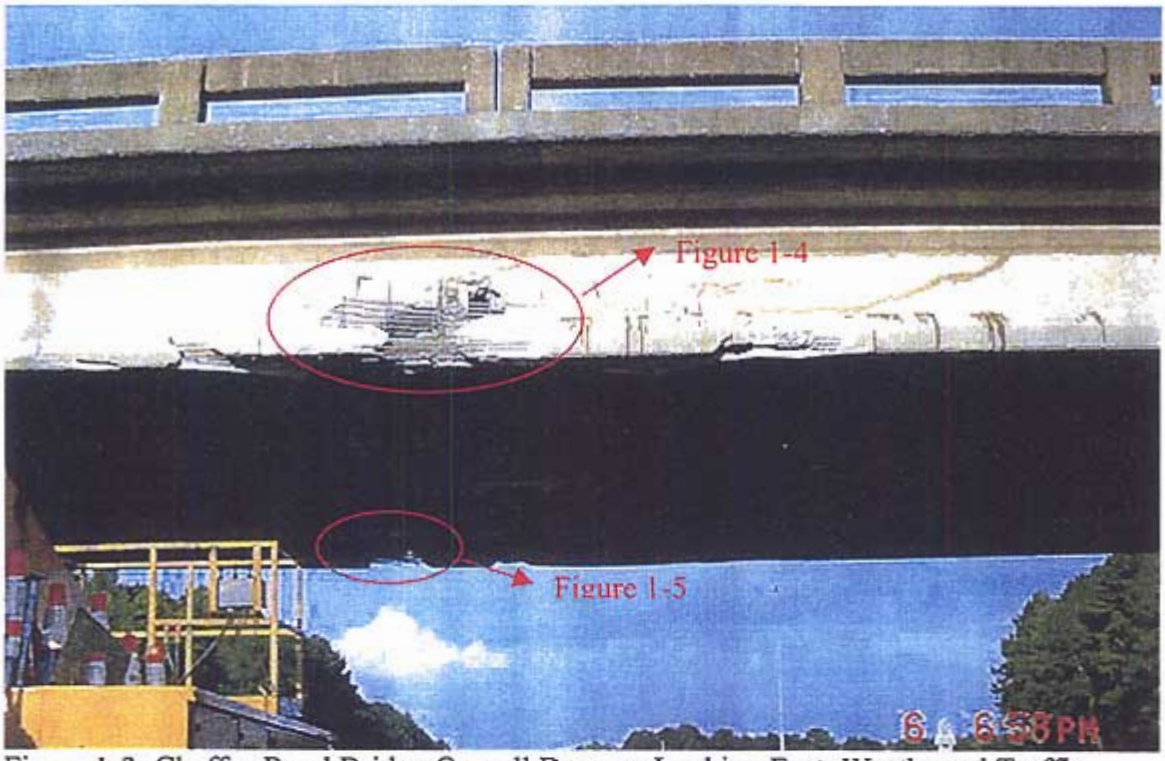

Figure 1-3: Chaffee Road Bridge Overall Damage Looking East, Westbound Traffic

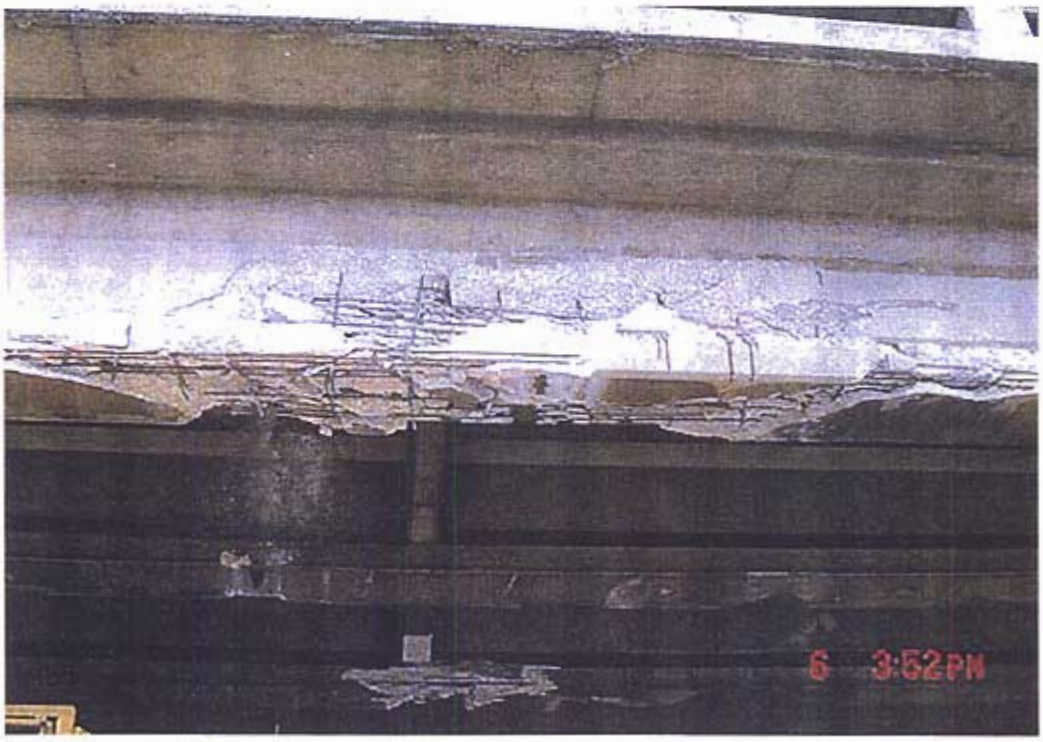

Figure 1-4: Close-up of Damage on the West Fascia Girder in the Vicinity of the Diaphragm

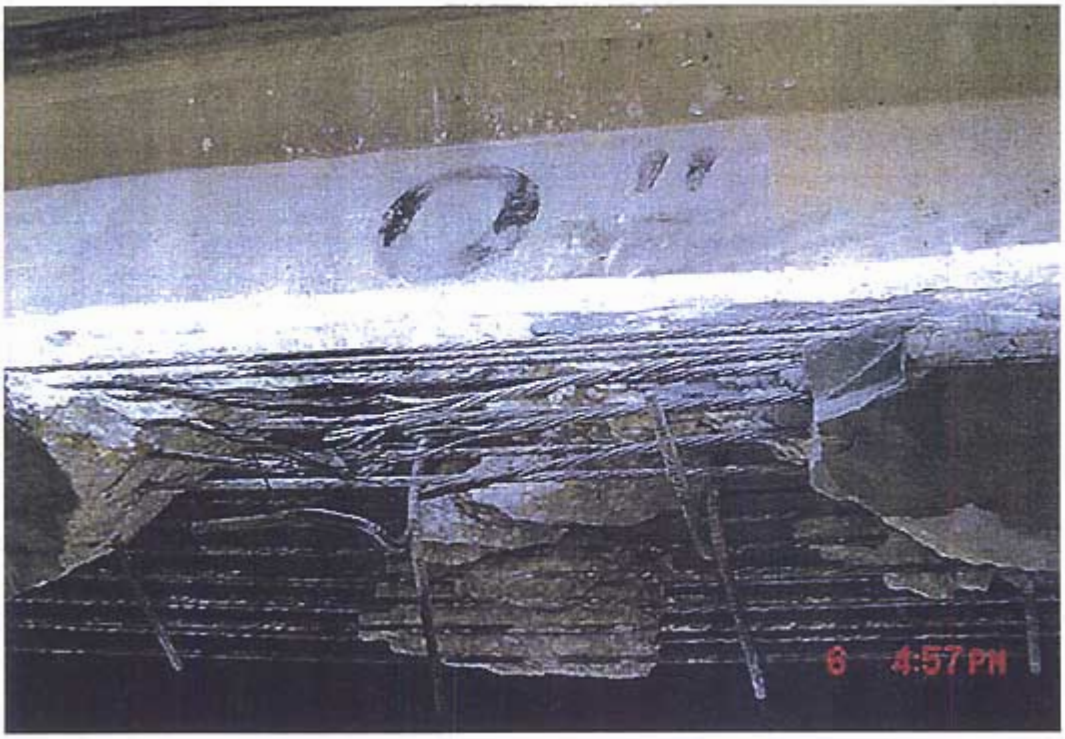

Figure 1-5: Close-up of Damage on the East Fascia Girder Showing Severed Prestressing Strands

CHAPTER 2
PREVIOUS RESEARCH

Fiber Reinforced Polymer Properties and Behavior

Previous research has shown a promising future for the use of fiber reinforced polymer systems as an efficient means to strengthen or retrofit concrete structures in order to resist increased design loads or repair damage (American Concrete Institute [ACI] 2002). Fiber reinforced polymer systems are lightweight, easy to install, noncorrossive, and inexpensive, when compared to prior repair techniques such as bonded steel plates, external post-tensioning, or concrete and steel jacketing (International Federation for Structural Concrete [FIB] 2001). When determining whether to repair or replace a structure, it is crucial that if failure of the FRP system occurs that it does not result in failure of the structure.

A fiber reinforced polymer system consists of fibers and a polymer matrix, namely a stress-bearing component, and a stress-transferring component (FIB 2001). Fibers are typically made of carbon, glass or aramid and all exhibit an almost linear elastic behavior to failure (ACI 2002). Figure 2-1 compares the stress-strain curves for carbon, glass and aramid fiber reinforced polymer systems to that of mild steel. The high tensile strength of an FRP system, provides increased axial strength by fully wrapping the cross-section to increase confinement, in shear capacity by placing the fibers perpendicular to potential shear crack development as shown in Figure 2-2, and in flexural capacity by placing the fibers in the tension areas. FRP systems can be used not only to increase flexural

strength but can also be used to increase the ductility in columns by providing confinement through wrapping the entire cross-section of the column.

Polymer matrices or adhesives are available in epoxies, polyesters, and vinyl-esters. Each type of fiber and adhesive has its advantages and disadvantages, which are dependent on application procedure, type of structure, reason for rehabilitation, and the configuration of the system. Table 2-1 provides a qualitative comparison of different fiber composites. An effective fiber reinforced polymer system consists of fibers and an adhesive working together so that the fibers can take on load from the original structure through an adhesive bond. If the bond is not capable of transferring the required load, the necessary capacity of the fibers can not be developed.

Fibers can be manufactured in a continuous or discontinuous form (FIB 2001). Also, the fiber strands can be manufactured into unidirectional, bi-directional, or multidirectional patterns or orientations forming a fabric which is capable of resisting and distributing load in the manufactured directions (ACI 2002). A fabric is the arrangement of fibers bound together in two or more directions.

Fiber reinforced polymer systems are divided into their different application techniques and can be classified as a wet-lay-up system, pre-impregnated system, pre-cured system or a sprayed system (ACI 2002, FIB 2001). A wet-lay-up system consists of applying a saturating adhesive in-place to a dry reinforcement forming a cured laminate on a structural member. A pre-impregnated system consists of an uncured fabric that has been previously impregnated off-site with a saturating resin which is then bonded to the surface of a structural member with or without an adhesive depending on system requirements. A pre-cured system is applied using an adhesive to bond the off-site

previously cured and formed laminate to a structural member. The spray technique combines the fiber, resin, and catalyst for the resin at the time of application and is sprayed directly onto the structural member (Boyd and Banthia 2001).

The placement of the system on a structure and the orientation of the fibers determines the type and amount of enhanced capacity which the rehabilitated structure will be capable of resisting (ACI 2002, FIB 2001). To resist moment in a flexural member, the fibers or fabric should be placed in the tension areas of the structural member and oriented in the direction of the highest tensile stresses. To resist shear in a flexural member, the fibers or fabric should be applied to the sides of the member and oriented either perpendicular to latent or visible shear cracks or at 45° from the longitudinal axis of the member as shown in Figure 2-2. When increasing the moment capacity of a structural member it is necessary to check that sufficient shear capacity is present to resist the corresponding increase in shear loads or additional shear reinforcement must be provided.

There are many possible failure modes for beams flexurally strengthened with FRP systems. If the ends of the FRP system are sufficiently anchored to the tension side of a flexural member, brittle failure will occur when the beam reaches its ultimate flexural capacity through tensile rupture of the FRP or concrete crushing as shown in Figures 2-3a and 2-3b, respectively (Teng et al. 2002). Figure 2-3c shows that a brittle failure in shear can occur if the flexural capacity exceeds the shear capacity of the strengthened member. Brittle and premature failure can result from debonding due to high interfacial stresses at or near the ends of an FRP system as shown in Figures 2-3d and 2-3e, respectively. Brittle and premature failure can also result from debonding due to high interfacial

stresses from a flexural or flexural-shear crack formed away from the ends of a FRP system as shown in Figures 2-3f and 2-3g, respectively. In addition, other failure modes are possible such as failure of the adhesive, slip at the concrete substrate to adhesive interface and slip at the adhesive to fabric interface or by a combination of any of the modes described above. If the retrofitted member is a prestressed element, additional failure modes can occur such as a prestressing strand steel failure.

Possible failure modes for shear strengthened beams are shear tension with FRP rupture, and shear tension without FRP rupture where the FRP debonds as shown in Figures 2-4a and 2-4b, respectively (Teng et al. 2001). Both failure modes for shear strengthened members are brittle that can lead to an abrupt and catastrophic failure.

Equations, examples, and methods for determining FRP contribution have been developed and included in the ACI (2002) code for reinforced concrete but not for prestressed concrete. The only guidelines are that strain compatibility regarding the state of strain in the prestressed member should be used to calculate FRP capacity increases and that rupture of prestressing strands should be considered as a failure mode (ACI 2002). The absence of code standards means that design repairs are being performed under increased engineering intuition, which could lead to incorrect assumptions.

Guidelines for detailing have been developed to avoid bond-related failures. Suggested details incorporate the use of mechanical anchorages to assist in stress transfer, tapering FRP lengths for multiple ply laminates, and providing sufficient overlap for splicing FRP plies (ACI 2002).

Condition Assessments

Shanafelt and Horn (1980) reported on the findings of an extensive research and compilation of statistics of all cooperating state departments of transportation. The responding departments of transportation showed that of the 23,344 prestressed concrete bridges in those states, an average of 201 bridges were damaged each year. The most significant finding was that over 80 percent of the damage to prestressed concrete bridges was due to over-height vehicles. The investigation produced the necessity for a standard method to evaluate damaged bridges, classify the amount and types of damage, and how to make decisions on the repairs. The types of repairs investigated in the report were repairs with externally bonded reinforcing bars, external post-tensioning using strands or bars, mild steel external sleeves, and internal strand splices. These repairs were investigated through analytical calculations on beams classified as severely damaged.

Shanafelt and Horn (1985) further investigated the findings of the research by performing repairs in the laboratory with external post-tensioning, mild steel external sleeves, and internal strand splices. The purpose of the experiments was to establish standards for evaluating damage to bridges, determining the amount of damage, and designing and applying appropriate repair techniques. Although some of the repair techniques investigated are no longer used solely for repairs, internal strand splicing is still currently being investigated as part of a potential repair technique system.

Zobel, Jirsa, Fowler, and Carrasquillo (1996, 1997 revised) reported on field inspections and laboratory experiments of an impact damaged prestressed concrete girder. The damaged fascia girder was removed from the bridge and used to evaluate non-destructive tests on impact damaged girders, and evaluate repairs with internal strand splicing and concrete patching. Inspection of the girder showed cracking extending into

the web with undamaged exposed prestressing strands. The non-destructive techniques used to evaluate the amount and type of damage to the girder were the rebound hammer, impact echo, and spectral analysis of surface waves. In addition to the above assessments, the girder was load tested without any repairs up to service load. The results showed that the girder had a lower flexural stiffness and had larger deflections at locations of significant damage and higher strains in strands with cross-sections that had significant damage. The girder was repaired using several cast-in-place repair methods: latex-modified vertical overhead mortars, single-component latex-modified mortars, and fiber reinforced silica fume modified mortars over different damaged sections. Epoxy was then injected to all remaining cracks and voids. After the repairs were completed, the girder was reevaluated with the rebound hammer which showed a sound repair and with the impact echo and spectral analysis of surface waves which showed that structural integrity was generally restored. The beam was then load tested again up to its service load. The results indicated that the girder had a higher flexural stiffness though it still had larger deflections at locations with significant damage. The slope of the load versus tendon strain curve showed significant improvement after the repair was completed.

The authors also investigated the effectiveness of internal strand splicing. Four strands were intentionally severed at midspan to be spliced with four different splicing assemblies. To determine the effectiveness of the splice, the girder was taken through a series of load tests in which all four strands had been severed, all four strands spliced, two splicing assemblies removed, and with all four splices removed. The load tests demonstrated that the strain in the undamaged strands decreased when the damaged

strands were spliced suggesting a redistribution of strain to the spliced strands and the capability of the splices to restore service load capacity.

Arockiasamy and Barbosa (2000) assessed techniques for the condition evaluation and repair of concrete bridges. The research provides condition evaluation, selection of repair types, repair design procedures, repair construction procedures, and case studies of implemented repairs for bridge deck, substructure and superstructure elements. The effective types of repairs that were considered in this study for prestressed girders were external post-tensioning, internal splicing of strands, metal sleeve splices, and replacement.

The Bridge Engineering Software and Technology (BEST) Center (2001) reported on a study in which the purpose was to determine the extent of over-height vehicle collisions and identify ways to prevent over-height vehicle collisions. A survey was sent to every state requesting the following: average clearance height of bridges, maximum vehicle height, fines for over-height vehicles, clearance postings, and collision data. Only 29 states replied to the survey. Of the responding states only 12 provided statistics on over-height collisions. Only 17 states stated that they keep records of over-height vehicle collisions. The researchers determined from the submitted data that the number of over-height vehicles increased by 1.3% per year from 1995 to 1999. In Maryland, 309 of the 1496 susceptible bridges or 20 percent have been damaged from over-height vehicles. Of the 309 bridges that have been damaged 106 or 34% cross over an interstate highway. To increase bridge clearances seven states or 24 percent indicated that they had ground down the pavement that resulted from repeated resurfacing. The state of Georgia

responded that a program was ongoing to raise all existing interstate bridges to a minimum clearance height of 16'-6".

Repairs with Fiber Reinforced Polymer Systems

Although a significant amount of research has been conducted on fiber reinforced polymer (FRP) strengthening systems of reinforced concrete elements, little research has been conducted on the use of FRP for the repair of prestressed concrete elements. This section contains the last 10 years of research concerning repairs with FRP systems. At present, standards for the design, application, and configuration of fiber reinforced polymer strengthening systems on prestressed concrete structures have not been developed.

Sen and Liby (1994) reported on the feasibility of using CFRP laminates to strengthen steel composite beams through experimental and analytical procedures. The composite beams were made of W8x24 steel sections with a 28" by 4 ½" concrete slab. The specimens were subjected to two loading cycles in four-point bending. The first cycle consisted of loading the specimen to yield of the tension flange to simulate distress. The second cycle consisted of loading the specimen to failure after the specimen was repaired with CFRP laminates along the tension flange. Clamps were installed at the ends of the laminates to resist peeling stresses. The clamps were designed based on the stresses determined from a finite element analysis in the laminate and adhesive. The test specimens consisted of two different steel yield strengths of 45 ksi and 54 ksi and were repaired with two different laminate thicknesses of 2mm and 5mm. Specimens 1 and 2 were 54 ksi yield steel repaired with 2mm thick CFRP laminates, Specimen 3 was 45 ksi yield steel repaired with 5 mm thick CFRP laminates, Specimen 4 was 54 ksi yield steel repaired with 5 mm thick CFRP laminates, and Specimens 5 and 6 were 45 ksi yield steel

repaired with 2 mm thick CFRP laminates. After testing Specimens 1, 2, and 3, additional bolts were used to further resist the stresses due to shear in the adhesive. These additional three rows of bolts were spaced 16 ½" apart at each end of the CFRP laminate. Figures 2-5, 2-6, 2-7, 2-8, 2-9, and 2-10 show the load deflection relationships for Specimens 1, 2, 3, 4, 5, and 6, respectively. The experimental results showed that the CFRP laminates significantly increased the ultimate capacity of the steel composite sections. A higher capacity with a more ductile failure mode could also be reached by properly anchoring the CFRP laminates with the additional bolts as compared to the unanchored repaired specimens.

Arockiasamy (1995) studied the flexural behavior of rectangular reinforced concrete beams with a varying number of CFRP plates on the tension face through experimental tests and analytical procedures. Six concrete specimens were tested to failure, one was a control with no FRP, one was strengthened with one layer of FRP, two were strengthened with two layers of FRP, and two were strengthened with three layers of FRP. The beam dimensions were 8" wide by 1'-0" deep and were 8'-0" long with a span to depth ratio of four. The beams were all tested to failure in two-point loading, and were instrumented with seven strain gauges on the bottom centerline of the beam, four strain gauges on one side of the beam, and five LVDT's equally spaced along the length of the beam. Table 2-2 compares the ultimate capacity, deflection at midspan, initial stiffness, and midspan crack width for all of the specimens, with the last number in the beam name indicating the number of layers of CFRP. Figure 2-11 shows the moment deflection relationship for all of the specimens. All of the beams with FRP systems failed due to concrete crushing at smaller deflections than the control specimen. The bonding

of the CFRP plates to the tension face increased the flexural capacity, increased the flexural stiffness, reduced crack widths, and reduced the CFRP, rebar, and concrete compressive strains at midspan as the number of FRP plates increased. Moment versus strain relationships for the CFRP, steel reinforcing bar, and concrete are shown in Figures 2-12, 2-13, and 2-14 respectively.

Tedesco, Stallings, and EL-Mihilmy (1998) investigated the effects of rehabilitating a deteriorated reinforced concrete bridge in the field with external bonding of FRP plates. The reinforced T-beam bridge was located on State Highway 110 near Union Springs, Alabama. The simple span bridge had significant flexural and shear cracking before repair. All of the reinforcing laminates used for repairs consisted of unidirectional fibers oriented parallel to the longitudinal axis of the plate. Three of the four beams were retrofitted with carbon fiber reinforced polymers on the tension face to increase flexural capacity and with glass fiber reinforced polymers on the sides to increase shear capacity. The remaining beam was only retrofitted with carbon fiber reinforced polymers on the tension face. Load tests were performed before and after the retrofit was applied to determine what affects the application of the FRP strengthening system had on the bridge. Retrofitting the bridge resulted in smaller strains in the longitudinal reinforcement and lower midspan deflections as shown in Tables 2-3 and 2-4. The beam with only FRP on the tension face exhibited the least reduction in strain and deflection indicating the significant effect of the GFRP on the overall structural behavior. To verify the effects that FRP laminates have on strengthening the bridge, a finite element analysis was performed. Results from the finite element analysis showed close

correlation to the in-field load tests for reinforcement strains and midspan deflections with an average percentage difference of 5.7% and 5%, respectively.

Klaiber, Wipf, Russo, Paradis, and Mateega (1999) reported on the repair of an impact damaged prestressed concrete bridge in Iowa in which field and laboratory tests were conducted. The impacted bridge carries Interstate 680 over County Road L34 located near Beebeetown, Iowa. The bridge consists of two separate structures of the same design and construction; one carries traffic eastbound and the other carries traffic westbound. Each bridge consists of a concrete deck set on eleven beams with varying vertical clearances. The westbound bridge was damaged while the eastbound bridge was undamaged, thus providing a means to compare in-place load tests on the damaged and undamaged structures. The three northernmost girders of the westbound bridge showed significant damage at their midspans ranging from exposed and slack multiple prestressing strands, a pre-existing severed strand, web cracking, and spalling of concrete. Figure 2-15 shows some of the damage to the bridge. As part of the study, the eastbound and westbound bridges were static load tested to determine whether they had a different response to the applied load and load distribution. Although the two northernmost damaged girders did not require replacement, they were subsequently removed from the bridge for laboratory testing of fiber reinforced polymer systems and the third northernmost girder was repaired insitu. Static load tests were again performed on the westbound bridge after the removed girders were replaced. The field test results showed that the behavior of the eastbound and westbound bridges were now basically the same.

Beam 1 was tested to failure as the control specimen. Beam 1 had two severed strands, which caused the beam to fail in combined shear and slab crushing at a moment of 2067 kip-ft and corresponding deflection of 8.62". Beam 2 was damaged by severing strands to be equivalent to Beam 1. Beam 2 was then repaired with three longitudinal carbon fiber reinforced plates with additional fiber stirrups along the length to restore the loss of capacity due to the severing of two strands and loaded to failure. Beam 2 ultimately failed due to debonding of the carbon fiber reinforcing system at a moment and corresponding deflection of 2480 kip-ft and approximately 6.4". Figure 2-16 provides a comparison of the moment deflection relationships for Beams 1 and 2, the series B1W is for Beam 1 and all of the other series are for Beam 2. By taking the experimental strain in the composite at ultimate and multiplying by the area of FRP material, the researchers determined that the force in the FRP was equivalent to three and a half 250 ksi strands with a diameter of 0.5". Only two strands had been severed, therefore the design goal of restoring the lost tensile capacity of the damaged strands was reached. A 12% increase in ultimate capacity of the repaired girder (Beam 2) over the control specimen (Beam 1) and a 10% increase in ultimate capacity over the theoretical ultimate capacity of an undamaged member was reported.

Mayo, Nanni, Watkins, Barker, and Boothby (1999) reported on the strengthening of a simple span reinforced concrete solid slab bridge in Iron County, Missouri. The bridge, located on a mining truck operation route, Route 32, was strengthened in order to remove weight restrictions. Through a comparison of design trucks in use at the time of design to the present and including the current condition of the bridge such as corrosion damage and cracking, it was determined that a 19% increase in flexural strength would be

required to remove the weight limit posting. To ensure the effectiveness of the FRP strengthening system, two full-scale reinforced concrete beams were constructed and tested to failure. The beams were constructed to simulate the existing bridge conditions and geometry. Beam 1 was a control beam with no FRP strengthening, and Beam 2 was strengthened with a one-ply carbon fiber reinforced polymer system to verify that a 20% increase in capacity could be restored. Beam 1 failed due to concrete crushing, and Beam 2 failed due to FRP rupture. Figure 2-17 provides a comparison of the experimental and theoretical load deflection relationships for Beams 1 (before strengthening) and 2 (after strengthening). The laboratory test results showed that a 27% increase in flexural strength with a finer crack pattern was achieved over the control beam test result. The durability of the bonding of the FRP system was also investigated through static and dynamic tests, confirming that peeling of the FRP should not be an issue. The bridge was instrumented with deflection gauges and then load tested while before and after FRP strengthening. The in-field load tests indicated a slight increase in stiffness due to decreased deflection of the rehabilitated bridge.

Shahawy and Beitelman (1999) studied the static performance of reinforced concrete beams strengthened with CFRP sheets. Eight T-beams of approximately 19'-0" long were tested to failure in four-point bending. One specimen was tested as a control with no FRP reinforcement. Five specimens had FRP applied to the entire stem, meaning the bottom and sides of the beam, with varying layers of FRP. For the five fully-wrapped specimens, there was one specimen with one layer of FRP, one specimen with three layers of FRP, one specimen with four layers of FRP, and two specimens with two layers of FRP. The remaining two specimens had two layers FRP applied only to the bottom

surface of the stem. All of the specimens were repaired with unidirectional carbon fiber sheets. The T-beams were instrumented with LVDT's at the load points, supports, and midspan and with strain gauges at the load points and midspan. The moment versus midspan deflection curve for the fully wrapped beams and control beam show an increase in capacity and a reduction in deflection of all of the repaired beams when compared to the control specimen shown in Figure 2-18. Figure 2-19 shows how the number of layers of FRP affects the flexural capacity at steel yield and ultimate for the fully wrapped beams. The partially wrapped specimens showed lower moment capacity and deflection than the fully wrapped sections presented in Figure 2-20. The partially wrapped beams failed prematurely due to concrete cover separation, demonstrating the significance of providing sufficient anchorage through wrapping the beams. A two-dimensional finite element program, which takes into account the non-linear response of the component materials was implemented. Four cross-sections were analyzed with this program representing the control specimen, the partially wrapped beam with two layers of FRP, and the remaining were fully wrapped cross-sections with two and three layers of FRP. The program resulted in very consistent values for midspan deflection for all cross-sections with slightly higher deflections and capacities at ultimate as shown in Figure 2-21.

Labossieere, Neale, Rochette, Demers, Lamothe, Lapierre, and Desgagne (2000) reported on the strengthening of the Sainte-Emelie Bridge that needed upgrading in order to withstand heavy loads due to a nearby timber distributor. The Sainte-Emelie Bridge carries Route 131 over the Riviere Noire near Sainte-Emelie-de-l-Energie in Quebec, Canada. The bridge is a one-span monolithic deck and T-section reinforced concrete

structure with no significant signs of deterioration such as concrete spalling or corrosion. The weight of standardized design trucks has increased since the design of this bridge. Therefore, to bring the bridge up to current standard design loads, the bridge required a 35% increase in moment and 20% increase in shear capacity. To ensure the strengthening procedure would be sufficient, numerous laboratory tests were performed on one-third scale test specimens and analytical models were evaluated. The laboratory tests included different potential climatic effects, behaviors of FRP materials, assessment of an assortment of strengthening configurations for the T-section, and the bonding capacity of the FRP system to concrete. Four beams were constructed and tested to failure. Beam 1 was a control beam with no additional reinforcement. Beam 2 was reinforced with six layers of carbon fiber for flexural strengthening on the full length with glass fiber stirrups at varying spacing with an additional continuous strip of glass at the top of the stirrups for added anchorage. Beam 3 was reinforced with one layer of carbon fiber for flexural strengthening on the full length with the glass fiber stirrup spacing of Beam 2 with an additional continuous strip of glass at the top of the stirrups for added anchorage wider than Beam 2. Beam 4 was reinforced with six layers of carbon fiber for flexural strengthening, three extending the full length and three apporximatley 3'-0" shorter on both ends with glass fiber stirrups at varying spacing and an additional continuous strip of glass at the top of the stirrups for added anchorage wider than Beam 2.

The control beam (Beam 1) failed in shear. Beam 2 failed in shear due to debonding of the FRP stirrups but with a 40% load capacity increase over Beam 1. Beam 3 failed when the flexural strengthening failed in tension with a 60% load capacity

increase over Beam 1. Beam 4 failed when the flexural strengthening ruptured in tension with a 50% load capacity increase over Beam 1. Figure 2-22 provides the load deflection relationships for Beams 1, 2, 3, and 4.

A larger deflection at failure was observed for the beams with FRP than the control beam consistent with the analytical models. The laboratory experiments showed the effectiveness of the FRP material on strengthening reinforced concrete structures. The final retrofit design for the Sainte-Emelie Bridge included three layers of carbon fiber oriented longitudinally for the full length of the beams. In addition, glass fiber stirrups with fibers oriented vertically anchored at the top with an additional glass fiber oriented longitudinally were applied to the beams. To determine the in-field effectiveness of the FRP system, the bridge was instrumented with strain gauges primarily at midspan and located on the reinforcing steel inside the beams, on the FRP strips. A displacement sensor was also placed under each beam at midspan. The bridge was load tested before and after the FRP application to observe the bridge behavior. Decreases in the midspan strains and deflections were observed after the FRP application as hypothesized in the design and demonstrated in the laboratory.

Tumialan, Huang, and Nanni (2001) reported on an in-field fiber reinforced polymer repair of an impact damaged bridge by an over-height vehicle in Missouri. The damaged bridge, Bridge A10062, is located at the interchange of Interstates 44 and 270 in St. Louis County, Missouri. After removal of the loose concrete, inspection of the prestressed concrete bridge girders showed that the exterior girder had sustained the most damage with two of the twenty prestressing strands severed. Figure 2-23 shows some of the damage to the bridge. From an analytical procedure it was determined that a 190 k-ft

moment capacity would be needed from the FRP system to restore the girder to its original strength. The repair called for a two-ply unidirectional carbon fiber reinforcing polymer system with stirrups along the fiber length. No load tests, field measurements, or laboratory simulations were conducted. After the repair was completed, it was inspected and any potential void areas that were identified were epoxy injected to ensure that a complete bond was provided.

Scheibel, Parretti, and Nanni (2001) investigated the effectiveness of fiber reinforced polymer strengthening of eleven prestressed concrete girders from another impact damaged bridge in Missouri. The damaged bridge, Bridge A4845, is located over Route 291 on Route 24 in Jackson County, Missouri. An inspection of the eleven girders showed only concrete spalling and the exposure of reinforcing steel and prestressing tendons. Further inspection revealed that only three girders had exposed prestressing tendons with a maximum of two tendons exposed in one girder. Figures 2-24 and 2-25 show overall and detailed views of the damaged bridge. For the design of the strengthening system, the exposed tendons were assumed to be 50% effective. From an analytical procedure it was determined that a 187 k-ft moment capacity would be needed from the FRP system to restore the girder to its original strength. The repair called for a two-ply unidirectional carbon fiber reinforcing polymer system with stirrups along the fiber length. Long-term durability was addressed by applying the repair in an area away from the damage to perform bond pull-off and torsion tests over five years. Initial durability tests indicated a strong bond between the concrete surface and the FRP. No load tests, field measurements, or laboratory simulations were conducted to show that the designed repair was sufficient to restore the girder's original load capacity.

Boyd and Banthia (2001) reported on a new application method of fiber reinforced polymer strengthening systems in which the fibers and matrix resin are simultaneously sprayed onto the member surface. The spraying equipment provides a two-dimensional random distribution of fibers with adjustable fiber lengths and has the ability to build up the FRP strengthening system to any desired thickness. To examine the effectiveness of this new method, three reinforced concrete channel beams that had been removed from a badly deteriorated bridge were tested under third point bending to failure. The damage to the beams consisted of cracking, loss of concrete cover, and reinforcement corrosion, which varied, in each specimen making direct comparisons invalid. From the three specimens, one was treated as a control with no repair while the other two were both repaired with E-glass fibers: one repaired with the spray technique and the other repaired with a continuous fiber system. Both applications were completed under laboratory conditions meaning that the beams were repaired while upside down, which is not possible in the field. The spray consisted of E-glass fibers embedded in a matrix consisting of a polyester resin and a catalyst for the resin. The researchers also conducted coupon tests and determined that the strength of the fiber reinforced polymer system increased with increasing fiber length. Figure 2-26 shows the load deflection relationship for the control specimen, the fabric repaired specimen, and the spray repaired specimen. The experiments showed a greater increase in stiffness with the spray repair over the fabric repair and a significant increase in strength for both repair fabric types. Also, for material costs only, the spray repair was determined to be less expensive than the continuous fiber repair.

Spadea, Swamy, and Bencardino (2001) reported on the laboratory testing of reinforced concrete beams repaired with carbon fiber reinforced polymer laminates reporting on respect to ductility, strength and failure modes. Eleven rectangular reinforced concrete beams were constructed. The beams were divided into three series, one control beam for each series with no external reinforcing referred to as A1, A2, and A3. Within a series the internal reinforcing remained constant and the external reinforcing was varied. Beams 1.1 and 3.1 were strengthened longitudinally with one sheet of CFRP and no additional reinforcement. Each series contained a beam (1.2, 2.2, and 3.2) that was strengthened longitudinally with one sheet of CFRP, a wide stirrup at each support, and four small stirrups spaced along the length of the beam. Beams 1.3 and 3.3 were strengthened longitudinally with one sheet of CFRP, a wide stirrup at each support, two small stirrups at midspan, and three small stirrups at each load point with a plate above. Beam 2.3 was strengthened longitudinally with one sheet of CFRP, a wide stirrup at each support, and ten small stirrups spaced along the length of the beam. The stirrups or anchorages were made of steel and applied to the beams with the same adhesive used for the CFRP. The steel plate anchorages were designed to either counteract stresses at the end of the plates and control bond slip between the CFRP plate and concrete, restrain movement of the plate, or provide lateral confinement for the concrete in compression. The beams were tested in four-point bending to failure to determine what increases in strength, ductility, and stiffness could be attained from the different reinforcing schemes. The control beams with no external reinforcing failed as expected due to concrete crushing. Beams 1.1 and 3.1 with only one sheet of CFRP and no anchorages, failed suddenly due to debonding of the CFRP at a capacity 60.7% and

30.8% greater than their corresponding control specimen. The other beams, with longitudinal and varying external stirrup reinforcing, all resisted a higher load than their respective control specimen and failed in a more ductile manner than the beam with only longitudinal reinforcing. The beams with anchorage reinforcing also reached higher strains in the concrete and in the CFRP than the beams with only longitudinal reinforcing. Structural ductility was quantified for deflection, curvature, and energy as defined by Equations 2-1, 2-2, and 2-3.

$$\mu_{\Delta} = \frac{\Delta_u}{\Delta_y} \tag{2-1}$$

$$\mu_{\phi} = \frac{\phi_u}{\phi_y} \tag{2-2}$$

$$\mu_{E} = \frac{E_{tot}}{E_y} \tag{2-3}$$

Where Δ_u = midspan deflection at ultimate load, Δ_y = midspan deflection at yield, ϕ_u = curvature at ultimate load, ϕ_y = curvature at yield load, E_y = area under the curve at yield load and E_{tot} = area under the curve at ultimate load. In Equation 2-3, E_{tot} is taken as the entire area under the load deflection curve and E_y is taken as the area under the load deflection curve up to yield. Table 2-7 provides the defined ductility ratios for all test specimens. Comparing the defined ductility ratios of the control beam to the other beams shows a significant reduction for all of the repaired beams and shows a more significant reduction in ductility of the beams repaired with only longitudinal reinforcing over the beams with longitudinal and stirrup reinforcing.

Table 2-1: Qualitative Comparison of Carbon, Aramid and Glass Fibers (Meier and Winistorfer 1995)

Criterion	Fiber Composite Sheets Made of:		
	Carbon Fibers	Aramid Fibers	E-Glass Fibers
Tensile Strength	Very Good	Very Good	Very Good
Compressive Strength	Very Good	Inadequate	Good
Young's Modulus	Very Good	Good	Adequate
Long-Term Behavior	Very Good	Good	Adequate
Fatigue Behavior	Excellent	Good	Adequate
Bulk Density	Good	Excellent	Adequate
Alkaline Resistance	Very Good	Good	Inadequate
Price	Adequate	Adequate	Very Good

Table 2-2: Comparison of Load, Deflection, Stiffness, and Crack Width (Arockiasamy 1995)

Beam	# of plates	Ultimate Load (kip)	% diff	Midspan Deflection at Ultimate (in)	% diff	Initial Stiffness (kip-in/in)	% diff	Midspan Crack Width at Ultimate (in)	% diff
S5-STL	0	13.442	-	1.65	-	674.685	-	0.0147	-
S5-PRE1	1	14.973	11.39	1.34	18.79	813.803	20.62	0.00294	80
S5-PRE2	2	19.878	47.88	0.994	39.76	980.725	45.36	0.0092	37.41
S6-PRE3	2	22.014	63.77	0.962	41.7	1004.555	48.89	0.00554	62.31
S6-PRE4	3	20.675	53.81	0.643	61.03	1011.465	49.92	0.00474	67.76
S6-PRE5	3	26.126	94.36	0.881	46.61	1197.95	77.56	0.00456	68.98

Table 2-3: Comparison of Midspan Deflection Before and After FRP Application (Tedesco et al. 1998)

Girder	Before FRP (mm)	After FRP (mm)	Percent Difference
Loading Position 1			
1	6	5.6	7
2	7.9	7.3	8
3	7	6.3	10
4	3.2	2.8	12
Loading Position 2			
1	5.4	5.2	5
2	7.7	7.1	8
3	7.3	6.6	10
4	3.7	3.3	12
Loading Position 3			
1	3.1	3	2
2	6.5	6	8
3	8.6	7.7	10
4	6.3	5.5	12
Loading Position 4			
1	3.6	3.5	4
2	6.9	6.3	9
3	8.3	7.4	11
4	5.6	5	12

Table 2-4: Comparison of Reinforcing Bar Stresses Before and After FRP Application (Tedesco et al. 1998)

Girder	Before FRP (MPa)	After FRP (MPa)	Percent Difference
Loading Position 1			
1	83	77	7
2	91	85	7
3	82	74	10
4	37	34	9
Loading Position 2			
1	75	72	4
2	88	82	7
3	84	77	8
4	45	41	9
Loading Position 3			
1	39	37	4
2	72	66	8
3	106	94	11
4	82	74	10
Loading Position 4			
1	47	44	6
2	76	69	9
3	102	90	12
4	73	66	10

Table 2-5: Comparison of Initial Stiffness and Strength for Various Retrofits (Boyd and Banthia 2001)

Retrofit Type	Stiffness		Strength	
	Initial (kN/mm)	Change (%)	Peak (kN)	Change (%)
None	6.69	-	214	-
Fabric	7.67	15	284	33
Spray	9	35	419	96

Table 2-6: Comparison of Stiffness Before and After Retrofit (Boyd and Banthia 2001)

Retrofit Type	Stiffness Before Retrofit (kN/mm)	Stiffness After Retrofit (kN/mm)	Change (%)
Fabric	6.9	7.67	11
Spray	7.78	9	16

Table 2-7: Comparison of Ductility Ratios (Spadea et al. 2001)

Beam	Failure Load (kN)	Deflection Ductility	Curvature Ductility	Energy Ductility
A1	54	6.2	8	11.6
A1.1	86.8	1.5	1.5	1.9
A1.2	98	4.3	2.9	9.5
A1.3	96.7	3.5	4	7.6
A2	29.2	7.5	11.5	17.4
A2.2	75	4.8	3	13.2
A2.3	77.7	5.8	4	16.1
A3	57.2	7	10.3	15.7
A3.1	74.8	2	2.2	3.2
A3.2	98.8	4.5	3.3	10.9
A3.3	98.3	3.8	4.9	8.4

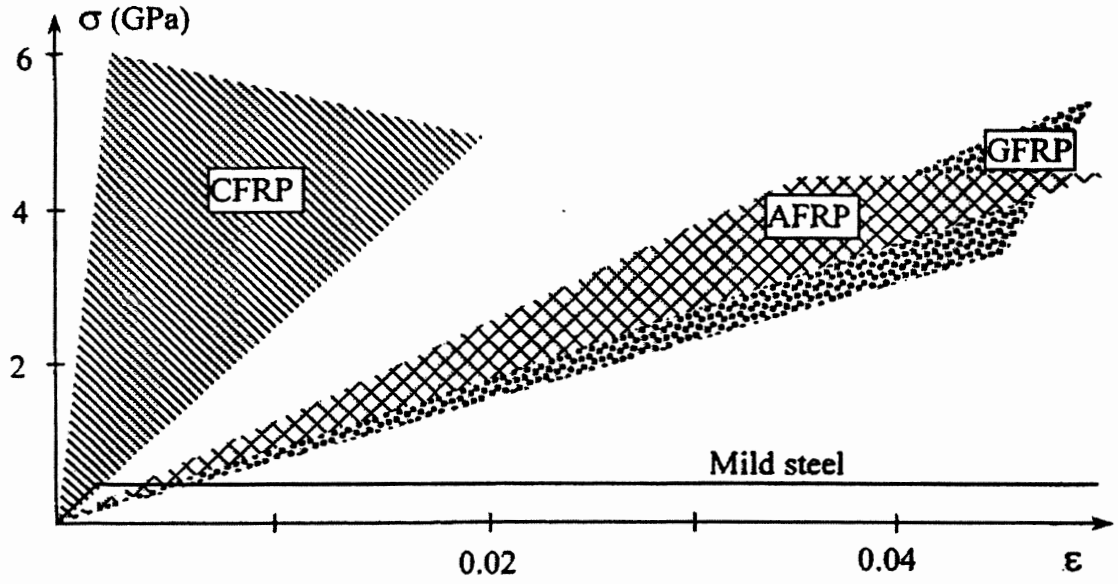

Figure 2-1: Stress-Strain Diagrams for Mild Steel and Carbon, Glass, and Aramid Fiber Reinforced Polymers (FIB 2001)

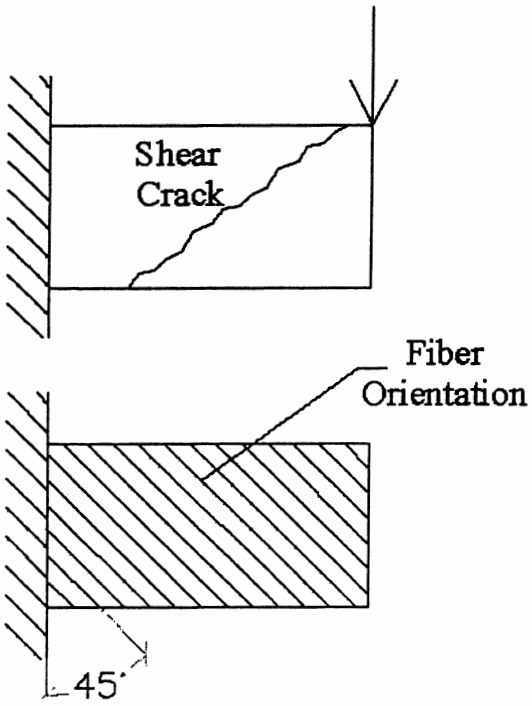

Figure 2-2: FRP Placement for Increase in Shear Capacity

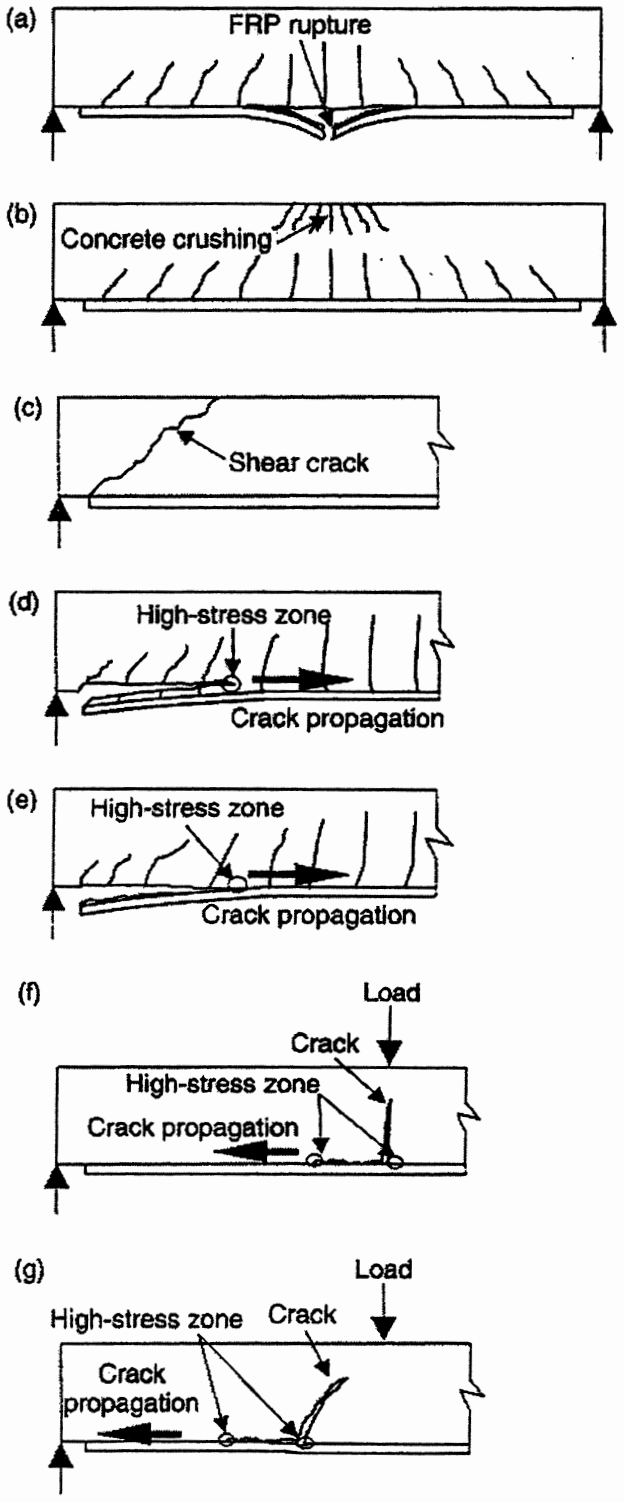

Figure 2-3: Flexural Failure Modes for FRP Strengthened Beams (Teng et al. 2002)

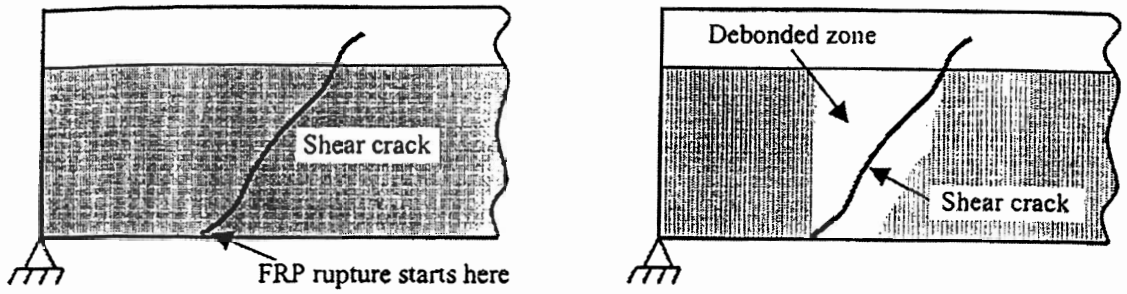

(a) (b)

Figure 2-4: Shear Failure Modes for FRP Strengthened Beams (Teng et al. 2001)

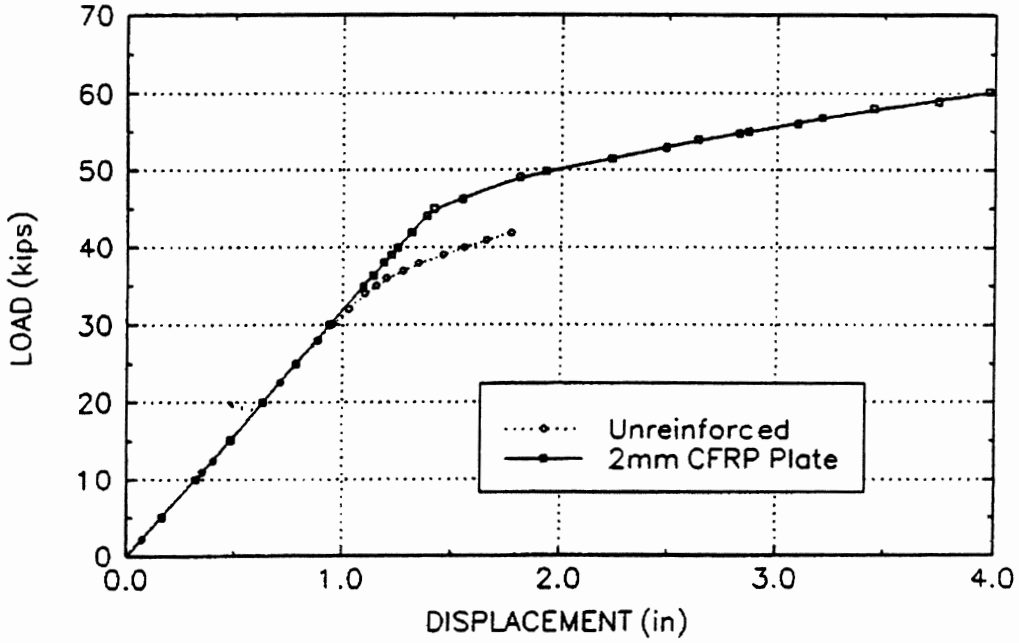

Figure 2-5: Load versus Midspan Deflection for Specimen 1 with 54 ksi yield steel (Sen and Liby 1994)

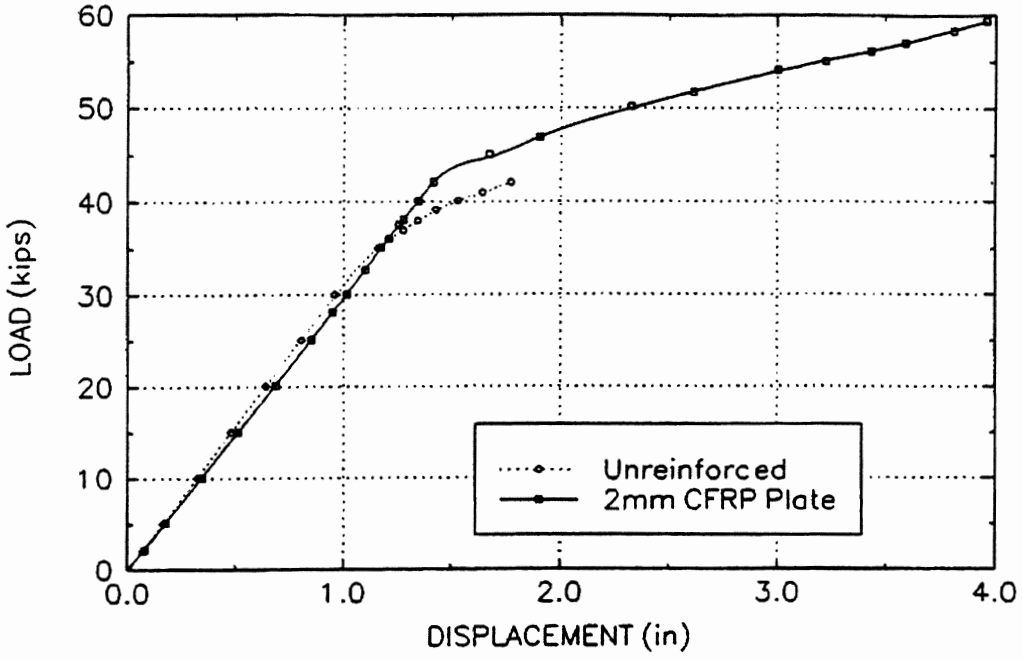

Figure 2-6: Load versus Midspan Deflection for Specimen 2 with 54 ksi yield steel (Sen and Liby 1994)

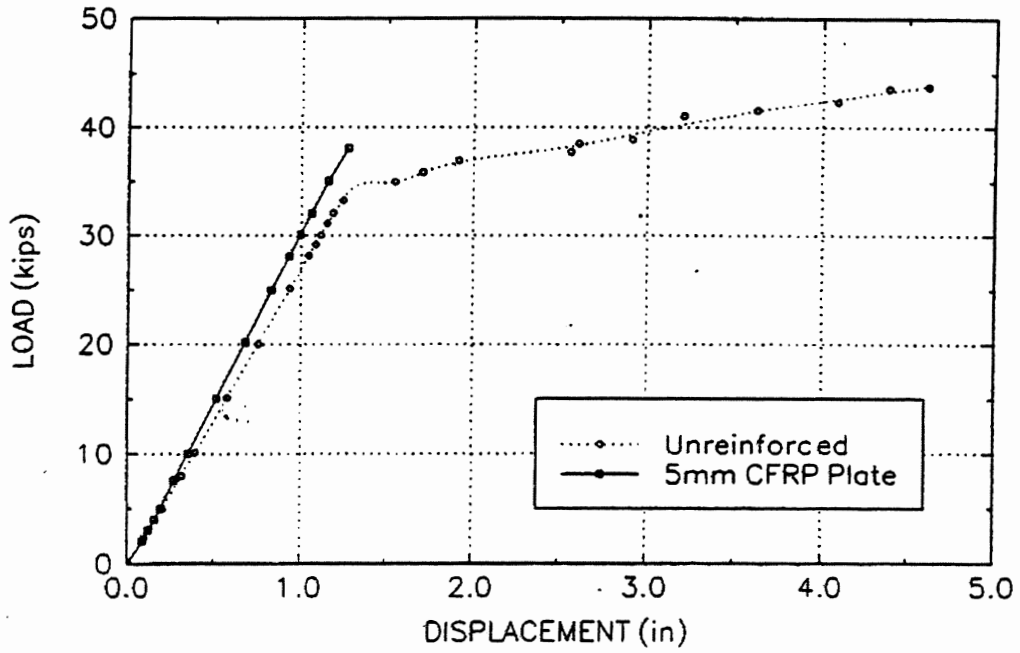

Figure 2-7: Load versus Midspan Deflection for Specimen 3 with 45 ksi yield steel (Sen and Liby 1994)

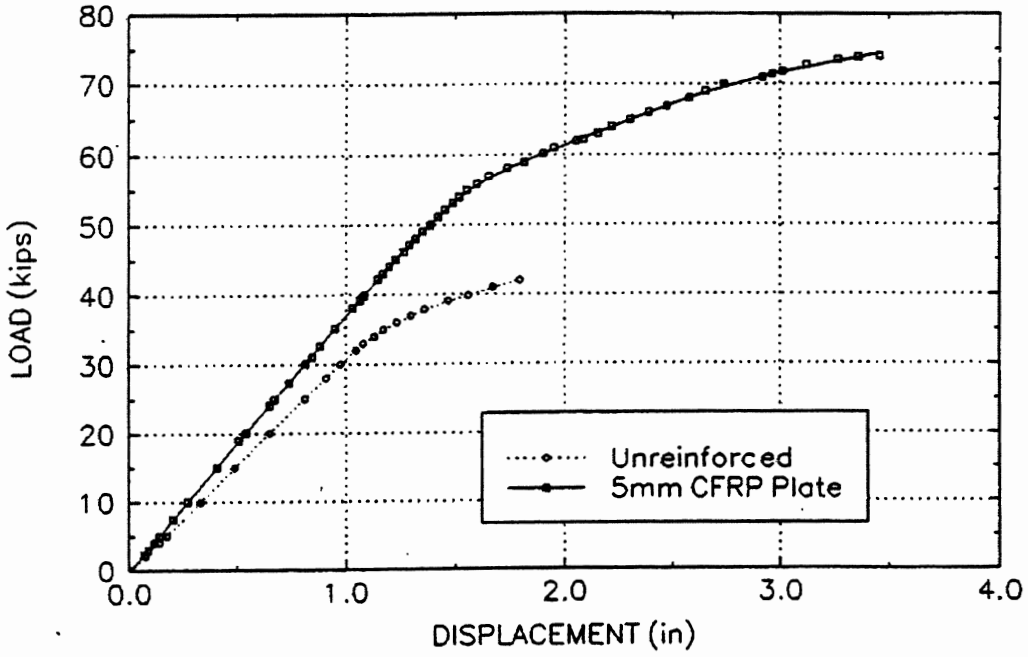

Figure 2-8: Load versus Midspan Deflection for Specimen 4 with 54 ksi yield steel (Sen and Liby 1994)

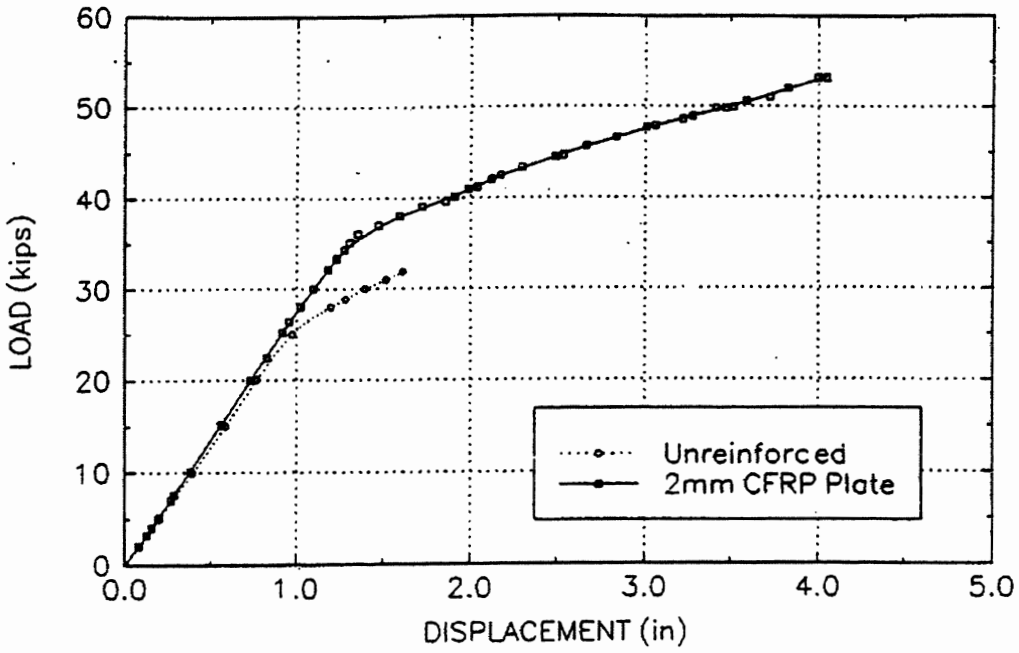

Figure 2-9: Load versus Midspan Deflection for Specimen 5 with 45 ksi yield steel (Sen and Liby 1994)

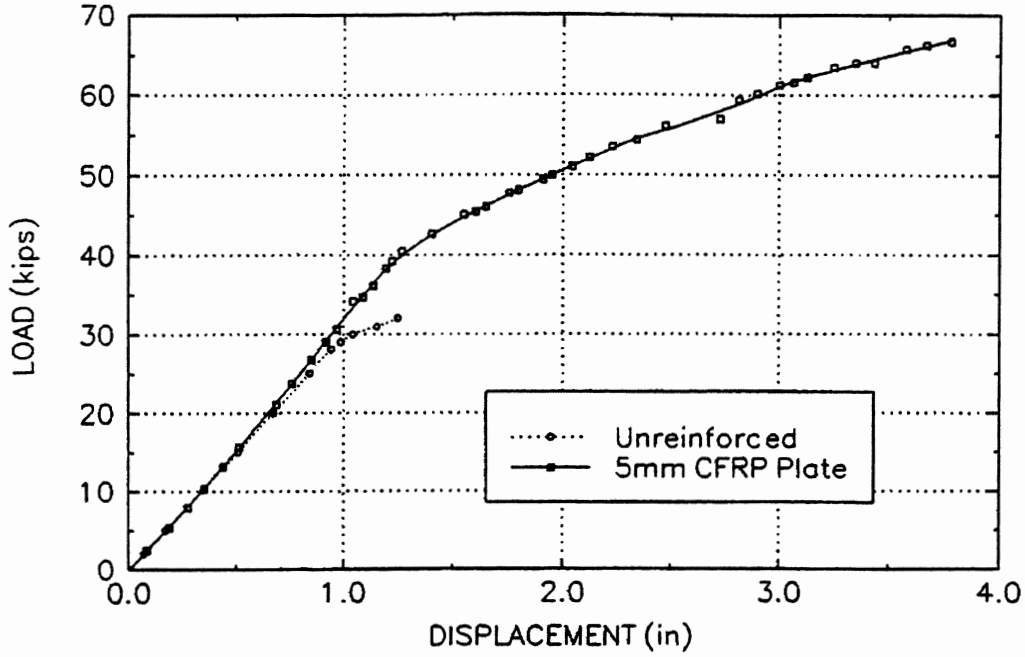

Figure 2-10: Load versus Midspan Deflection for Specimen 6 with 45 ksi yield steel (Sen and Liby 1994)

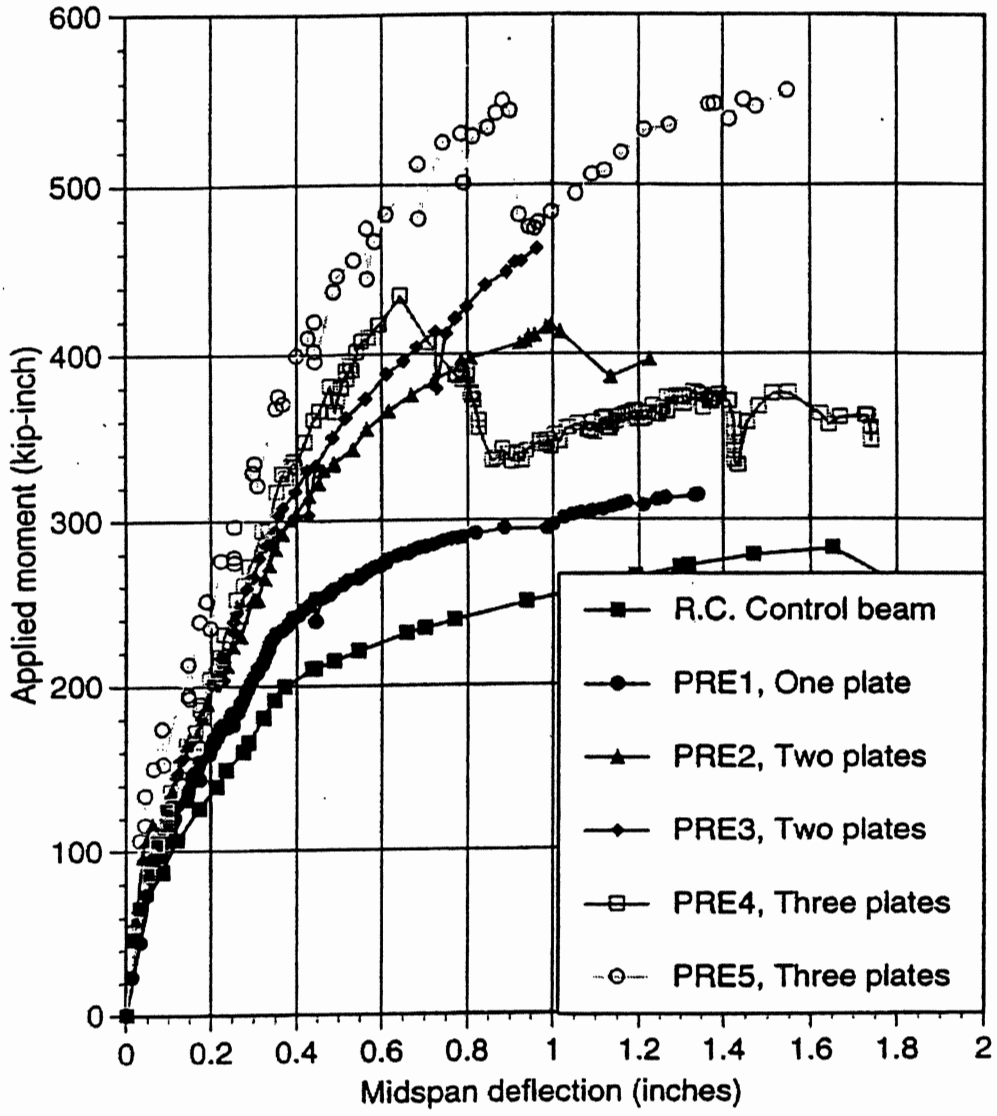

Figure 2-11: Moment Deflection Relationship for Six Specimens (Arockiasamy 1995)

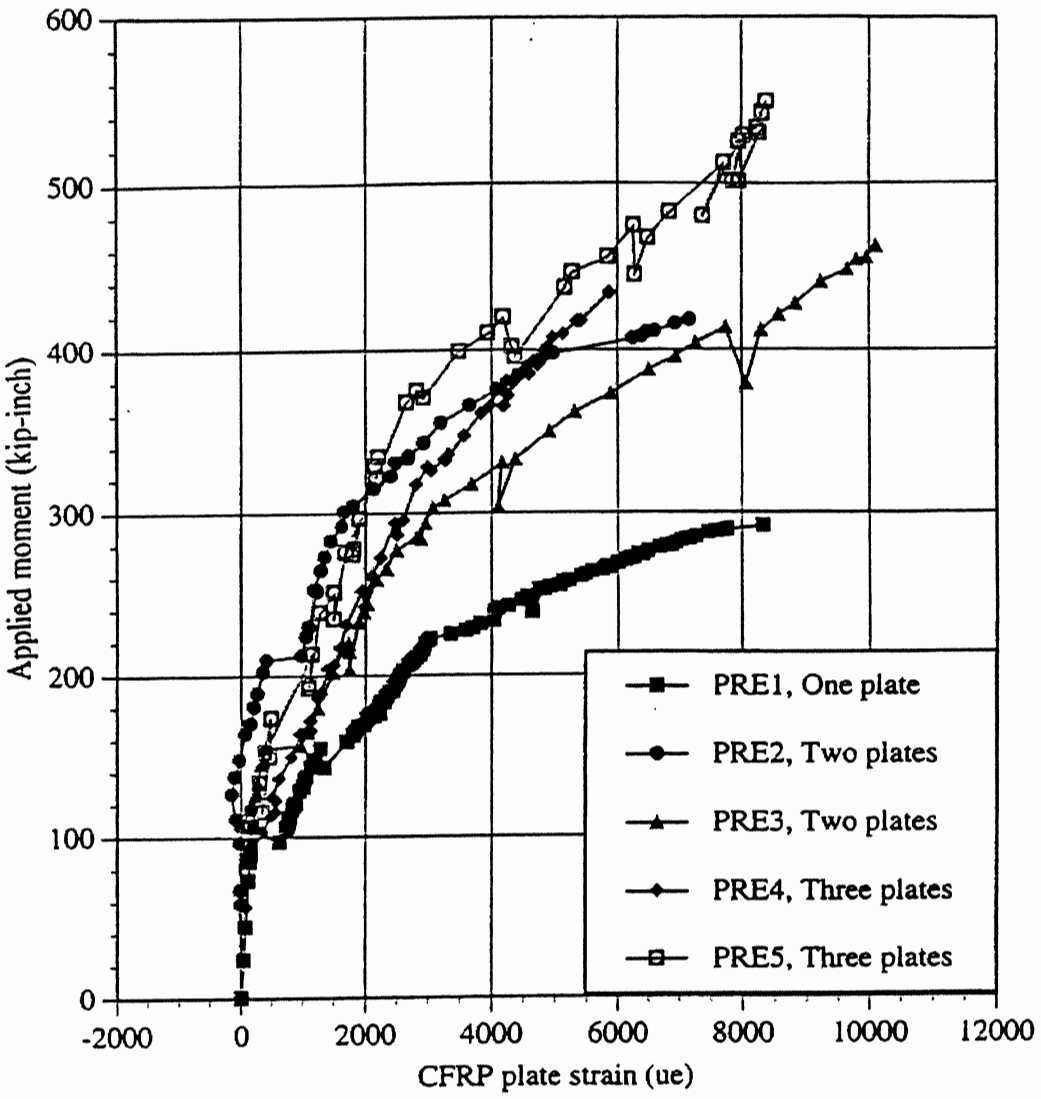

Figure 2-12: Moment versus CFRP Strain for Repaired Specimens (Arockiasamy 1995)

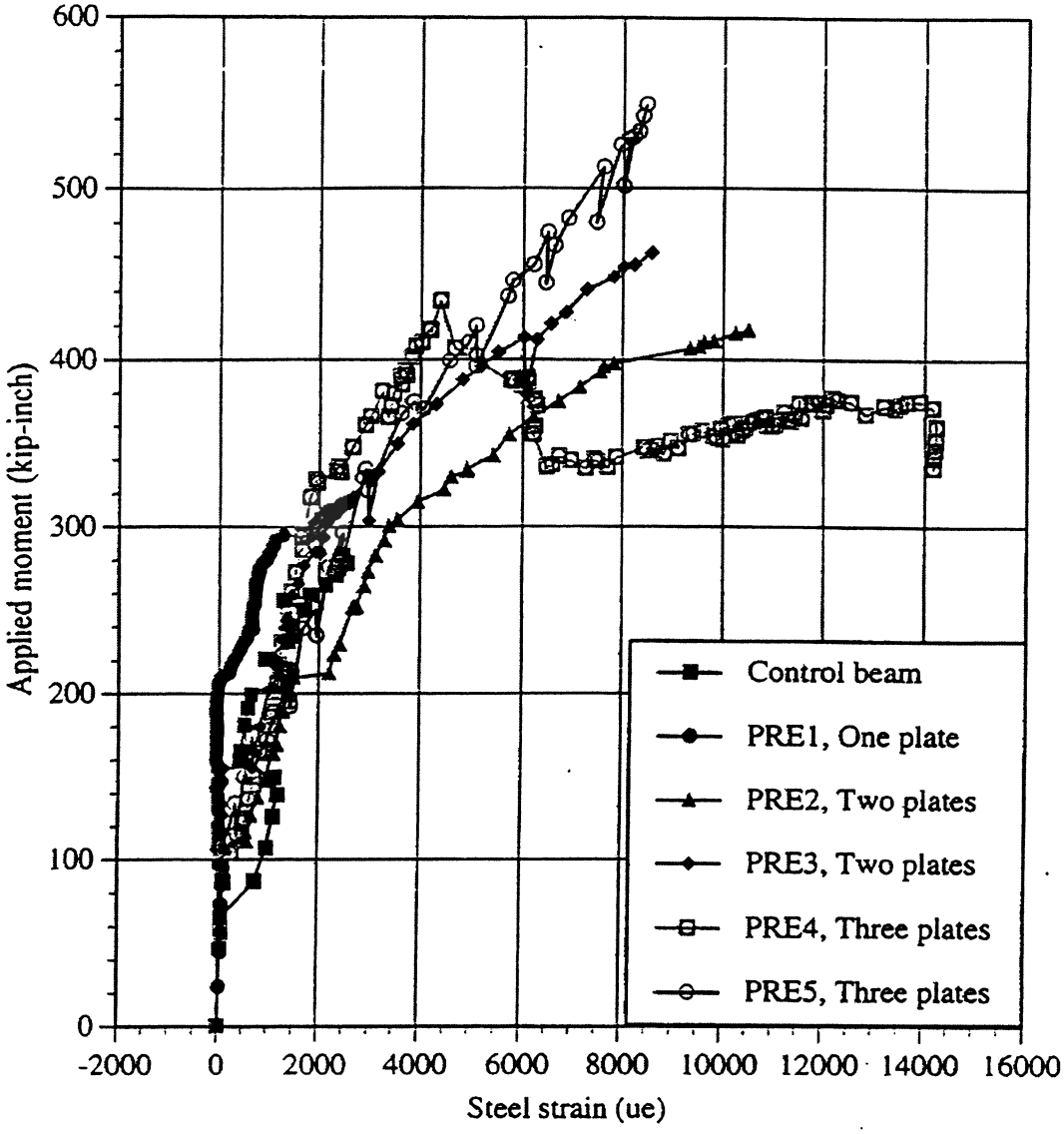

Figure 2-13: Moment versus Reinforcing Bar Strains for Six Specimens (Arockiasamy 1995)

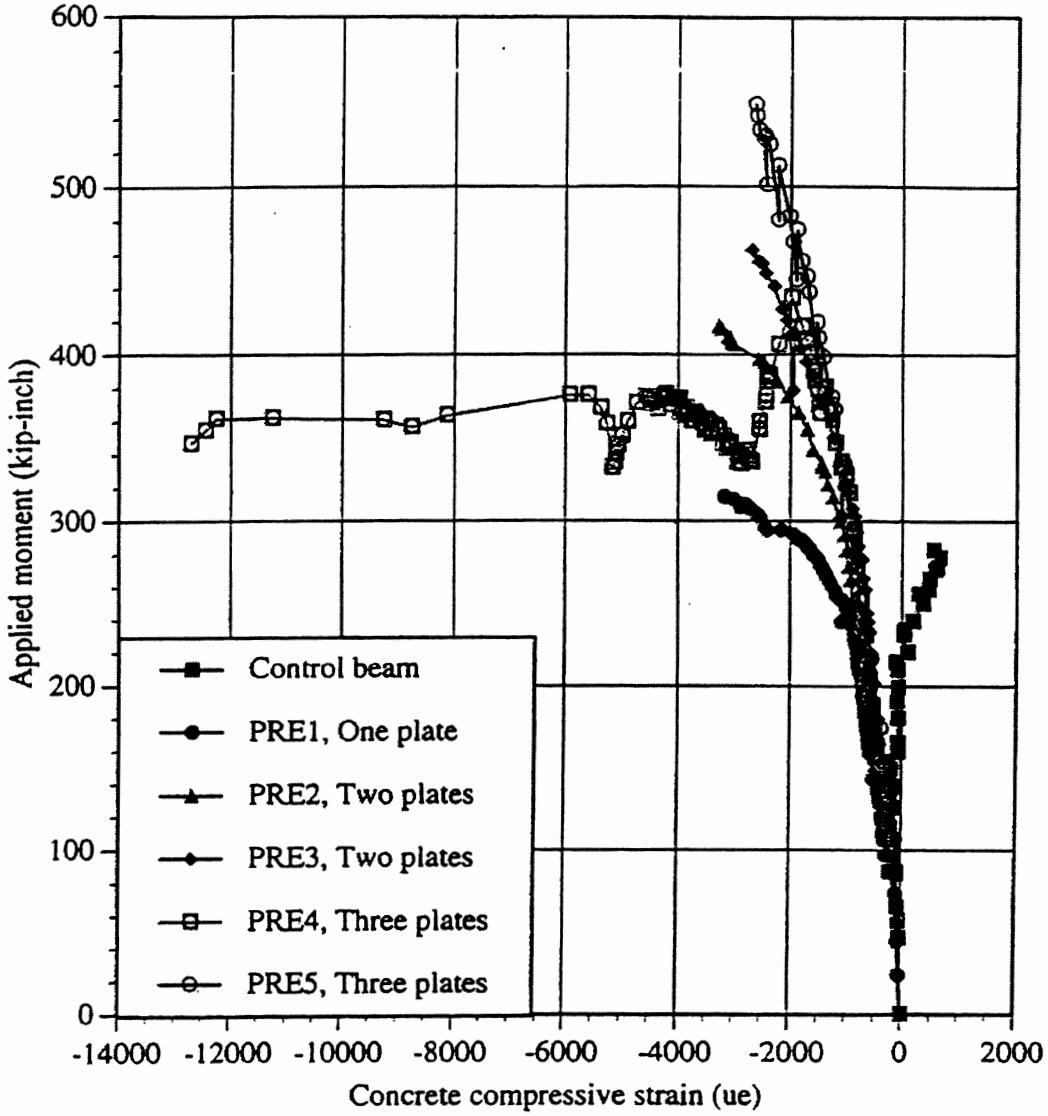

Figure 2-14: Moment versus Concrete Compressive Strain for Six Specimens (Arockiasamy 1995)

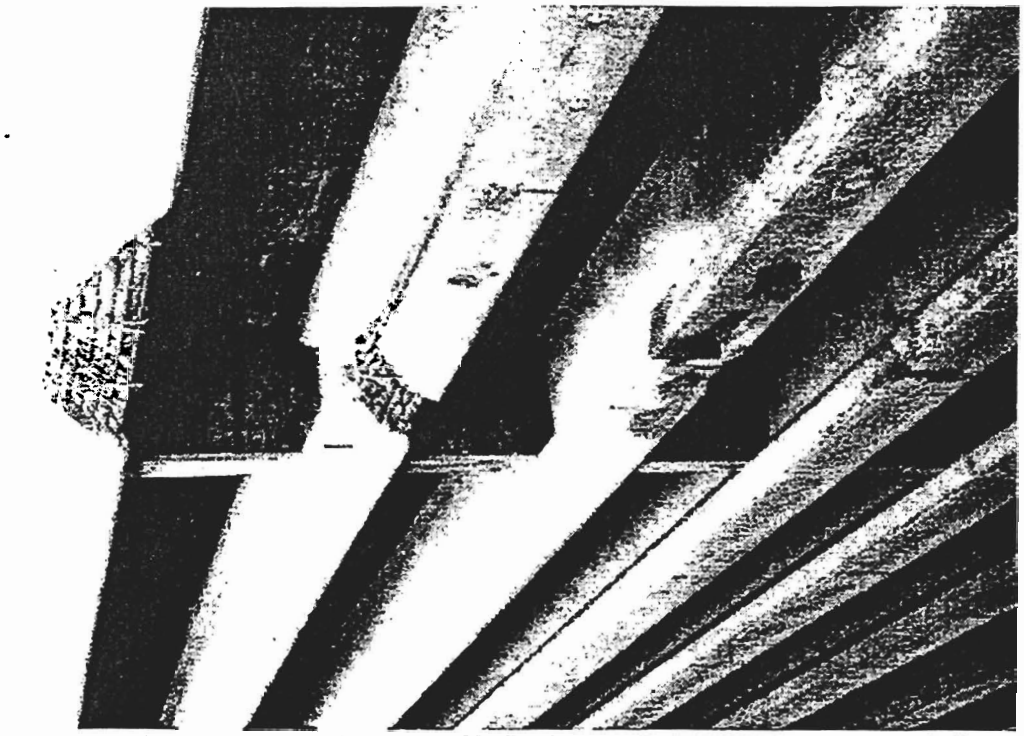

Figure 2-15: Overall Damage to I-680 over CR L34, near Beebeetown, Iowa (Klaiber et al. 1999)

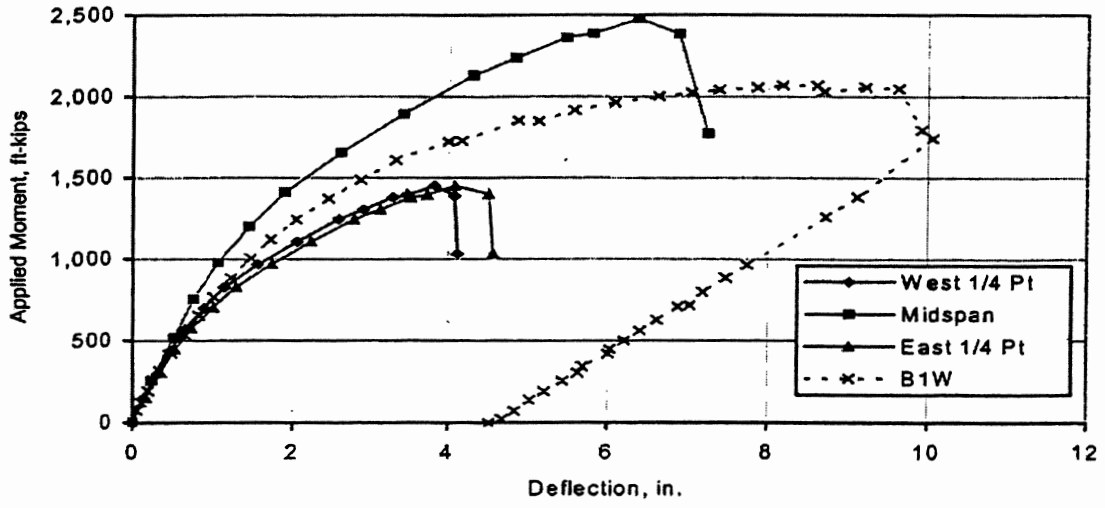

Figure 2-16: Moment Deflection Relationships for Beams 1 and 2 (Klaiber et al. 1999)

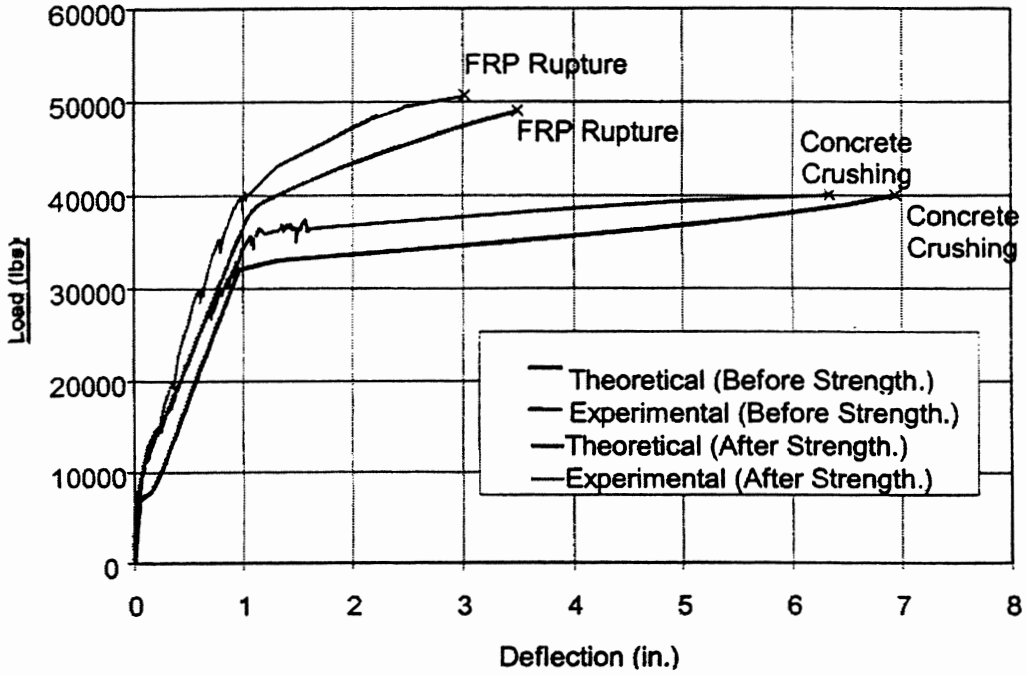

Figure 2-17: Experimental and Theoretical Load Deflection Relationship for Beams 1 and 2 (Mayo et al. 1999)

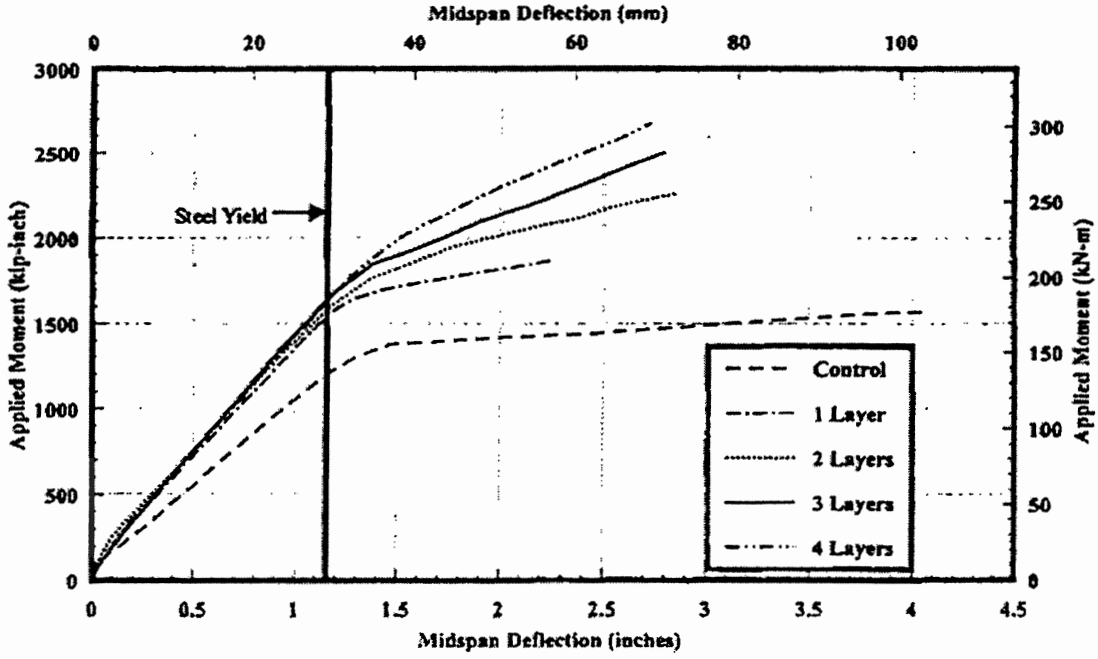

Figure 2-18: Load Deflection Relationship of Fully-Wrapped Beams (Shahawy and Beitelman 1999)

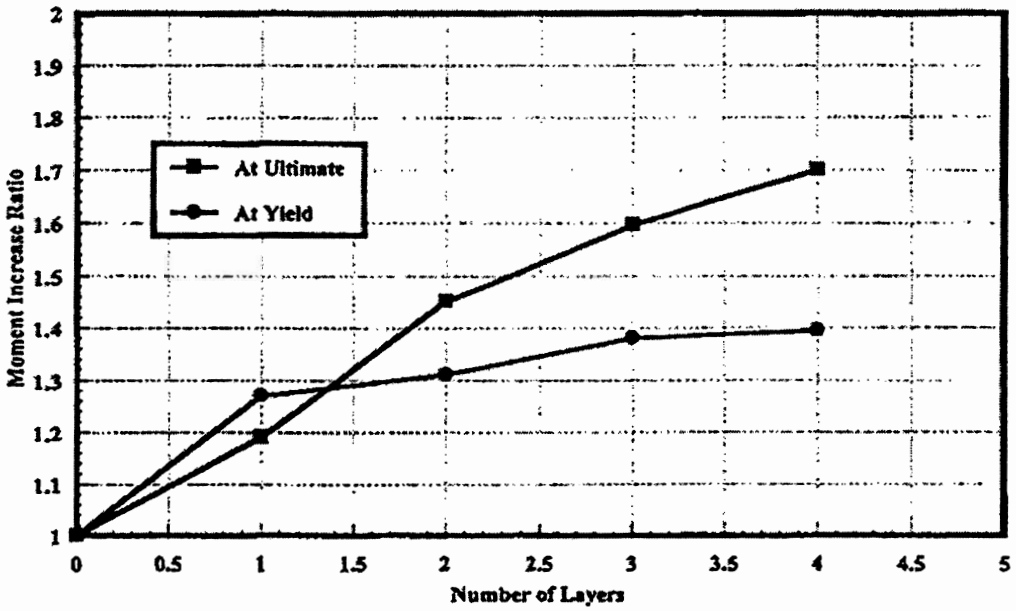

Figure 2-19: Relationship Between Number of FRP Layers to Moment Capacity at Steel Yield and Ultimate (Shahawy and Beitelman 1999)

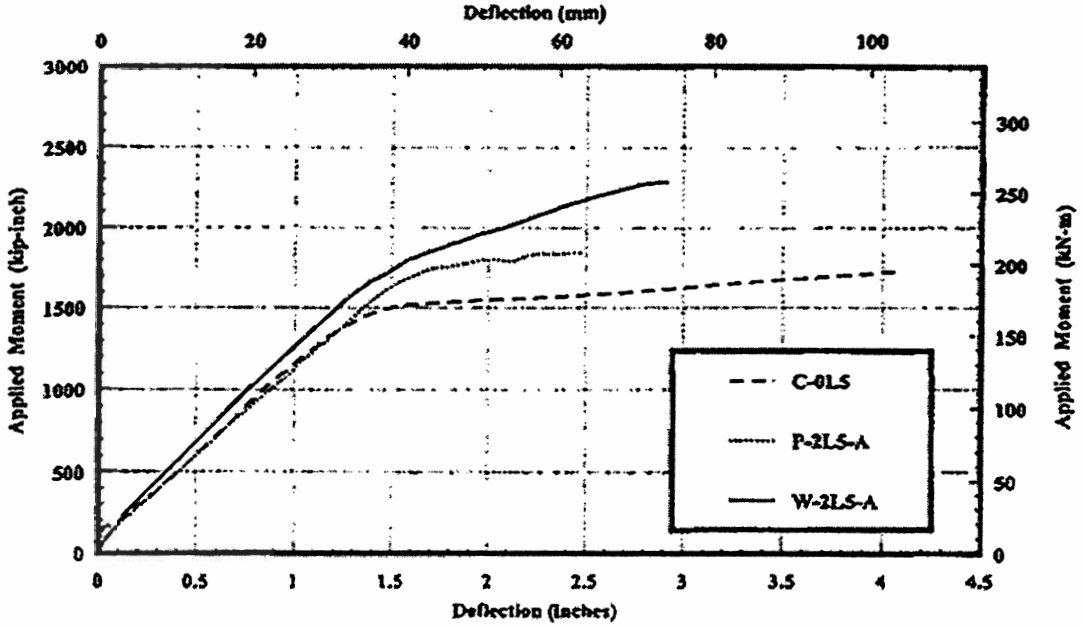

Figure 2-20: Load Deflection Relationships for Fully-Wrapped and Partially-Wrapped Sections with 3 Layers of FRP (Shahawy and Beitelman 1999)

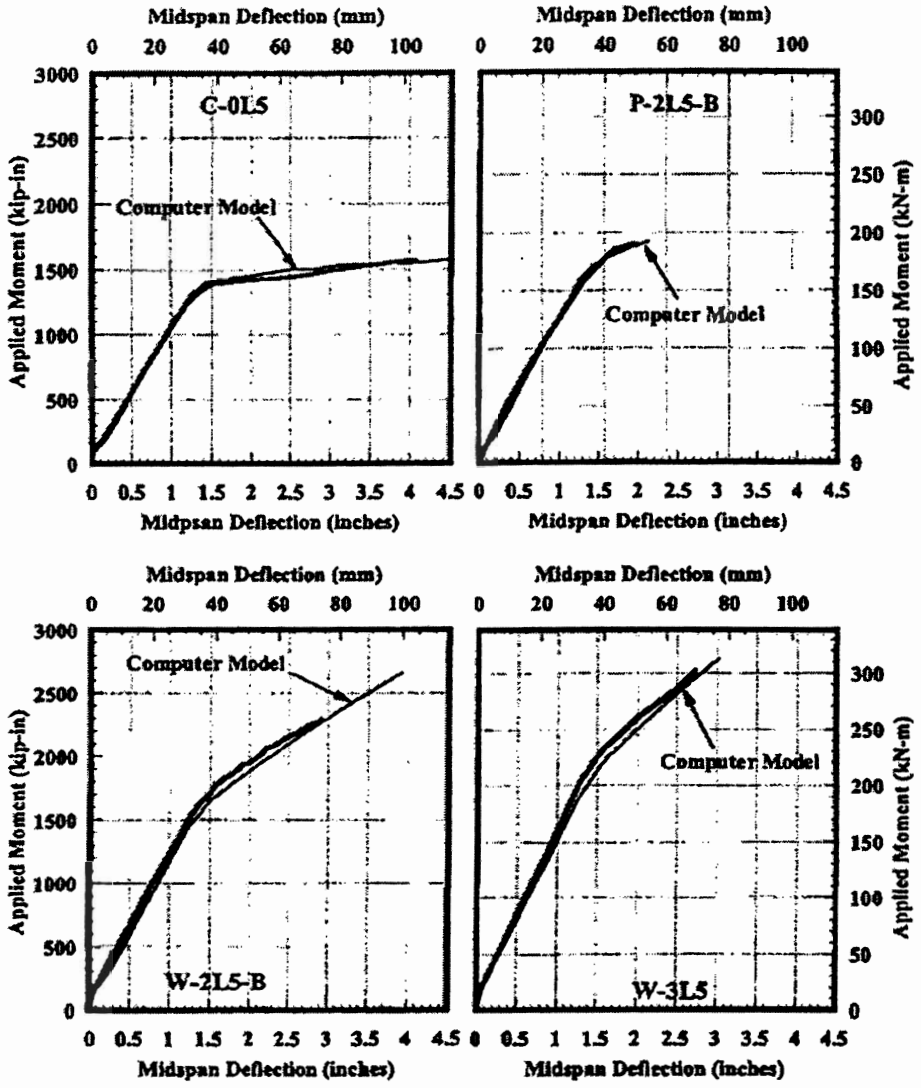

Figure 2-21: Theoretical and Experimental Midspan Deflection for the Analyzed Sections (Shahawy and Beitelman 1999)

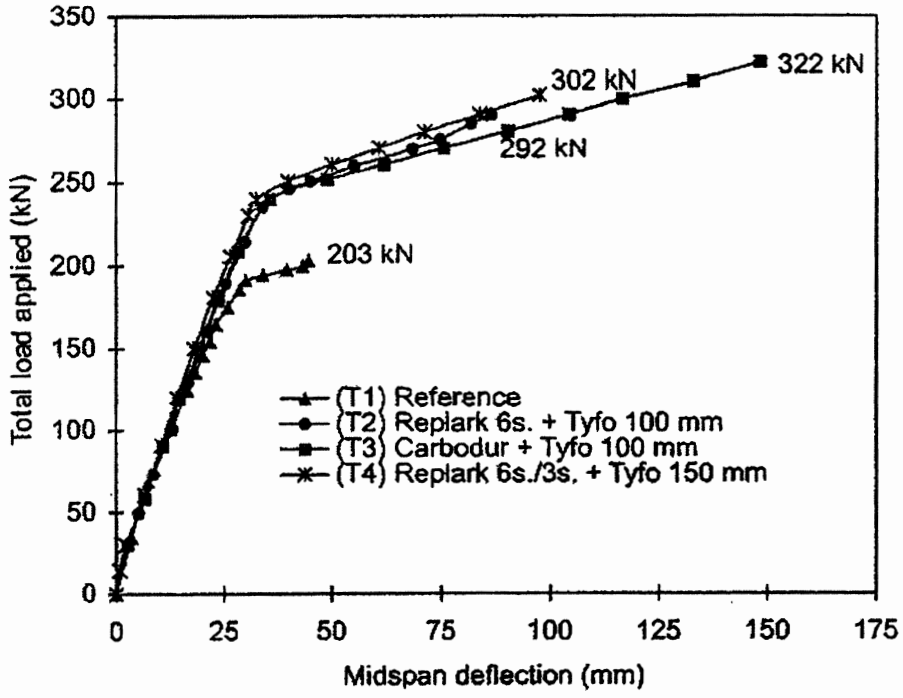

Figure 2-22: Load Deflection Relationship for Beams 1, 2, 3, and 4 (Labossieere et al. 2000)

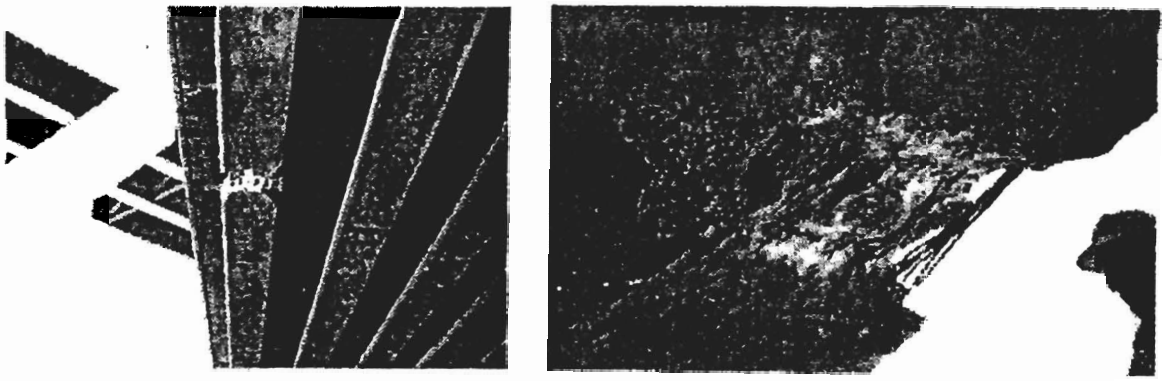

Figure 2-23: Damage to Bridge A10062, St. Louis County, Missouri (Tumialan et al. 2001)

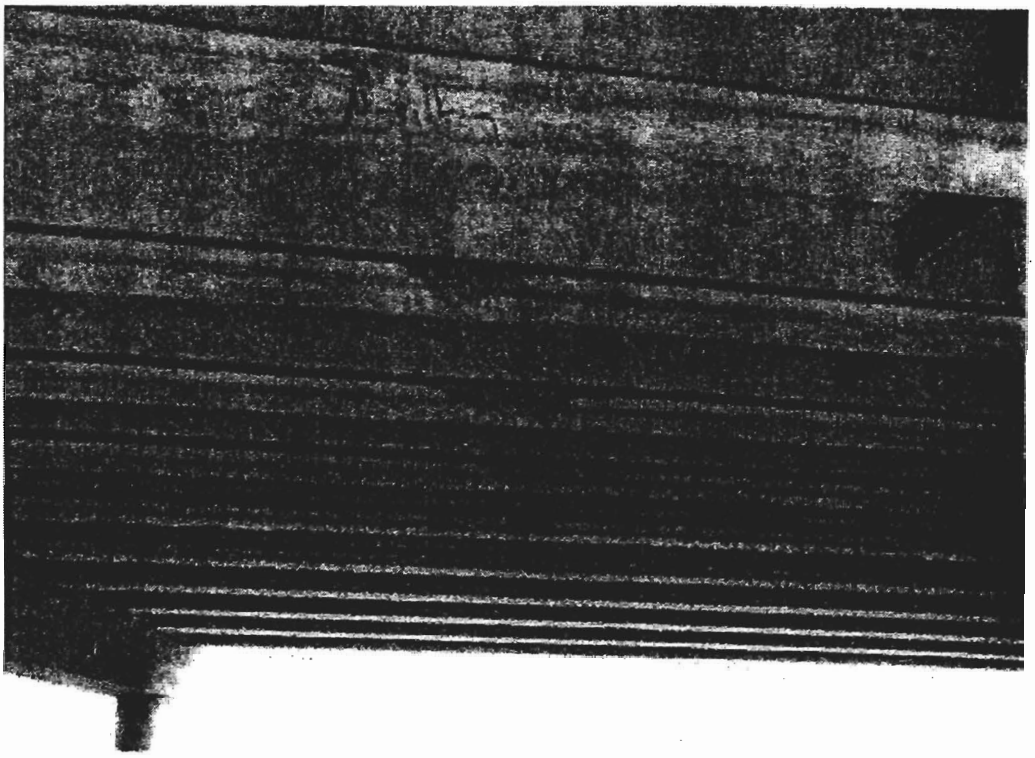

Figure 2-24: Overall Damage to Bridge A4845, Jackson County Missouri (Scheibel et al. 2001)

Figure 2-25: Close-up Damage to Bridge A4845, Jackson County Missouri (Scheibel et al. 2001)

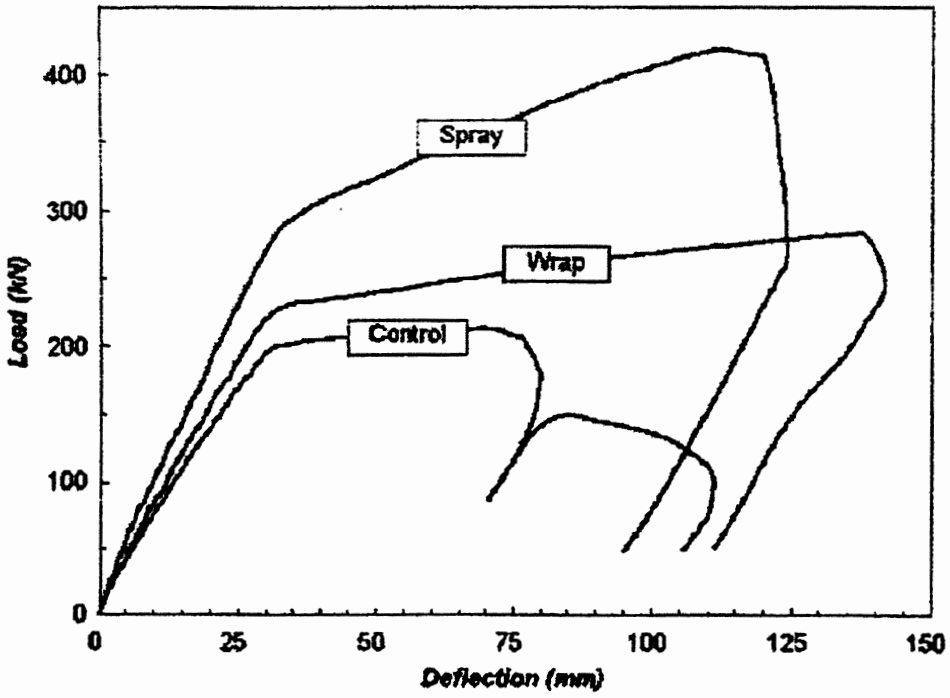

Figure 2-26: Load Midspan Deflection Relationship for the Control, Repaired with Fabric, and Repaired with Spray Specimens (Boyd and Banthia 2001)

CHAPTER 3
DESCRIPTION OF EXPERIMENTAL STUDY

In order to test different repair methods several identical test specimens were needed that were in similar conditions. Six unutilized prestressed concrete type II AASHTO bridge girders were found in a pre-cast yard in south Florida. The 43'-9" girders were thought to be approximately 26 years old and to have the same constituents based on corresponding lengths, strand patterns, and stirrup locations. These six girders provided the testing of four repair methods leaving two girders as control specimens. Two control specimens were needed to establish the moment and shear capacities at an undamaged and damaged condition and therefore verify that sufficient additional moment and shear strength would be attained from the various repair techniques to restore the original moment and shear capacities of the girder.

Before any testing was initiated, a 1'-0" deep by 2'-0" wide slab having an average 6300 psi compressive strength was cast on each of the girders. The slabs were cast in order to counteract the effect of camber due to prestressing and to duplicate in-field conditions of having a deck or dead load acting on the girders. Figure 3-1 shows a detailed cross-section and profile of the girders in the undamaged state.

Description of Test Specimens in Damaged State

All of the test specimens except for the undamaged control specimen were damaged to replicate the most probable conditions that impact of an over-height vehicle would cause. To simulate the impact damage in the laboratory, first a 5'-0" long section of concrete was removed from each side of the bottom flange centered about midspan.

The hatched area in Figure 3-2 represents the removed concrete. After removal of the concrete, four prestressing strands were exposed, two on each side, that were severed representing an 18% loss in capacity. A concrete patch was then applied to the removed concrete area to restore the original gross cross-section. An average 4500 psi concrete compressive strength for all of the girders was determined by testing cores taken from one test specimen. The location of the prestressing hold downs at the third points was determined when the concrete was removed to damage the specimens. Direct tension tests were performed of the removed 7/16" diameter, 250 ksi strands. Figure 3-2 shows the cross-section of the girders at their midspans and ends and gives details as to the damage executed on the girders. Figure 3-3 shows a typical girder in the damaged state before the concrete patch was applied. The results of the direct tensile tests for the removed strands are shown in Figure 3-4. The surfaces of all of the girders were sandblasted on the sides and bottom in order that a good bond surface for the FRP repairs would be produced.

Test Setup for Four Point Bending Tests

All girders were tested in a four point bending configuration where a uniform moment exists between the load points and shear is only present between the load points and reactions. Figure 3-5 shows the load diagram and resulting shear and moment diagrams for the experiments. For the test setup, the load points were 10'-0" apart and the supports were 40'-0" apart centered about the midspan. Figure 3-6 shows the test setup for all test specimens and includes the locations of crack gauges, LVDTs, and load cells. Figures 3-6b and 3-6c show the location of instruments corresponding to the instrumentation lines shown in Figure 3-6a. The girders were loaded statically to failure noting crack locations, sizes, and propagations during loading. The data from the tests

was reduced to determine the moment capacity, shear capacity, and midspan deflection of the undamaged and damaged control specimens to be used for comparison and to later verify if the FRP repair of the damaged girders had reached the required capacities. The capacities would also provide the necessary values to be utilized in the design. The supports for Test Specimen 4 were moved out an additional 6" on both ends due to the termination of the FRP laminates occurring at the location of the supports for Tests 1, 2, 3, 5 and 6.

Repair Designs and Design Properties

The company that was to perform the repair was responsible for the design calculations. No method or procedure, factors of safety, assumption for failure mode, or fiber or resin material type was specified for the repair designs by the FDOT. Appendix A contains the repair designs for Test Specimens 3, 4 and 5.

A comparison of the repair design properties and the corresponding description of the repair for Test Specimens 3, 4, 5 and 6 is shown in Table 3-1. The design properties in Table 3-1 for the repairs of Test Specimens 3, 4, and 6 are from data sheets provided by the manufacturers through direct tensile coupon tests. ASTM D3039 (2000) gives standards for determining tensile properties of polymer matrix composite materials. The standards state that the extensometer gage length should be in the range of 0.5 to 2.0 inches. An extensometer gauge length of 0.5" was used for the direct tensile coupon test data for Test Specimen 3. An extensometer gauge length of 2" was used for the direct tensile coupon test data for Test Specimen 4. The design properties in Table 3-1 for the repairs of Test Specimen 5 were taken from previous tensile coupon tests of representative properties in which an extensometer gauge length of approximately 2

inches was utilized (Boyd 2000). For the Test Specimen 6 laminate properties, an average of 0.12" elongation over an 8" long specimen was reported.

Repair Application Procedures

For Test 3, employees of RJWatson performed the installation procedure in which a wet lay-up procedure was implemented. First a layer of epoxy was applied to the tension face of the girder where the FRP strengthening system would be applied. After the epoxy became tacky, one layer of pre-cut fabric was placed on the tension face of the girder and rolled out to remove voids and prevent wrinkling of the fabric. Epoxy was then applied to the exposed side of the fabric. When the exposed epoxy became tacky the next layer of FRP was applied. This procedure was followed for each successive layer of FRP applied. Figure 3-7 shows the installed repair for Test Specimen 3 in which the fabric direction is oriented parallel to the longitudinal axis of the member. It should be noted that all four layers are terminated at the same location.

For Test 4, the installation procedure was performed by Air Logistics in which pre-cut fabric sizes of pre-impregnated resin were applied to the tension face with additional stirrups of fabric placed to resist peeling of the fabric. A primer was first applied to the tension side of the girder. When the primer became tacky, the fabric was unrolled directly onto the surface. After two of the four layers were applied, water was sprayed over the fabric with a garden hose activating the resin. The remaining two layers were then applied and water was again sprayed over the fabric to activate the resin. As each layer was applied, it was necessary to stretch the fabric in order to reduce air voids and wrinkling of the fabric. After all of the layers were applied to the tension face, two layers of bi-directional fabric were applied as stirrups following the above procedure with two bolts placed through the ends into the web. Figure 3-8 shows the installed repair for Test

Specimen 4 in which the fabric direction is oriented parallel to the longitudinal axis of the member and the layers are terminated at varying locations. In addition to longitudinal reinforcement, a two-ply stirrup was installed just within the termination of the second shortest layer to enhance the behavior of the FRP strengthening system. The stirrup fabric was oriented at 0° and 90° as represented in Figure3-8 by the hatched area.

Magnum Venus Products (MVP) and graduate students from the University of Florida performed the installation for Test 5. Figure 3-9 shows the equipment used for the spray application procedure. The fibers in a roving form are routed into a chopper mechanism attached to the spray gun. A detailed view of the gun is shown in Figure 3-10. The chopping mechanism has two rollers with adjustable blades to vary fiber lengths as the fiber roving passes through the rollers. The final FRP composite is comprised of a resin, catalyst, and fibers that are fed separately into the spray gun and meet simultaneously beyond the gun either in mid-air or on the application surface shown in Figure 3-11. After an application of spraying was complete to an average thickness of 5 mils ,ribbed metal rollers were used to compact the fibers, resin, and catalyst onto the surface, remove air voids, and assist in bonding the material to the surface and underlying layers. The above procedure was followed making each pass in which about 5 mils was sprayed onto the surface and rolled out until the desired thickness was reached. The repair was originally designed with fibers approximately 1.9 inches in length and its representative properties with a laminate thickness of 0.35 inches. While attempting the installation with the 1.9 inch fiber length, it was determined that it would be necessary to reduce the fiber lengths. Since it was known from previous research that reducing fiber length causes a reduction in composite strength, the repair was redesigned (Boyd 2000).

A new fiber length of 1.25 inches was utilized with a desired thickness of 0.50 inches to produce an equivalent strength as specified in the original design. Figure 3-12 shows the installed repair for Test Specimen 5 in which the multidirectional or randomly oriented fibers were applied to the entire bottom of the girder and up 6" on both sides of the bottom flange for 20'-0" centered about midspan. In addition a 2-0" wide stirrup of randomly oriented fibers was applied up to the bottom of the top flange at the termination of the repair at each end of the girder to enhance the shear strength of the repair and ensure a good bond of the FRP strengthening system.

Difficulties were encountered during the two-day application of the spray FRP. The spray application procedure had not been used in this type of application previously where the spray had to be projected up onto the tension face of the beam simulating in-field conditions with multiple layers having to be applied to reach the desired thickness. In order to apply another layer, the underlying layer must be set such that the additional layer does not pull the underlying layer off due to its self-weight. The FRP thickness measurement device was incapable of piercing through the hardened underlying layers to get accurate measurement of applied thickness so it was not known during or after the application exactly what thickness was actually applied. Therefore, FRP cores were taken from the specimen after loading. Figure 3-13 shows where samples were taken from the cross-section and profile of the specimen.

A total of 73 samples were taken from the sides and bottom of the test specimen to evaluate if the desired thickness was reached. The side samples are defined as those taken from the web, and the angled and vertical side of the flange (numbers 1 through 5 and 9 through 13) as shown in Figure 3-13. The 73 samples yielded an average thickness

of 0.479" with a standard deviation of 0.196". Of the 21 samples taken from the tension face of the girder none had a thickness equal to the desired thickness of 0.5". The maximum and minimum thicknesses taken from the tension face of the girder were 0.368" and 0.139", respectively with an average thickness of 0.266" and a standard deviation of 0.065". A total of 52 samples, 26 per side, were taken from the sides of the test specimen with an average thickness of 0.565" with a standard deviation of 0.161". There is a significant difference in thickness between the two sides of the specimen from the two days of spraying in which only one side of the beam was repaired each day. When the sides were evaluated by day, the results of the first day showed an average thickness of 0.506" with a standard deviation of 0.102", and the results of the second day had an average thickness of 0.625" with a standard deviation of 0.188".

The average thickness, as previously stated, for all of the 73 specimens was 0.479". This was reasonably close to the desired thickness of 0.50", although it is apparent from the bottom thickness measurements that the desired 0.50" was not reached during the application of the FRP to the tension face of the girder.

The application procedure for Test Specimen 6 was performed by Edge Composite employees, in which a wet lay-up procedure was implemented. All surface voids, in which any FRP strengthening system was to be applied, were filled with a West System Filler Epoxy containing micro-fibers to form a flat surface for a maximum bond. Then a layer of resin was applied to the tension face of the beam in which the fabric would be applied. When the resin became tacky the first layer of pre-cut fabric was applied to the girder. A plastic trowel or scraper was used to remove any excess resin and to obtain the desired constant thickness of resin between the layers. Each layer of fabric was rolled out

to remove voids and prevent wrinkling of the fabric. Resin was then applied to the exposed side of the first layer of fabric. The procedure described above was followed for the two successive layers. After the three layers were applied to the tension face, a two ply stirrup was applied at the end of the longitudinal fabric to provide resistance against peeling of the longitudinal fabric. The stirrups were applied to the girder using the above described procedure. Figure 3-13 shows the installed repair for Test Specimen 6 in which the fabric direction is oriented parallel to the longitudinal axis of the member and the layers are terminated at the same location. In addition to the longitudinal reinforcement, a two-ply stirrup was installed just within the termination of the fabric to enhance the behavior of the FRP strengthening system. The stirrup fabric was unidirectional and oriented perpendicular to the length of the girder as represented in Figure3-14 by the striped area.

Table 3-1: Comparison of Design Repairs for Test Specimens 3, 4, 5, and 6

Test Specimen	3	4	5	6
Fiber Material and Description	Carbon Uni-directional with Aramid Cross Fibers	Carbon Uni-directional with Cross Fibers	E-Glass Multi-directional Fibers	Carbon Uni-directional Fibers
Resin Material	Epoxy	Polyurethane	Vinyl Ester	Epoxy
Elongation at Failure	1.21%	1.05%	1.43%	1.50%
Tensile Modulus (ksi)	10500	11000	1522	10100
Ultimate Tensile Strength (ksi)	127	115	15.08	150
Total Laminate Thickness from Data Sheets (in.)	0.160	0.124	0.500	0.069
Total Average Laminate Thickness Measured (in.)	0.276	0.236	0.138 to 0.386	0.169
Number of Laminates	4	4	1	3
Total Length of Laminates (ft.)	20 20 20 20	40 32 24 16	20	20 20 20
Width of Laminates (in.)	16	12	18	18
Vertical FRP Anchorage Description	None	2 Plies CFRP Oriented at 0 and 90 Degrees, 12 ft from Midspan	Sprayed GFRP ~ 1/2" Thick 2 ft Wide up to Bottom Flange	2 Plies CFRP at 0 Degrees up to Bottom Flange

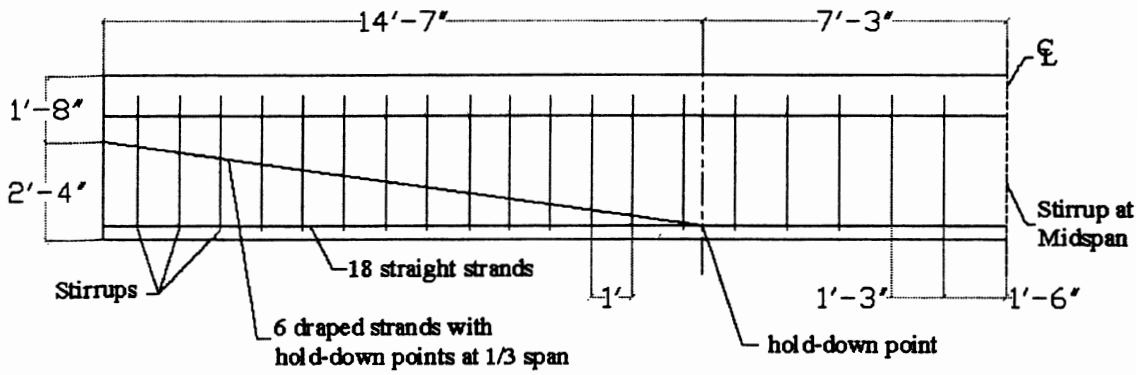

a) Typical Profile of Test Specimens in Undamaged State

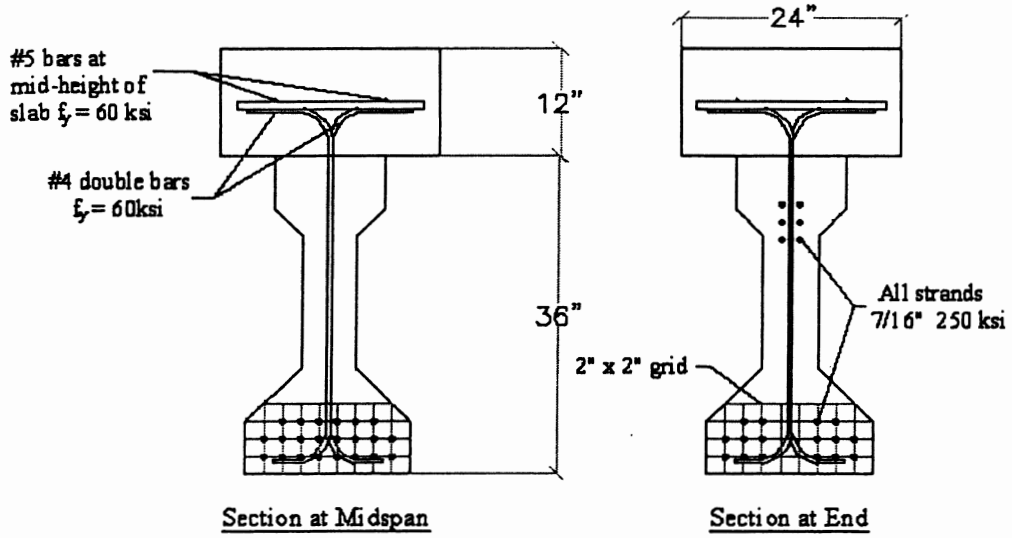

b) Typical Cross-Sections of Test Specimens in Undamaged State

Figure 3-1: Typical Profile and Cross-Sections of Test Specimens in Undamaged State

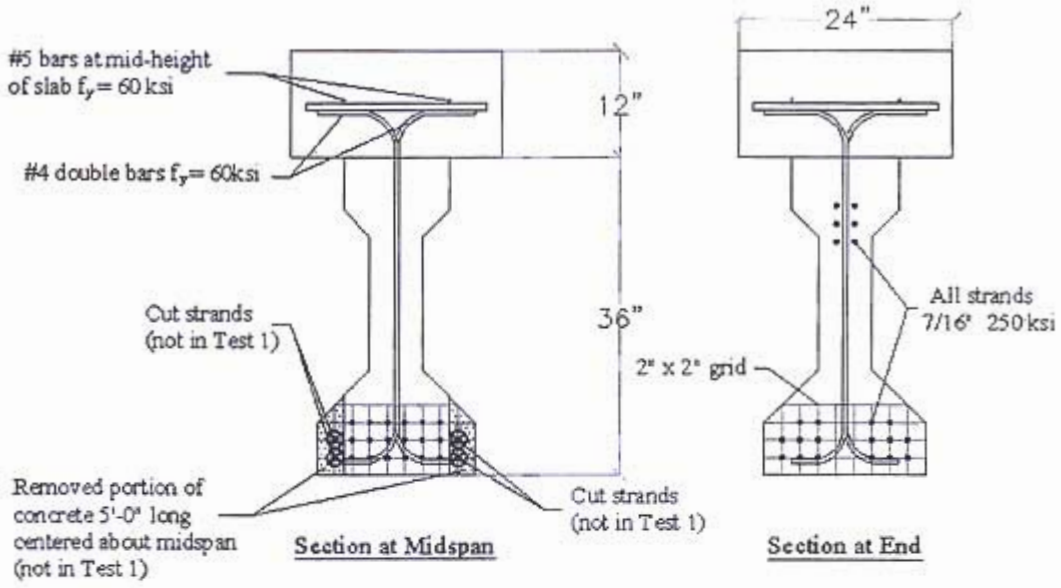

Figure 3-2: Typical Cross-Section Details for Test Specimens 2, 3, 4, 5, and 6

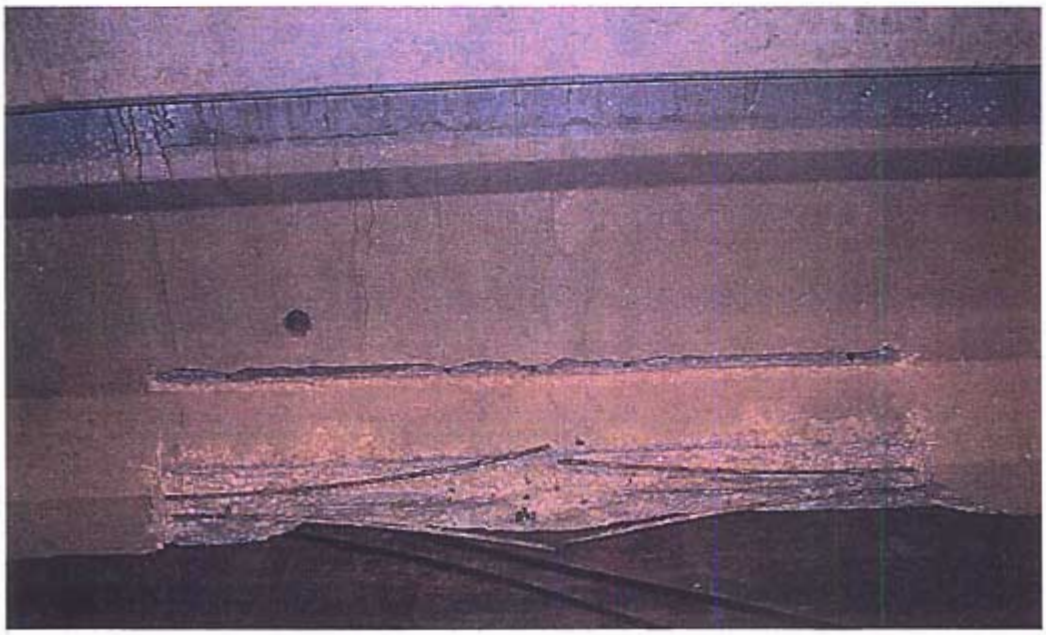

Figure 3-3: Typical Damage for Test Specimens 2, 3, 4, 5, and 6 Showing Removed Concrete and Two Severed Prestressing Strands

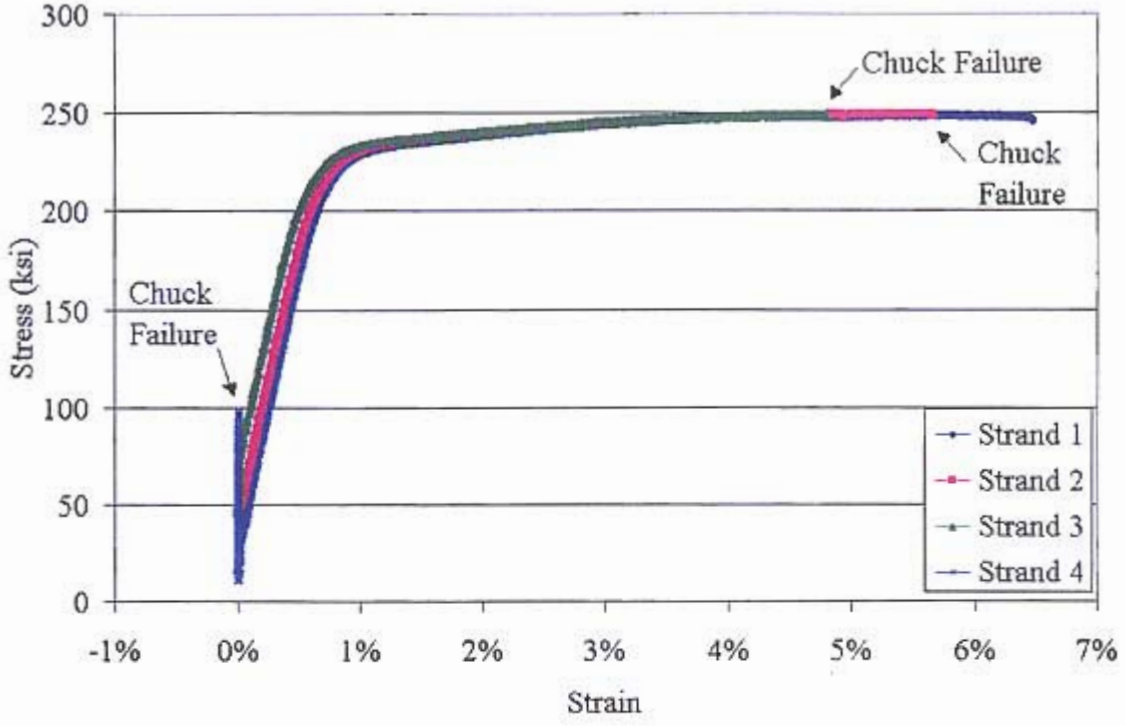

Figure 3-4: Stress-Strain Curves for Removed Strands from Test Specimen 2

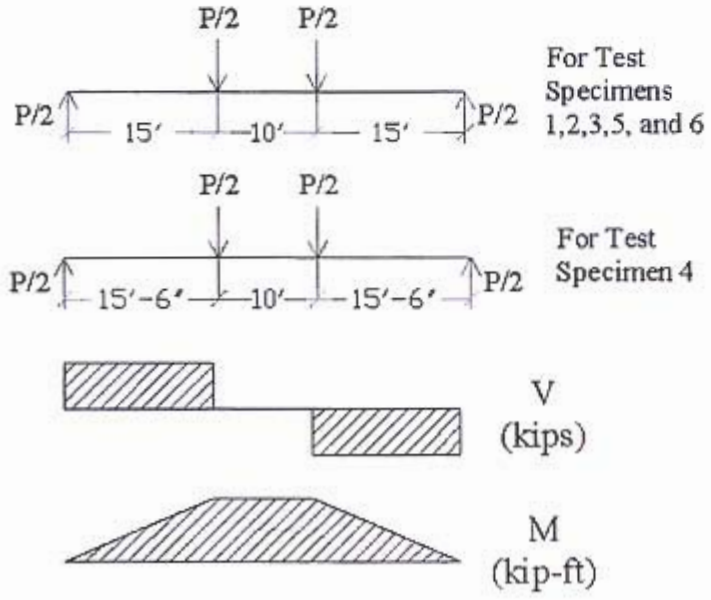

Figure 3-5: Load, Shear, and Moment Diagrams for All Four-Point Bending Tests

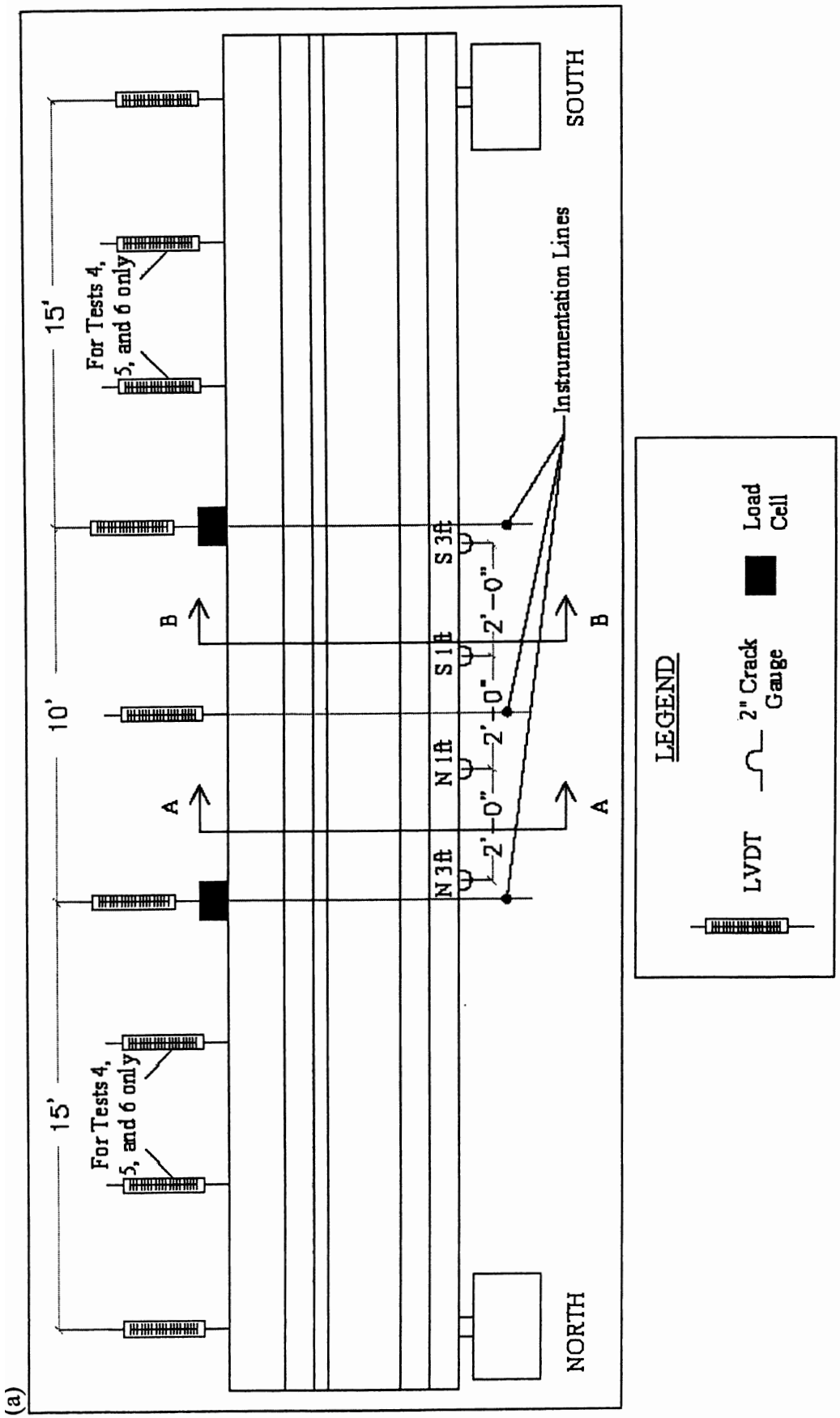

Figure 3-6: Typical Instrumentation for Four-Point Bending Tests a)Typical Instrumentation Layout for Test Specimens 1, 2, 3, 4, 5, 6

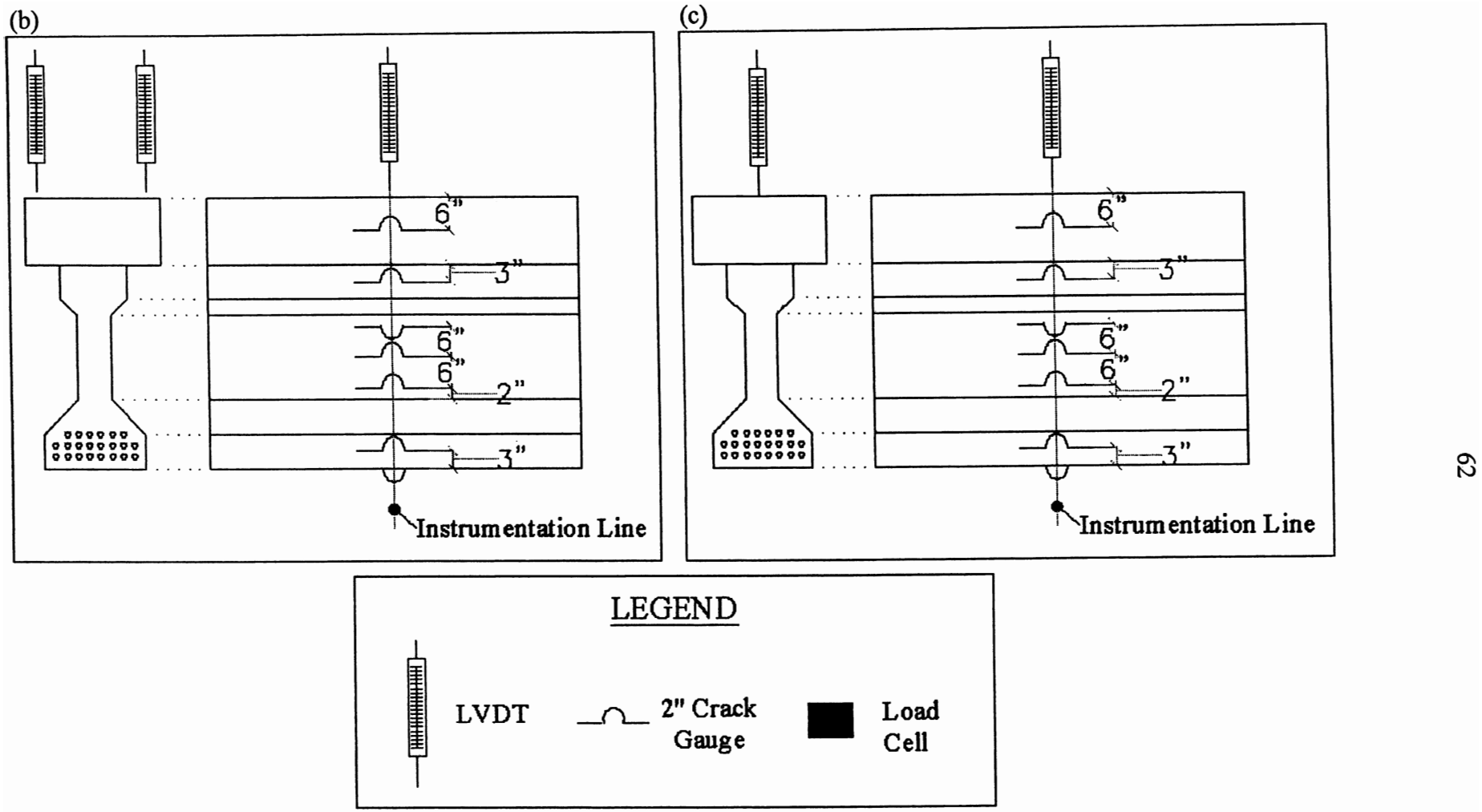

Figure 3-6(continued): Typical Instrumentation for Four-Point Bending Tests b)Typical Instrumentation Locations for Section A-A Cross-Section in Figure 3-6a; c) Typical Instrumentation Locations for Section B-B Cross-Section in Figure 3-6a

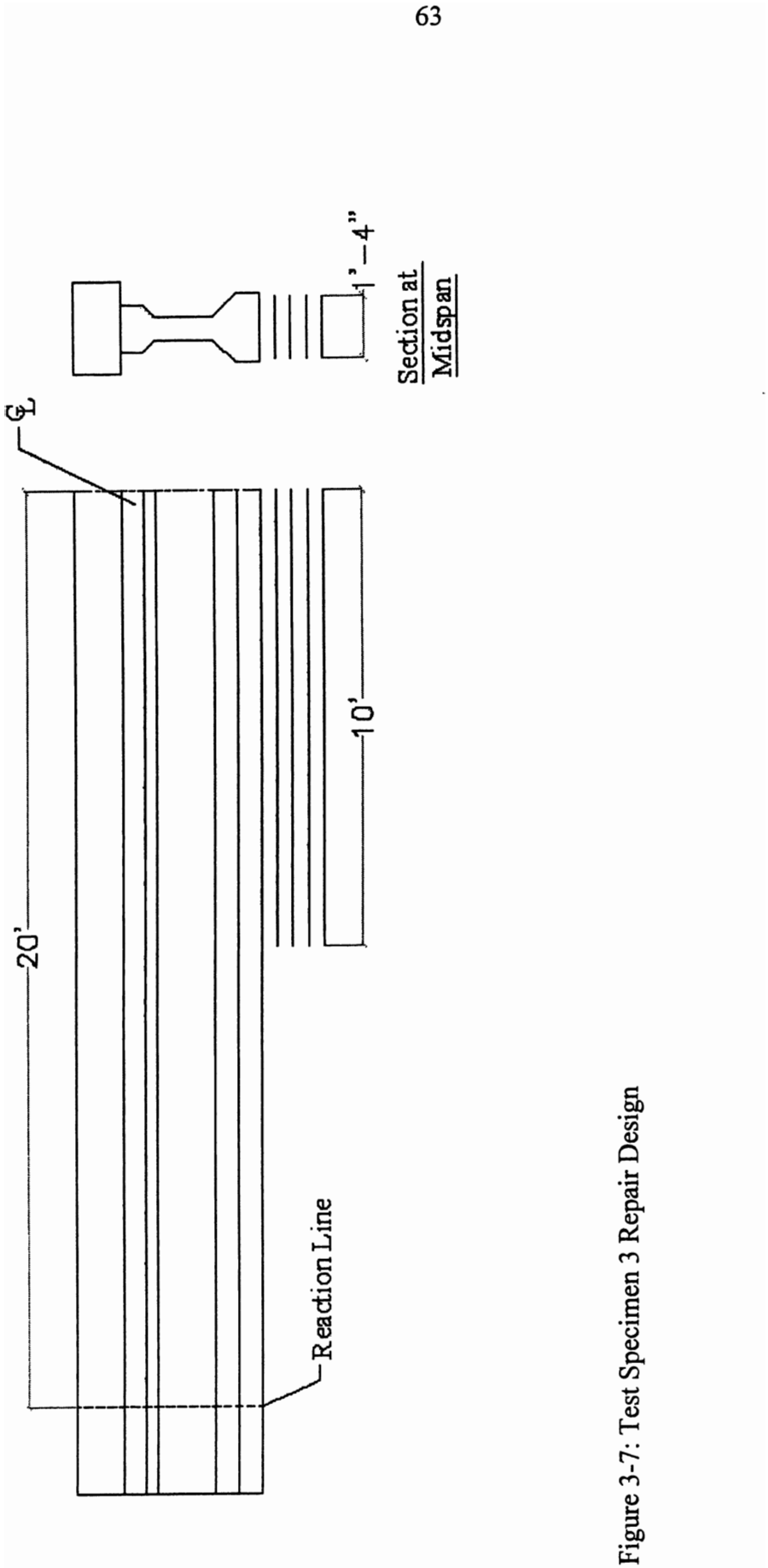

Figure 3-7: Test Specimen 3 Repair Design

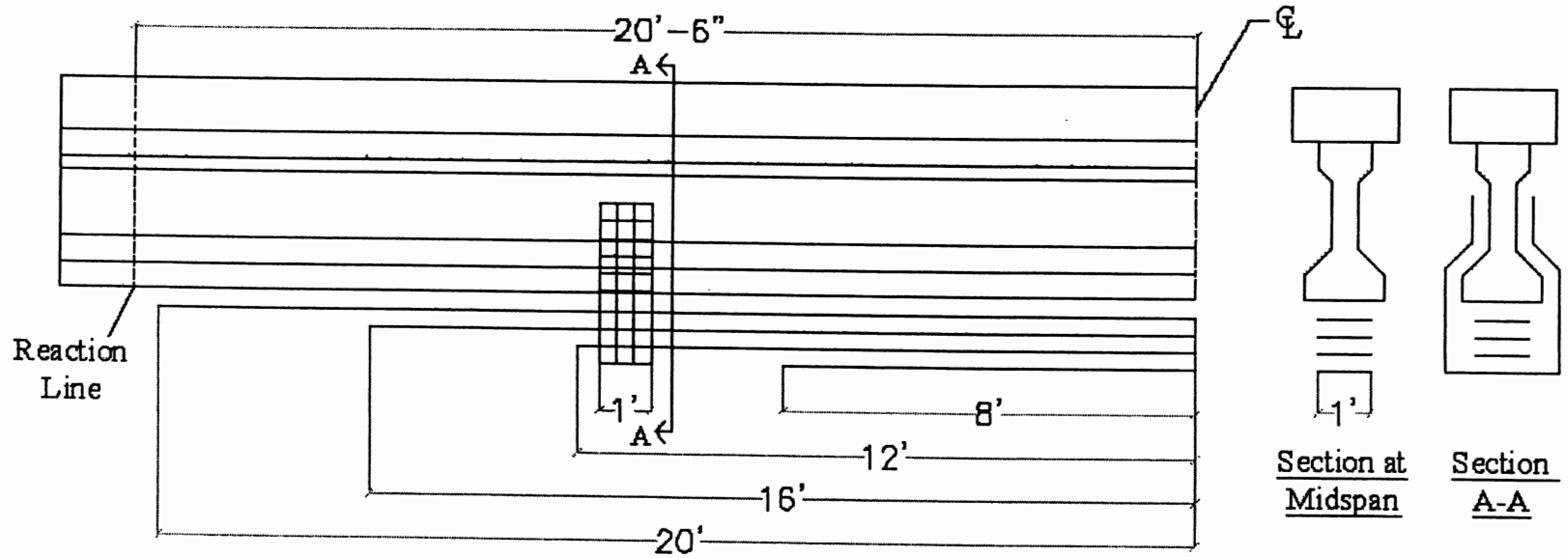

Figure 3-8: Test Specimen 4 Repair Design

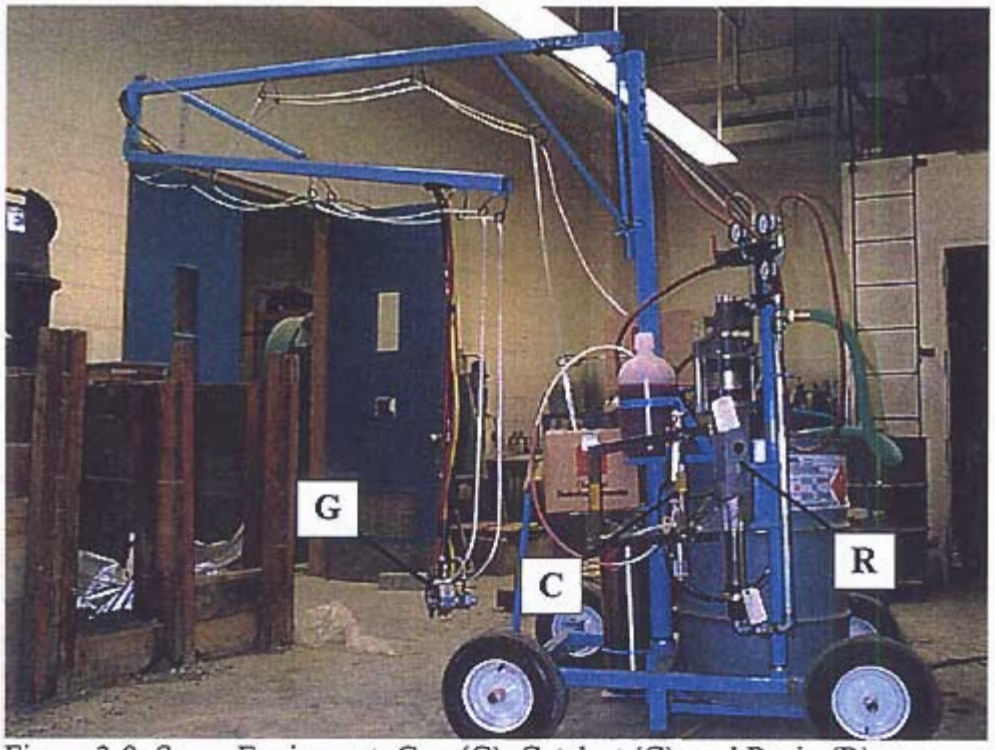

Figure 3-9: Spray Equipment: Gun (G), Catalyst (C), and Resin (R)

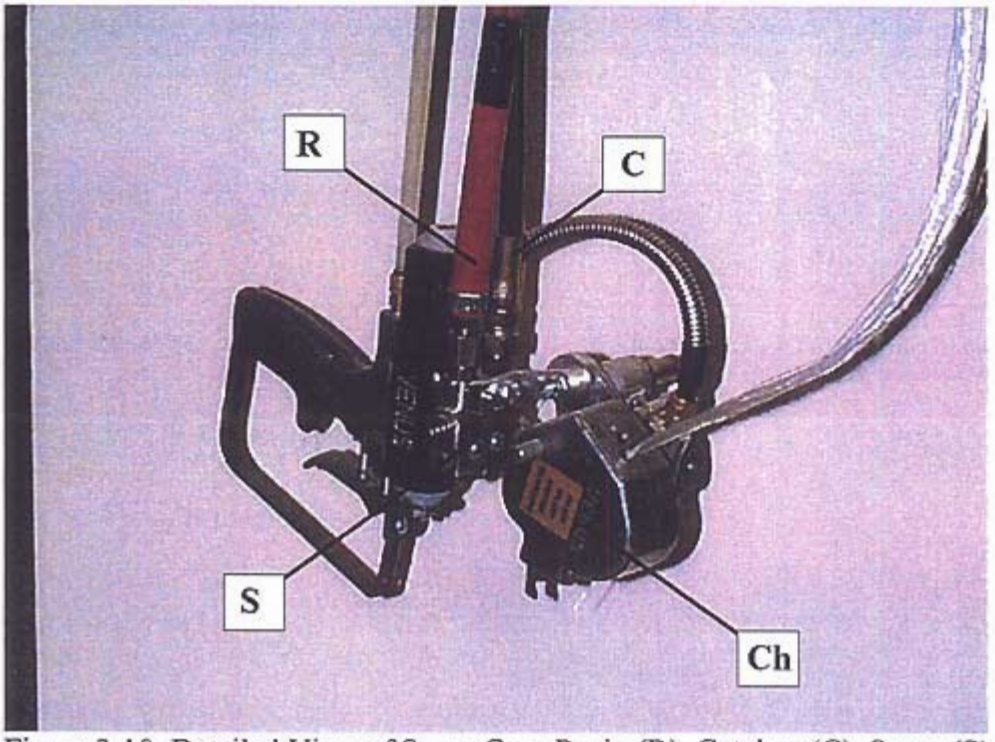

Figure 3-10: Detailed View of Spray Gun: Resin (R), Catalyst (C), Spray (S), and Chopper (Ch)

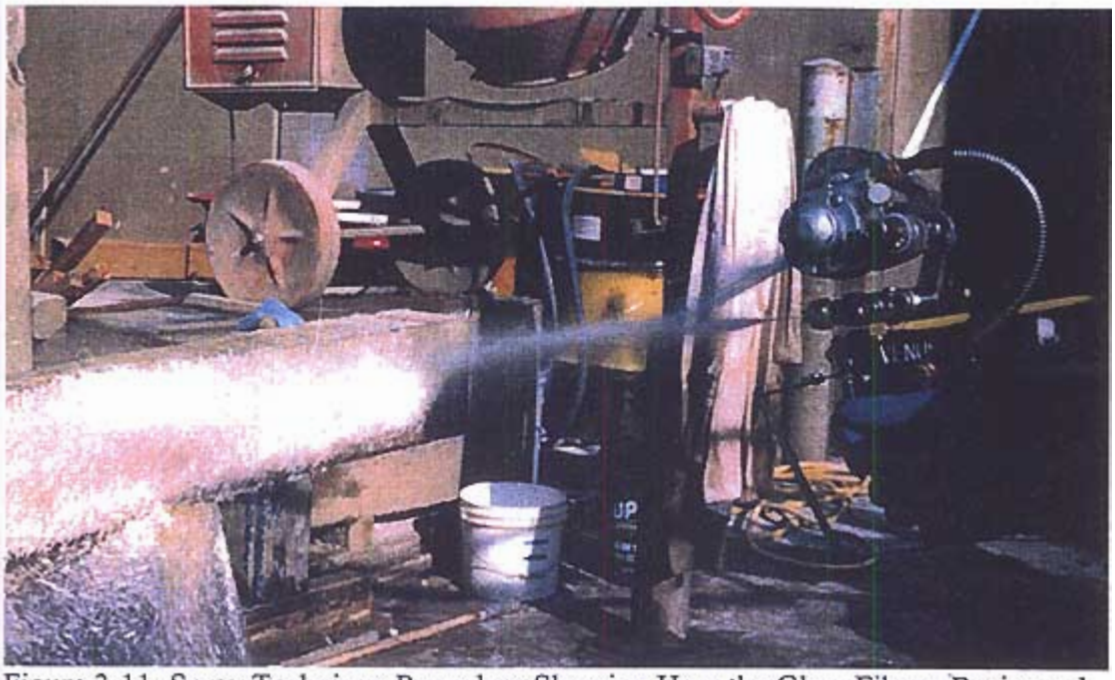

Figure 3-11: Spray Technique Procedure Showing How the Glass Fibers, Resin, and Catalyst for Resin are Combined in Mid-Air

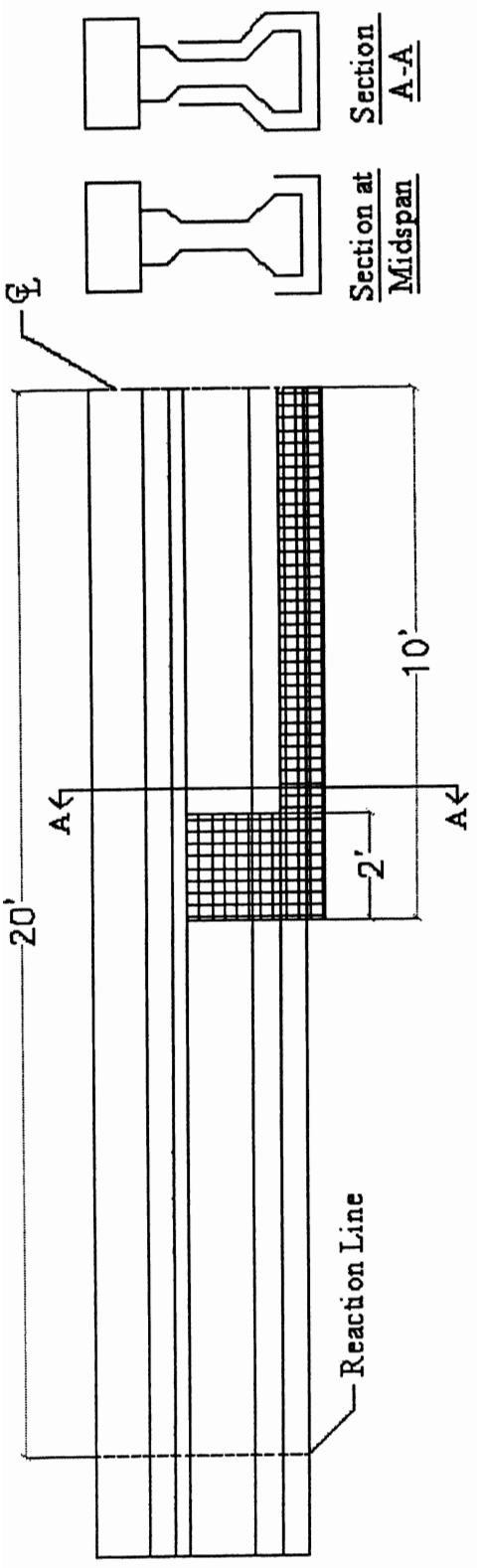

Figure 3-12: Test Specimen 5 Repair Design

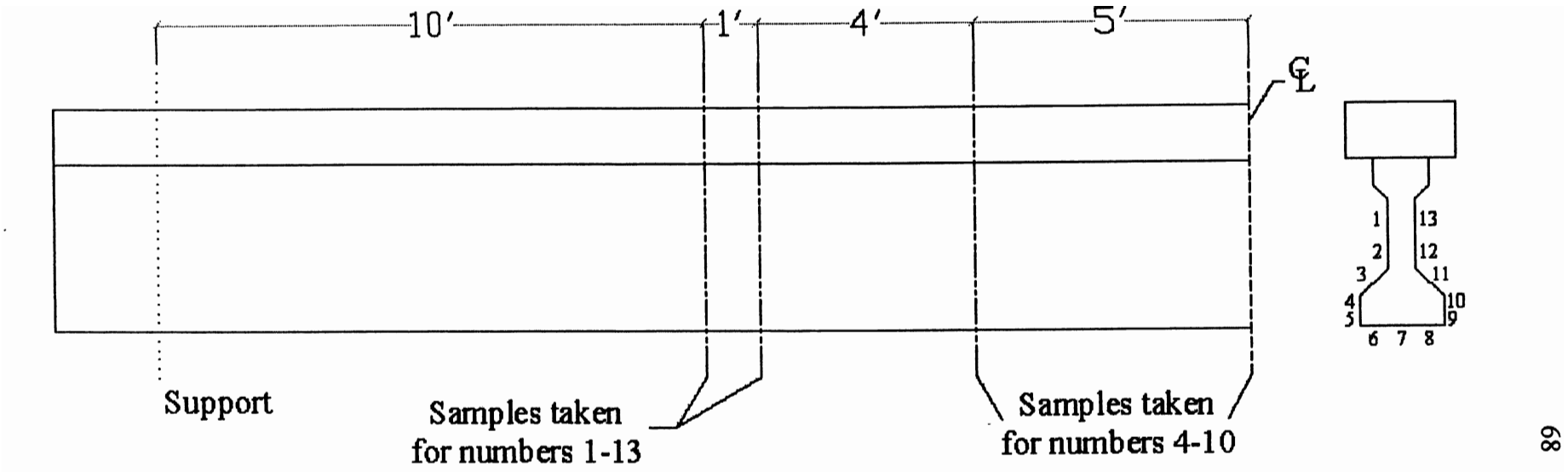

Figure 3-13: FRP Sampling Cores for Test Specimen 5

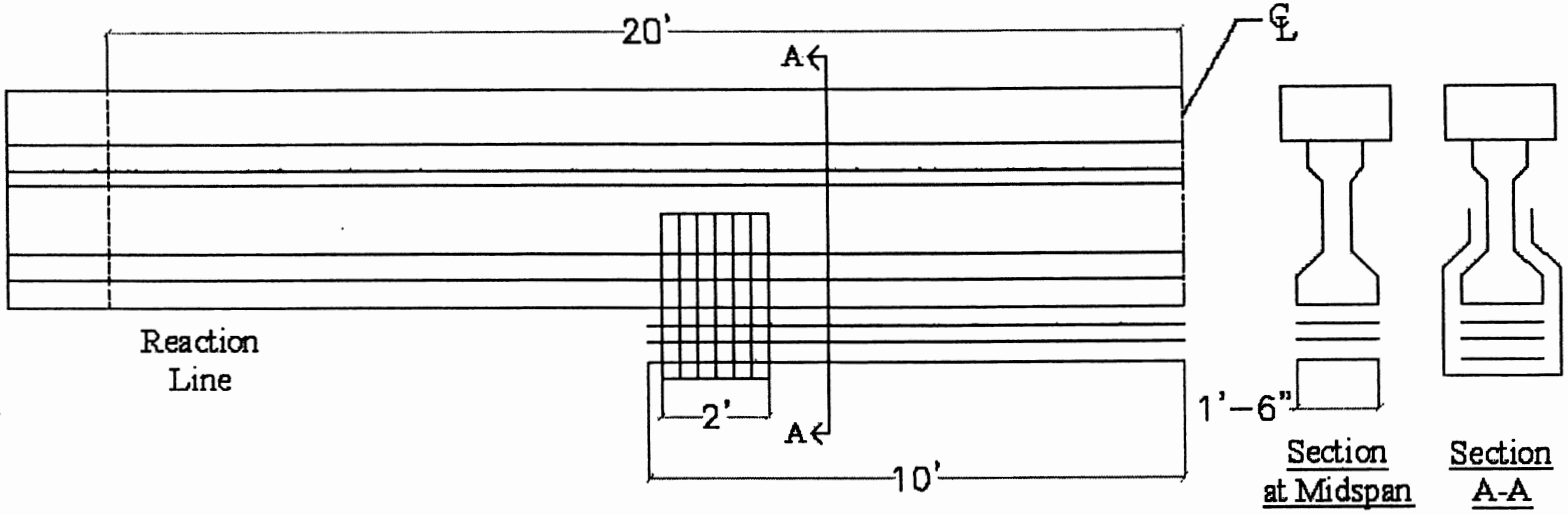

Figure 3-14: Test Specimen 6 Repair Design

CHAPTER 4
EXPERIMENTAL TEST RESULTS

This chapter contains the experimental data for the six, four-point bending tests that were conducted. Chapter 5 will serve as a comparison of the experimental results shown in this chapter to calculated theoretical values.

Loading was terminated for each specimen once either load cell showed a reduced reading therefore, no post ultimate data is shown for any of the tests. The total applied load is the sum of the two load cell measurements shown in Figure 3-6a. The moment in the constant moment region is calculated by taking one-half the total applied load and multiplying it by 15'-0" for Test Specimens 1, 2, 3, 5, and 6 and 15'-6" for Test Specimen 4. Strain and deflection profiles are plotted at 25, 50, 75, 90, and 100 percent of the maximum load attained during each experiment. Strain gauges that either were initially defective, or after a certain load level no longer functioned properly, were omitted from the strain profiles. Large increases in the strain readings for a particular gauge can be attributed to crack formation occurring inside of the two-inch gauge length causing increased strain due to stress redistribution. The experimental neutral axis depths were determined by assuming a best-fit linear strain distribution through the cross-section for a specified load level using all properly functioning strain gauges. In order to compare strain values at a certain load level and strain increases between load levels, the strain gauge closest to the prestressing steel, 45 inches down from the top of the slab, was chosen for comparison between all test specimens. In a case where the strain value was unavailable at the steel level the value was determined by linear interpolation between the

compressive strain measured 6" down from the top of the slab and the extreme tensile strain measured 48" down from the top of the slab. If the extreme tensile strain value at 48" down from the top of the slab was also unavailable, the strain at 48" down was set equal to the bottom strain being measured closest to the unavailable data at the same load level.

Test 1 Undamaged Control Results

The load versus midspan deflection for Test Specimen 1 is shown in Figure 4-1. The experimental load capacities at cracking and ultimate are 131 kips and 268 kips with corresponding midspan deflections of 0.50 and 5.95 inches, respectively. The load deflection relationship, as shown in Figure 4-1, is linear up to the cracking load and nonlinear between the cracking load and maximum load. Symmetrical deflections occurred about the midspan of the beam as shown in Figure 4-2, except for a slightly larger deflection at the south load point at the maximum load, P_{max}. Figure 4-2 also shows similar increases in deflection between 0 and 25 percent and between 25 and 50 percent of the maximum load, with larger increases in deflection between 50 and 75 percent and between 75 and 90 percent of the maximum load, and a substantial increase in deflection between 90 and 100 percent of the maximum load.

The strain profiles in Figures 4-3, 4-4, and 4-5 all show an upward movement of the neutral axis from the initial location of 20.7 inches down from the top of the slab into the slab at P_{max}. The final depths of the neutral axis at the north load point, midspan, and south load point locations are 11.27", 9.05", and 5.73", respectively, down from the top of the slab at the maximum load. The variation in neutral axis depths can be attributed to either a slight imbalance of 4 kips at the maximum applied load with a higher load at the south load point location, larger deflections, slipping of prestressing strands, yielding of

the strands, or a compression failure all on the south end of the girder. Figures 4-3, 4-4, and 4-5 also show a significant increase in strain between 90 and 100 percent of the maximum load that can be attributed to the formation of multiple cracks or the further opening up of existing cracks that developed under the applied load. Figure 4-3 shows only slight increases in strain when compared to the strain increases of Figures 4-4 and 4-5. Figures 4-4 and 4-5 show similar strain profiles for the midspan and south load point, which is reasonable since both locations are in the constant moment region. Strain increases between the load levels at the prestressing steel layer at the north load point shown in Figure 4-3 are 245 x 10^{-6} in/in, 1741 x 10^{-6} in/in, 1933 x 10^{-6} in/in, and 3508 x 10^{-6} in/in. Strain increases between the load levels at the prestressing steel layer at midspan shown in Figure 4-4 are 456 x 10^{-6} in/in, 3612 x 10^{-6} in/in, 2615 x 10^{-6} in/in, and 7240 x 10^{-6} in/in. Strain increases between the load levels at the prestressing steel layer at the south load point shown in Figure 4-5 are 339 x 10^{-6} in/in, 3303 x 10^{-6} in/in, 2224 x 10^{-6} in/in, and 7680 x 10^{-6} in/in. Comparing the strain increases at the prestressing steel level shows significantly larger increases in strain at the south load point than at the north load point, and strain increases at the south load point similar to the increases at midspan. The larger strains at the south load point location can be attributed to either unbalanced load cells with a higher load at the south load point location, larger deflections, slipping of prestressing strands, yielding of the strands, or a compression failure all on the south end of the girder. Figure 4-6 shows the load versus strain data for the strain gauges shown in Figure 3-6a along the bottom centerline of the test specimen. The figure shows similar strain readings for the four gauges up to the cracking load, and similar strains up to failure for the two strain gauges at 1'-0" from midspan and for the two strain gauges

3'-0" from midspan. The maximum recorded bottom centerline strain at P_{max} was 0.018447 in/in and occurred at 3'-0" north of midspan.

Concrete crushing was not the failure mode as expected, which allows for slipping of the strands to be assessed as the failure mode. The slightly larger deflections and larger strains recorded at the south load point location provide an assumption that the slipping of strands occurred on the south end of the girder. The shear, moment, and midspan deflection recorded at failure for the undamaged girder were 268 kips, 2012 kip-ft, and 5.95 inches, respectively.

Test 2 Damaged Control Results

The load versus midspan deflection for Test Specimen 2 is shown in Figure 4-7. The experimental load capacities at cracking and ultimate are 112 kips and 210 kips with corresponding midspan deflections of 0.54 and 6.42 inches, respectively. The load deflection relationship, as shown in Figure 4-7, is linear up to the cracking load and nonlinear between the cracking load and maximum load. Symmetrical deflections occurred about the midspan of the beam as shown in Figure 4-8, except for a slightly larger deflection at the south load point at the maximum load, P_{max}. Figure 4-8 also shows similar increases in deflection between 0 and 25 percent and between 25 and 50 percent of the maximum load, with larger increases in deflection between 50 and 75 percent and between 75 and 90 percent of the maximum load, and a substantial increase in deflection between 90 and 100 percent of the maximum load.

The strain profiles in Figures 4-9, 4-10, and 4-11 all show an upward movement of the neutral axis from the initial location of 20.7 inches down from the top of the slab into the slab at the maximum load. The final depths of the neutral axis at the north load point, midspan, and south load point locations are 10.78", 8.16", and 5.33", respectively, down

from the top of the slab at the maximum load. The variation in neutral axis depths can be attributed to either a slight imbalance of 1 kip at the maximum applied load with a higher load at the south load point location, larger deflection, slipping of prestressing strands, yielding of the strands, or a compression failure all on the south end of the girder. Figures 4-9, 4-10, and 4-11 also show a significant increase in strain between 90 and 100 percent of the ultimate load possibly due to the formation of multiple cracks or the further opening up of existing cracks. The strain profiles in Figures 4-9 and 4-11 for the north and south load point locations show similar strain values for all load increments. A comparison of the strains in Figures 4-9, 4-10, and 4-11 show that there were larger increases at midspan than at the load point locations for all profiles up to $0.90P_{max}$. This can be attributed to the damage imparted to the specimen only in the midspan area prior to testing. Strain increases between the load levels at the prestressing steel layer at the north load point shown in Figure 4-9 are 254 x 10^{-6} in/in, 1364 x 10^{-6} in/in, 1121 x 10^{-6} in/in, and 11759 x 10^{-6} in/in. Strain increases between the load levels at the prestressing steel layer at midspan shown in Figure 4-10 are 536 x 10^{-6} in/in, 6392 x 10^{-6} in/in, 16971 x 10^{-6} in/in, and 1140 x 10^{-6} in/in. Strain increases between the load levels at the prestressing steel layer at the south load point shown in Figure 4-11 are 277 x 10^{-6} in/in, 1243 x 10^{-6} in/in, 800 x 10^{-6} in/in, and 11832 x 10^{-6} in/in. Comparing the strain increases at the prestressing steel level shows larger increases in strain at the midspan location than at either of the load point locations except for the last load step where similar increases in strain at the north and south load point locations were recorded. Larger increases at the midspan location than at the load point locations are reasonable since the midspan is within the constant or maximum moment region and the load points are not located in the

constant moment region. Figure 4-12 shows the load versus strain for the strain gauges shown in Figure 3-6a along the bottom centerline of the test specimen. Similar strain readings were recorded up to the cracking load for the four strain gauges. The two strain gauges at 1'-0" from the midspan show similar strains up to failure and the two strain gauges 3'-0" from midspan show similar strains up to failure. Figure 4-12 also shows higher strains for the strain gauges 1'-0" from midspan at the maximum load than the strain gauges 3'-0" from midspan, which were located one foot from the end of the damaged area. The maximum recorded bottom centerline strain at P_{max} was 0.023338 in/in and occurred at 1'-0" south of midspan.

Concrete crushing was not the failure mode as expected, which allows for slipping of the strands to be assessed as the failure mode. The slightly larger deflections and larger strains recorded on the south load point location provide an assumption that the slipping of strands occurred on the south end of the girder. The shear, moment, and midspan deflection recorded at failure for the damaged girder were 210 kips, 1576 kip-ft, and 6.42 inches, respectively.

Test 3 RJWatson Repair Results

Two cycles of loading and unloading of Test Specimen 3 were performed before the specimen was taken to failure as shown in Figure 4-13. The data provided in Figures 4-15 through 4-18 was taken from the last series of loading. The two initial cycles of loading caused a slight softening in the load deflection curve, meaning that there was some measurable reduction in the stiffness of the specimen at the beginning of the loading cycle to failure. The load versus midspan deflection for Test Specimen 3 is shown in Figure 4-14. The experimental load capacities at cracking and ultimate are 125 kips and 244 kips with corresponding midspan deflections of 0.60 and 3.15 inches,

respectively. The experimental cracking load for Test Specimen 3 was attained during the second series of loading which means that for the third or final loading series, the cracking load had previously been exceeded. The load deflection relationship, as shown in Figure 4-14 is still linear up to the cracking load and nonlinear between the cracking load and maximum load. Symmetrical deflections occurred about the midspan of the beam as shown in Figure 4-15, except for a slightly larger deflection at the south load point at the maximum load. Figure 4-15 also shows similar increments of deflection between 0 and 25 percent and between 25 and 50 percent of the maximum load, with increasingly larger increments of deflection between 50 and 75 percent , 75 and 90 percent, and 90 and 100 percent of the maximum load.

The strain profiles in Figures 4-16, 4-17, and 4-18 all show an upward movement of the neutral axis from the initial location of 20.81 inches down from the top of the slab into the slab at P_{max}. The final depths of the neutral axis at the north load point and midspan locations are 10.98" and 10.52", respectively, down from the top of the slab at the maximum load. The neutral axis depth at the south load point location can not be determined due to an insufficient number of data points. The determined final depths of the neutral axis for the north load point and midspan locations are similar with a slightly smaller neutral axis depth for the midspan location. This difference can be attributed to either the midspan location being within the constant or maximum moment region and the north load point location being located at the transition between the moment gradient and constant moment regions or a slight imbalance of 7 kips at the maximum applied load with a higher load at the south load point location. The strain profiles in Figures 4-9 and 4-11 for the north and south load point locations show similar strain patterns for all

load steps with slightly larger strains at the north load point. A comparison of the strains in Figures 4-9, 4-10, and 4-11 show that there were larger increases at midspan than at the load point locations for all profiles. This can be attributed to the damage imparted on the specimen only in the midspan area prior to testing. Strain increases between the load levels at the prestressing steel layer at the north load point shown in Figure 4-16 are 254 x 10^{-6} in/in, 1610 x 10^{-6} in/in, 1210 x 10^{-6} in/in, and 753 x 10^{-6} in/in. Strain increases between the load levels at the prestressing steel layer at midspan shown in Figure 4-17 are 503 x 10^{-6} in/in, 1454 x 10^{-6} in/in, 1118 x 10^{-6} in/in, and 1174 x 10^{-6} in/in. Strain increases between the load levels at the prestressing steel layer at the south load point shown in Figure 4-18 are 209 x 10^{-6} in/in, 810 x 10^{-6} in/in, 650 x 10^{-6} in/in, and 2347 x 10^{-6} in/in. The largest increases for the strain gauges near the level of prestressing were located at midspan for the first two load steps of 0.25 and 0.50P_{max}, the north load point for the next two load steps of 0.75 and 0.90P_{max}, and the south load point for the last load step up to P_{max}. The pattern of strain increase shows fairly symmetric strains about midspan up to 0.50P_{max} equal to 122 kips which is approximately equal to the experimental cracking load of 125.28 kips. Also, the largest strain increase occurred between 0.90P_{max} and 1.00P_{max} at the south load point, which is at the location where a portion of the girder completely separated from the rest of the girder at failure. Figure 4-19 shows the load versus strain data for the strain gauges shown in Figure 3-6a along the bottom centerline of the test specimen. Similar strain readings were recorded for the two strain gauges on the north end of the beam up to failure. The figure shows slightly larger strains for the strain gauges located 3'-0" from midspan than the strain gauges 1'-0" from

midspan throughout loading. The maximum recorded bottom centerline strain at P_{max} was 0.005083 in/in and occurred at 3'-0" north of midspan.

The failure mode of Test Specimen 3 was concrete cover separation as shown in Figures 4-20 and 4-21. A crack formed at both ends of the FRP plate at the bottom layer of prestressing and propagated towards midspan. The severe cracking at the south end of the girder caused a portion of the bottom flange of the girder up to the bottom layer of prestressing to fall to the ground with the adhered FRP. The shear, moment, and midspan deflection recorded at failure for the repaired girder were 244 kips, 1829 kip-ft, and 3.15 inches, respectively. The ultimate shear and moment capacity corresponds to restoring 91% of the experimental ultimate capacity of the undamaged girder. The measured deflection at P_{max} for Test Specimen 3 corresponds to a 47% reduction in the deflection of the undamaged girder (Test Specimen 1) at its maximum load.

Test 4 Air Logistics Repair Results

The load versus midspan deflection for Test Specimen 4 is shown in Figure 4-22. The experimental load capacities at cracking and ultimate are 111 kips and 247 kips with corresponding midspan deflections of 0.47 and 3.50 inches, respectively. The load deflection relationship, as shown in Figure 4-22 is linear up to the cracking load and nonlinear between the cracking load and maximum load. Symmetrical deflections occurred about the midspan of the beam as shown in Figure 4-23, except for a slightly larger deflection at the south load point at the maximum load. Figure 4-23 also shows similar increases in deflection between 0 and 25 percent and between 25 and 50 percent of the maximum load, with slightly larger increases in deflection between 50 and 75 percent , 75 and 90 percent, and 90 and 100 percent of the maximum load.

The strain profiles in Figures 4-24, 4-25, and 4-26 all show an upward movement of the neutral axis from the initial location of 20.76 inches down from the top of the slab into the slab at P_{max}. The final depths of the neutral axis at the north load point, midspan, and south load point locations are 6.68", 7.81", and 7.22", respectively, down from the top of the slab at the maximum load. It is reasonable that the neutral axis depth at midspan would be greater than the neutral axis depths at the load point locations due to the midspan location being within the constant or maximum moment region and the load point locations being located at the transition between the moment gradient and constant moment regions. The difference of the neutral axis depths at the load point locations can be attributed to either a slight imbalance of 2.9 kips at the maximum applied load with a higher load at the north load point location, larger deflections, slipping of prestressing strands, yielding of the strands, compression failure, or failure of the FRP all on the north end of the girder. The strain profiles in Figures 4-24 and 4-26 for the north and south load points show similar strain patterns for all load increments with slightly larger strains at the north load point. A comparison of the strains in Figures 4-24, 4-25, and 4-26 show that there were larger increases at midspan than at the load points for all profiles. This can be attributed to the damage imparted to the specimen only in the midspan area prior to testing. Strain increases between the load levels at the prestressing steel layer at the north load point shown in Figure 4-24 are 160 x 10^{-6} , 372 x 10^{-6} , 1203 x 10^{-6} , 1992 x 10^{-6} , and -867 x 10^{-6} in/in. Strain increases between the load levels at the prestressing steel layer at midspan shown in Figure 4-25 are 143 x 10^{-6} , 2635 x 10^{-6} , 4396 x 10^{-6} , 5962 x 10^{-6} , and 6856 x 10^{-6} in/in. Strain increases between the load levels at the prestressing steel layer at the south load point shown in Figure 4-26 are 139 x 10^{-6} , 287 x

10^{-6} , 1045 x 10^{-6} , 1889 x 10^{-6} , and 789 x 10^{-6} in/in. The largest increases for the strain gauges near the level of prestressing were located at the north load point for the first load step up to $0.25P_{max}$, and the midspan for the next four load steps up to P_{max}. The strain increase pattern shows overall symmetric strain increases about midspan except between 0.90 and P_{max}. Figure 4-27 shows the load versus strain data for the strain gauges shown in Figure 3-6a along the bottom centerline of the test specimen. Similar strain readings were recorded for the four strain gauges up to the maximum load. Figure 4-27 also shows slightly larger strains at the maximum load for the strain gauges located on the north end of the girder than for the strain gauges located on the south end of the girder. The maximum recorded bottom centerline strain at P_{max} was 0.009211 in/in and occurred at 1'-0" north of midspan.

The failure mode of Test Specimen 4 was a combination of FRP rupture and adhesive failure as shown in Figure 4-28. Before failure, the FRP system had debonded between the stirrups and was stretched in tension due to the deflection of the girder. At failure, the FRP had reached its tensile capacity in which the FRP ruptured just before the stirrup at the south end and debonded past the stirrup at the north end. By debonding past the stirrup, the longitudinal FRP sheared through the stirrup, which had fibers oriented at 0° and 90° as shown in Figure 4-29. The shear, moment, and midspan deflection recorded at failure for the repaired girder were 246.7 kips, 1912 kip-ft, and 3.50 inches, respectively. The ultimate shear and moment capacity corresponds to restoring 92% and 95%, respectively, of the experimental ultimate capacity of the undamaged girder. The restored percentages for shear and moment capacity differ due to the supports being moved out an additional 6" for the test as shown in Figure 3-5. The measured deflection

at P_{max} for Test Specimen 4 corresponds to a 41% reduction in the deflection of the undamaged girder at its maximum load. Loading was discontinued for Test Specimen 4 when the FRP system failed at a load corresponding to less than the ultimate experimental load of Test Specimen 2, representing the girder in the damaged state. It can be assumed that Test Specimen 4 would have ultimately failed at approximately the ultimate load of Test Specimen 2.

Test 5 UF Sprayed Repair Results

The load versus midspan deflection for Test Specimen 5 is shown in Figure 4-30. The experimental load capacities at cracking and ultimate are 125 kips and 255 kips with corresponding midspan deflections of 0.53 and 3.16 inches, respectively. The load deflection relationship, as shown in Figure 4-30 is linear up to the cracking load and nonlinear between the cracking load and maximum load. Symmetrical deflections occurred about the midspan of the beam as shown in Figure 4-31, except for a slightly larger deflection at the north load point at the maximum load. Figure 4-31 also shows similar increases in deflection between 0 and 25 percent and between 25 and 50 percent of the maximum load, with slightly larger increases in deflection between 50 and 75 percent , 75 and 90 percent, and 90 and 100 percent of the maximum load.

The strain profiles in Figures 4-32, 4-33, and 4-34 all show an upward movement of the neutral axis from the initial location of 20.96 inches down from the top of the slab into the slab at P_{max}. The final depths of the neutral axis at the north load point, midspan, and south load point locations are 16.05", 9.18", and 9.12", respectively, down from the top of the slab at the maximum load. The significant difference between the neutral axis depths at the load point locations can be attributed to either a slight imbalance of 6 kips at the maximum applied load with a higher load at the south load point location, larger

deflections, slipping of prestressing strands, yielding of the strands, compression failure, or failure of the FRP all on the south end of the girder. The strain profiles in Figures 4-32 and 4-34 for the north and south load point locations show similar strain patterns for all load increments with slightly larger strains at the south load point. A comparison of the strains in Figures 4-32, 4-33, and 4-34 show that there were larger increases at midspan than at the load point locations for all profiles. This can be attributed to the damage imparted to the specimen only in the midspan area prior to testing. Strain increases between the load levels at the prestressing steel layer at the north load point shown in Figure 4-32 are 254 x 10^{-6} in/in, 2084 x 10^{-6} in/in, 1451 x 10^{-6} in/in, and 952 x 10^{-6} in/in. Strain increases between the load levels at the prestressing steel layer at midspan shown in Figure 4-33 are 808 x 10^{-6} in/in, 2714 x 10^{-6} in/in, 2487 x 10^{-6} in/in, and 2814 x 10^{-6} in/in. Strain increases between the load levels at the prestressing steel layer at the south load point shown in Figure 4-34 are 209 x 10^{-6} in/in, 1149 x 10^{-6} in/in, 1733 x 10^{-6} in/in, and 1303 x 10^{-6} in/in. Comparing the strain increases at the prestressing steel level shows larger increases in strain at the midspan location than at either of the load point locations and similar increases in strain at the north and south load point locations. These larger increases at the midspan location are reasonable since the midspan is within the constant or maximum moment region and the load points are located outside the constant moment region. Figure 4-35 shows the load versus strain data for the strain gauges shown in Figure 3-6a along the bottom centerline of the test specimen. Similar strain readings were recorded for the two strain gauges at 1'-0" from midspan up to failure and for the two strain gauges 3'-0" from midspan up to failure. In Figure 4-35, the strain gauge located 3'-0" from midspan on the south end of the girder is experiencing increased

sensitivity noted by the repeated back and forth motion although the gauge remained functional throughout the loading. Figure 4-35 also shows larger strains after the cracking load for the strain gauges 1'-0" from midspan than the strain gauges 3'-0" from midspan which are located one foot from the end of the damaged area. The maximum recorded bottom centerline strain at P_{max} was 0.009234 in/in and occurred at 1'-0" north of midspan.

The failure mode of Test Specimen 5 was FRP rupture as shown in Figures 4-36 and 4-37. A crack formed near midspan of the beam rupturing completely through the FRP applied to the perimeter of the section. The FRP remained attached over the entire length and perimeter of the girder. The shear, moment, and midspan deflection recorded at failure for the repaired girder were 255 kips, 1911 kip-ft, and 3.16 inches, respectively. The ultimate shear and moment capacity corresponds to restoring 95% of the experimental ultimate capacity of the undamaged girder. The deflection at P_{max} for Test Specimen 5 corresponds to a 47% reduction in the deflection of the undamaged girder at its maximum load.

Test 6 Edge Composites Repair Results

The load versus midspan deflection for Test Specimen 6 is shown in Figure 4-38. The experimental load capacities at cracking and ultimate are 141 kips and 288 kips with corresponding midspan deflections of 0.47 and 4.34 inches, respectively. The load deflection relationship, as shown in Figure 4-38 is linear up to the cracking load and nonlinear between the cracking load and maximum load. Symmetrical deflections occurred about the midspan of the beam as shown in Figure 4-39, except for a slightly larger deflection at the north side of the girder point at the maximum load. The deflection data of the LVDT just north of midspan (36 in) is not shown in Figure 4-39

due to a malfunction of this instrument. Figure 4-39 also shows similar increases in deflection between 0 and 25 percent and between 25 and 50 percent of the maximum load, with increasingly larger increments of deflection between 50 and 75 percent , 75 and 90 percent, and 90 and 100 percent of the maximum load.

The strain profiles in Figures 4-40, 4-41, and 4-42 all show an upward movement of the neutral axis from the initial location of 20.73 inches down from the top of the slab into the slab at P_{max}. The final depths of the neutral axis at the north load point and midspan locations are 6.30" and 7.04", respectively, down from the top of the slab at the maximum load. The neutral axis depth at the south load point location can not be determined due to a tension strain being measured in the slab at the maximum load. The slight difference between the neutral axis depths at the north load point and midspan locations can be attributed to either a slight imbalance of 15 kips at the maximum applied load with a higher load at the south load point location, larger deflections, slipping of prestressing strands, yielding of the strands, or compression failure all on the south end of the girder. The strain profiles in Figures 4-40 and 4-42 for the north and south load point locations show larger strains at the south load point location for all load increments. A comparison of the strains in Figures 4-40, 4-41, and 4-42 show that there were larger increases at midspan than at the load point locations for all profiles. This can be attributed to the damage imparted to the specimen only in the midspan area prior to testing. Strain increases between the load levels at the prestressing steel layer at the north load point shown in Figure 4-40 are 261 x 10^{-6} in/in, 1977 x 10^{-6} in/in, 1950 x 10^{-6} in/in, and 4199 x 10^{-6} in/in. Strain increases between the load levels at the prestressing steel layer at midspan shown in Figure 4-41 are 973 x 10^{-6} in/in, 6165 x 10^{-6} in/in, 30473 x 10^{-6}

in/in, and -2768 x 10^{-6} in/in. Strain increases between the load levels at the prestressing steel layer at the south load point shown in Figure 4-42 are 236 x 10^{-6} in/in, 1598 x 10^{-6} in/in, 3079 x 10^{-6} in/in, and 5155 x 10^{-6} in/in. Comparing the strain increases at the prestressing steel level shows larger increases in strain at the midspan location than at either of the load point locations and similar increases in strain at the north and south load point locations. These larger increases at the midspan location are reasonable since the midspan is within the constant or maximum moment region and the load points are located outside the constant moment region. Figure 4-43 shows the load versus strain data for the strain gauges shown in Figure 3-6a along the bottom centerline of the test specimen. Similar strain readings were recorded up to the maximum load for the three functioning strain gauges. Figure 4-43 also shows higher strains for the strain gauges 3'-0" from midspan at the maximum load than the strain gauge 1'-0" from midspan. The maximum recorded bottom centerline strain at P_{max} was 0.011293 in/in and occurred at 3'-0" north of midspan.

The failure mode of Test Specimen 6 was due to an anchorage failure at the north end of the girder which caused the longitudinal FRP to slip as shown in Figures 4-44 and 4-45. The anchorage remained attached to the girder although it was debonded on the tension face of the specimen. The uniform 18" width longitudinal FRP separated into three longitudinal pieces with the middle strip remaining adhered to the girder and the two edge strips slipping at the north end of the girder. The slipping of the two edge strips caused these edge strips to debond between the stirrups and sag about midspan. The shear, moment, and midspan deflection recorded at failure for the repaired girder were 288 kips, 2162 kip-ft, and 4.34 inches, respectively. The ultimate shear and moment

capacity corresponds to restoring 108% of the experimental ultimate capacity of the undamaged girder. The deflection at P_{max} for Test Specimen 6 corresponds to a 27% reduction in the deflection of the undamaged girder at its maximum load.

Evaluation of Experimental Observations

Table 4-1 shows the capacities, midspan deflections, strains, and initial flexural stiffness at the cracking load and Table 4-2 shows the capacities, midspan deflections, and strains at the maximum load.

Effect of Fiber Reinforced Polymers on Stiffness

A significant reduction in stiffness occurred when four prestressing strands were severed in the test specimens to simulate the impact damage. This stiffness loss resulted in larger deflections at reduced load levels. The maximum load and subsequent failure also occurred at reduced load levels. The experimental initial flexural stiffness of the test specimens was determined by dividing the load at cracking by the deflection at cracking. The initial flexural stiffness calculated for Test Specimen 1 was 262 kips/in while Test Specimen 2 had an initial flexural stiffness of 208 kips/in as shown in Table 4-1. Therefore, a 21% reduction in initial flexural stiffness was simulated by the severing of four prestressing strands as shown in Table 4-1.

The application of FRP materials to the tension face of a girder provides resistance to deflection through the high tensile strength of the FRP materials in comparison to concrete or mild steel. The resulting amount of resistance or stiffness increase is dependent on FRP laminate properties, FRP location on the girder, thickness of the FRP laminate, and an effective bond. Test Specimen 3, repaired with carbon fibers and an epoxy adhesive had an initial stiffness that was only of 79.5% of Test Specimen 1; Test Specimen 4, repaired with carbon fibers with a polyurethane adhesive had an initial

stiffness that was 89.4% of Test Specimen 1; Test Specimen 5, repaired with glass fibers with a polyester adhesive had a comparable initial stiffness that was 89.5% of Test Specimen 1; and Test Specimen 6, repaired with carbon fibers with a epoxy adhesive had a comparable initial stiffness that was 113.8% of Test Specimen 1 as shown in Table 4-1. The resulting initial flexural stiffness increases of Test Specimens 3, 4, 5, and 6 over Test Specimen 2 were 0%, 12.8%, 12.9%, and 43.6%, respectively, as shown in Table 4-1.

At the cracking load, the experimentally measured midspan deflections of Test Specimens 2, 3, 4, 5, and 6 varied in comparison to the measured midspan deflection of Test Specimen 1. The measured midspan deflection at cracking load for Test Specimen 1 was 0.50" while Test Specimen 2 had a midspan deflection at cracking load of 0.54" as shown in Table 4-1. Therefore, a 7.6% increase in midspan deflection at cracking load was simulated by the severing of four prestressing strands. Test Specimen 3, with a midspan deflection at cracking load equal to 0.60", had a midspan deflection at cracking load 20% greater than Test Specimen 1; Test Specimen 4, with a midspan deflection at cracking load equal to 0.47", had a midspan deflection at cracking load 5.3% less than Test Specimen 1; Test Specimen 5, with a midspan deflection at cracking load of 0.53", had a midspan deflection at cracking load 6.6% greater than Test Specimen 1; and Test Specimen 6, with a midspan deflection at cracking load of 0.47", had a midspan deflection at cracking load 5.8% less than Test Specimen 1 as shown in Table 4-1. The measured midspan deflection at maximum load for Test Specimen 1 was 5.95" while Test Specimen 2 had a midspan deflection at cracking load of 6.42" as shown in Table 4-2. Therefore, a 8% increase in midspan deflection at maximum load was simulated by the severing of four prestressing strands. Test Specimen 3, with a midspan deflection at

maximum load equal to 3.15", had a midspan deflection at maximum load 47% less than Test Specimen 1; Test Specimen 4, with a midspan deflection at maximum load equal to 3.50", had a midspan deflection at maximum load 41% less than Test Specimen 1; Test Specimen 5, with a midspan deflection at maximum load of 3.16", had a midspan deflection at maximum load 47% less than Test Specimen 1; and Test Specimen 6, with a midspan deflection at maximum load of 4.34", had a midspan deflection at maximum load 27% less than Test Specimen 1 as shown in Table 4-2.

Effect of Fiber Reinforced Polymers on Capacity

A significant reduction in capacity occurred when four prestressing strands were severed in the test specimens to simulate impact damage. This loss in capacity resulted in failures at reduced load levels. The shear and moment capacity of Test Specimen 1 at the cracking load was 131 kips and 984 kip-ft while the shear and moment capacity of Test Specimen 2 at the cracking load was 112 kips and 839 kip-ft as shown in Table 4-1. Therefore, a 15% reduction in the shear and moment capacity at the cracking load was simulated by the severing of four prestressing strands. The experimental capacity at the cracking load for Test Specimen 3 was 125 kips which was equal to 95% of the capacity of Test Specimen 1, and equal to 112% gain over the capacity of Test Specimen 2 as shown in Table 4-1. The experimental capacity at the cracking load for Test Specimen 4 was 111 kips which was equal to 85% of the capacity of Test Specimen 1, and equal to 99% of the capacity of Test Specimen 2 as shown in Table 4-1. The experimental capacity at the cracking load for Test Specimen 5 was 125 kips which was equal to 95% of the capacity of Test Specimen 1, and equal to 112% gain over the capacity of Test Specimen 2 as shown in Table 4-1. The experimental capacity at the cracking load for Test Specimen 6 was 141 kips which was equal to 107% of the capacity of Test

Specimen 1, and equal to 126% gain over the capacity of Test Specimen 2 as shown in Table 4-1. The shear and moment capacity of Test Specimen 1 at the maximum load was 268 kips and 2012 kip-ft, respectively. While the shear and moment capacity of Test Specimen 2 at the maximum load was 210 kips and 1576 kip-ft, respectively as shown in Table 4-2. Therefore, a 22% reduction in the shear and moment capacity at the maximum load was simulated by the severing of four prestressing strands. The experimental capacity at the maximum load for Test Specimen 3 was 244 kips which was equal to 91% of the capacity of Test Specimen 1, and equal to 116% over the capacity of Test Specimen 2 as shown in Table 4-2. The experimental capacity at the maximum load for Test Specimen 4 was 247 kips which was equal to 92% of the capacity of Test Specimen 1, and equal to 118% of the capacity of Test Specimen 2 as shown in Table 4-2. The experimental capacity at the maximum load for Test Specimen 5 was 255 kips which was equal to 95% of the capacity of Test Specimen 1, and equal to a 121% over the capacity of Test Specimen 2 as shown in Table 4-2. The experimental capacity at the maximum load for Test Specimen 6 was 288 kips which was equal to 108% of the capacity of Test Specimen 1, and equal to a 137% over the capacity of Test Specimen 2 as shown in Table 4-2. The amount of capacity increase that the FRP can provide to a structural member is dependent on FRP laminate properties, FRP location on the girder, thickness of the FRP laminate, and an effective bond.

Effect of Fiber Reinforced Polymers on Strains on Bottom Centerline of Test Specimens

As a result of smaller midspan deflections of the girders repaired with FRP systems than the unrepaired test specimens, strains at the extreme tensile face of the girder at maximum load were also reduced. The measured tensile strain for Test Specimen 1 at

maximum load was 0.018447 in/in while the measured tensile strain for Test Specimen 2 at maximum load was 0.023338 in/in as shown in Table 4-2. Therefore, a 26.5% increase in measured tensile strain was simulated by the severing of four prestressing strands. Test Specimen 3, with a tensile strain equal to 0.005083 in/in at maximum load, had a tensile strain at maximum load that was 27.5% of Test Specimen 1; Test Specimen 4, with a tensile strain equal to 0.009211 in/in at maximum load, had a tensile strain at maximum load that was 49.9% of Test Specimen 1; Test Specimen 5, with a tensile strain equal to 0.009234 in/in, had a tensile strain at maximum load that was only 50.1% of Test Specimen 1; and Test Specimen 6, with a tensile strain equal to 0.011293 in/in, had a tensile strain at maximum load that was only 61.2% of Test Specimen 1 as shown in Table 4-2.

Other Effects – Initial Imperfections and Bond

A rough transition from the patch material to the original girder was present on all of the test specimens especially on the sides of the girder. This rough transition made it difficult to obtain a even bond of the FRP material in these areas and could cause high stress concentrations in surrounding areas. This imperfection caused problems for the repair application on Test Specimen 5 due to a significant amount of the repair material being placed on the sides of the girder. The rough transition did not affect the resulting capacities or failure modes of the test specimens since no significant cracking was present in the FRP near these areas.

Before testing the repaired test specimens, an infrared camera was used to scan over the repaired areas of Test Specimens 3, 4, 5, and 6 to determine if existing voids in the bond resulted from the application procedure or from curing. In order to locate voids in the repaired areas, a heat source was passed over the repaired areas. Then when

infrared images are taken, a void location is determined by a hotspot in which the heat is collecting. The infrared scanning of Test Specimen 3 showed that no voids were present in the bond at the surface or between the applied layers. The infrared camera scanning did not result in any usable results for Test Specimen 4 since the polyurethane adhesive behaved as an insulator to the heat. Therefore, the FRP material bonded in one area and unbonded in a separate area showed that both locations were unbonded. The infrared scanning of Test Specimen 5 showed the presence of numerous small voids at the exterior surface of the FRP located on the tension face of the girder. The infrared scanning of Test Specimen 6 showed that only a few small voids were present in the bond at the surface or between the applied layers.

Summary of Test Specimen Failure Modes

Steel yielding followed by concrete crushing is the expected failure mode for any flexural member. Concrete crushing results when the capacity of the steel is exceeded and therefore the neutral axis depth is reduced to the top of the member such that the section can withstand the applied load in tension. Test Specimens 1 and 2 failed due to slipping of the prestressing strands, not as concrete crushing as expected.

Test Specimen 3 failed due to concrete cover separation. Concrete cover seperation is a premature failure, which means that if the ends of the FRP had been properly anchored to the girder a higher capacity would have been attained (Teng et al 2002). At failure of Test Specimen 3, a portion of the bottom flange was completely separated from the girder. This piece of concrete that was still adhered to the FRP resulted from the concrete being only attached to the girder through the FRP.

The failure mode of Test Specimen 4 was FRP rupture following an adhesive failure, which is a premature failure mode meaning that further capacity could have been

gained if the FRP material had been applied with a better adhesive. In addition, at failure of Test Specimen 4, the FRP material was no longer adhered to the concrete and was hanging from the bottom of the girder at one end. The resulting failure states of Test Specimens 3 and 4 are not desirable. Overhanging materials with the possibility of falling onto a roadway system, like the failure modes of Test Specimens 3 and 4 would be very dangerous.

Test Specimen 5 failed due to FRP rupture, which is not a premature failure mode. Therefore, the full capacity of the installed FRP system was reached at the failure load.

Test Specimen 6 failed due to anchorage failure, which is a premature failure mode. It was assumed that if failure of the anchorage had not occurred, a significant capacity of the girder would not have been attained over the experimentally measured capacity meaning a mature failure would have occurred at approximately the same capacity. Although the longitudinal FRP was debonded from the girder is still remained attached due to the anchorages remaining adhered to the girder.

Table 4-1: Experimental Capacities, Deflections, Strains, and Initial Flexural Stiffness of All Test Specimens at Cracking Load

Test Specimen	P_{cr} (kip)	% diff from Test Specimen 1	% gain from Test Specimen 2	M_{cr} (kip-ft)	Δ_{cr} (in)	% diff from Test Specimen 1	ε_{cr} (in/in) maximum in profile	Location of maximum ε_{cr} in profile	ε_{cr} (in/in) maximum on bottom	Location of maximum ε_{cr} on bottom	Initial stiffness (kip/in)	% diff from Test Specimen 1
1	131.3	0.0	N/A	984.4	0.50	0.0	0.000626	S 48" down	0.000664	N 3'	262.0	100.0
2	111.9	14.7	0.0	839.4	0.54	-7.6	0.001838	C 48" down	0.000597	S 1'	207.6	79.2
3	125.3	4.6	11.9	939.6	0.60	-20.0	0.000569	S 48" down	0.000901	N 3'	208.3	79.5
4	111.0	15.4	-0.8	860.5	0.47	5.3	0.00122	C 45" down	0.000691	N 1'	234.1	89.4
5	125.2	4.6	11.8	938.7	0.53	-6.6	0.00103	C 48" down	0.000824	S 1'	234.4	89.5
6	140.6	-7.1	25.6	1054.5	0.47	5.8	0.001070	C 45" down	0.000636	N 3'	298.1	113.8

Table 4-2: Experimental Capacities, Deflections, and Strains of All Test Specimens at Maximum Load

Test Specimen	P_{max} (kip)	% diff from Test Specimen 1	% gain from Test Specimen 2	M_{max} (kip-ft)	Δ_{max} (in)	% diff from Test Specimen 1	ε_{max} (in/in) maximum in profile	Location of maximum ε_{max} in profile	ε_{max} (in/in) maximum on bottom	Location of maximum ε_{max} on bottom
1	268.3	0.0	N/A	2012.1	5.95	0.0	0.021053	S 48" down	0.018447	N 3'
2	210.1	21.7	0.0	1575.9	6.42	-8.0	0.025185	N 48" down	0.023338	S 1'
3	243.9	9.1	16.1	1829.1	3.15	47.1	0.004207	S 45" down	0.005083	N 3'
4	246.7	8.0	17.4	1911.9	3.50	41.1	0.00875	C 48" down	0.009211	N 1'
5	254.8	5.0	21.3	1910.8	3.16	46.9	0.00911	C 45" down	0.009234	N 1'
6	288.3	-7.5	37.2	2162.3	4.34	27.0	0.035074	C 45" down	0.011293	N 3'

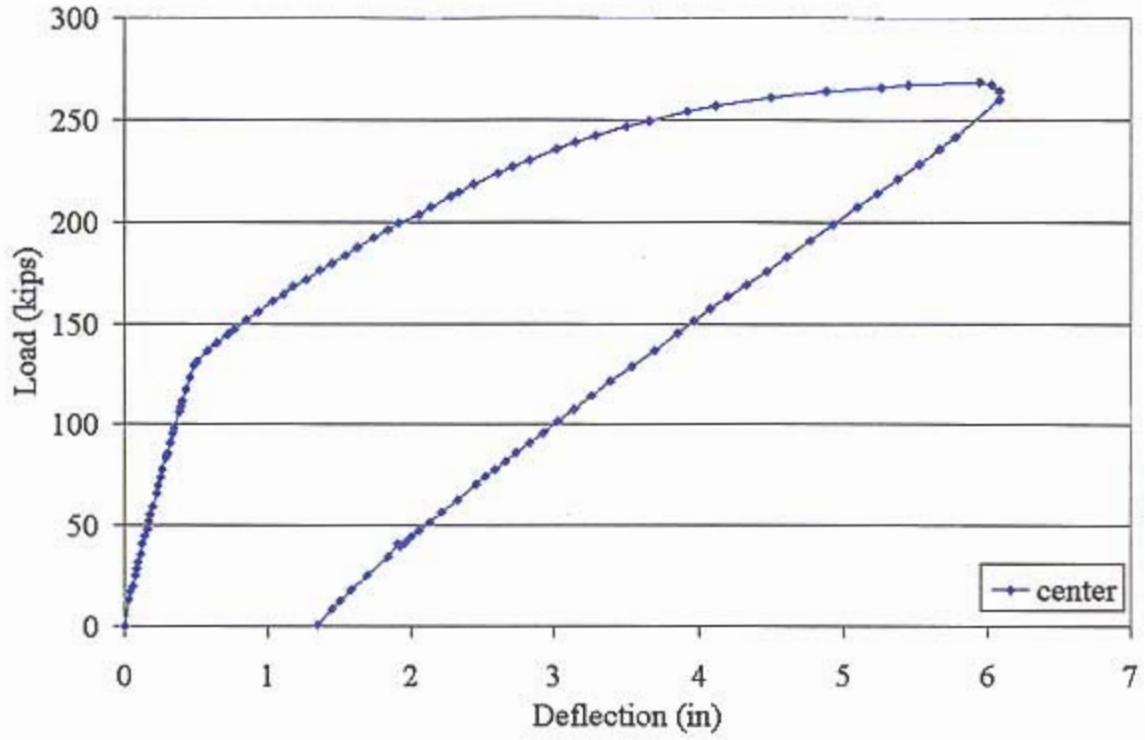

Figure 4-1: Test Specimen 1 Load versus Midspan Deflection Curve

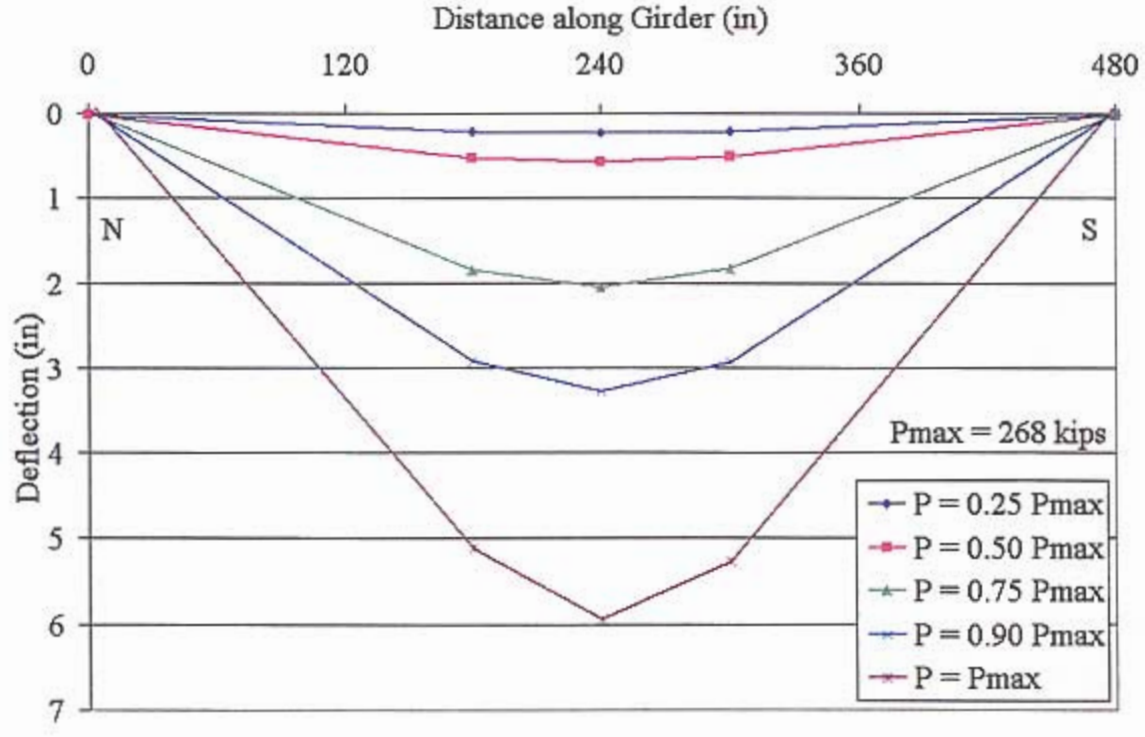

Figure 4-2: Test Specimen 1 Measured Deflection Profile

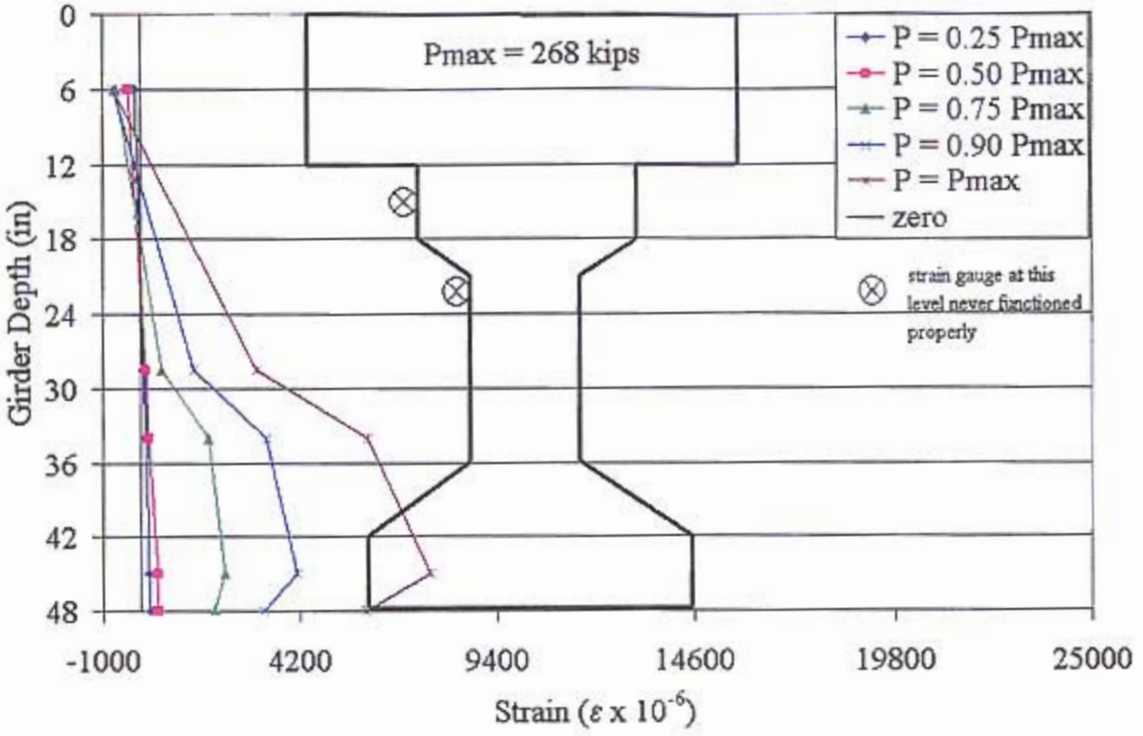

Figure 4-3: Test Specimen 1 Strain Profile at North Load Point

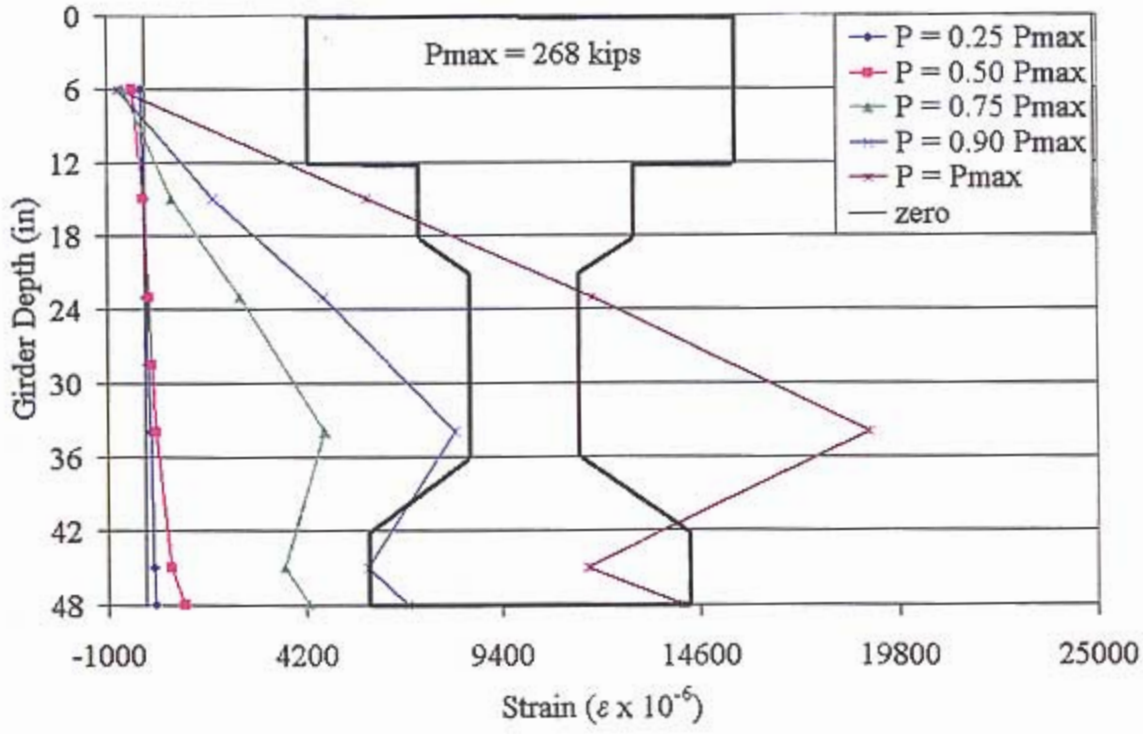

Figure 4-4: Test Specimen 1 Strain Profile at Midspan

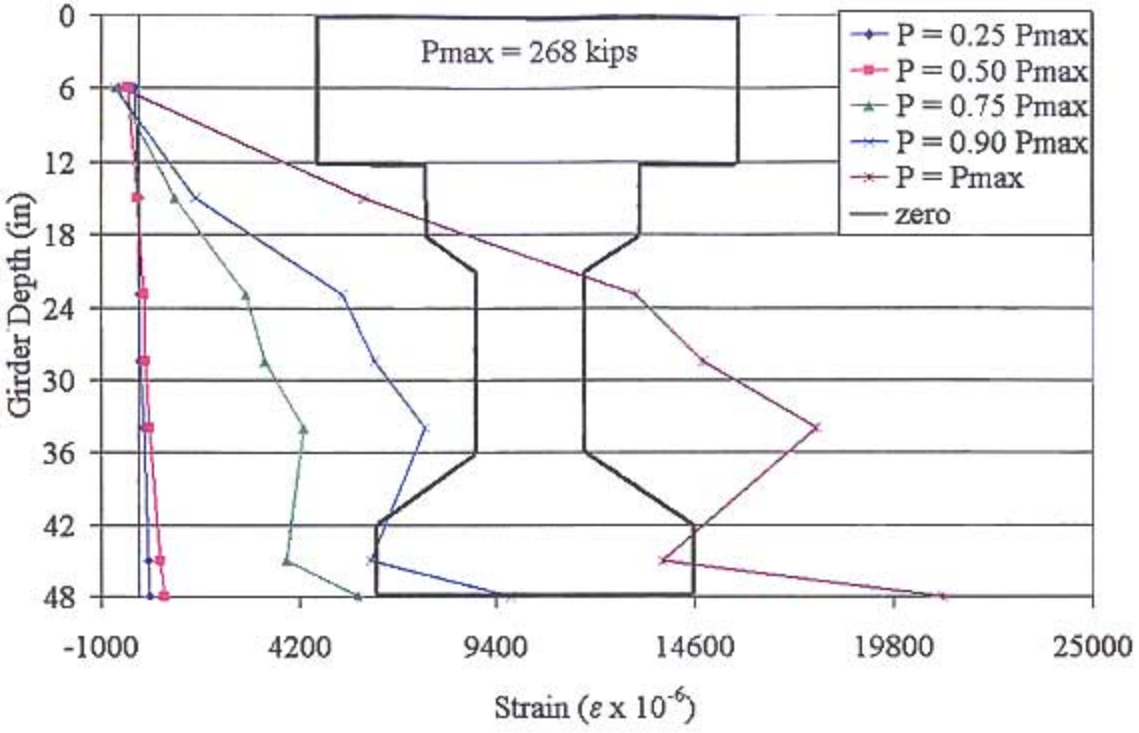

Figure 4-5: Test Specimen 1 Strain Profile at South Load Point

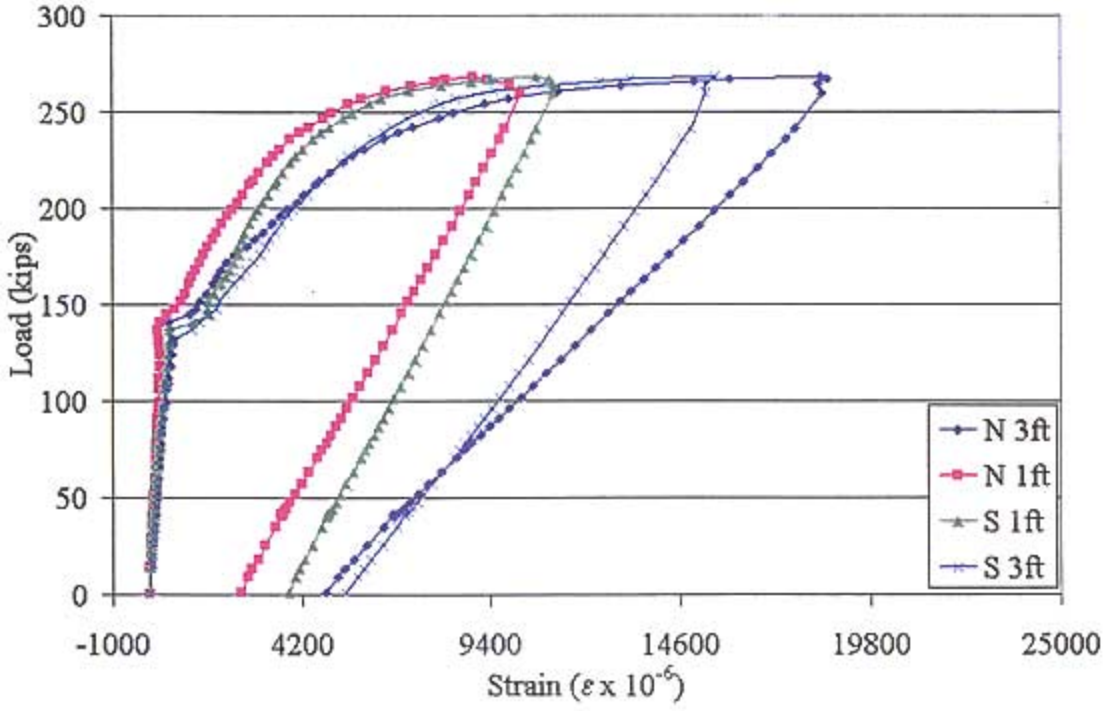

Figure 4-6: Test Specimen 1 Load versus Measured Strain Along Bottom Centerline of Beam

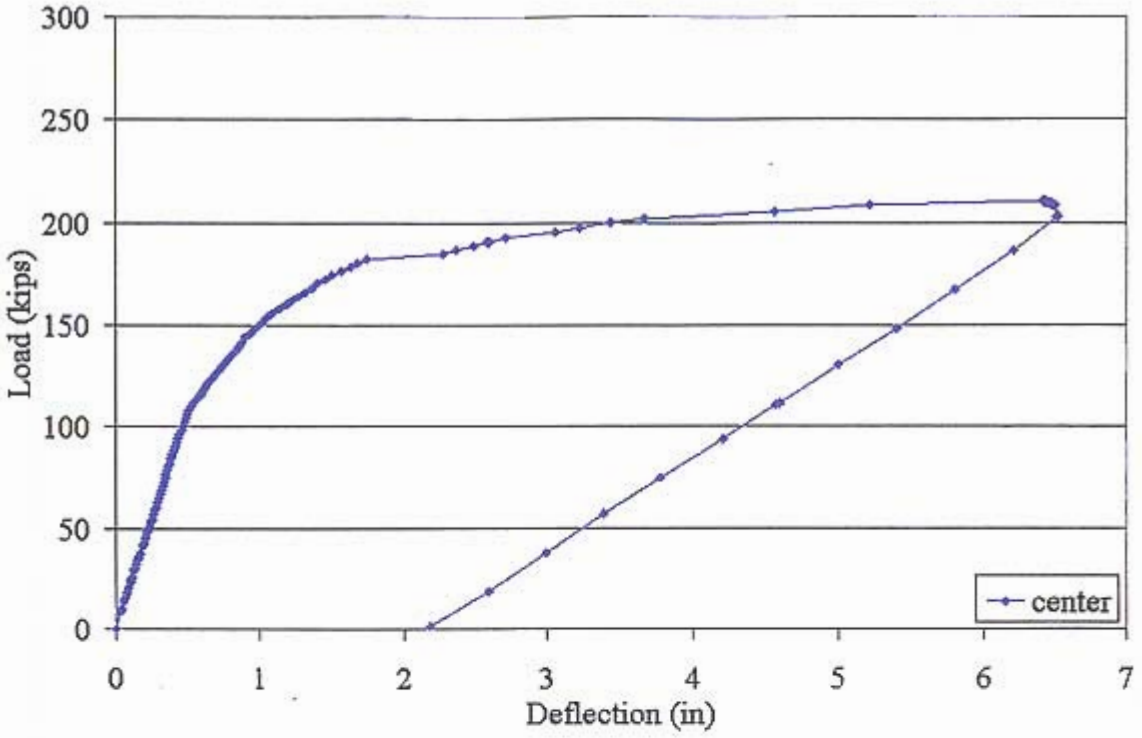

Figure 4-7: Test Specimen 2 Load versus Midspan Deflection Curve

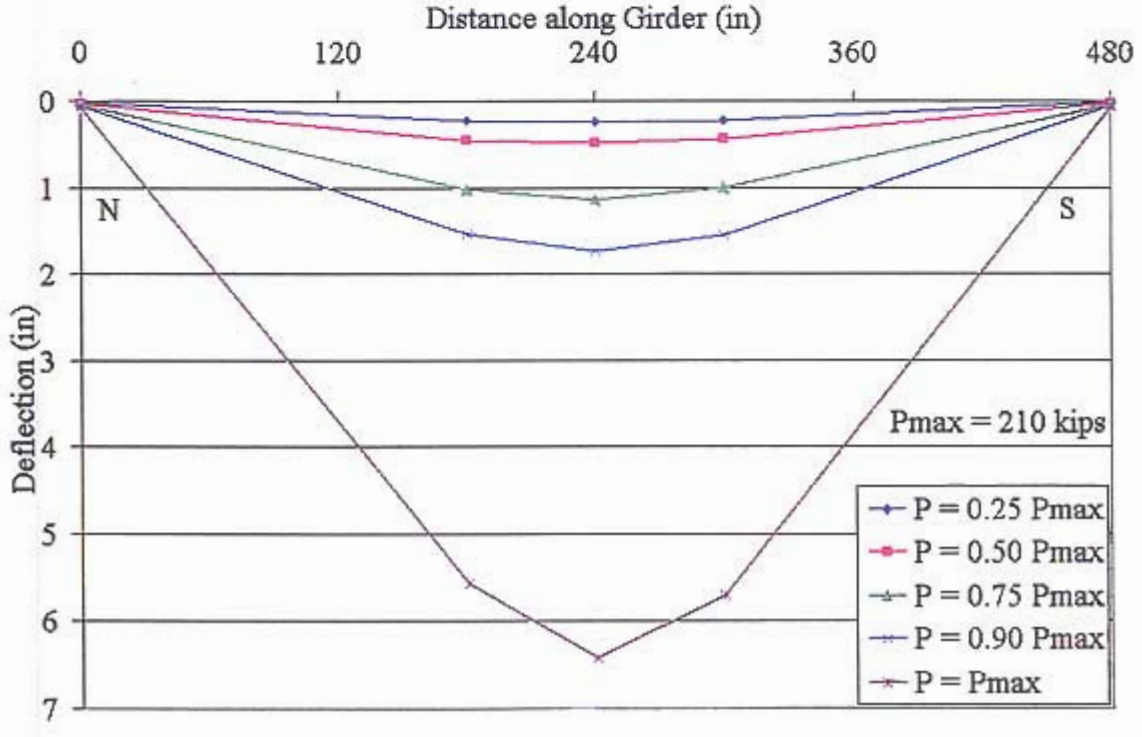

Figure 4-8: Test Specimen 2 Measured Deflection Profile

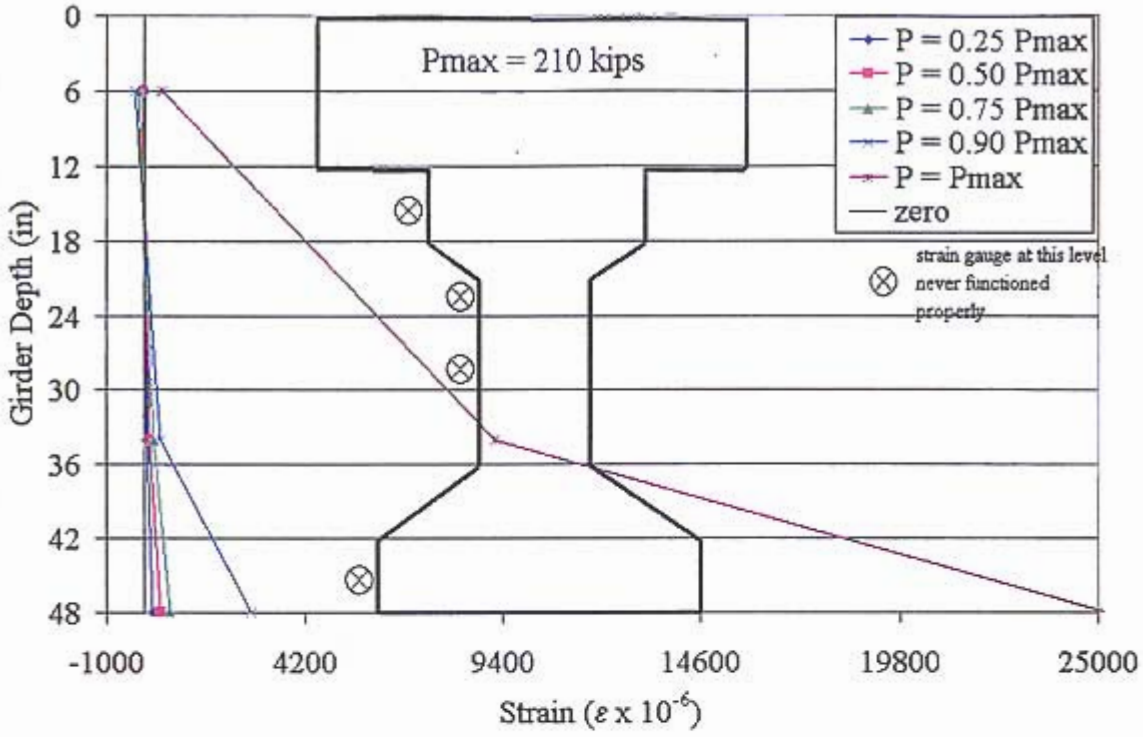

Figure 4-9: Test Specimen 2 Strain Profile at North Load Point

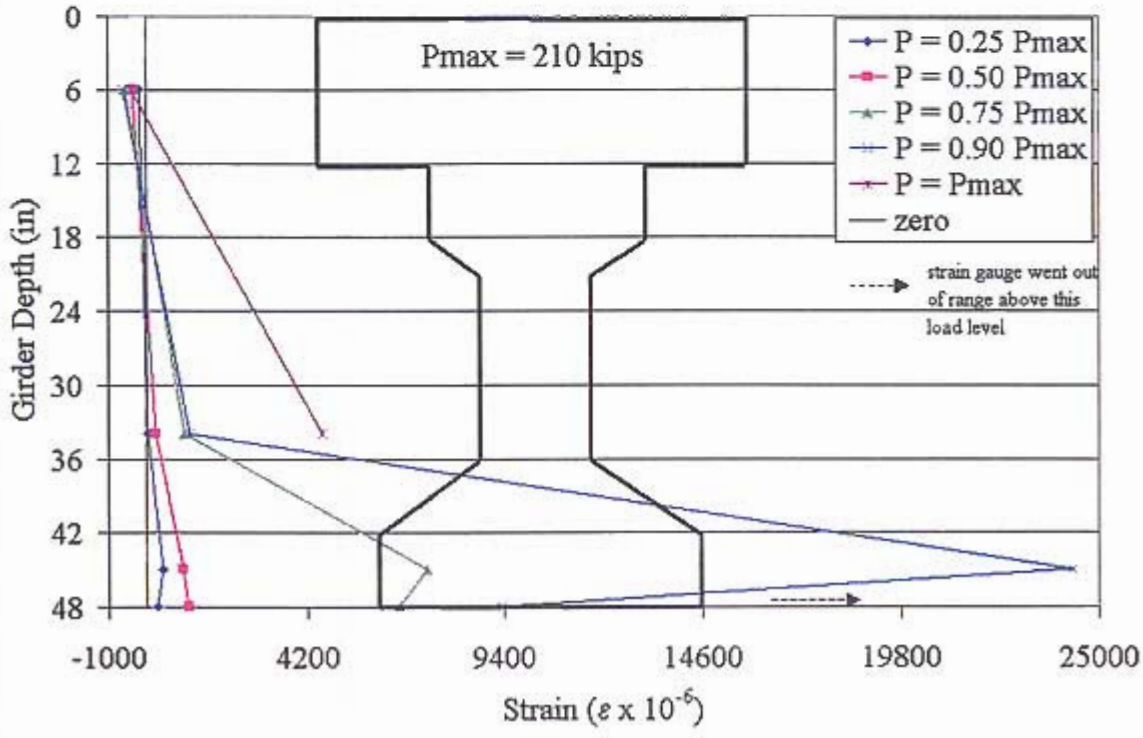

Figure 4-10: Test Specimen 2 Strain Profile at Midspan

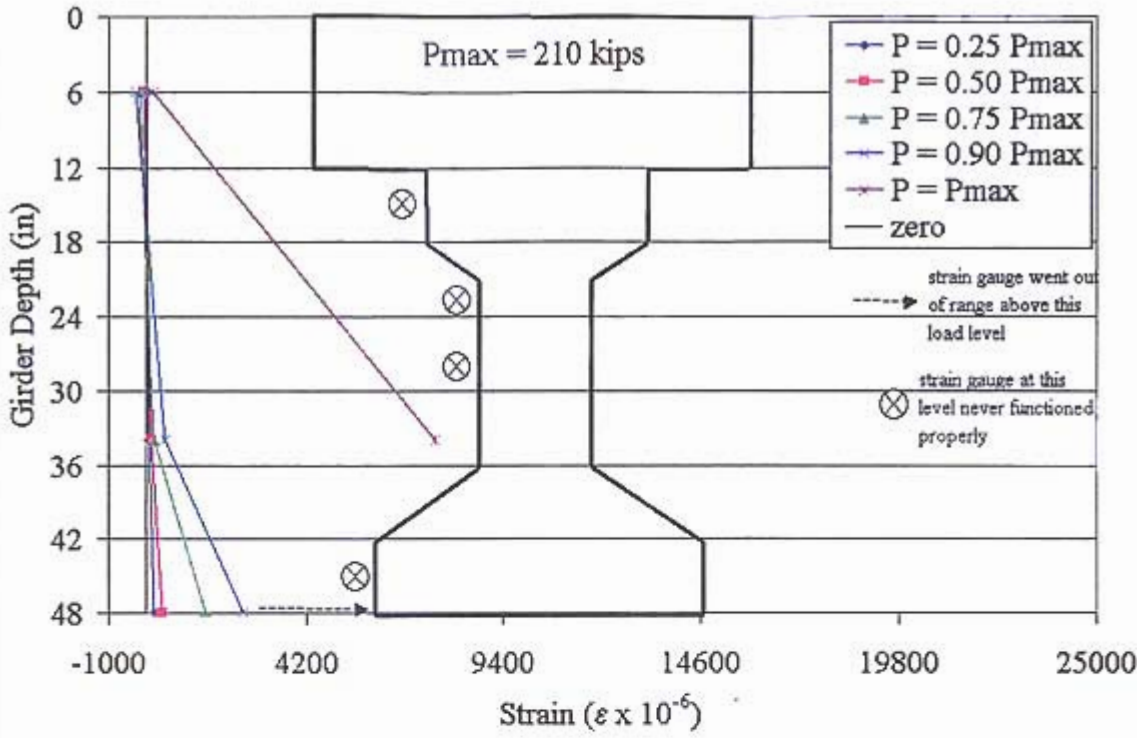

Figure 4-11: Test Specimen 2 Strain Profile at South Load Point

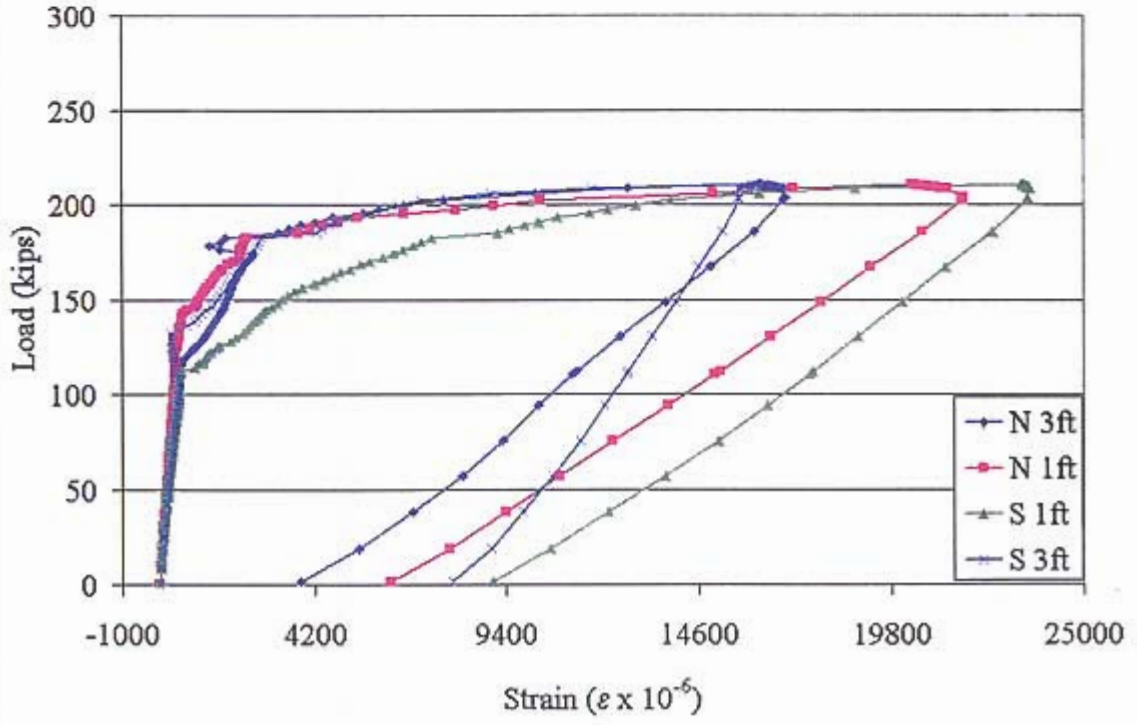

Figure 4-12: Test Specimen 2 Load versus Measured Strain Along Bottom Centerline of Beam

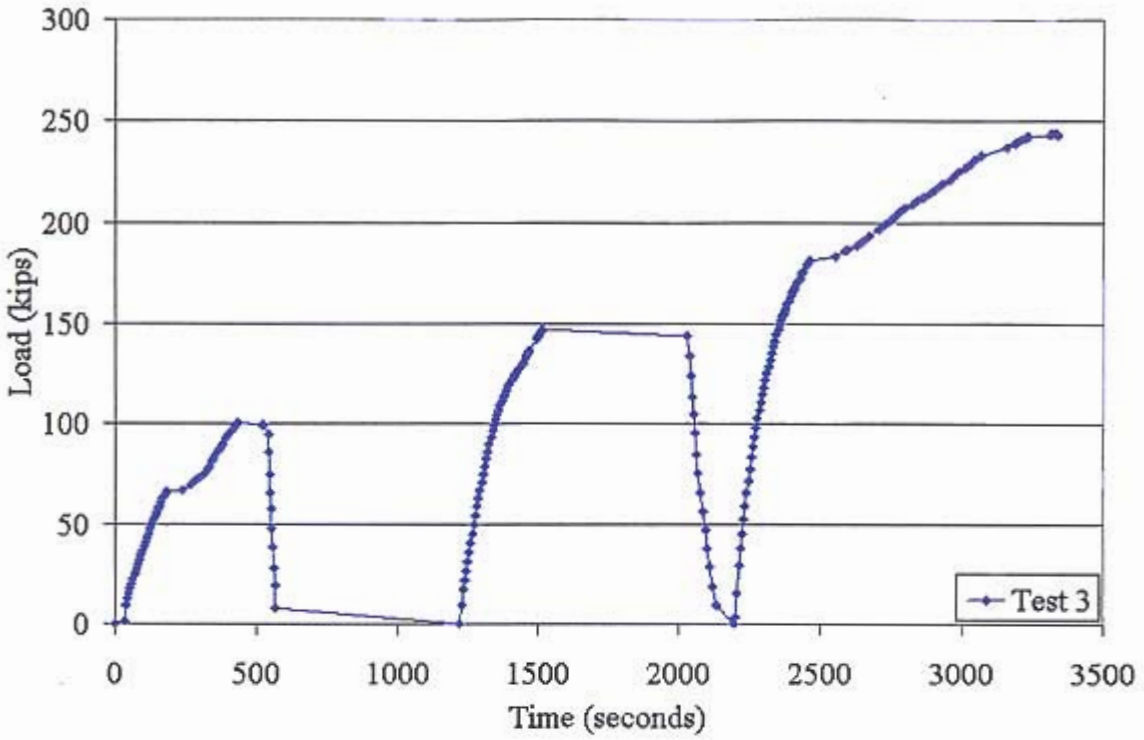

Figure 4-13: Test Specimen 3 Load versus Time Showing Loading and Unloading Cycles

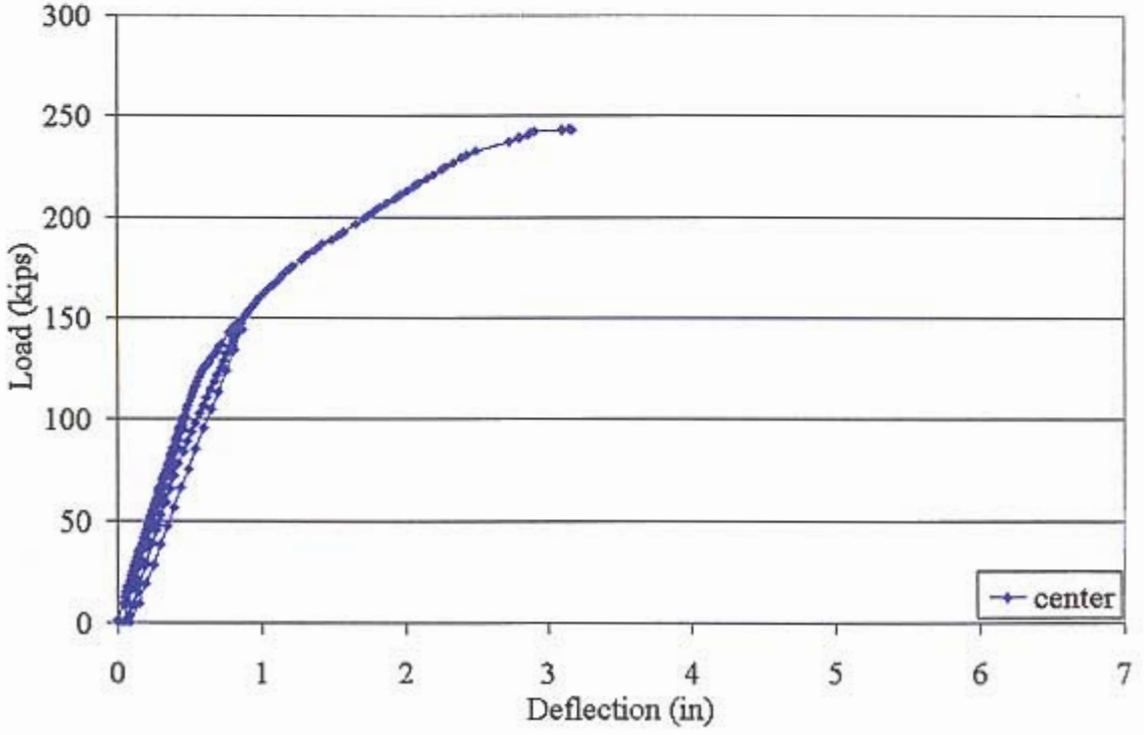

Figure 4-14: Test Specimen 3 Load versus Midspan Deflection Curve

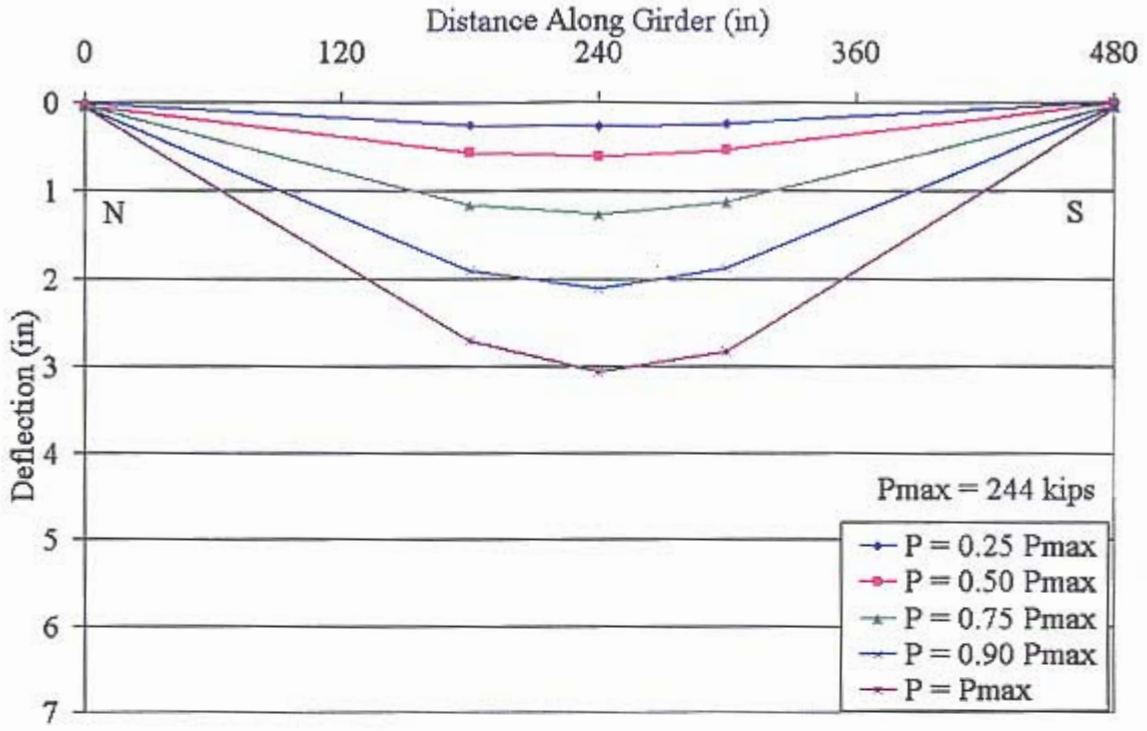

Figure 4-15: Test Specimen 3 Measured Deflection Profile

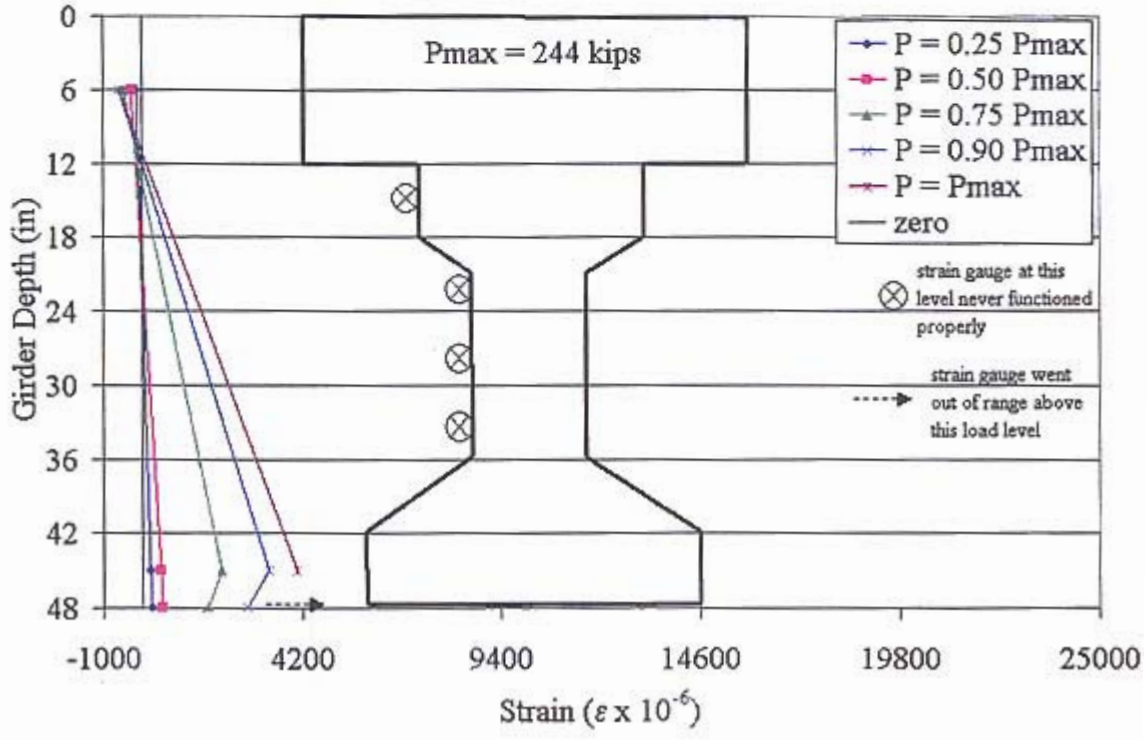

Figure 4-16: Test Specimen 3 Strain Profile at North Load Point

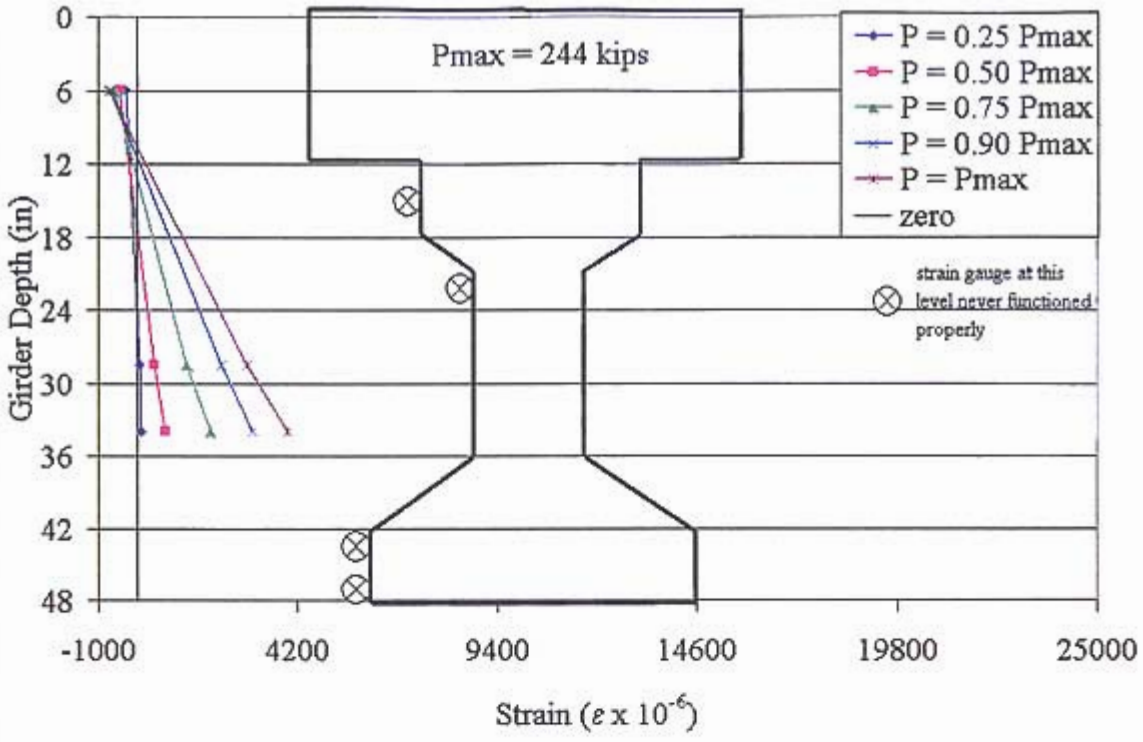

Figure 4-17: Test Specimen 3 Strain Profile at Midspan

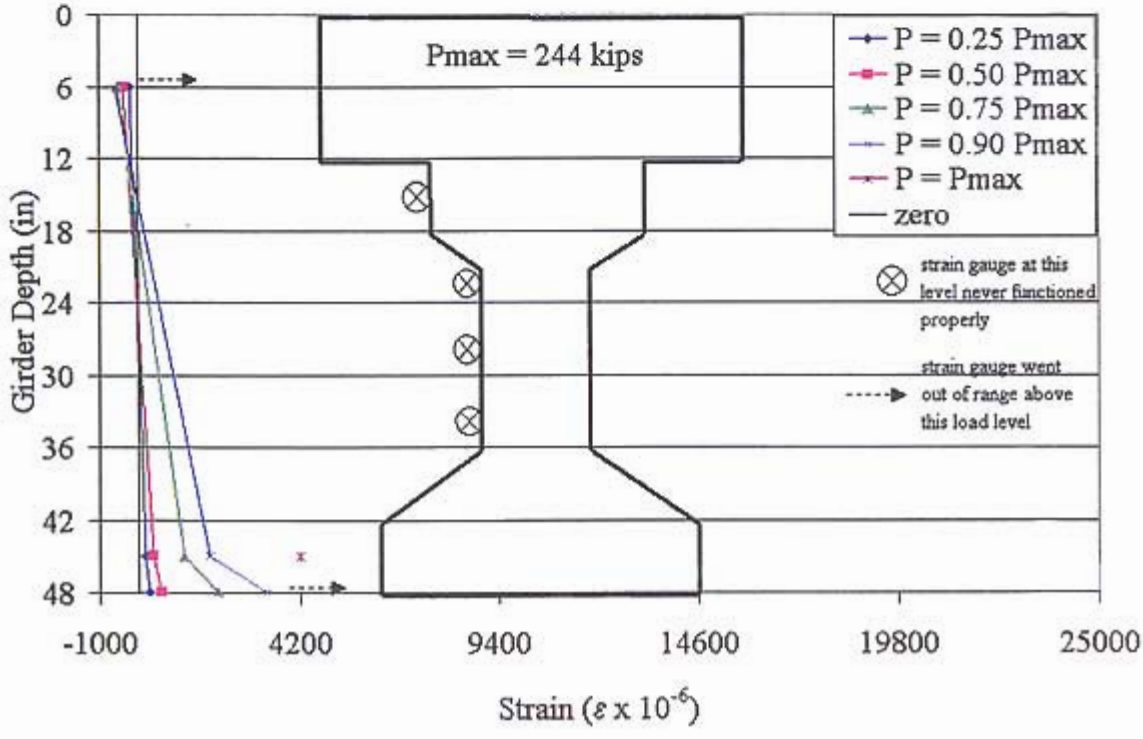

Figure 4-18: Test Specimen 3 Strain Profile at South Load Point

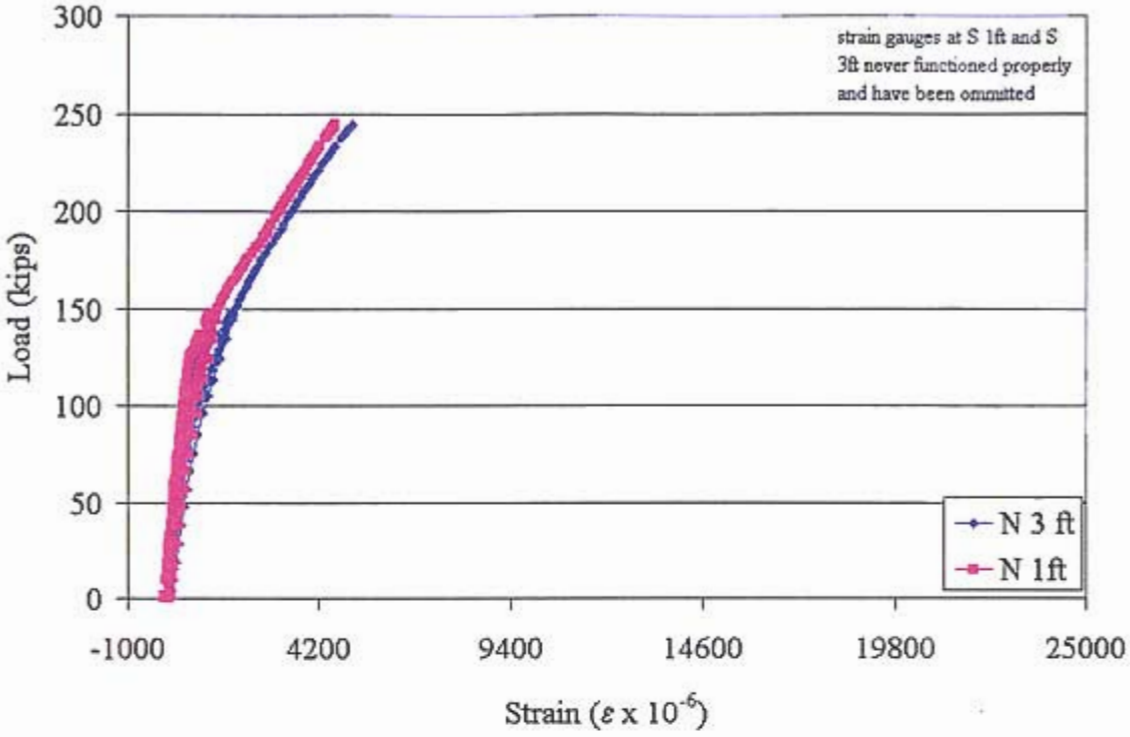

Figure 4-19: Test Specimen 3 Load versus Measured Strain Along Bottom Centerline of Beam

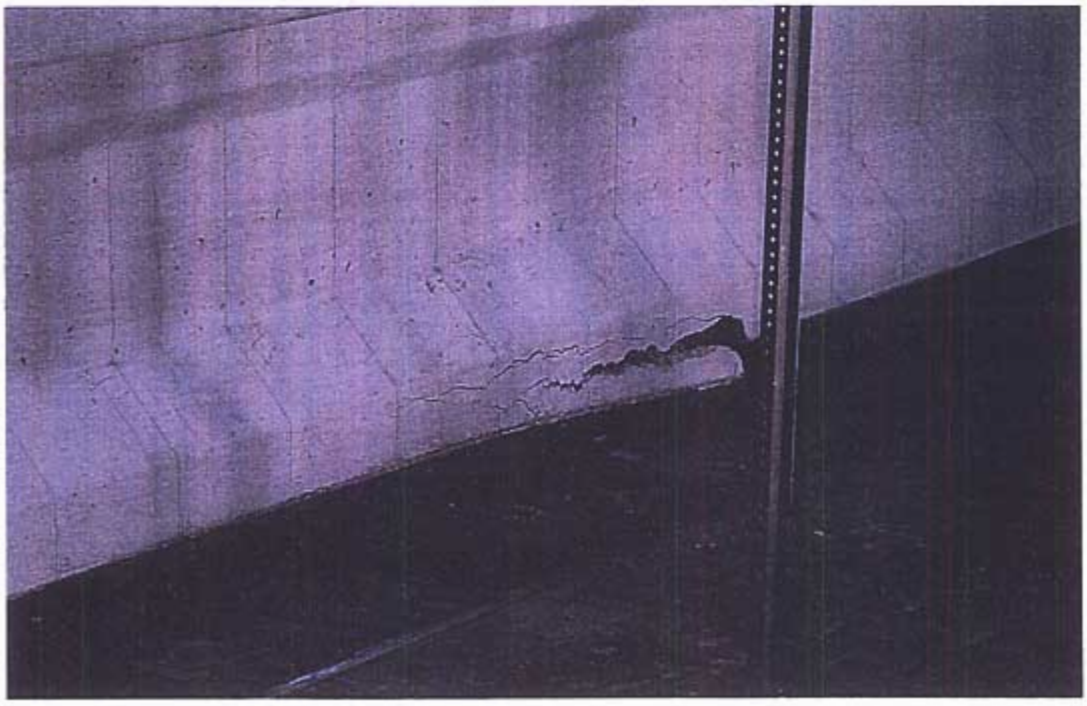

Figure 4-20: Test Specimen 3 During Loading Showing Crack Propagation on South End of Girder at the Bottom Layer of Prestressing

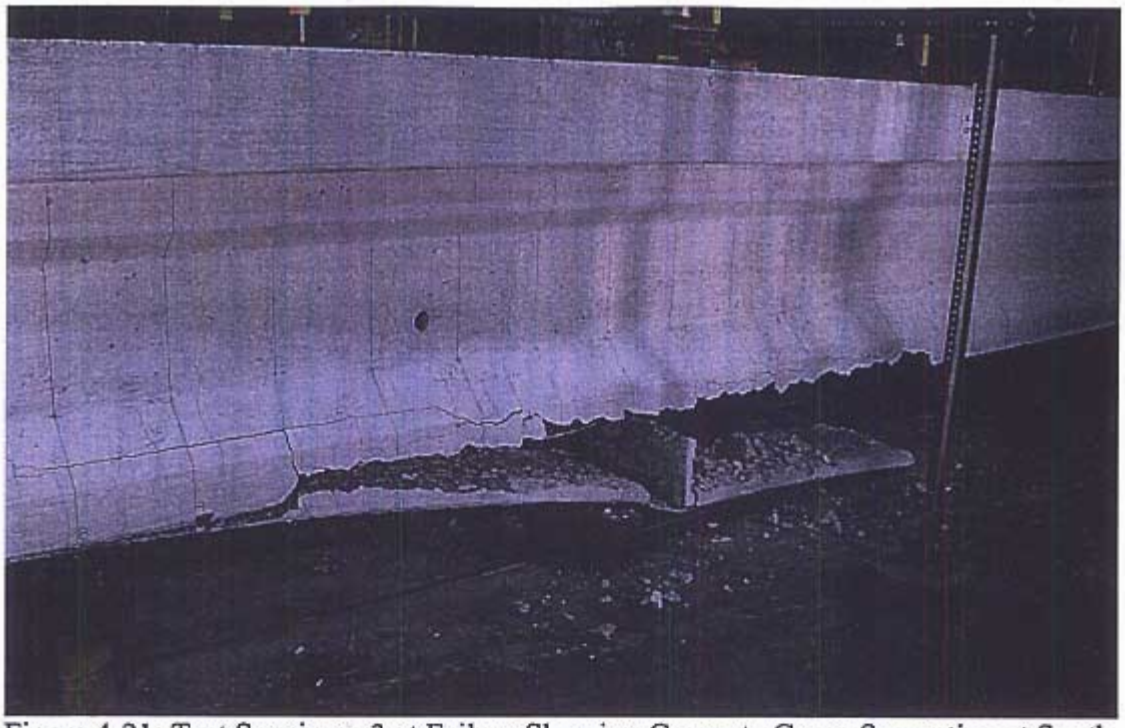

Figure 4-21: Test Specimen 3 at Failure Showing Concrete Cover Separation at South End

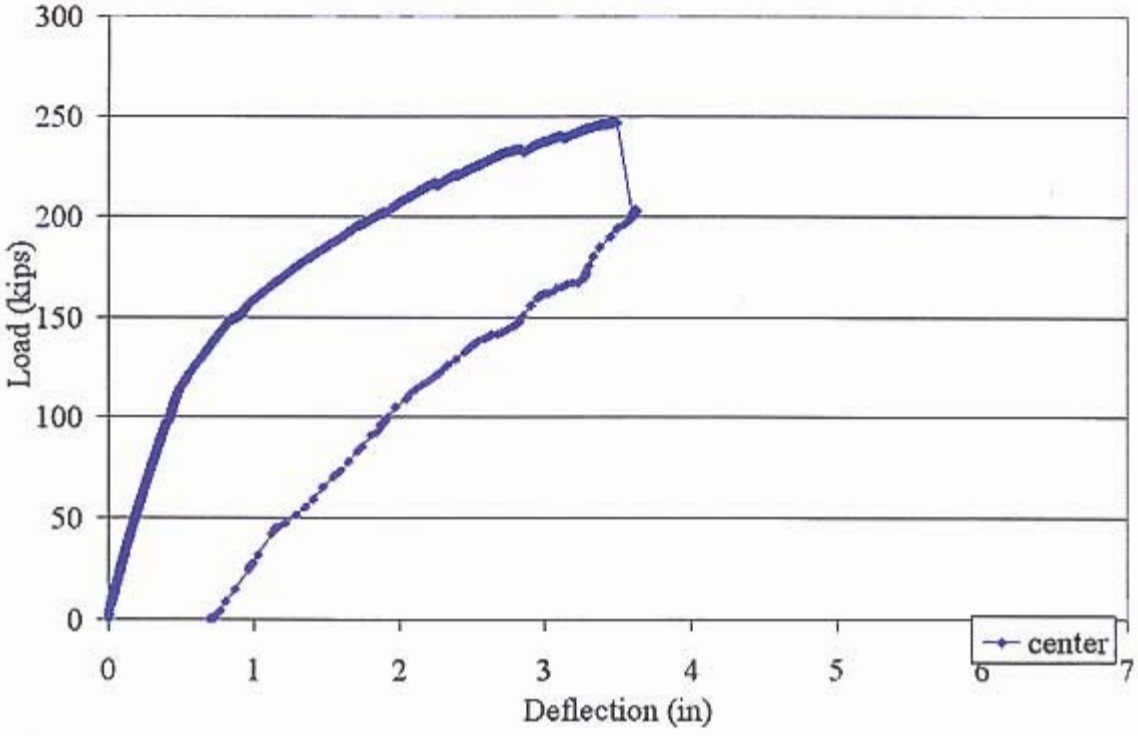

Figure 4-22: Test Specimen 4 Load versus Midspan Deflection Curve

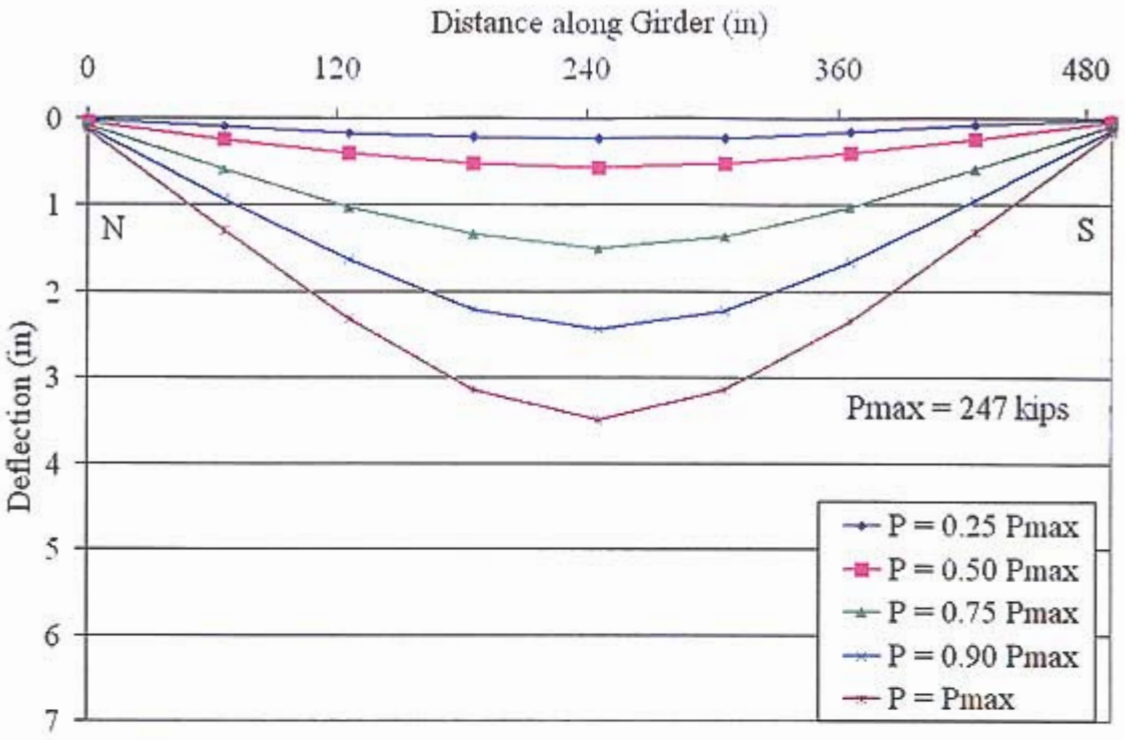

Figure 4-23: Test Specimen 4 Measured Deflection Profile

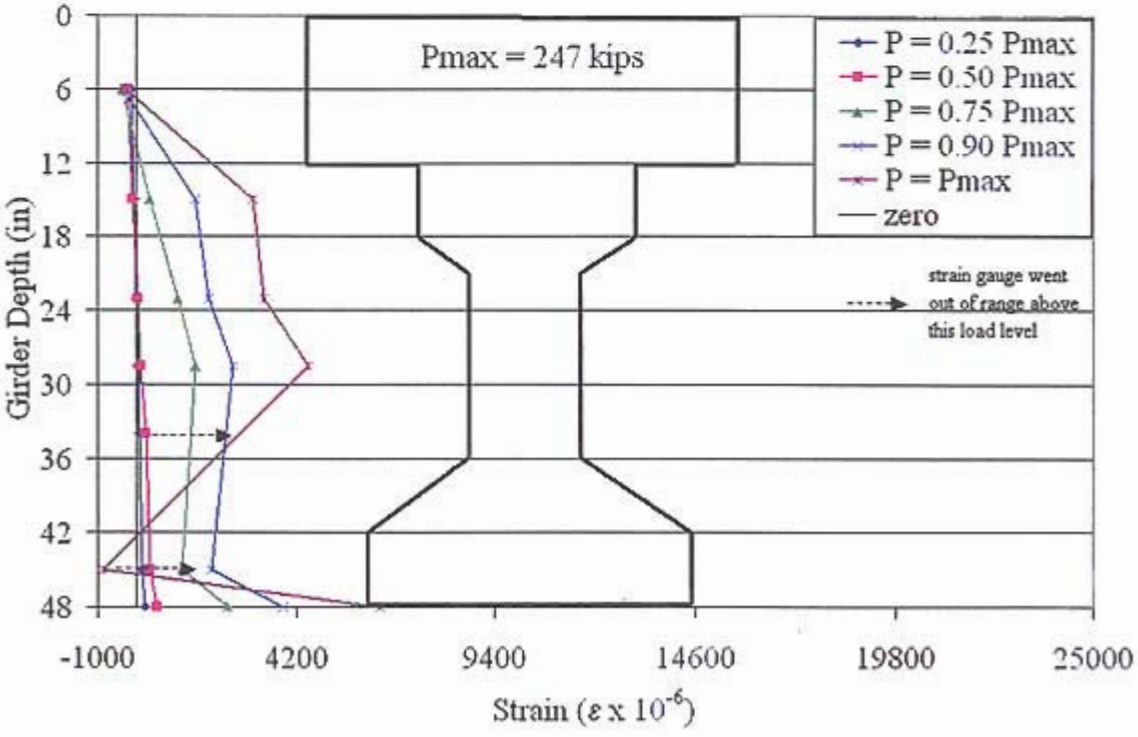

Figure 4-24: Test Specimen 4 Strain Profile at North Load Point

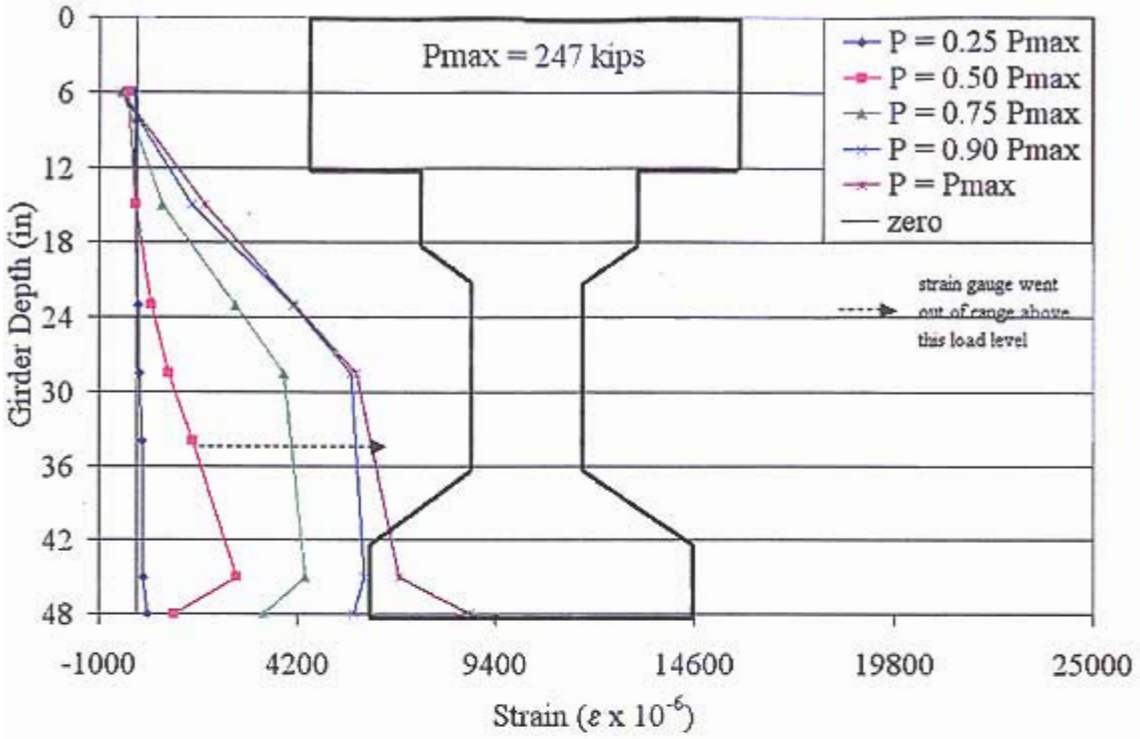

Figure 4-25: Test Specimen 4 Strain Profile at Midspan

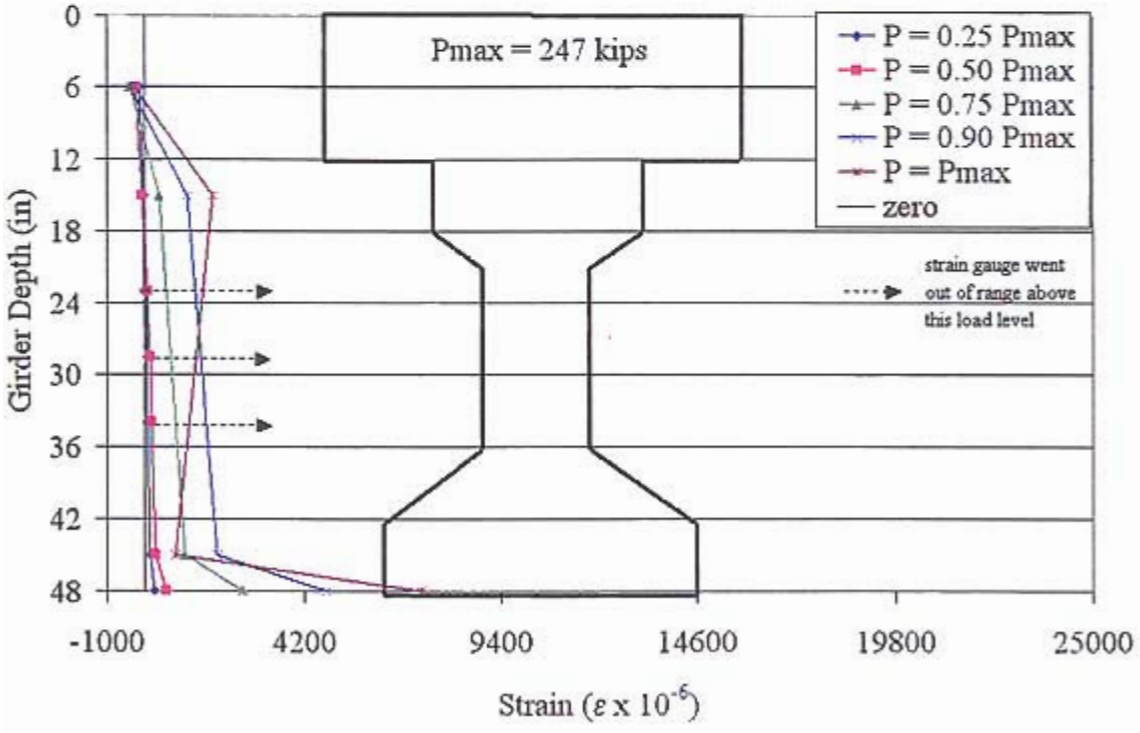

Figure 4-26: Test Specimen 4 Strain Profile at South Load Point

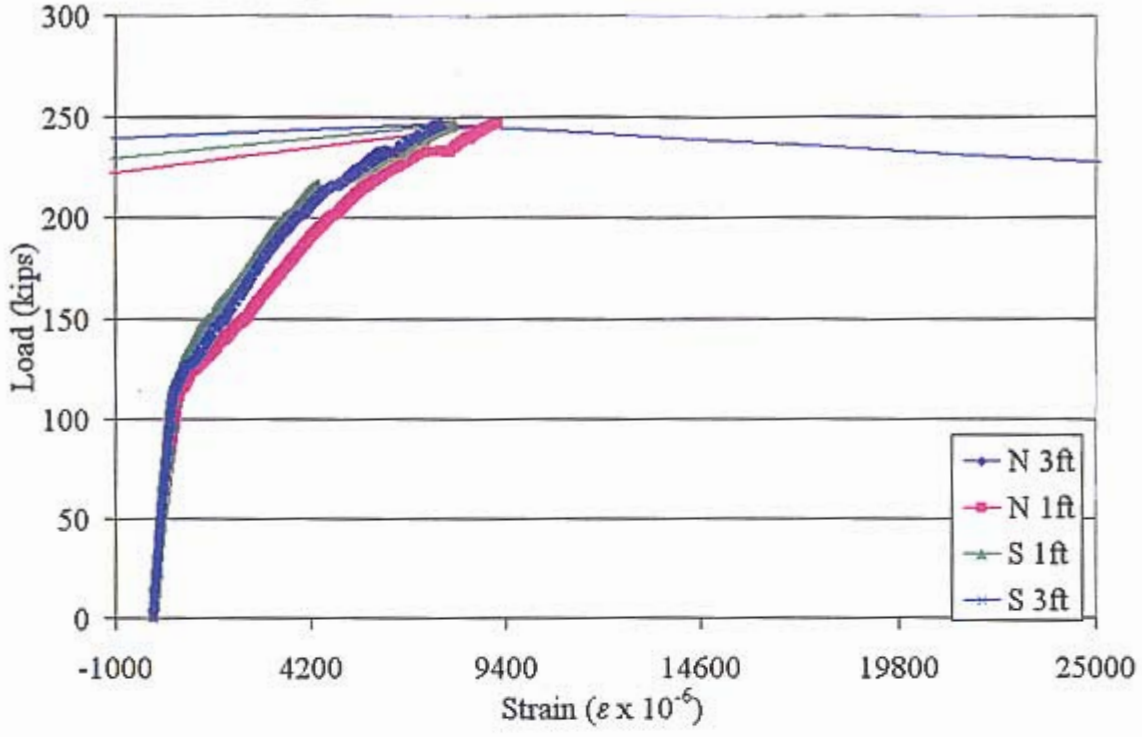

Figure 4-27: Test Specimen 4 Load versus Measured Strain Along Bottom Centerline of Beam

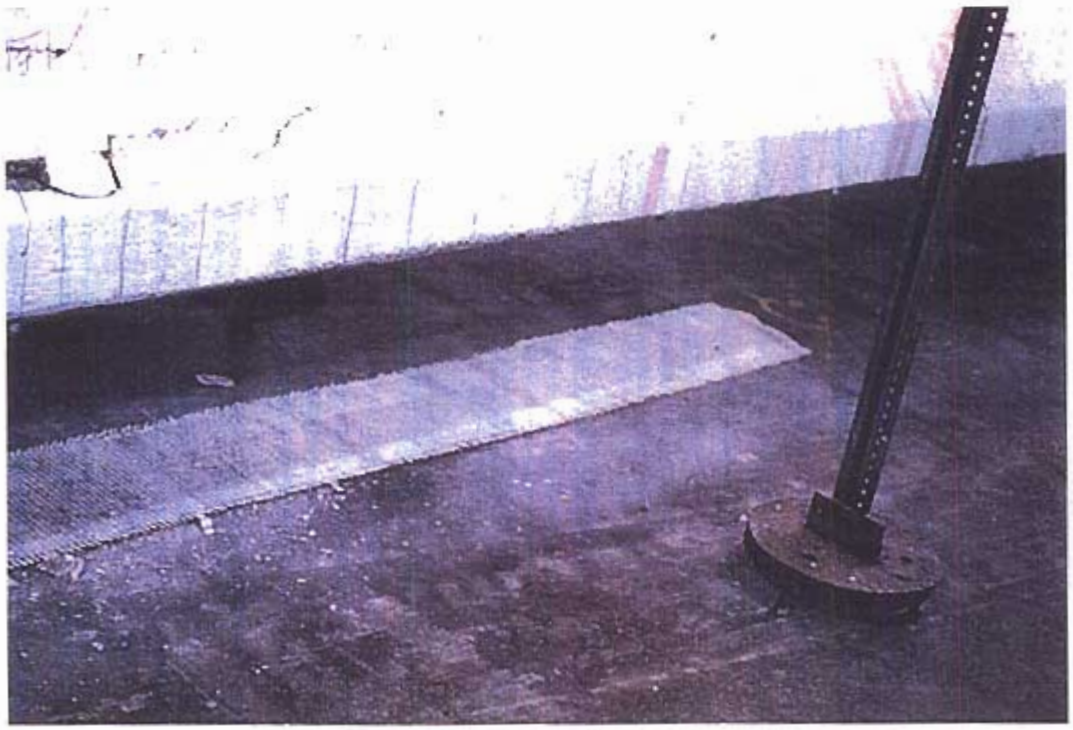

Figure 4-28: Test Specimen 4 at Failure Showing Separation of FRP

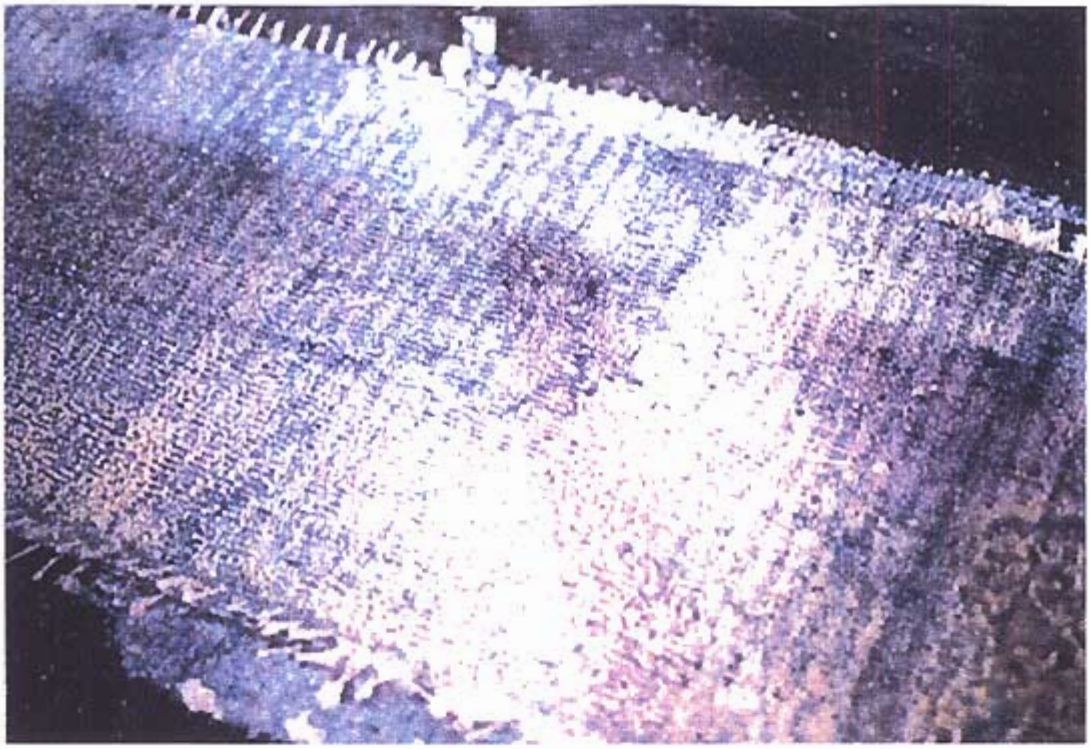

Figure 4-29: Test Specimen 4 at Failure Showing Shearing of FRP Stirrup

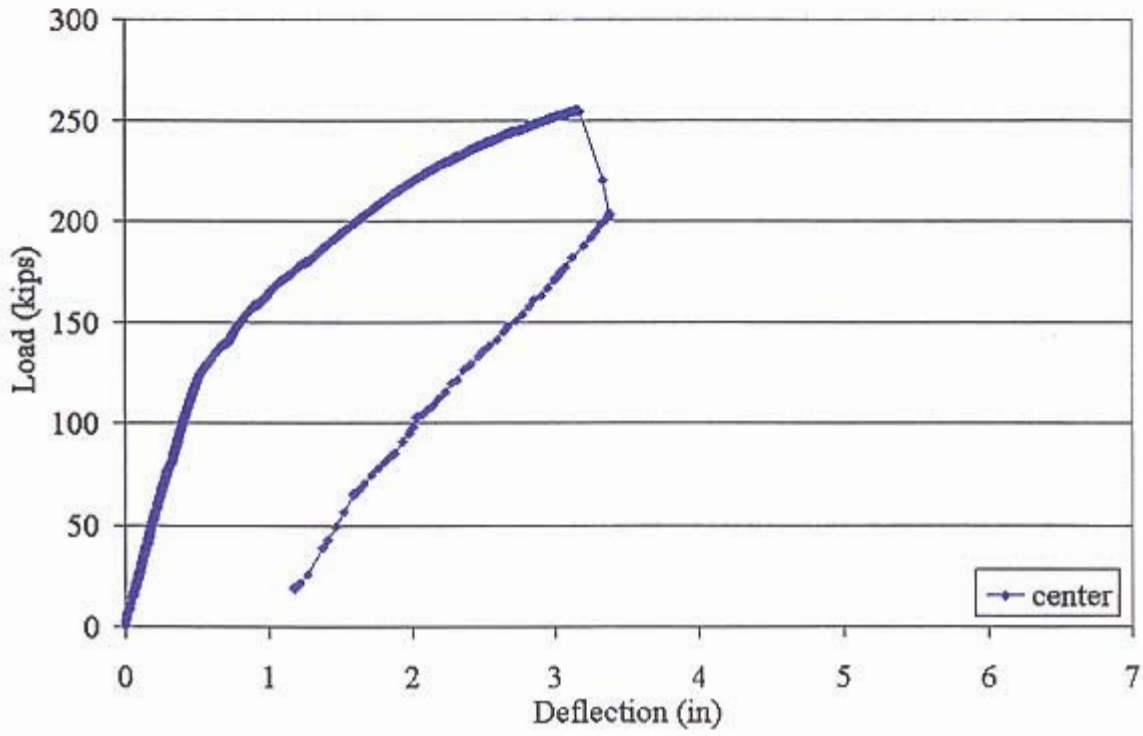

Figure 4-30: Test Specimen 5 Load versus Midspan Deflection Curve

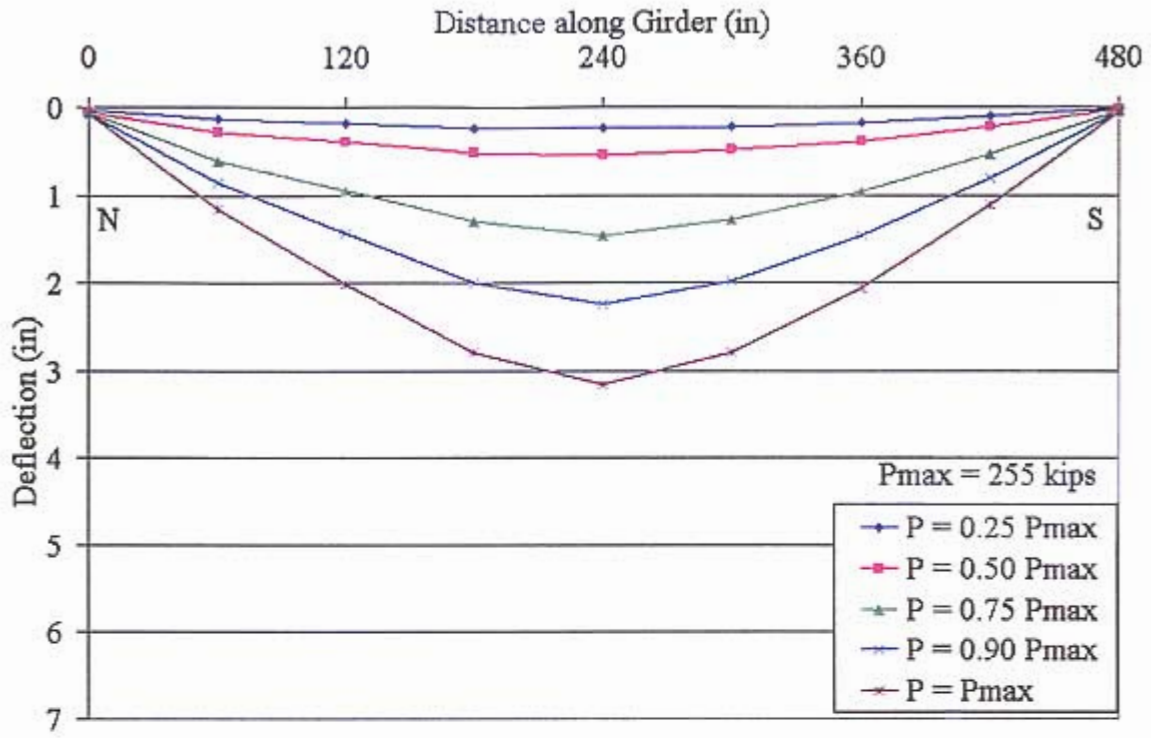

Figure 4-31: Test Specimen 5 Measured Deflection Profile

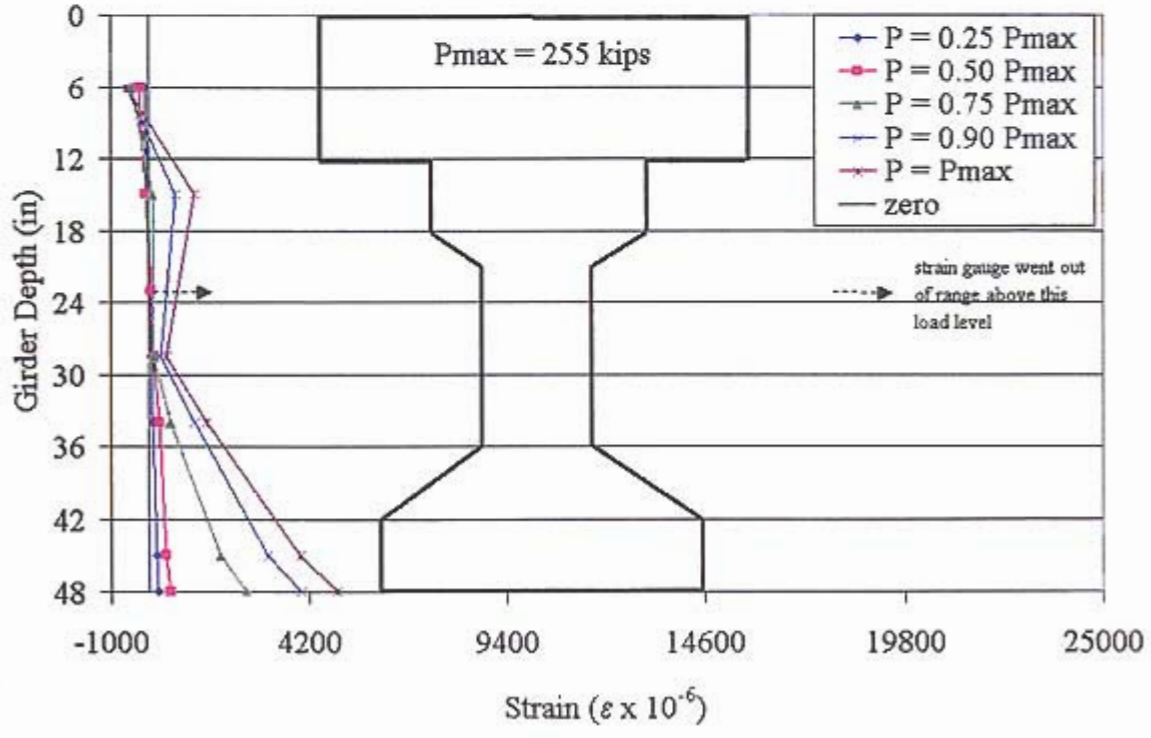

Figure 4-32: Test Specimen 5 Strain Profile at North Load Point

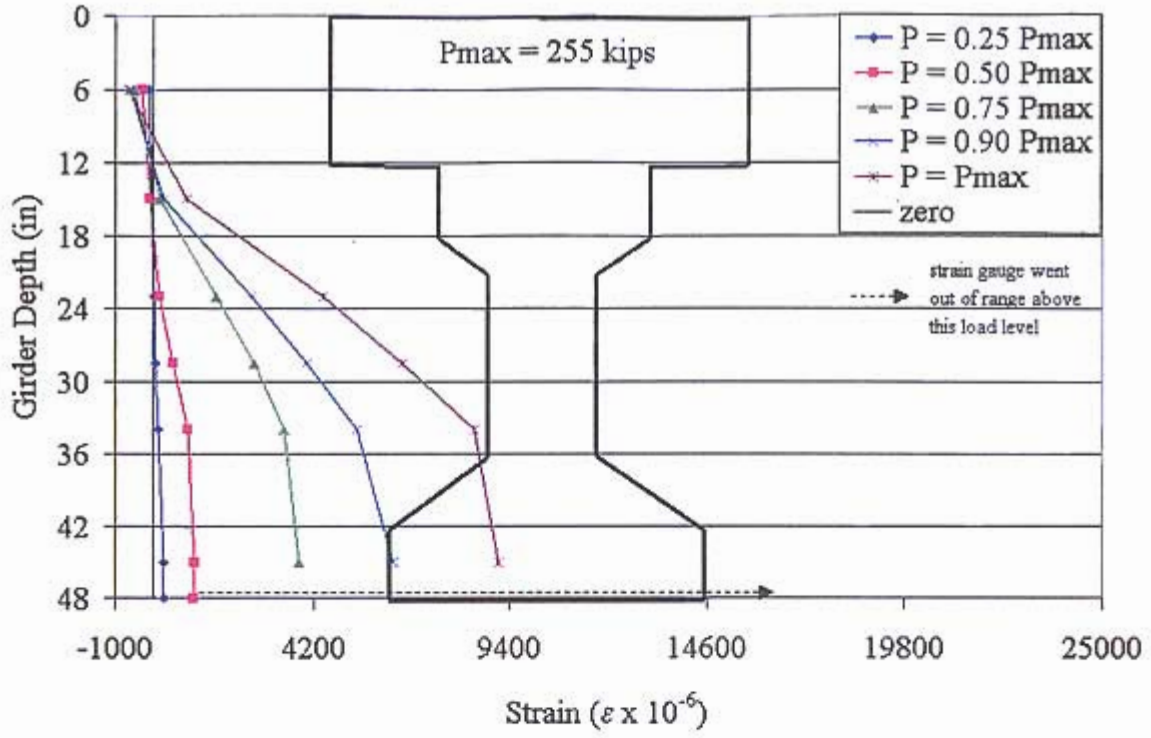

Figure 4-33: Test Specimen 5 Strain Profile at Midspan

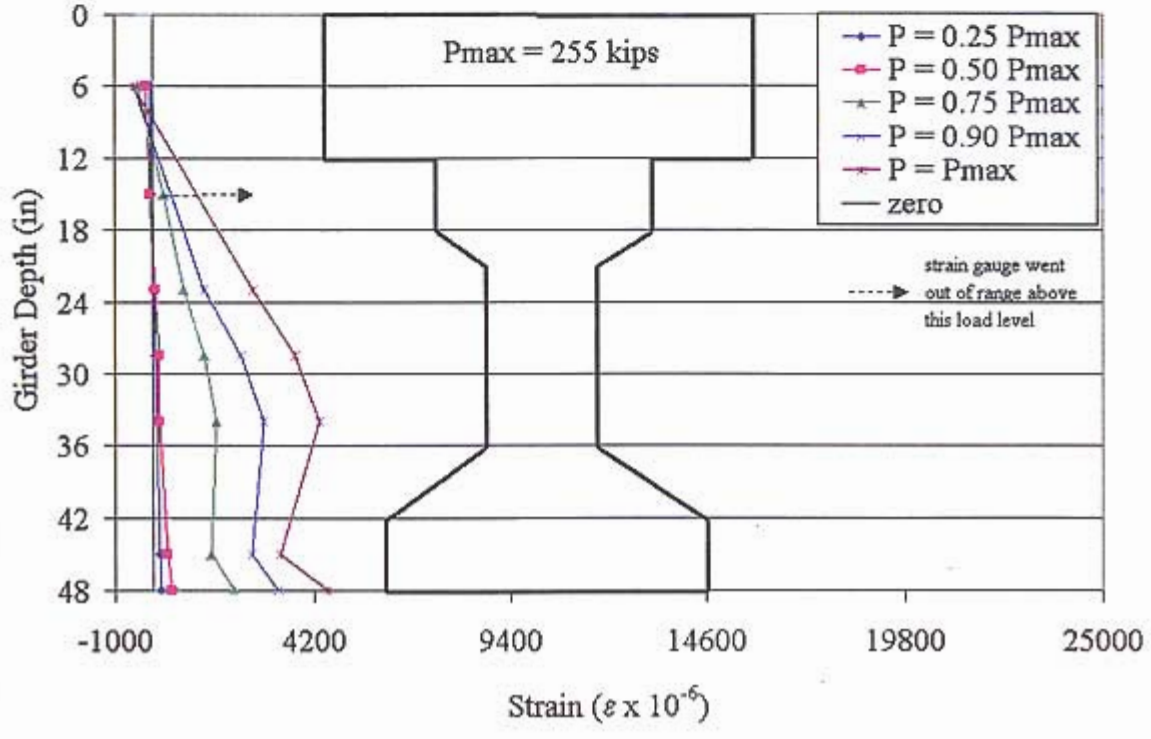

Figure 4-34: Test Specimen 5 Strain Profile at South Load Point

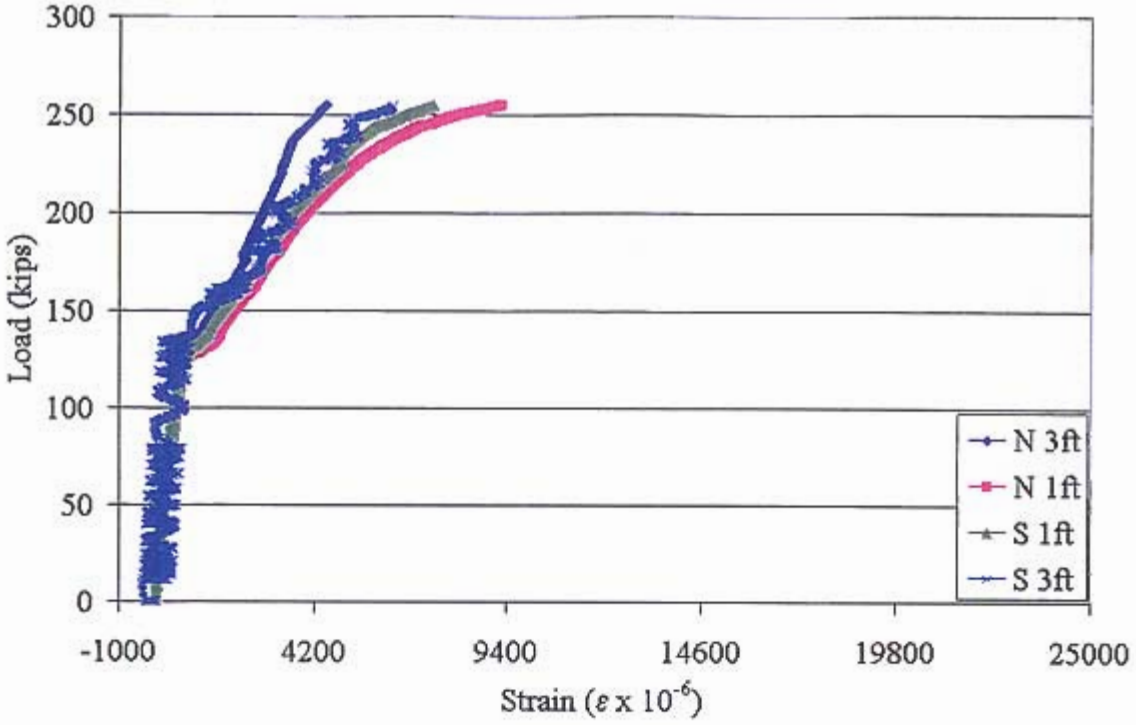

Figure 4-35: Test Specimen 5 Load versus Measured Strain Along Bottom Centerline of Beam

Figure 4-36: Test Specimen 5 at Failure Showing Rupture of FRP at Midspan

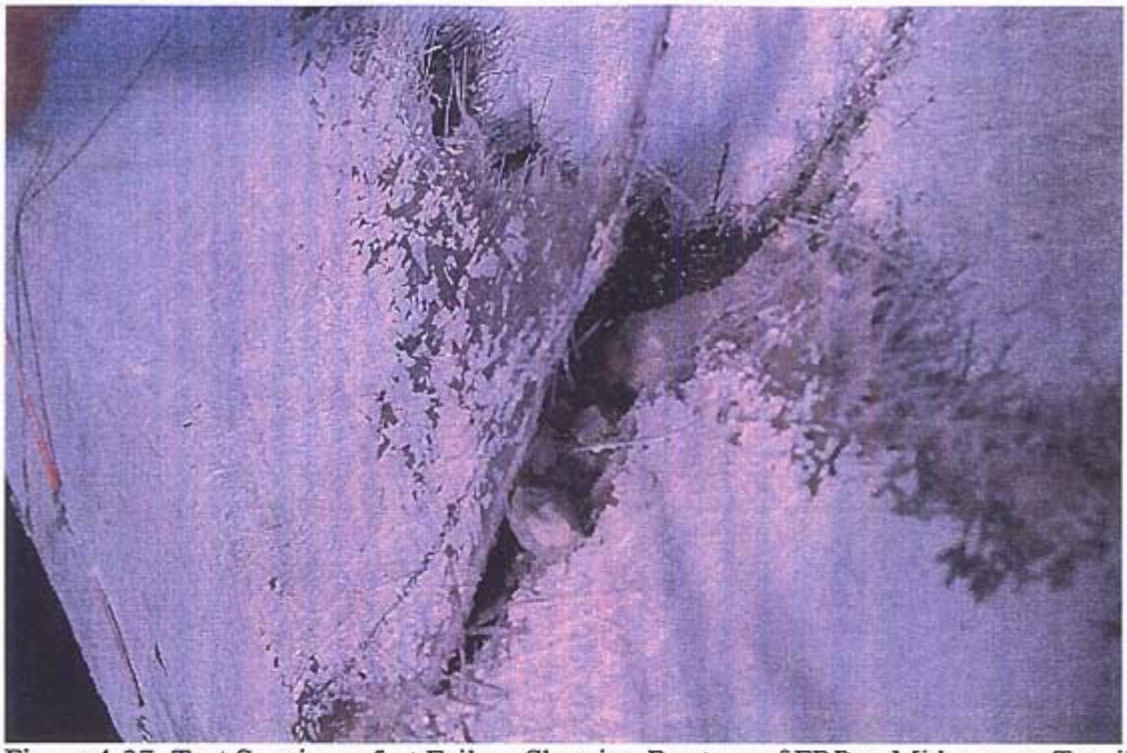

Figure 4-37: Test Specimen 5 at Failure Showing Rupture of FRP at Midspan on Tensile Face of Girder

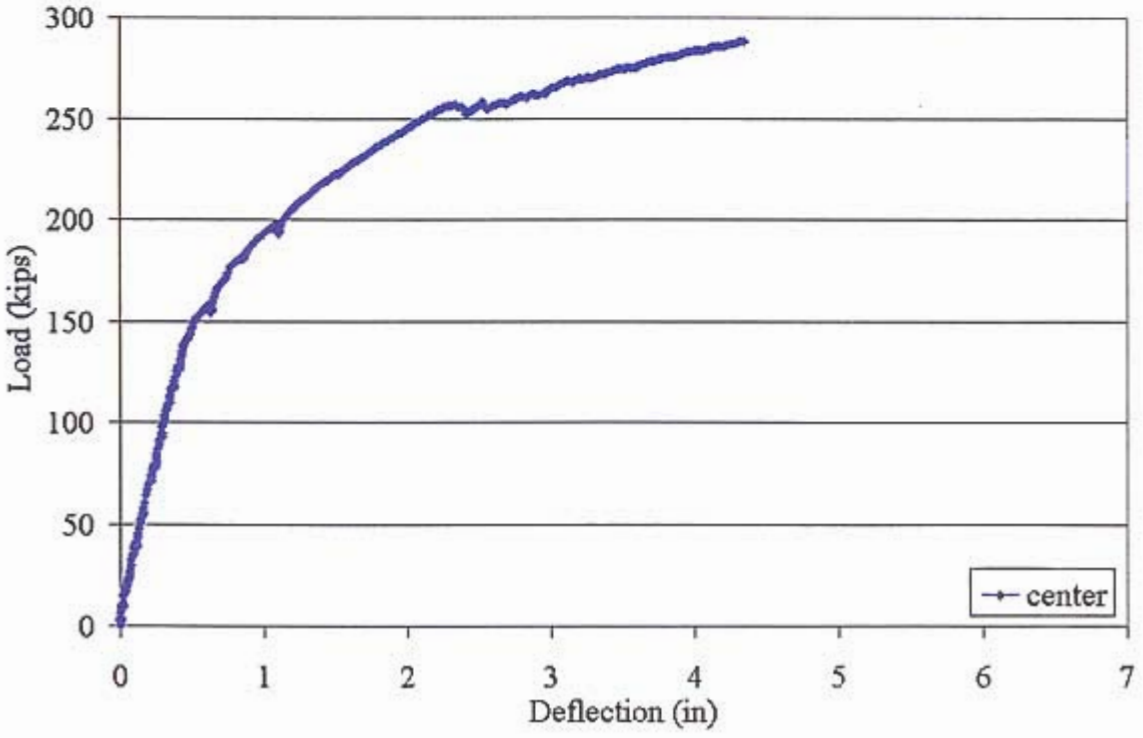

Figure 4-38: Test Specimen 6 Load versus Midspan Deflection Curve

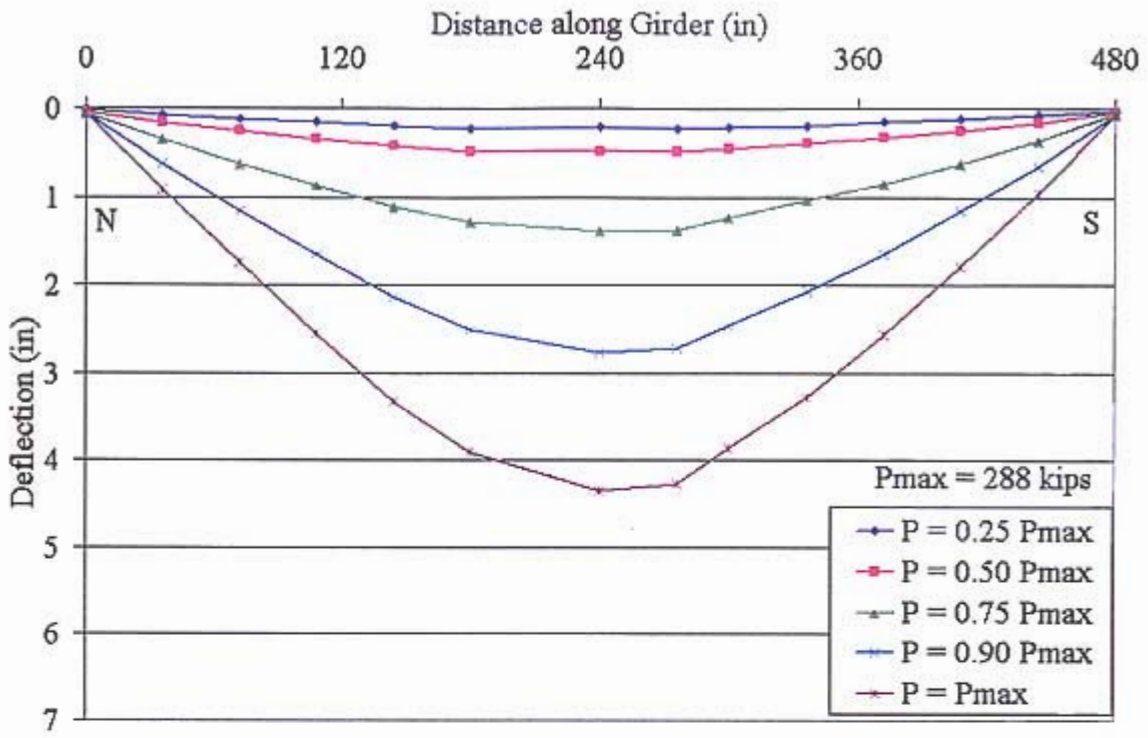

Figure 4-39: Test Specimen 6 Measured Deflection Profile

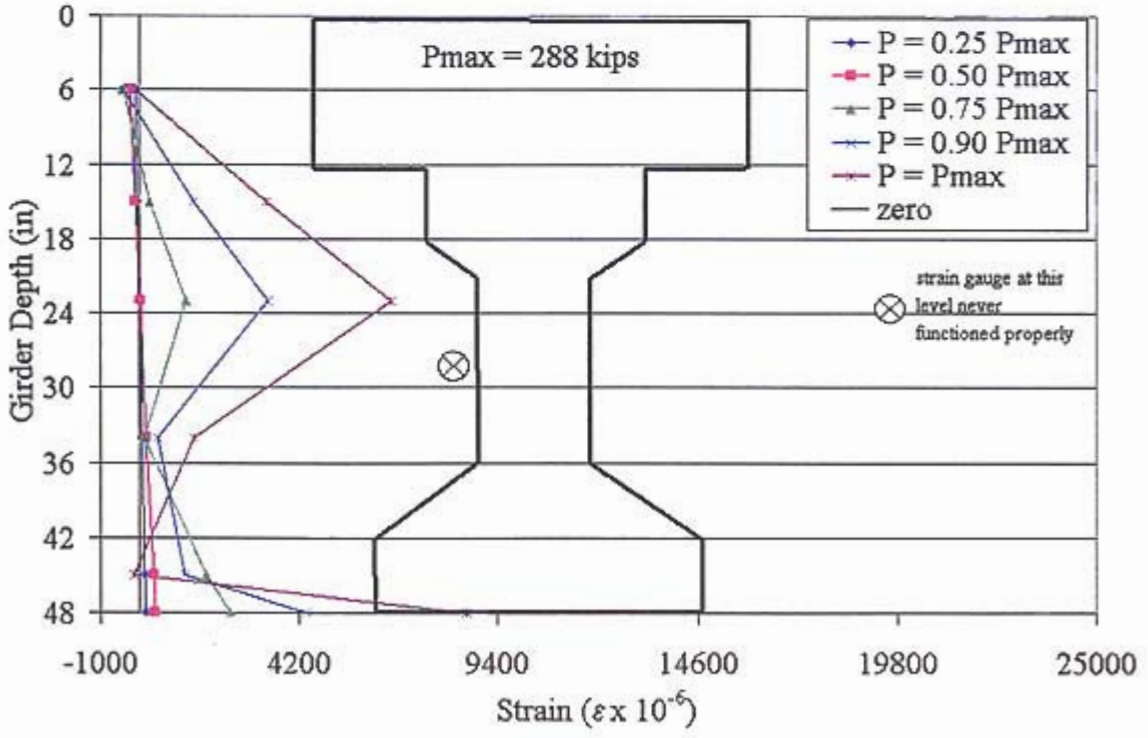

Figure 4-40: Test Specimen 6 Strain Profile at North Load Point

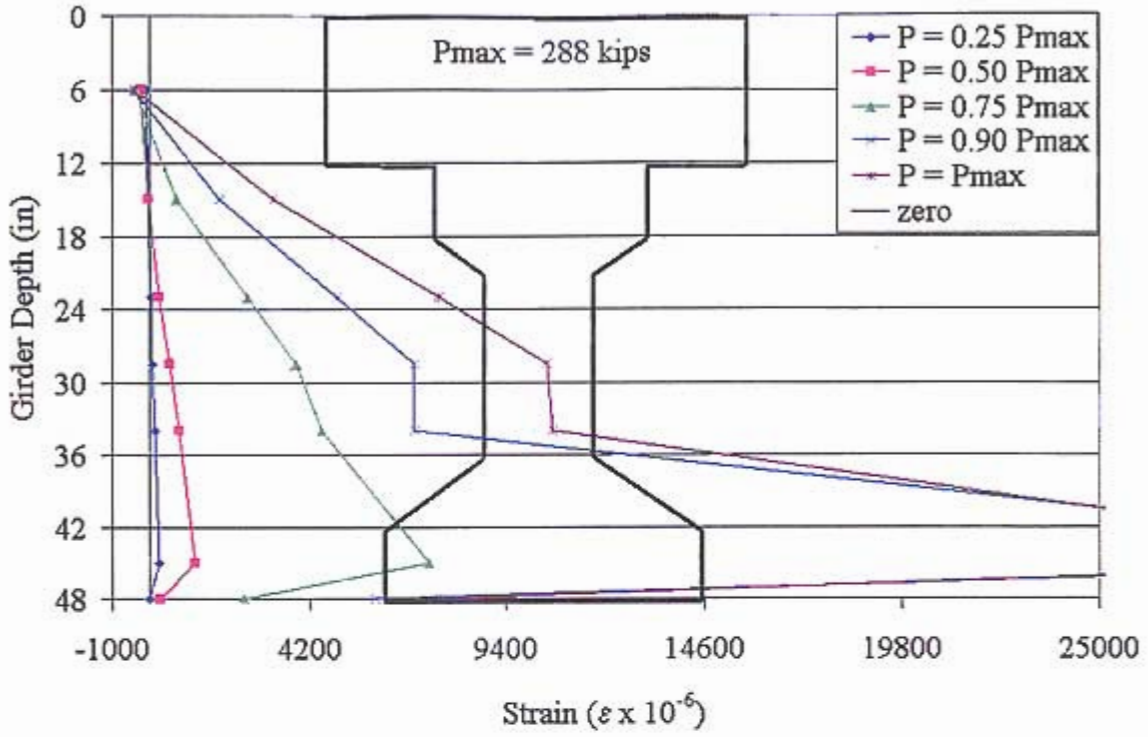

Figure 4-41: Test Specimen 6 Strain Profile at Midspan

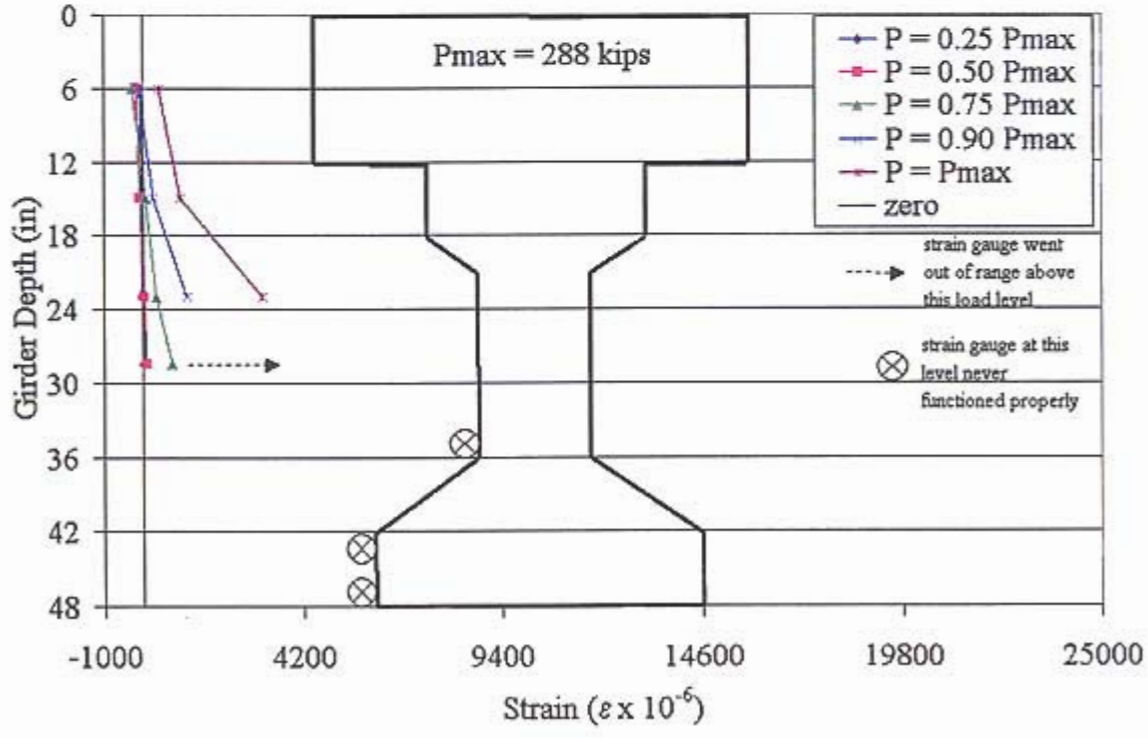

Figure 4-42: Test Specimen 6 Strain Profile at South Load Point

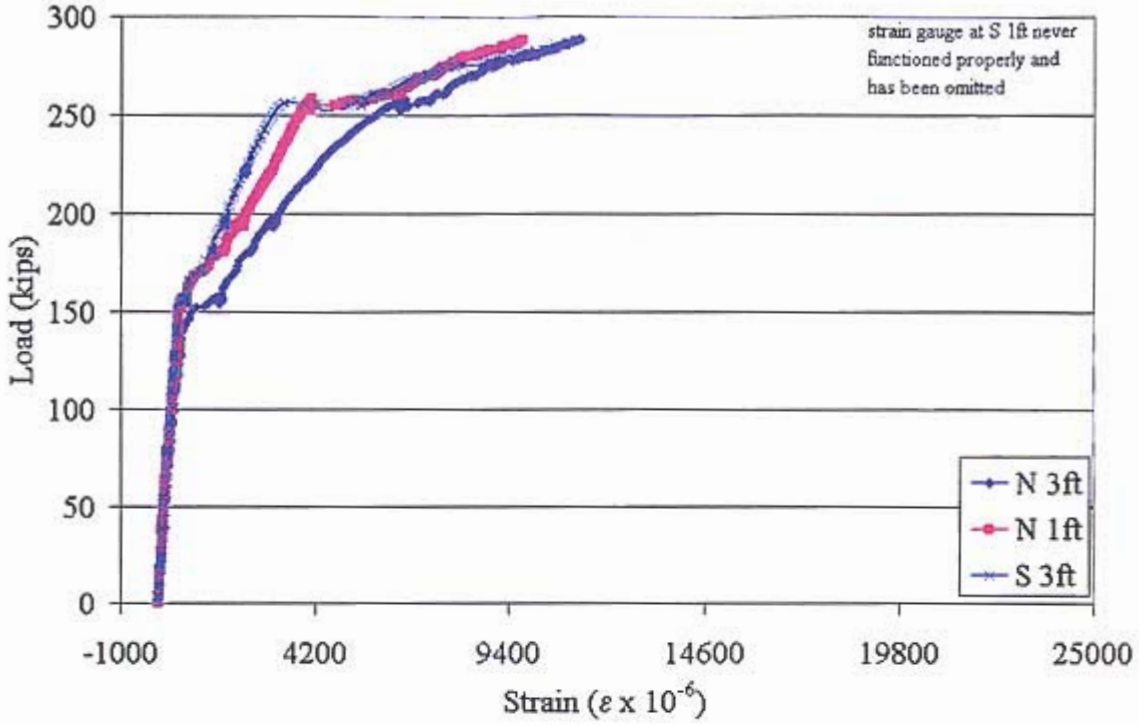

Figure 4-43: Test Specimen 6 Load versus Measured Strain Along Bottom Centerline of Beam

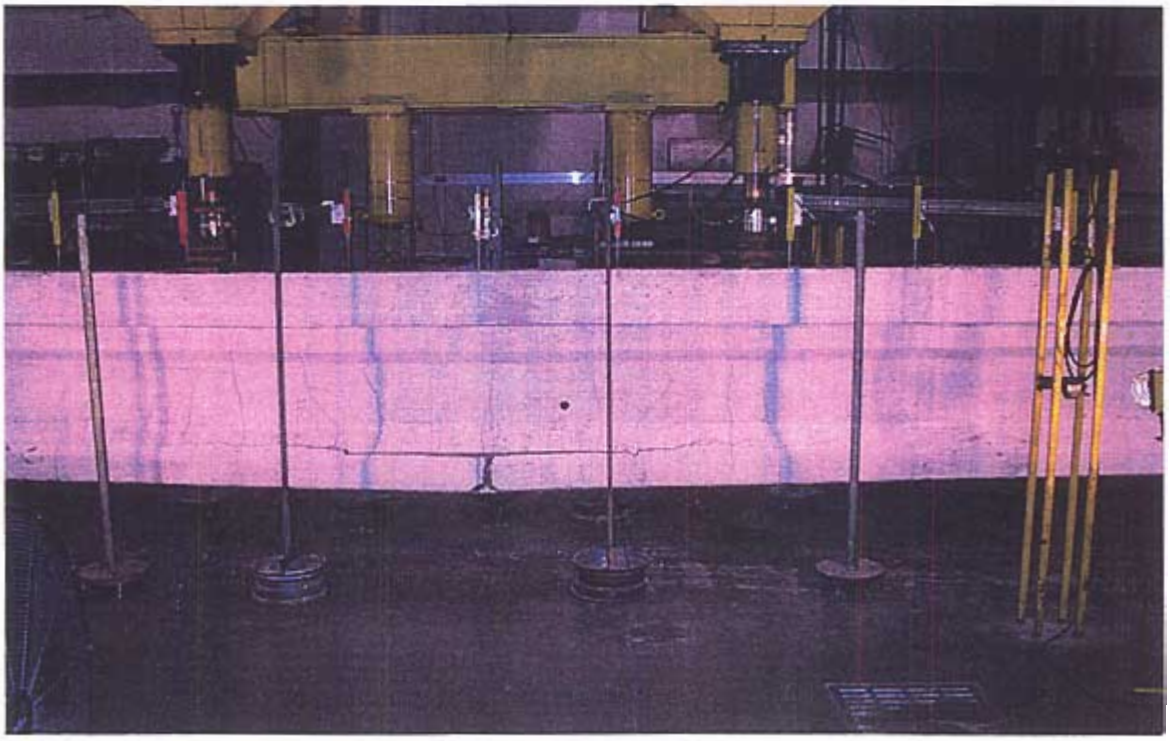

Figure 4-44: Test Specimen 6 at Failure Showing Significant Cracking in Patched Area

Figure 4-45: Test Specimen 6 at Failure Showing Anchorage Slip

CHAPTER 5
ANALYTICAL TEST RESULTS

This chapter provides a description of the methods used to calculate theoretical capacities of the test specimens and a comparison between the calculated theoretical capacities and experimental capacities. Appendix B contains the following theoretical computations presented in this chapter: effective prestress, theoretical cracking capacity for the test specimens in the undamaged and damaged state, theoretical maximum capacity for the test specimens in the undamaged and damaged state, maximum capacities of Test Specimens 3, 4, 5, and 6, support conditions, and midspan deflection at the maximum load for Test Specimen 1.

Calculation of Effective Prestress

In order to calculate theoretical values of the cracking and ultimate loads for the test specimens, it was necessary to determine the effective prestress for stress-relieved prestressing strands. Effective prestress is defined as the stress remaining in the prestressing steel after all losses have occurred (ACI 1996). The total losses that result from prestressing, Δf_T, were found by summing the losses due to elastic shortening of concrete, Δf_{ES}, creep of concrete, Δf_{CR}, shrinkage of concrete, Δf_{SH}, and steel stress relaxation, Δf_{RE}, as shown in Equation 5-1.

$$\Delta f_T = \Delta f_{ES} + \Delta f_{CR} + \Delta f_{SH} + \Delta f_{RE} \tag{5-1}$$

Equations 5-2, 5-3, 5-4, and 5-5 were used to determine the losses due to concrete elastic shortening, concrete creep, concrete shrinkage, and steel stress relaxation, respectively (Precast/Prestressed Concrete Institute 1999).

$$\Delta f_{ES} = K_{ES} n f_{cs} \tag{5-2}$$

where K_{ES} = 1.0 for pretensioned members, n = modular ratio, and f_{cs} = compressive stress in concrete at the level of prestressing steel immediately after prestress transfer (ksi).

$$\Delta f_{CR} = K_{CR} n (f_{cs} - f_{cds}) \tag{5-3}$$

where K_{CR} = 2.0 for normal weight concrete and f_{cds} = stress from all superimposed permanent dead and sustained loads after prestressing (ksi).

$$\Delta f_{SH} = (8.2 \times 10^{-6}) K_{SH} E_{ps} \left(1 - 0.06 \frac{V}{S}\right)(1 - RH) \tag{5-4}$$

where K_{SH} = 1.0 for pretensioned members, E_{ps} = modulus of elasticity of prestressing reinforcement (ksi), V/S = volume to surface ratio (in), and RH = average ambient relative humidity (%).

$$\Delta f_{RE} = [K_{RE} - J(\Delta f_{ES} + \Delta f_{CR} + \Delta f_{SH})]C \tag{5-5}$$

where K_{RE} = 185 ksi, J = 0.14 for 250 ksi grade stress-relieved strand, and C = variable that is a function of the initial stress in the prestressing strands, f_{pi} and of the ultimate stress in the prestressing strands, f_{pu}.

Since the majority of prestress losses occurred soon after transfer of prestress force to the girder, the section properties were determined for the girder only (Precast/Prestressed Concrete Institute 1999). The gross concrete area of the girder, A_g, the gross moment of inertia about the major axis for the girder, I_g, and the neutral axis

were taken for the girder only as shown in Figure 5-1a. The eccentricity of the strands at midspan, e, was taken as 11.83 inches representing the vertical difference between the centroid of the harped strands and the neutral axis of the cross-section.

To determine the losses due to elastic shortening and creep, it was necessary to calculate the compressive stress in the concrete at the level of the prestressing steel immediately after prestress transfer with the effects for harped strands, f_{cs}, as shown in Equation 5-6 (Precast/Prestressed Concrete Institute 1999).

$$f_{cs} = \left[K_{csi} \frac{P_i}{A_g} \left(1 + \frac{e^2}{r^2} \right) \right] - \frac{M_D e}{I_g} \tag{5-6}$$

where $K_{csi} = 0.9$ for pretensioned members, P_i = initial prestress force after anchorage seating losses (kip), r = radius of gyration of girder about the major axis (in), M_D = moment due to dead load (kip-in). The initial prestress force after anchorage seating losses, P_i, was calculated by multiplying the area of prestressing by the initial steel stress, f_{pi}. The initial stress of the prestressing steel after anchorage seating losses, f_{pi}, was taken as 0.70 of the ultimate strength of the prestressing steel, f_{pu}, which was 250 ksi (Precast/Prestressed Concrete Institute 1999, ACI 1996). The area of prestressing was taken as 2.376 in^2 representing 22 strands of 7/16" diameter wire. The modulus of elasticity of the prestressing reinforcement was taken as 27500 ksi and the modulus of elasticity of the concrete, E_c, was calculated using Equation 5-7 with a concrete compressive strength, f'_c, of the girder of 4500 psi.

$$E_c = 57000\sqrt{f'_c} \tag{5-7}$$

where f'_c is in psi.

The radius of gyration, r, was calculated by Equation 5-8 using the area and moment of inertia corresponding to the gross cross-sectional area of the girder as shown in Figure 5-1a.

$$r = \sqrt{\frac{I_g}{A_g}} \tag{5-8}$$

The moment due to dead load, M_D, was calculated using Equation 5-9 with an unsupported length of 40'-0" and distributed load, w_D, as shown in Figure 5-1a.

$$M = \frac{wl^2}{8} \tag{5-9}$$

The stress due to all superimposed permanent dead and sustained loads after prestressing or in this case from the slab, f_{cds}, was calculated by Equation 5-10.

$$f_{cds} = \frac{M_{sd}e}{I_g} \tag{5-10}$$

The moment, M_{sd}, was calculated using Equation 5-9 with the distributed load as shown in Figure 5-1b and an unsupported length of 40'-0". The volume to surface ratio in Equation 5-4 was calculated by taking the volume of the girder divided by its surface area giving 109.45". The average ambient relative humidity, RH, in Equation 5-4 was taken as 75% (Precast/Prestressed Concrete Institute 1999). The variable C in Equation 5-5 was calculated using Equation 5-11 with the ratio of initial to ultimate strength of prestressing steel, f_{pi}/f_{pu} being 0.70 as assumed above to solve for P_i in Equation 5-6.

$$C = 1 + 9\left(\frac{f_{pi}}{f_{pu}} - 0.7\right) \tag{5-11}$$

for $0.70 \leq f_{pi}/f_{pu} \leq 0.75$. The effective prestress, f_{pe}, was calculated as shown in Equation 5-12 by taking the initial stress of the steel, f_{pi}, minus the sum of all of the losses from Equation 5-1.

$$f_{pe} = f_{pi} - \Delta f_T \tag{5-12}$$

The resulting effective prestress, f_{pe}, was 120 ksi.

Theoretical Cracking Capacity for Test Specimens in Undamaged and Damaged State without Repair

To calculate the theoretical cracking moment capacity of the test specimens in the undamaged state Equation 5-13 was utilized.

$$M_{cr} = \frac{I_g}{y_T}\left[\frac{P_e}{A_g}\left(1+\frac{ec_b}{r^2}\right)+7.5\lambda\sqrt{f'_c}\right]-M_D \tag{5-13}$$

where y_T = distance from the centroid of the section to the extreme tensile fibers of the concrete (in) and was taken as 27.3", P_e = effective prestress force (kips), c_b = distance from the bottom of the section to the neutral axis(in) and equals 15.83" (see Figure 5-1a), and $\lambda = 1.0$ for normal weight concrete.

All of the terms inside of the brackets in Equation 5-13 were representative of the girder only and the terms outside of the brackets were representative of the girder with the slab. Therefore, the gross area of concrete, location of the neutral axis, and the input values for the radius of gyration using Equation 5-8 were taken from Figure 5-1a. The effective prestress force, P_e, was calculated by multiplying the area of prestress, A_{ps}, by the effective prestress, f_{pe}. The moment due to dead load of the girder with the slab, M_D, was calculated using Equation 5-9 with an unsupported length of 40'-0" and distributed load, w_D, as shown in Figure 5-1c. Using these input values for Equation 5-13 resulted in a theoretical cracking moment of 1034.73 kip-ft for the live load of the test specimen in

the undamaged state. This theoretical cracking moment for the undamaged specimen corresponds to a cracking load equal to 137.96 kips (see Figure 3-5).

The theoretical cracking load for the girders in the damaged state can also be calculated using Equation 5-13. This equation is for an undamaged section and is not directly applicable to a damaged section. However, if Equation 5-13 was used for a damaged section, the calculated cracking moment capacity would be less accurate as a result of the simulated damage. To calculate the damaged theoretical cracking moment capacity the above procedure was followed except that the effective prestress force, P_e, was calculated by taking the effective prestress, f_{pe}, multiplied by the reduced area of prestressing reinforcement, A_{ps}. The reduced area of prestress was taken as 1.944 in^2 representing 18 strands or 22 strands minus the four removed strands each being 7/16" in diameter. Using these values as input in Equation 5-13 resulted in a cracking moment capacity of 867.84 kip-ft for the live load of the specimen in the damaged state. This theoretical cracking moment for the damaged specimen corresponds to a cracking load equal to 115.71 kips (see Figure 3-5).

Theoretical Ultimate Capacity for Test Specimens in Undamaged and Damaged State without Repair

The guidelines suggested by ACI Committee 440 (2002) were used to calculate the theoretical ultimate moment capacity of the test specimens in the undamaged state. ACI guidelines suggest first setting the compressive strain at the top of the section equal to 0.003 in/in to solve through iterations the location of the neutral axis. The location of the neutral axis is then used to solve for the capacities of the steel and concrete. The girder with the slab was used to determine the ultimate capacity for the test specimens in the undamaged and damaged state (see Figure 5-1c). The depth to the individual steel layers

from the top of the section and corresponding area of prestressing steel were taken as shown in Figure 5-2a.

The force contribution from the concrete was found by multiplying the stress in the concrete at a given level by the width of the section at that level only for the portion of the section above the neutral axis. Linear interpolation between the strain at the top of the section equal to 0.003 in/in and the strain at the neutral axis location equal to zero was used to determine the strain in the concrete at that given level. The moment contribution of the concrete was found by integrating, from the neutral axis to the top of the section, the force at each level by the corresponding distance to the elastic centroid of the section. The force contribution from the steel was found by integrating over the three layers of steel the area of prestressing at each level times the stress in the prestressing steel at that corresponding level.

The Ramberg-Osgood function shown as Equation 5-14 was used for determining the stress in the prestressing steel (Collins and Mitchell 1991).

$$f_{ps} = E_{ps}\varepsilon\left(A + \frac{1-A}{\left[1+(B\varepsilon)^{C}\right]^{\frac{1}{C}}}\right) \tag{5-14}$$

The Ramberg-Osgood coefficients, A, B, and C, were found from direct tensile tests of the removed strands of Test Specimen 2, and determined to be 0.1091, 115.09, and 10, respectively (see Figure 3-4). The strain in any given layer of prestressing steel was determined by linear extrapolation with the strain at the top of the section equal to 0.003 in/in and the strain at the neutral axis location equal to zero. The strain input into Equation 5-14 was the sum of the strain in the layer of prestressing from linear extrapolation and the effective prestress strain. The moment contribution of the

prestressing steel was found by summing the force at the level of prestressing times the corresponding distance to the elastic centroid of the section for each layer of prestressing. The total load capacity was determined by taking the force contribution of the prestressing steel minus the force contribution of the concrete. The total moment capacity was determined by summing the moment contributions of the concrete and prestressing steel. Using the above procedure, the total ultimate moment capacity was determined to be 2034.02 kip-ft for the specimen in the undamaged state. The ultimate moment due to live load was determined by taking the resulting ultimate moment capacity minus the dead load moment. The resulting live load ultimate moment capacity was 1897.15 kip-ft. This theoretical ultimate moment for the undamaged specimen corresponds to an ultimate load equal to 252.95 kips (see Figure 3-5).

The theoretical ultimate load for the girders in the damaged state can also be calculated by the same procedure. This procedure is for an undamaged section and is not directly applicable to a damaged section. However, if the procedure were used for a damaged section, the maximum moment capacity would be less accurate as a result of the simulated damage. To calculate the damaged theoretical ultimate moment capacity, the above procedure was followed except that the area of steel was reduced for the bottom two layers of prestressing steel. The depth to the individual steel layers from the top of the section and corresponding area of prestressing steel were taken as shown in Figure 5-2b. Using the above procedure, the total ultimate moment capacity was determined to be 1679.59 kip-ft for the specimen in the damaged state. The ultimate moment due to live load was determined by taking the resulting ultimate moment capacity minus the dead load moment. The resulting live load ultimate capacity was 1542.72 kip-ft. This

theoretical ultimate moment for the damaged specimen corresponds to an ultimate load equal to 205.7 kips (see Figure 3-5).

Theoretical Ultimate Capacities of Test Specimens 3, 4, 5, and 6

The guidelines suggested by ACI Committee 440 (2002) were used to calculate the theoretical ultimate moment capacity of the test specimens. ACI guidelines suggest first setting the tensile strain at the extreme bottom of the section equal to ultimate strain of the laminate and then solve through iterations the location of the neutral axis. The location of the neutral axis was then used to solve for the capacities of the steel, concrete, and FRP. No factors of safety were used for the analysis, such as the environmental reduction factor, C_e, to be applied to the ultimate tensile strength or the bond dependent coefficient, κ, to be applied to the rupture strain suggested by the ACI guidelines. The cross-section properties at midspan for the girder with the slab were utilized for the analysis of all of the repaired test specimens (see Figure 5-1c). The depth to the individual steel layers from the top of the section and corresponding area of prestressing steel were taken as shown in Figure 5-2a.

The force and moment contribution from the concrete was determined as described in the previous section except that the limits for linear interpolation of the concrete stress have changed. Linear interpolation between the strain at the bottom of the section equal to the rupture strain of the laminate and the strain at the neutral axis location equal to zero was used to determine the stress in the concrete at any level. The force and moment contribution from the steel was determined as described in the previous section except that the limits for linear extrapolation of the steel strain have changed. The strain in any given layer of prestressing steel was determined by linear interpolation between the strain

at the bottom of the section equal to the rupture strain of the laminate and the strain at the neutral axis location equal to zero. The strain input into Equation 5-14 was the sum of the strain in the layer of prestressing from linear interpolation and the effective prestress strain. The force contribution of the FRP was determined by multiplying the cross-sectional area of the FRP by the stress in the FRP. The stress in the FRP was found by multiplying the rupture strain or elongation at break strain by the tensile modulus of elasticity of the FRP. The moment contribution of the FRP was determined by multiplying the force contribution of the FRP by the distance of the FRP to the elastic centroid of the section. The total load capacity of the section was determined by taking the force contribution of the concrete minus the force contribution of the prestressing steel and minus the force contribution of the FRP. The total moment capacity was determined by summing the moment contributions of the concrete, prestressing steel, and FRP. Using the above procedure, the total ultimate theoretical moment capacity for Test Specimens 3, 4, 5, and 6 were determined to be 2914.69 kip-ft, 2326.74 kip-ft, 2206.13 kip-ft (2412.58 kip-ft actual), and 2140.13 kip-ft, respectively. The ultimate theoretical moment capacity due to live load was determined by taking the resulting ultimate moment capacity minus the corresponding dead load moment. The resulting theoretical live load ultimate capacities for Test Specimens 3, 4, 5, and 6 are 2777.82 kip-ft, 2182.94 kip-ft, 2069.26 kip-ft (2275.71 kip-ft actual), and 2003.26 kip-ft, respectively. These theoretical ultimate moment capacities for the repaired specimen correspond to ultimate loads equal to 370.38 kips, 281.67 kips, 275.90 kips (303.43 kips actual), and 267.1 kips, respectively (see Figure 3-5).

The disadvantages to using this procedure were that the FRP thickness on the bottom flange could not be varied as in the case of Test Specimen 5. Also, FRP on the sides of the specimens could not be included as additional flexural capacity only as shear capacity.

Support Conditions

To determine the behavior of the support conditions during the experimental tests, analytical midspan (maximum) deflections were determined for the undamaged girder for two cases. Case 1 assumes that the girder is a simple beam with two equal concentrated loads symmetrically placed and Case 2 assumes that the girder is fixed at both ends with two loads symmetrically placed. Equations 5-15 and 5-16 represent the deflection equations for Case 1, pinned supports, and Case 2, fixed supports, respectively (AISC 2001).

$$\Delta_{max}(at\ center) = \frac{Pa}{24EI}\left(3l^2 - 4a^2\right) \tag{5-15}$$

for pinned supports, where P = load at one load cell, l = unsupported length and a = distance from support to load point.

$$\Delta_{max}(at\ center) = 2\left[\frac{Pb^2x^2}{6EIl^3}(3al - 3ax - bx)\right] \tag{5-16}$$

for fixed supports, where b = distance to the load point, x = distance to calculated deflection.

The concrete compressive strength, f'_c, is taken as 4500 psi and used in Equation 5-6 to determine the modulus of elasticity of the concrete, E_c. The unsupported length, l, is taken as 40'-0" representing the distance between the supports. The girder with the slab was used to determine the support conditions for the test specimen in the undamaged

state (see Figure 5-1c). The distance to the load point, a, was taken as 15'-0" representing the distance between one support and the nearest load point during the experiment. The distance to the load point, b, was taken as 25'-0" representing the distance between the load point and the support at the other end of the beam during the experiment. The distance to the deflection, x, was taken as 20'-0" representing the distance from one support to where the deflection was being calculated on the beam. The experimental load and midspan deflection chosen for analytical comparison was 98.4 kips and 0.349" where the load is the sum of the two load points on the beam (see Figure 3-5). The experimental load, equal to 98.4 kips, was chosen for the support condition evaluation since it was less than the experimental cracking load for Test Specimen 1 (131.3 kips) as well as the analytical cracking load equal to 132.69 kips. The load, P, to be input into Equations 5-15 and 5-16 was 49.2 kips representing the measured load from one load cell. The analytical midspan deflections determined for the pinned supported case and fixed supported case using a load, P, of 49.2 kips were 0.328" and 0.076", respectively. Therefore, the analytical and experimental results for the deflection at midspan of Test Specimen 1 confirm that the case with pinned supports provides a verification that the supports for the experiments behaved as pinned supports as assumed. For Test Specimen 6, additional instruments at the south support were utilized to calculate the rotation that occurs at the support (see Figure 3-6c). The measured rotation at the south support was 1.7° that corresponds to the supports behaving as pinned supports as confirmed above by the theoretical deflection calculation.

Theoretical Midspan Deflection at the Theoretical Ultimate Capacity of the Girder in the Undamaged State

In order to normalize the experimental data for comparison it was necessary to determine the ultimate theoretical deflection at midspan. The ultimate deflection at midspan was calculated using Equation 5-15 with the assumption that the supports behave as pinned supports during testing. The maximum load was 135.6 kips which represents the theoretical load at one load point as solved previously for Test Specimen 1. The area of prestressing, A_{ps}, was taken as 2.376 in^2 representing 22 strands each with a diameter of 7/16". The gross moment of inertia can not be used to determine the midspan deflection at the maximum load. For Equation 5-15, the cracked moment of inertia must be used to obtain a deflection representative of the state of the girder at maximum load. The cracked moment of inertia was determined using Equation 5-17 (Precast/Prestressed Concrete Institute 1999).

$$I_{cr} = nA_{ps}d_p^2\left(1-\left(1.6\sqrt{n\rho_p}\right)\right) \tag{5-17}$$

where d_p = depth to the prestressing strands and ρ_p = ratio of prestressed reinforcement. The depth to the prestressing strands, d_p, was taken as 44" representing the distance from the top of the section to the middle layer of prestressing strands (see Figure 5-2a). The ratio of prestressed reinforcement, ρ_p, was calculated using Equation 5-18 with the width of the section, b, taken as 24" representing the width of the section in compression.

$$\rho_p = \frac{A_{ps}}{b \times d_p} \tag{5-18}$$

The resulting theoretical midspan deflection at ultimate was 5.67".

Comparison of Theoretical and Experimental Capacities and Deflections

Tables 5-1 and 5-2 provide a comparison between the live load theoretical (T) and experimental (E) capacities at cracking load and at maximum load, respectively. The percent differences, shown in Tables 5-1 and 5-2, were calculated by dividing the difference between the two quantities by the calculated theroetical capacity.

Table 5-1 presents the theoretical cracking capacities for Test Specimens 1 and 2 calculated with the assumption of fully composite action existing between the slab and girder. Test Specimen 1 had a theoretical cracking load of 138 kips and an experimental cracking load of 131 kips while Test Specimen 2 had a theoretical cracking load of 116 kips and an experimental cracking load of 112 kips as shown in Table 5-1. Therefore, a 16.1% reduction in the theoretical cracking load capacity was estimated by the severing of four prestressing strands. Therefore, for Test Specimen 1 the experimental and theoretical capacities at the cracking load for Test Specimen 1 differed by 4.9%. Test Specimen 2 had an experimental cracking load of 112 kips and had a theoretical cracking load of 116 kips as shown in Table 5-1. Therefore, for Test Specimen 2 the experimental and theoretical capacities at the cracking load differed by 3.3%. The calculated theoretical cracking capacity was slightly higher than the observed experimental cracking capacity for Test Specimens 1 and 2. The calculated theoretical cracking capacities were based on the previously determined effective prestress force in the steel of 120 ksi. Although the theoretical cracking capacity was higher than the experimental cracking capacity, the difference can be attributed to several factors such as the assumption that the initial prestressing force should be 70% of the ultimate and the camber of the girders increasing over time due to being out of service without an applied dead load.

Test Specimen 1 had a theoretical maximum load of 253 kips and an experimental maximum load of 268 kips while Test Specimen 2 had a theoretical maximum load of 206 kips and an experimental maximum load of 210 kips as shown in Table 5-2. Therefore, an 18.7% reduction in maximum load capacity was estimated by the severing of four prestressing strands, the experimental and theoretical capacities at the maximum load for Test Specimen 1 differed by 6.1%, and the experimental and theoretical capacities at the maximum load for Test Specimen 2 differed by 2.1%. Test Specimen 3 had an experimental maximum load of 244 kips and had a theoretical maximum load of 371 kips as shown in Table 5-2. Therefore, the experimental and theoretical capacities at the maximum load differed by 34.3%. Test Specimen 4 had an experimental maximum load of 247 kips and had a theoretical maximum load of 282 kips as shown in Table 5-2. Therefore, the experimental and theoretical capacities at the maximum load differed by 12.4%. The theoretical capacities presented in Table 5-2 for Test Specimen 5 were the result of a constant FRP laminate thickness of 0.5" with a fiber length of approximately 1.25" applied only to the tension face of the girder. Test Specimen 5 had an experimental maximum load of 255 kips and had a theoretical maximum load of 304 kips as shown in Table 5-2. Therefore, the experimental and theoretical capacities at the maximum load differed by 16.2%. Test Specimen 6 had an experimental maximum load of 288 kips and had a theoretical maximum load of 268 kips as shown in Table 5-2. Therefore, the experimental and theoretical capacities at the maximum load differed by 7.5%. The unrepaired theoretical capacities were consistent with the experimental findings whereas the repaired theoretical capacities were much larger than the observed experimental capacities, which could be due to premature failure modes for Test Specimens 3 and 4,

imperfect application of the FRP systems, unconservative repair guidelines set by ACI 440, or FRP material flaws.

The theoretical midspan deflection at ultimate for Test Specimen 1 was calculated, with the assumption of pinned supports, as 5.67" and the measured midspan deflection at ultimate load of Test Specimen 1 was 5.95". Therefore, at ultimate load the experimental and theoretical midspan deflection differed by only 6%. The observed midspan deflection at ultimate was slightly higher than the theoretical deflection possibly due to shear deformations being neglected in the midspan deflection calculation with the girder having a shear span to depth ratio of 3.75.

Figure 5-3 shows the moment deflection relationship that was normalized to the theoretical live load moment and deflection values at ultimate for Test Specimen 1. The data shown for Test Specimen 3 only contains values for the last series of loading up to failure. Figure 5-3 shows consistent calculations of the theoretical deflection and capacity of Test Specimen 1 and substantial reductions in deflection and ductility of the girders repaired with FRP systems.

Computer Program Implementation for all Test Specimens

A computer program was implemented to calculate theoretical moment curvature diagrams and ultimate capacities of the six test specimens for comparison with experimental values (Fung 2002, Consolazio et al. in press). The computer program evaluates capacities based on section properties. The cross-section properties at midspan were input into the computer program for all test specimens. The major advantage of the program was the evaluation of a cross-section including the effects of fiber reinforced polymer systems with any dimensions.

The input dimensions are based on a coordinate system for the cross-section contour, steel locations, FRP locations and properties, the concrete compressive strength of the girder, f'_c, and the effective prestress of the prestressing strands, f_{pe}. The required steel properties were the yield strength of the mild steel, tensile modulus of the prestressing steel, area of steel, type of steel, and location of the mild steel and/or prestressing steel. Some of the disadvantages of the program were that the cross-section could not be entered as two parts with different concrete compressive strengths as existed in the test specimens, and that all of the FRP failure modes such as bond failures were not considered.

By taking the experimental strain profiles and solving for the location of the neutral axis at a specific load, the experimental curvature was determined for that specific load. The calculated experimental curvature has a corresponding load and moment which were used for comparing the theoretical moment curvature values from the computer program output. Figure 5-4 shows the theoretical moment curvature relations for Test Specimens 1, 2, 3, 4, 5, and 6 and the experimental moment curvature relations for Test Specimens 1, 2, 3, 4, 5 and 6 with T and E denoting the theoretical and experimental relationships, respectively. Figure 5-4 shows three separate theoretical moment curvature relations for Test Specimen 5. The first two series 5a and 5b represent the repair with a fiber length of approximately 2" with a thickness of 0.35" and the repair with a fiber length of approximately 1.25" with a thickness of 0.50". The last series of theoretical moment curvature points, 5c, was generated with the average thickness of the FRP applied at the midspan which was measured from samples taken from the girder after the load test. This program generated the first point at a value of negative curvature. Therefore, the

theoretical values shown in Figure 5-4 were offset by the initial negative curvature of the evaluated cross-section such that all of the moment curvature relationships start at zero curvature and zero moment. The theoretical moment curvature points in Figure 5-4 were fairly consistent with the experimental data in the elastic range but vary greatly in the inelastic range. The theoretical ultimate capacities computed by this program are shown in Table 5-3 with E in Column 2 denoting experimental data. The computer program produced consistent moment capacities for the unrepaired specimens with a 1.78% difference for Test Specimen 1 and a 3.74% difference for Test Specimen 2. Generally the computer program produced moment capacities for the repaired specimens higher than the observed experimental capacities. For Test Specimens 3 and 4, the experimental and theoretical maximum moment capacities differed by 32.6% and 30%, respectively. This significant difference can be attributed to the specimens failing prematurely and not at full capacity. For Test Specimen 5, three analyses were performed (5a, 5b, and 5c) in which the 5c analysis represents the actual repair that was applied to the girder. The experimental and theoretical maximum moment capacities for the 5c analysis differed only by 6.1%. For Test Specimen 6, the experimental and theoretical moment capacities differed by only 5.3%.

Table 5-1: Comparison of Experimental and Theoretical Capacities of Test Specimens 1 and 2 at Cracking

Test Specimen	P_{cr} (kip) E	M_{cr} (kip-ft) E	P_{cr} (kip) T	M_{cr} (kip-ft) T	% difference of M_{cr} T of test specimen 1 and T per test specimen	% difference of M_{cr} T and E per test specimen
1	131.3	984.4	138.0	1034.7	0.0	4.9
2	111.9	839.4	115.7	867.8	16.1	3.3

Table 5-2: Comparison of Experimental and Theoretical Capacities of Test Specimens 1, 2, 3, 4, 5 and 6 at Maximum Load

Test Specimen	P_{max} (kip) E	M_{max} (kip-ft) E	P_{max} (kip) T	M_{max} (kip-ft) T	% difference of M_{max} T of test specimen 1 and T per test specimen	% difference of M_{max} T and E per test specimen
1	268.3	2012.1	253.0	1897.2	0.0	6.1
2	210.1	1575.9	205.7	1542.7	18.7	2.1
3	243.9	1829.1	371.0	2782.6	46.7	34.3
4	246.9	1913.5	282.0	2185.4	15.2	12.4
5	254.8	1910.8	304.1	2280.6	20.2	16.2
6	288.3	2162.3	268.1	2011.1	6.0	7.5

Table 5-3: Theoretical Moment Capacity at Ultimate Generated by Computer Program for all Test Specimens

Test Specimen	M_{test} (kip-ft) E	M_{test} (kip-ft)	% difference of M_{test} experimental per test specimen
1	2012.1	1976.9	1.8
2	1575.9	1637.0	3.7
3	1829.1	2713.9	32.6
4	1913.8	2224.8	14.0
5a	1910.8	2395.6	20.2
5b	1910.8	2652.0	28.0
5c	1910.8	2035.4	6.1
6	2162.3	2054.3	5.3

Table 5-4: Experimental Midspan Deflection at the Theoretical Service Load Moment for all Test Specimens

Test Specimen	Δ at service load moment (in)
1	0.27
2	0.36
3	0.34
4	0.30
5	0.32
6	0.24

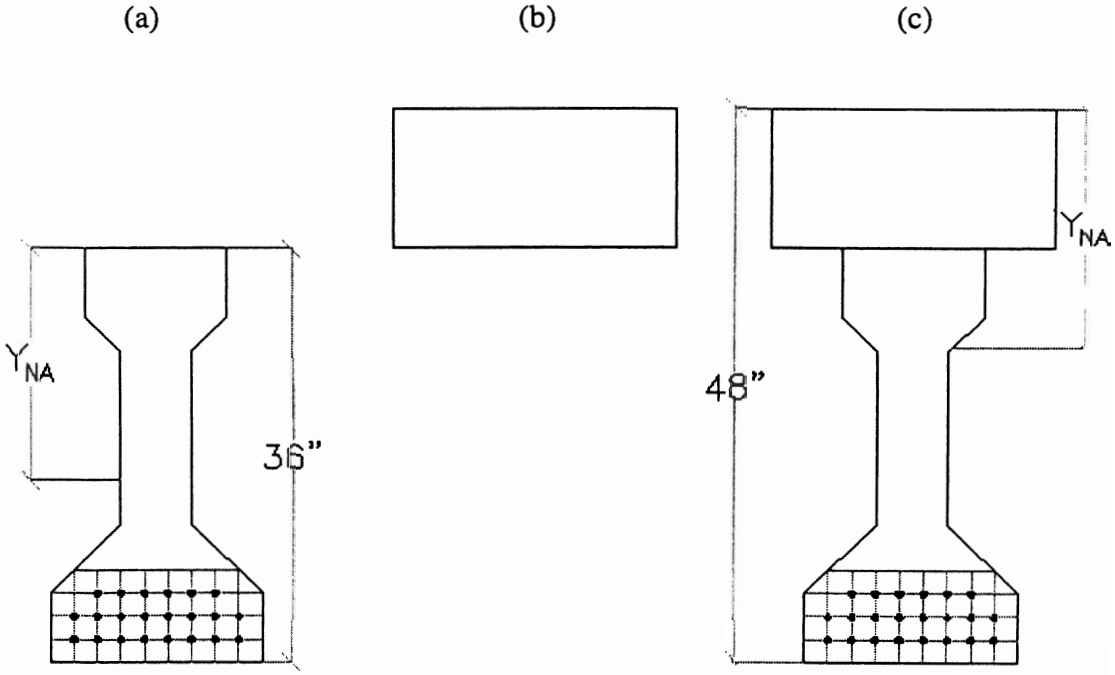

Girder Without Slab Properties

$A = 369\ in^2$
$I = 50979\ in^4$
$w = 0.384\ kip/ft$
$y_{NA} = 20.17\ in$

Slab Properties

$A = 288\ in^2$
$w = 0.30\ kip/ft$

Girder With Slab Properties

$A = 657\ in^2$
$I = 165220.83\ in^4$
$w = 0.684\ kip/ft$
$y_{NA} = 20.7\ in$

Figure 5-1: Geometric Properties of the Cross-Section a) Girder without the Slab; b) Slab; and c) Girder with the Slab

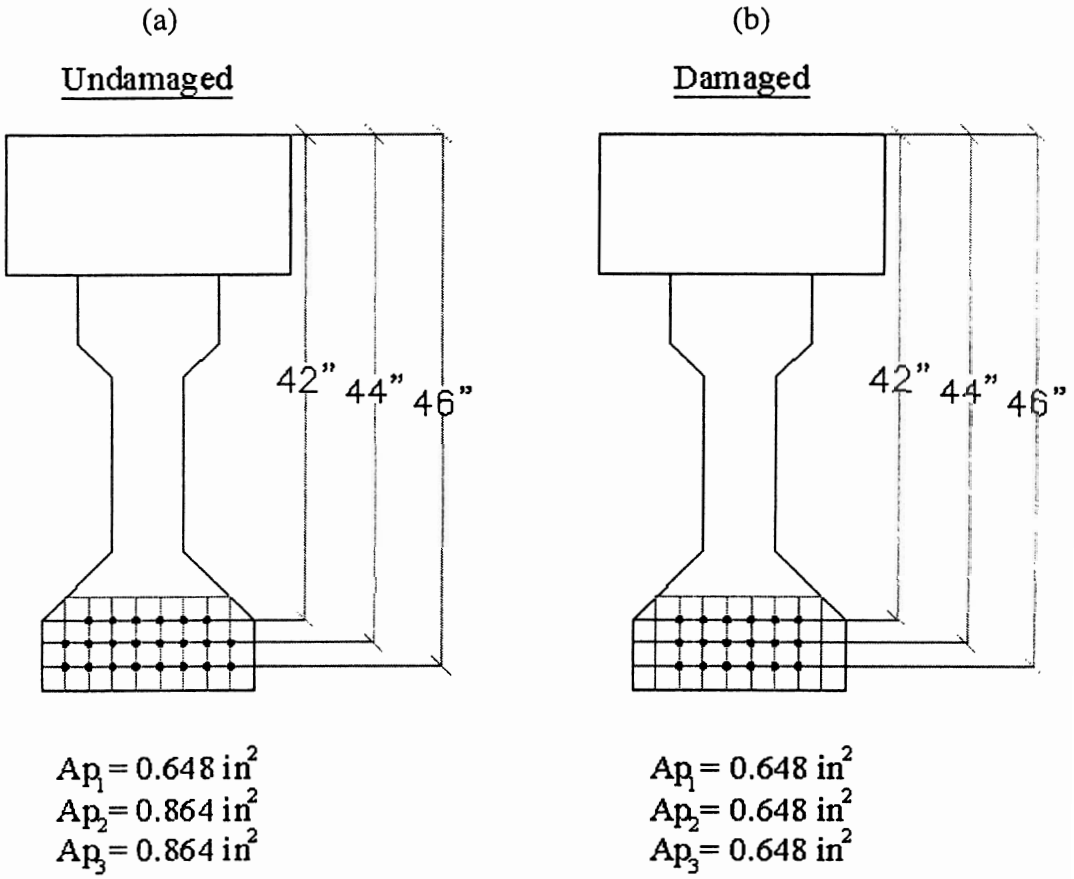

Figure 5-2: Steel Areas and Location for a) an Undamaged Section; and b) a Damaged Section

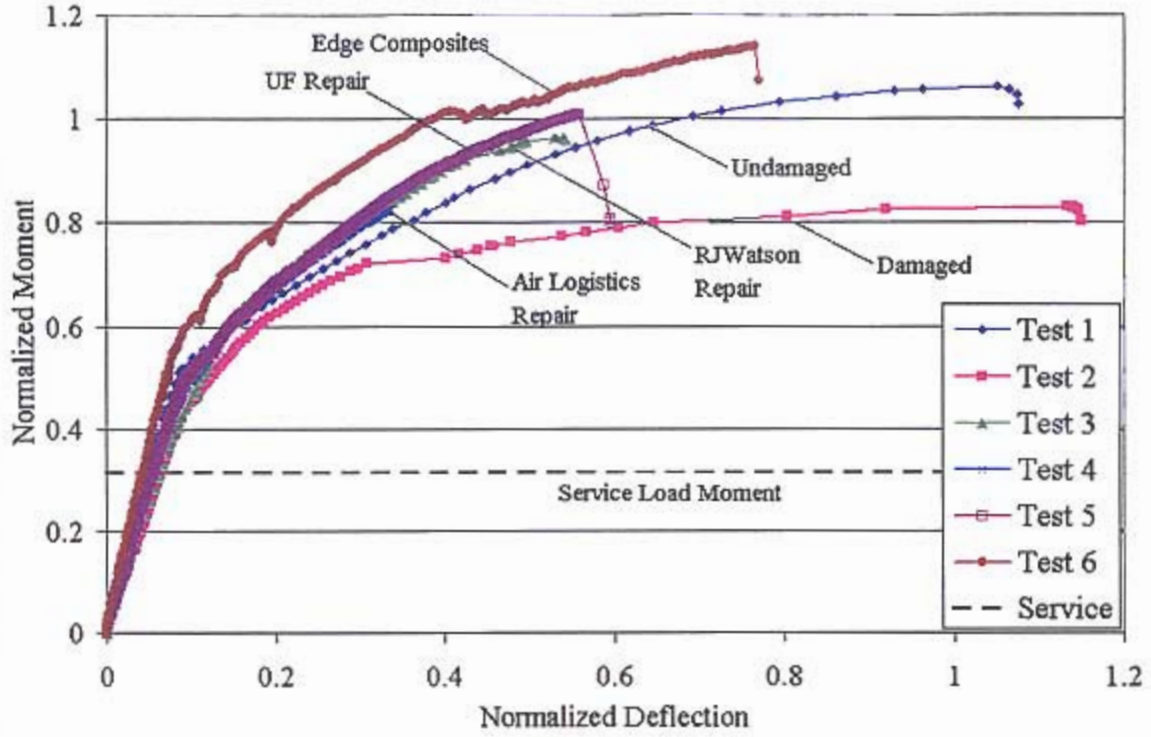

Figure 5-3: Normalized Moment versus Deflection for all Test Specimens and the Service Load Moment

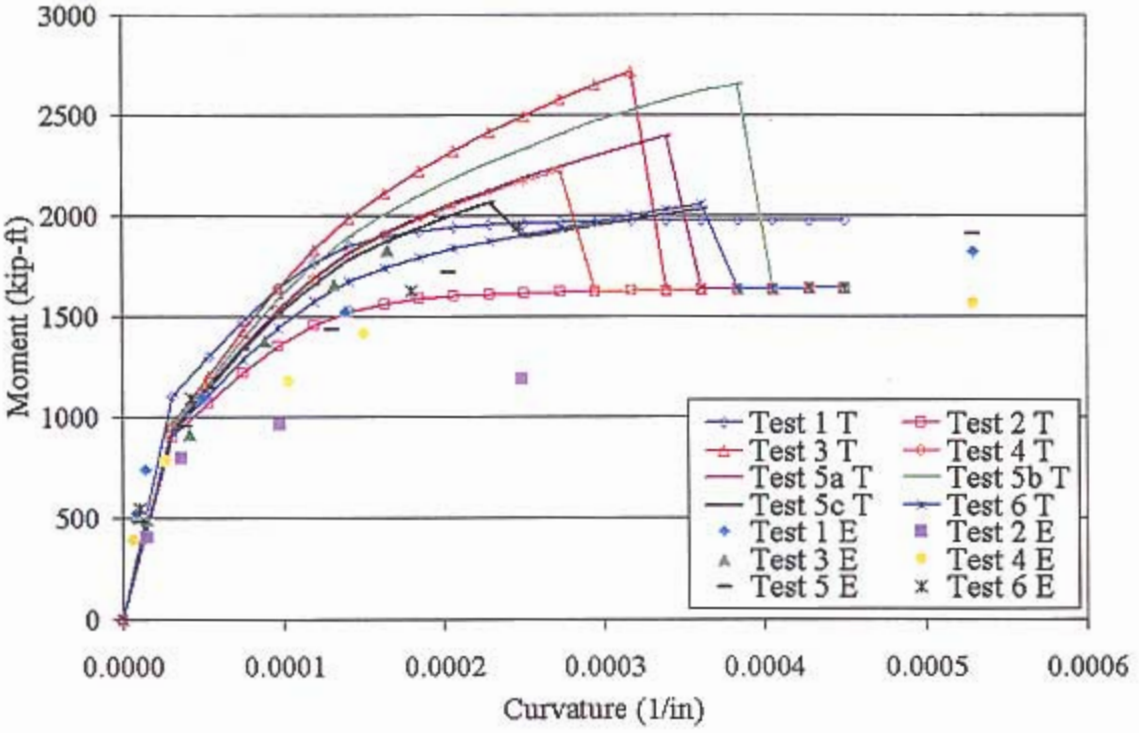

Figure 5-4: Moment Curvature Comparison of Theoretical Data from Computer Program and Experimental Data

CHAPTER 6
DESIGN RECOMMENDATIONS AND PRELIMINARY DESIGN SPECIFICATIONS

All of the repair design procedures for the FRP strengthening systems of the damaged girders were reasonable and followed typical prestressed and FRP behavior. Each repair design for the damaged girder using FRP used different factors of safety based on engineering judgement and not guideline procedures. All of the design procedures consisted of determining an ultimate capacity, which was not based on a critical limit state or critical failure mode that would be attained if perfect application and bonding was ensured. The biggest issue with repair design procedures using FRP strengthening systems is that code standards do not exist, only guidelines. Guidelines have been established for FRP repair of reinforced concrete structures but only a limited part of these guidelines address or even relate to FRP repair of prestressed concrete girder systems (ACI 2002).

For the computation of the ultimate capacity of a reinforced concrete member flexurally strengthened with a FRP system, ACI guidelines suggest setting the tensile strain at the extreme bottom of the section equal to ultimate strain of the laminate. The neutral axis is then determined through iterations with the limit on the extreme tensile strain equal to the laminate rupture strain. The location of the neutral axis can then used to solve for the contributions of the steel, concrete, and FRP. ACI suggests the use of an environmental reduction factor, C_e, to be applied to the ultimate tensile strength of the laminate, which is a function of the expected exposure condition, fiber type, and resin type as shown in Table 6-1. The purpose of the environmental reduction factor, C_e, is to

take into the account how the mechanical properties of an FRP system are affected by long-term exposure to the environment. ACI also suggests the use of a factor, κ_m, to be applied to the rupture strain of the laminate that is computed as shown in Equation 6-1 (ACI 2002).

$$\kappa_m = \begin{cases} \frac{1}{60\varepsilon_{fu}}\left(1-\frac{nE_f t_f}{2{,}000{,}000}\right) \le 0.90 \text{ for } nE_f t_f \le 1{,}000{,}000 \\ \frac{1}{60\varepsilon_{fu}}\left(\frac{500{,}000}{nE_f t_f}\right) \le 0.90 \text{ for } nE_f t_f > 1{,}000{,}000 \end{cases} \quad (6\text{-}1)$$

where ε_{fu} = rupture strain of FRP reinforcement, n = number of plies of FRP reinforcement, E_f = tensile modulus of elasticity of the FRP, and t_f = nominal thickness of one ply of FRP reinforcement. The κ_m factor limits the strain developed in the laminate in order to prevent debonding of the FRP laminate.

ACI (2002) also provides the following guidance for the flexural capacity calculation of a prestressed concrete member when the member is strengthened with longitudinal FRP reinforcment to its tension face,

> In the case of prestressed concrete members, strain compatibility, with respect to the state of strain in the stressed member, should be used to evaluate the FRP contribution.

The setting of standards for FRP repairs to reinforced and prestressed concrete would reduce the amount of engineering judgment used in current designs, and therefore would reduce errors and ensure that a proper repair was designed.

Although the repair of the test specimens focused mainly on flexural strengthening due to the damage imparted to only the flexural reinforcement, shear capacity must also be an issue in the repair design. Shear resistance is provided through the internal stirrups of prestressed concrete girders. Even though the damage procedure did not involve any

damage to the internal shear stirrups, the shear capacity was reduced by 14.7% experimentally and 6.2% theoretically when compared to the undamaged shear capacity. This reduction in shear capacity can be attributed to the removal and replacement of the 5'-0" section centered about midspan. The damage process interrupted the original shear load path. In the undamaged specimen, the load moves through a continuous section without initial cracks. In the damaged specimens, the load moves through a discontinuous section that results from having adjoining concrete of differing properties. To regain the shear capacity through an FRP strengthening system, it is necessary to provide a load path from the FRP being applied primarily for flexure, back to the internal shear stirrups, which were designed for the undamaged shear capacity.

A way to ensure that an adequate shear load path will be restored to a flexurally damaged member, is to require that FRP material be applied to the girders for shear reinforcement. For example, if the structural capacity being restored is due to flexural inadequacies, then a cross-sectional area equal to a certain percentage of the applied flexural reinforcement needs to be applied to ensure adequate shear capacity.

Based on the findings of this experimental testing program, preliminary design specifications for prestressed concrete girder repairs with FRP materials are as follows:

- All concrete surfaces should be cleaned and sandblasted prior to FRP application. Cracks, voids, and discontinuities should be repaired to ensure that there will be a good bond of the FRP materials.
- FRP materials used for flexural reinforcement on the tension face of a structural member should extend, at a minimum, 0.80 times the unsupported length
- For flexurally repaired structural members, an area equal to a percentage of flexural reinforcement should be applied to the sides of a member for shear strength. This percentage needs to be determined through further investigation;

- Stirrups should be used at the termination points of FRP flexural reinforcement for proper anchorage and to avoid the failure modes due to concrete cover separation and FRP debonding;

- The stirrups should be made of bi-directional fabric with fibers oriented in the direction of and perpendicular to the longitudinal axis of the structural member;

Table 6-1:Environmental Reduction Factor for Various FRP Systems and Exposure Conditions (ACI 2002)

Exposure Conditions	Fiber and resin type	Environmental reduction factor, C_e
Interior exposure	Carbon/epoxy	0.95
	Glass/epoxy	0.75
	Aramid/epoxy	0.85
Exterior exposure (bridges, piers, and unenclosed parking garages)	Carbon/epoxy	0.85
	Glass/epoxy	0.65
	Aramid/epoxy	0.75
Aggressive environment (chemical plants and waste water treatment plants)	Carbon/epoxy	0.85
	Glass/epoxy	0.50
	Aramid/epoxy	0.70

CHAPTER 7
SUMMARY, CONCLUSIONS, AND RECOMMENDATIONS FOR FUTURE RESEARCH

A short term way to avert collisions due to over-height vehicles would be to regulate that all bridges including underpasses to the Interstate System meet the current minimum desired height requirements. This would mean that pre-existing bridges would have to be replaced or lifted, or underlying roadways would have to be lowered requiring a tremendous amount of work and funding. Also this would mean that in a couple of years vehicle heights would increase and bridges would again be subject to impacts due to over-height vehicles resulting in a continuous cycle of increased bridge heights followed by increased vehicle heights. Until drastic measures are taken to ensure that collisions due to over-height vehicles will not occur, it is necessary to investigate emergency repair methods, especially of prestressed concrete bridges. The repair of prestressed concrete structures with FRP systems needs additional research for the following reasons: to determine that all failure modes have been observed, to determine solutions to undesirable failure modes, to determine if the necessary capacity of a damaged member can be regained through FRP strengthening, and to determine standards for the repair designs of FRP strengthened systems of prestressed concrete structures. To minimize over-height vehicle collisions some preventative measures could be used such as additional warning signs, more aggressive enforcement, higher fines for violators, placement of video cameras on previously impacted bridges, or over-height vehicle detection systems with communication devices.

Summary

Full-scale girder tests of six type II AASHTO girders were performed. The six tests represented an undamaged control specimen, a control specimen with simulated damage, and the four specimens with simulated damage that were then repaired with different fiber reinforced polymer systems. The FRP systems varied in material types, laminate properties, application procedures, reinforcing schemes, and repair design procedures and assumptions. The specimens were tested to failure to determine moment and shear capacities, as well as deformation and ductility behavior of the undamaged, damaged, and repaired girders. Through experimental and analytical comparisons of the behavior of the repaired girders to the undamaged girder, the specific fiber reinforced polymer systems were evaluated for acceptance to the FDOT Quality Products List. The FRP systems were evaluated structurally on their ability to restore the undamaged shear and moment capacity of the prestressed concrete girder, type of failure mode, cost of repair system including installation and ease of installation.

Conclusions

Although Test Specimen 3 failed prematurely, it still regained 96.4% of the theoretical capacity and 90.9% of the experimental capacity of Test Specimen 1. The use of stirrups at the ends of the FRP laminate could have provided sufficient resistance to the peeling stresses that led to premature failure. Test Specimen 4, repaired with carbon fibers and a polyurethane adhesive, failed prematurely due to adhesive failure followed by FRP rupture. The test specimen did not regain any of the lost capacity due to the simulated damage. Test Specimen 5 failed due to FRP rupture with a regained theoretical capacity equal to 100.7% and with a regained experimental capacity equal to 95% of Test Specimen 1. The desired thickness of the spray FRP for the tensile face of the beam was

0.50", although only an average thickness of 0.27" was achieved. If the desired thickness of 0.50" had been achieved, Test Specimen 5 could have, at a minimum, attained the same capacity as the undamaged girder. The failure mode of Test Specimen 6 was failure of an FRP anchorage which allowed the longitudinal FRP to slip between the anchorages. The test specimen still regained 114% of the theoretical capacity and 108% of the experimental capacity of Test Specimen 1.

The midspan deflections at the maximum capacity for all of the repaired test specimens showed significant reductions with a minimum reduction equal to 23% of the theoretical deflection at maximum capacity of Test Specimen 1. The measured strains on the bottom centerline of the girder at maximum capacity for all of the repaired test specimens showed significant reductions with a minimum reduction equal to 39% of the experimental maximum strain at maximum capacity of Test Specimen 1.

Future Testing Recommendations for Measurements to Assess Adequacy and Performance of FRP Repair

The lack of instrumentation and properly functioning instruments used for the girder tests resulted in minimal conclusions being drawn from the experiments in some cases. By increasing the number and type of instruments used on each specimen, better information can be obtained to help understand what is occurring in the specimens during loading. Additional load cells at the supports are needed to determine if unequal loading is resulting in unequal reactions at the supports. More strain gauges are needed in the compression region to make up for gauges that were located too close to the neutral axis resulting in unusable data. If possible, strain gauges should be placed directly on the prestressing strands to obtain more accurate data than from the crack gauges applied to the concrete surface at the level of prestressing. By instrumenting the prestressing

strands directly, the problems encountered with the crack gauges might have been avoided. Instrumenting both the damaged and undamaged prestressing strands would show if the damaged strands should be fully or partially neglected in repairs and if the damaged strands have similar strains to the surrounding concrete over only a portion of their length due to their loss of development and transfer length. Instrumenting the damaged and undamaged strands would also provide information related to strand slip or strand failure during testing.

For future tests, camber measurements before the slab is poured, after the slab is cast, after the concrete is removed (damage), after the strands are severed, after the concrete patch is applied, and after the FRP system is applied will all be valuable for determining stresses in the test specimens.

APPENDIX A
REPAIR DESIGNS

This appendix contains the design procedures for the repairs of Test Specimens 3, 4, and 5.

RJWatson Repair Design

The RJWatson repair design is shown below as provided to the FDOT for installation.

CLIENT: Florida DOT SHEET 1 OF 2
PROJECT NAME: Test Program PROJECT #:
CALCULATION BY: SEW DATE: 11-15-02

Design Goal: To provide additional flexural capacity to the damaged beams.

Existing Beam Properties:

$b := 18$	beam width (on bottom) (in)
$d := 36$	beam depth (in)
$t_s := 12$	slab thickness (in)
$d_f := d + t_s$	total depth of beam and slab for flexure (in)
$d_f = 48$	
$l := 43.75$	beam span length (ft)
$f'_c := 4.5$	concrete compressive strength (ksi)

Tyfo® SCH 41S Unidirectional Carbon Composite Properties:

$E_u := 10500$	typical test value for tensile modulus (ksi)
$C_E := 0.85$	environmental reduction factor for carbon
$E := C_E \cdot E_u$	guaranteed design value for tensile modulus (ksi)
$E = 8925$	
$\varepsilon := 0.006$	allowable design strain in composite for flexure

$f := E \cdot \varepsilon$ guaranteed design stress in composite (ksi)

$f = 53.6$

$t := 0.04$ layer thickness of SCH 41S composite (in)

Moment capacity enhancement with one layer of composite:

The moment capacity enhancement of the beam provided by the composite is:

$$\Phi M = \Phi\ A\ f\ (jd)$$

$\Phi := 0.9$ ACI reduction factor for flexure

$A := t \cdot b$ area of one layer of composite (in^2)

$A = 0.72$

$jd := 0.9 \cdot d_f$ assumed moment lever arm (in)

$jd = 43.2$

$$\Phi M := \Phi \cdot A \cdot f \cdot \frac{jd}{12}$$

$\Phi M = 124.9$ additional moment capacity of beam with one layer of composite (k-ft)

Required number of layers of composite:

The number of layers of composite needed on the beam is based on the additional moment demand required.

$M_{req} := 2012 - 1576$

required additional moment capacity (k-ft)

$$layers := \left(\frac{M_{req}}{\Phi M} \right)$$

number of layers required

$layers := ceil(layers)$ round up to closest number of layers

$layers = 4$

Design Conclusions:

Providing 4 layers of the Tyfo® SCH 41S System will enhance the flexural capacity of the beam to restore the original design strength.

Air Logistics Repair Design

The Air Logistics repair design is shown below as provided to the FDOT for installation except that the written calculations have been duplicated in computer format for presentation.

$kip := 1000lbf$ $ksi := 1000psi$

Client: Air Logisitcs Corporation
-FDOT

Project: FLDOT AASHTO Girder Test Program

Structure: AASHTO Type II Girder
-Control
-Damaged: 4 prestressing strands severed

Objective: Use CFRP retrofit system to strengthen the damaged girder

Goal: Strengthen the damaged girder in a manner that results in the girder resembling or exceeding the performance of the control girder

TEST DATA

Theoretical Capacities

$M_{controlT} := 2007kip \cdot ft$ $M_{damagedT} := 1624kip \cdot ft$

$P_{controlT} := 133.8kip$ $P_{damagedT} := 108.3kip$

Experimental Capacities

$M_{controlE} := 2012kip \cdot ft$ $M_{damagedE} := 1576kip \cdot ft$

$P_{controlE} := 134.1kip$ $P_{damagedE} := 105.1kip$

Experimental Deflections

Δ is for deflection at midspan and δ is for deflection at the load points 15 feet from supports

$\Delta_{control} := 6.34in$ $\Delta_{damaged} := 6.37in$

$\delta_{control} := 5.58in$ $\delta_{damaged} := 5.57in$

Experimental Strains

E is for maximum strain at center on bottom at failure and ε is for maximum strain on bottom at load points 15 feet from supports

$E_{control} := .0095\frac{in}{in}$ $E_{damaged} := 0.027\frac{in}{in}$

$\varepsilon_{control} := 0.018\frac{in}{in}$ $\varepsilon_{damaged} := 0.021\frac{in}{in}$

$l := 40ft$ $P_1 := P_{controlE}$

$s := 10ft$ $P_2 := P_1$

$x := 20ft$

$$M_{midspan} := x \cdot \frac{(l - x)}{l} \cdot \left[P_1 + P_2 \cdot \frac{(x - s)}{x} \right] \qquad M_{midspan} = 2011.5kip \cdot ft$$

$V_{midspan} := 0kip$

$x := 15ft$

$$M_{loadpoint} := x \cdot \frac{(l - x)}{l} \cdot \left[P_1 + P_2 \cdot \frac{(x - s)}{x} \right] \qquad M_{loadpoint} = 1676.25kip \cdot ft$$

$$V_{loadpoint} := P_1 \cdot \frac{(l - x)}{l} + P_2 \cdot \frac{(l - x - s)}{l} \qquad V_{loadpoint} = 134.1kip$$

$x := 0ft$

$$M_{support} := x \cdot \frac{(l - x)}{l} \cdot \left[P_1 + P_2 \cdot \frac{(x - s)}{x} \right] \qquad M_{support} = 0kip \cdot ft$$

$$V_{support} := P_1 \cdot \frac{(l - x)}{l} + P_2 \cdot \frac{(l - x - s)}{l} \qquad V_{support} = 234.67kip$$

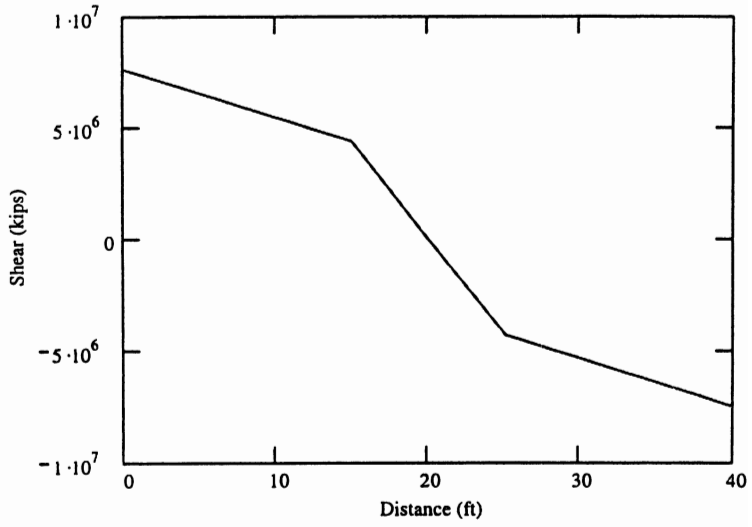

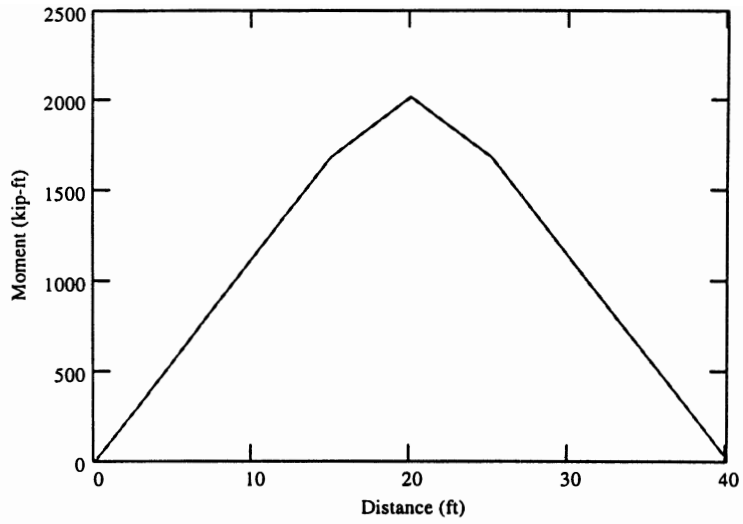

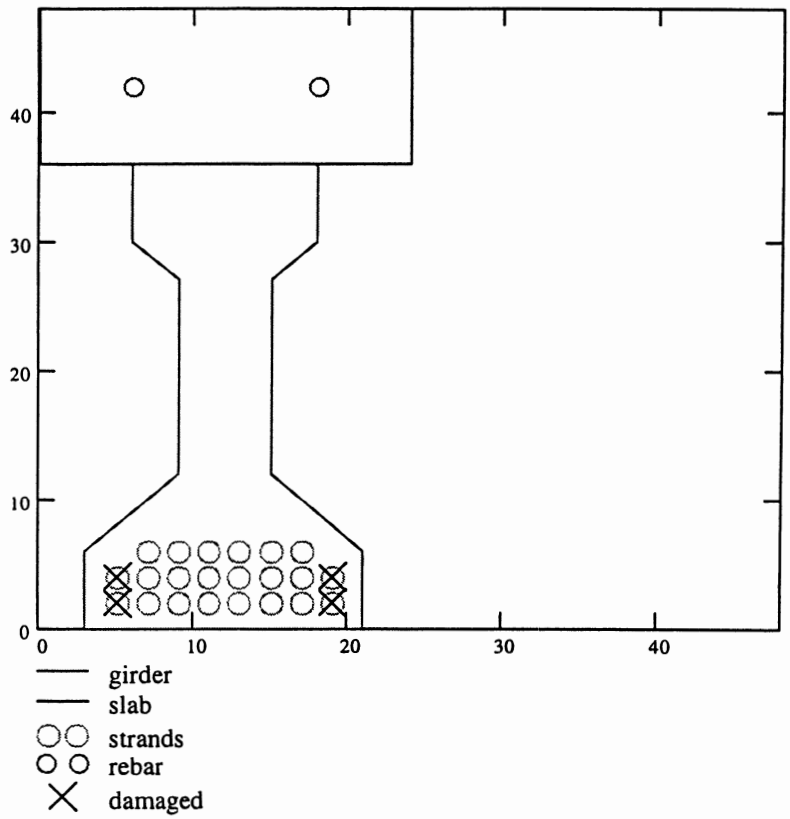

$A_g := (12 \cdot in \cdot 24 \cdot in) + (12 \cdot in \cdot 6 \cdot in) + (6 \cdot in \cdot 3 \cdot in) + 2 \cdot (.5 \cdot 3in \cdot 3in) + 6in \cdot 15in + (6in \cdot 6in) \ldots$
$+ 2 \cdot (.5 \cdot 6in \cdot 6in) + (6in \cdot 18in)$

$A_g = 657in^2$

$A_g = 4.56ft^2$

$V_c := A_g \cdot 43.75ft$ $V_c = 199.61ft^3$

$\gamma := 150\frac{lbf}{ft^3}$

$W := \gamma \cdot V_c$ $W = 29.94kip$

$w := \frac{W}{43.75ft}$ $w = 0.684\frac{kip}{ft}$

$M_{dead} := \frac{w \cdot l^2}{8}$ $M_{dead} = 136.87kip \cdot ft$ moment at midspan due to self-weight

Calculate Cracked Transformed Section

$d_1 := 42in$

$f'c := 6300psi$ compression is in the slab

$d_2 := 44in$

$E_s := 29000ksi$

$d_3 := 46in$

$E_c := 57000\left(psi^{.5}\sqrt{f'c}\right)$ $E_c = 4524.23ksi$

$d := 48in$

$t_s := 24in$

$n := \frac{E_s}{E_c}$ $n = 6.41$

$d_s := 12in$

$A_{stop} := 0.31in^2$ Area of #5 bars at midheight of slab

$A_s := .115in^2$ Area of strand of 7/16 inch diameter and 250 ksi steel

Transformed Areas

$A_{s1} := 6 \cdot A_s$

$A_{s2control} := 8 \cdot A_s$ $A_{s2damaged} := 6 \cdot A_s$

$A_{s3control} := 8 \cdot A_s$ $A_{s3damaged} := 6 \cdot A_s$

$$Acontrol := \begin{pmatrix} A_{s1} \\ A_{s2control} \\ A_{s3control} \end{pmatrix} \quad Adamaged := \begin{pmatrix} A_{s1} \\ A_{s2damaged} \\ A_{s3damaged} \end{pmatrix}$$

Concrete

$A_c := A_g$ $A_c = 4.56ft^2$

Steel

$A_{spos} := 2 \cdot A_{stop} \cdot (n - 1)$ $A_{spos} = 3.35in^2$

$A_{scontrol} := n \cdot (A_{s1} + A_{s2control} + A_{s3control})$ $A_{scontrol} = 16.22in^2$

$A_{sdamaged} := n \cdot (A_{s1} + A_{s2damaged} + A_{s3damaged})$ $A_{sdamaged} = 13.27in^2$ only 18 strands carrying load for damaged condition

Bottom Carbon

$E_f := 11000ksi$

$t_f := 0.028in$

$w_f := 12in$

$f_{fabric} := 120ksi$

$\varepsilon_{fabric} := .012\frac{in}{in}$

$z := 3$ number of layers

$A_{f3} := \frac{E_f}{E_c} \cdot w_f \cdot z \cdot t_f$ $A_{f3} = 2.45in^2$ for 3 layers

$z := 4$ number of layers

$A_{f4} := \frac{E_f}{E_c} \cdot w_f \cdot z \cdot t_f$ $A_{f4} = 3.27in^2$ for 4 layers

Calculate Neutral Axis for Three Cases

CASE 1: CONTROL

$$X(c) := \left[t_s \cdot c \cdot \left(\frac{c}{2}\right)\right] + A_{spos} \cdot \left(c - \frac{d_s}{2}\right) + A_{scontrol} \cdot (c - d_2)$$

$c := 7.0462in$ comparable to data points from tested strain gauges

$X(c) = 0.01in^3$ $c_{control} := c$

CASE 2: DAMAGED

$$X(c) := \left[t_s \cdot c \cdot \left(\frac{c}{2} \right) \right] + A_{spos} \cdot \left(c - \frac{d_s}{2} \right) + A_{sdamaged} (c - d_2)$$

$c := 6.4354\text{in}$

$X(c) = 0.01\text{in}^3$ $\quad c_{damaged} := c$

CASE 3: REPAIRED

for 4 layers of FRP

$$X(c) := \left[t_s \cdot c \cdot \left(\frac{c}{2} \right) \right] + A_{spos} \cdot \left(c - \frac{d_s}{2} \right) + A_{sdamaged} (c - d_2) + A_{f4} \cdot (c - d)$$

$c := 7.1766\text{in}$

$X(c) = -0\text{in}^3$ $\quad c_{repaired4} := c$

for 3 layers of FRP

$$X(c) := \left[t_s \cdot c \cdot \left(\frac{c}{2} \right) \right] + A_{spos} \cdot \left(c - \frac{d_s}{2} \right) + A_{sdamaged} (c - d_2) + A_{f3} \cdot (c - d)$$

$c := 7.0004\text{in}$

$X(c) = 0.01\text{in}^3$ $\quad c_{repaired3} := c$

STRESS DISTRIBUTION

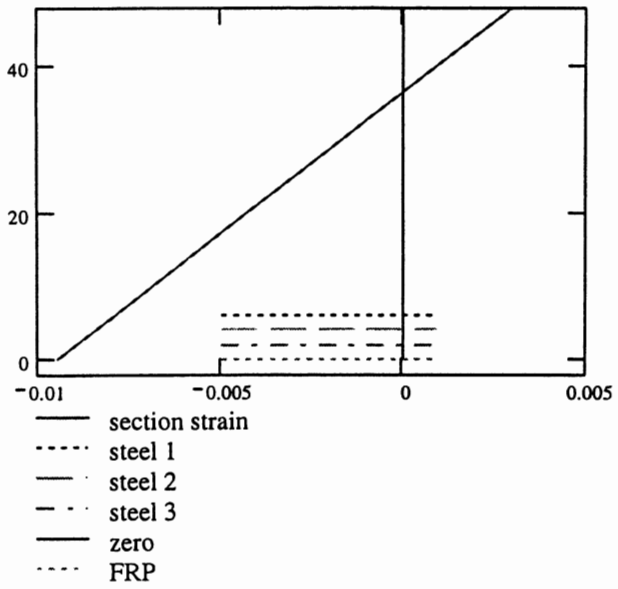

ASSUMPTIONS

$f_u := 250ksi$

$f_y := 0.85 \cdot f_u$ $\quad f_y = 212.5ksi$

$f_i := 0.85 \cdot f_y$ $\quad f_i = 180.62ksi$ initial tendon stress

At failure assume 1) concrete is at limit $\varepsilon_{cu} = 0.003$
2) bottom steel is at ultimate limit $f_u = 250$ ksi (3 layers of steel)
3) other two layers of steel at reduced stress

Find Steel Stresses by Similar Triangles

REPAIRED 4 LAYERS

$$f_2 := (d_2 - c_{repaired4}) \cdot \frac{f_u}{d_3 - c_{repaired4}} \qquad f_2 = 237.12ksi$$

CONTROL

$$f_2 := (d_2 - c_{control}) \cdot \frac{f_u}{d_3 - c_{control}} \qquad f_2 = 237.16ksi$$

$$f_1 := (d_1 - c_{control}) \cdot \frac{f_u}{d_3 - c_{control}} \qquad f_1 = 224.33ksi$$

$f_3 := f_u$ $\qquad f := \begin{pmatrix} f_1 \\ f_2 \\ f_3 \end{pmatrix}$

CALCULATE MOMENT CAPACITY

CONTROL

$a := 0.85 \cdot c_{control}$

$$jd := \begin{pmatrix} d_1 - \frac{a}{2} \\ d_2 - \frac{a}{2} \\ d_3 - \frac{a}{2} \end{pmatrix} \qquad jd = \begin{pmatrix} 39.01 \\ 41.01 \\ 43.01 \end{pmatrix} in$$

$$Mc := \sum_{i=0}^{2} Acontrol_i \cdot f_i \cdot jd_i \qquad Mc = 2072.98\,kip\cdot ft$$

DAMAGED

$$a := 0.85 \cdot c_{damaged}$$

$$jd := \begin{pmatrix} d_1 - \frac{a}{2} \\ d_2 - \frac{a}{2} \\ d_3 - \frac{a}{2} \end{pmatrix} \qquad jd = \begin{pmatrix} 39.26 \\ 41.26 \\ 43.26 \end{pmatrix} in$$

$$Md := \sum_{i=0}^{2} Adamaged_i \cdot f_i \cdot jd_i \qquad Md = 1691.14\,kip\cdot ft$$

REPAIRED

$$jdf := 45in$$

$$\phi := \frac{E_{control}}{\varepsilon_{fabric}} \qquad \phi = 0.792 \qquad \phi := 0.8$$

by setting the ultimate strain for the FRP fabric equal to the ultimate strain found experimentally, a strength reduction of ϕ = 0.8 has to be applied for capacity calculations

with 4 layers

$$z := 4$$

$$a := 0.85 \cdot c_{repaired4}$$

$$jd := \begin{pmatrix} d_1 - \frac{a}{2} \\ d_2 - \frac{a}{2} \\ d_3 - \frac{a}{2} \end{pmatrix} \qquad jd = \begin{pmatrix} 38.95 \\ 40.95 \\ 42.95 \end{pmatrix} in$$

$$Mr4 := \left(\sum_{i=0}^{2} Adamaged_i \cdot f_i \cdot jd_i \right) + \left(z \cdot t_f \cdot w_f \cdot \phi \cdot f_{fabric} \cdot jdf \right) \qquad Mr4 = 2162.09\,kip\cdot ft$$

with 3 layers

$z := 3$

$a := 0.85 c_{repaired3}$

$$jd := \begin{pmatrix} d_1 - \frac{a}{2} \\ d_2 - \frac{a}{2} \\ d_3 - \frac{a}{2} \end{pmatrix} \qquad jd = \begin{pmatrix} 39.02 \\ 41.02 \\ 43.02 \end{pmatrix} \text{ in}$$

$$Mr3 := \left(\sum_{i=0}^{2} Adamaged_i \cdot f_i \cdot jd_i \right) + \left(z \cdot t_f \cdot w_f \cdot \phi \cdot f_{fabric} \cdot jdf \right) \qquad Mr3 = 2044.2 \text{kip} \cdot \text{ft}$$

$$M = \begin{pmatrix} 0 \\ 1676.25 \\ 2011.5 \\ 1676.25 \\ 0 \end{pmatrix} \text{kip} \cdot \text{ft} \qquad M_{damaged} := \begin{pmatrix} Md \\ Md \\ Md \\ Md \\ Md \end{pmatrix} \qquad M_{repair4} := \begin{pmatrix} Mr4 \\ Mr4 \\ Mr4 \\ Mr4 \\ Mr4 \end{pmatrix} \qquad M_{repair3} := \begin{pmatrix} Mr3 \\ Mr3 \\ Mr3 \\ Mr3 \\ Mr3 \end{pmatrix}$$

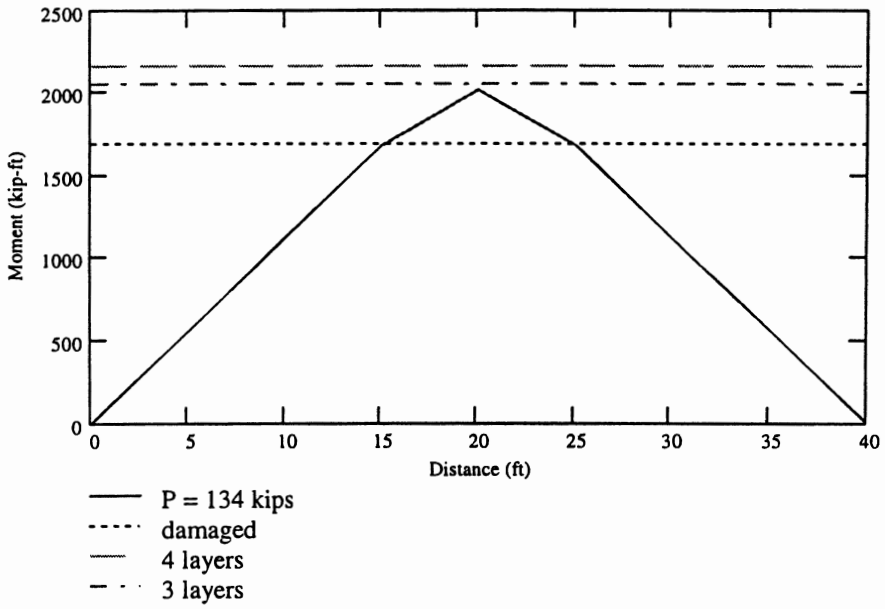

$P_1 := 140kip \qquad P_2 := P_1$

$x := 20ft$

$$M_{midspan} := x \cdot \frac{(l - x)}{l} \cdot \left[P_1 + P_2 \cdot \frac{(x - s)}{x} \right]$$

$x := 0ft$

$$M_{support} := x \cdot \frac{(l - x)}{l} \cdot \left[P_1 + P_2 \cdot \frac{(x - s)}{x} \right]$$

$x := 15ft$

$$M_{lp} := x \cdot \frac{(l - x)}{l} \cdot \left[P_1 + P_2 \cdot \frac{(x - s)}{x} \right]$$

$$M_{140} := \begin{pmatrix} M_{support} \\ M_{lp} \\ M_{midspan} \\ M_{lp} \\ M_{support} \end{pmatrix} \qquad xx := \begin{pmatrix} 0ft \\ 15ft \\ 20ft \\ 25ft \\ 40ft \end{pmatrix}$$

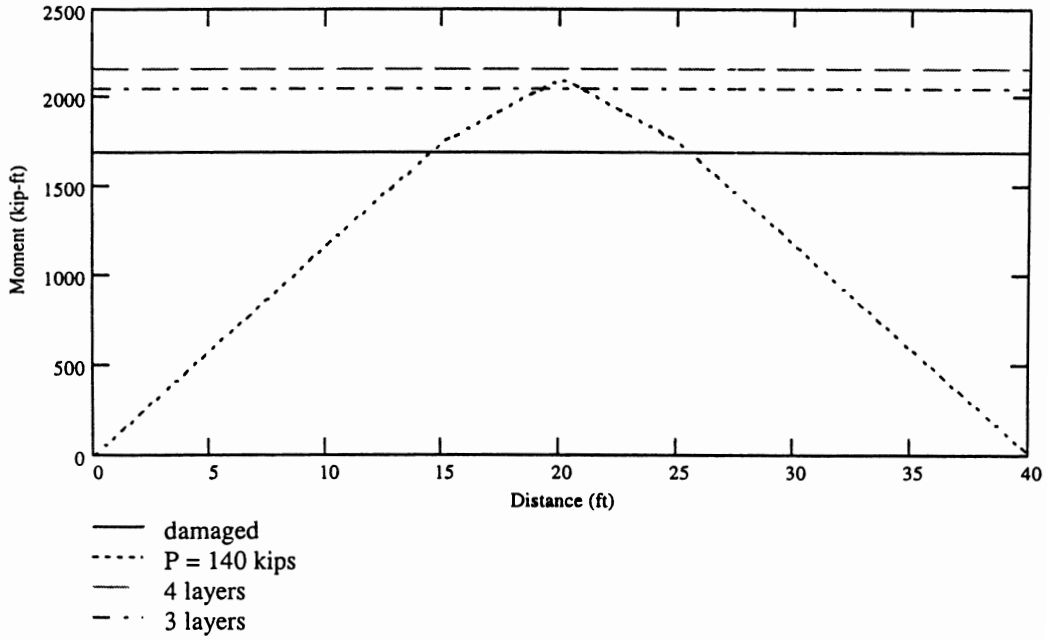

Minimum Theoretical Strip Lengths

layer1 := l – (2·14ft) + (2·7.5ft) layer1 = 27ft

layer2 := l – (2·16ft) + (2·5ft) layer2 = 18ft

layer3 := l – (2·18ft) + (2·4ft) layer3 = 12ft

layer4 := l – (2·20ft) + (2·3.5ft) layer4 = 7ft

The numbers inside the first parenthesis to be subtracted above represents the theoretical cutoff and the numbers inside the second parenthesis to be added above represents the providing of Le beyond the theoretical cut off.

Proposed Lengths

layer1 := 40ft

layer2 := 32ft to be centered at midspan

layer3 := 24ft

layer4 := 16ft

Alternatively, all 4 layers could be carried over full length

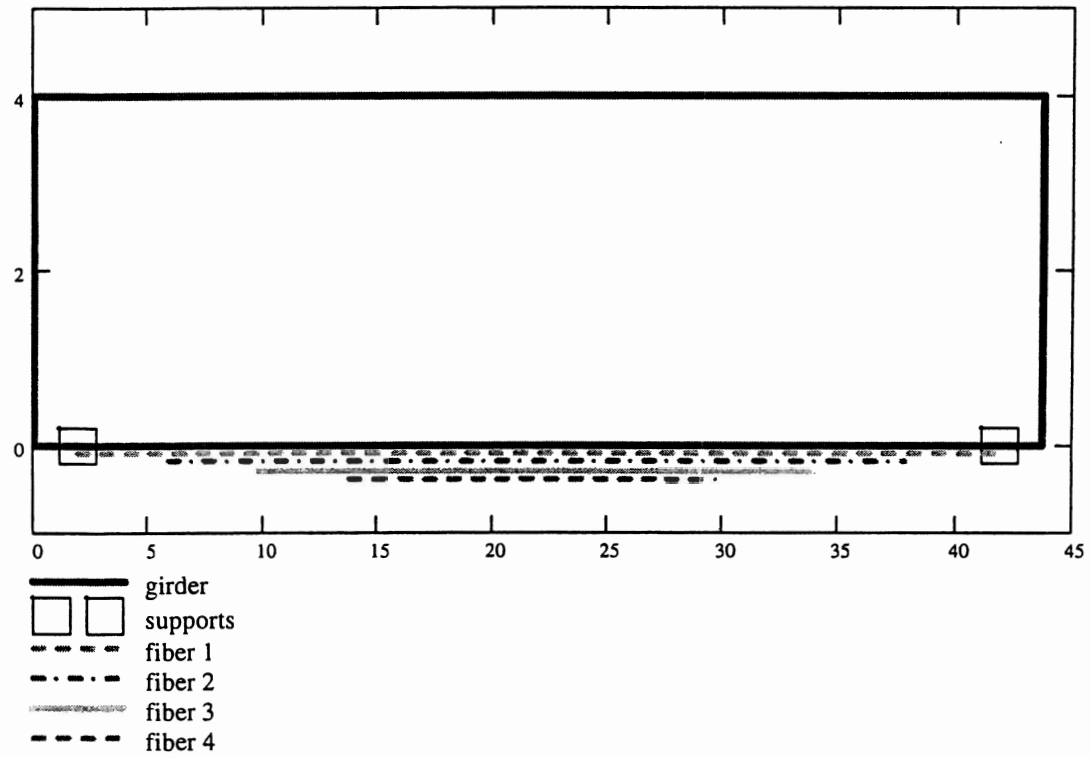

UF Repair Design-As Designed

The UF repair design is shown below as it was initially designed and provided to the FDOT

$h := 48$ (in) height of section

$width := 18$ (in) width of flange that the FRP will be applied to, to assist in carrying moment

$f'_c := 4.5$ (ksi)

Input thickness $t_f := 0.35$ (in) Thickness of FRP to be applied varied until desired moment of 2012 kip-ft is reached

$$RefCentY := \frac{13599 + 48 \cdot width \cdot t_f + \frac{width}{2} \cdot t_f^2}{657 + width \cdot t_f}$$

Elastic Centroid

$RefCentY = 20.96$ (in)

STEEL

$Ap1 := 6 \cdot 0.108$ (in^2) 1st layer of steel from the bottom

$Ap2 := 6 \cdot 0.108$ (in^2) 2nd layer of steel from the bottom

$Ap3 := 6 \cdot 0.108$ (in^2) 3rd layer of steel from the bottom

$d1 := 46$ (in) distance of first layer of steel from the top of section

$d2 := 44$ (in) distance of second layer of steel from the top of section

$d3 := 42$ (in) distance of third layer of steel from the top of section

$E_p := 27500$ (ksi) Modulus of elasticity of prestressing steel typical for 250 ksi steel

$f_{pe} := 120$ (ksi) Inputted value from calculation of prestress losses

FRP

$E_f := 1711$ (ksi) Modulus of FRP for spray-up from Boyd's thesis of 2 in fiber length

$\varepsilon_{fu} := 0.0132$ Material failure strain for spray-up from Boyd's thesis of 2 in fiber length

$\varepsilon_{fiber} := 0.0132$

$f_{fiber} := \varepsilon_{fiber} \cdot E_f$

$F_{fiber} := width \cdot t_f \cdot f_{fiber}$

$$M_{fiber} := F_{fiber} \left[\left(h + \frac{t_f}{2} \right) - RefCentY \right]$$

CONCRETE

$$\varepsilon top(c) := \frac{\varepsilon_{fu} \cdot c}{h - c}$$

Concrete compressive strain at the top of the section in terms of strain in FRP being at ultimate

$$\varepsilon_c(c,z) := \frac{\varepsilon top(c)}{c} \cdot z$$

$$fcs(c,z) := \left| \begin{array}{l} nf \leftarrow \frac{1}{2.5} \cdot f'_c + 0.8 \\ \varepsilon fc \leftarrow \frac{f'_c}{1265\sqrt{f'_c} + 1000} \cdot \left[\frac{\left(\frac{f'_c}{2.5} + 0.8 \right)}{\left(\frac{f'_c}{2.5} + 0.8 \right) - 1} \right] \\ k \leftarrow \frac{f'_c}{9} + 0.67 \\ \varepsilon peak \leftarrow \exp\left[\frac{\ln\left[\frac{(nf - 1)}{(-1 + nf \cdot k)} \right]}{(nf \cdot k)} \right] \cdot \varepsilon fc \\ f_{c\_peak} \leftarrow \frac{nf \cdot \left(\frac{\varepsilon peak}{\varepsilon fc} \right)}{nf - 1 + \left(\frac{\varepsilon peak}{\varepsilon fc} \right)^{nf \cdot k}} \cdot f'_c \\ adjust \leftarrow \frac{f'_c}{f_{c\_peak}} \\ fcs\_actual \leftarrow \frac{nf \cdot \left(\frac{\varepsilon_c(c,z)}{\varepsilon fc} \right)}{nf - 1 + \left(\frac{\varepsilon_c(c,z)}{\varepsilon fc} \right)^{nf \cdot k}} \cdot f'_c \cdot adjust \\ fcs\_actual \end{array} \right.$$

Width of Section: z is the distance from the neutral axis; c is the neutral axis position from the top fiber of concrete

$$b(c,z) := \begin{cases} 24 & \text{if } c \geq z \geq (c-12) \\ 12 & \text{if } (c-12) > z \geq (c-18) \\ 6 + 2\cdot[-(c-z)+21] & \text{if } (c-18) > z \geq (c-21) \\ 6 & \text{if } (c-21) > z \geq (c-36) \\ [6 - 2\cdot[36-(c-z)]] & \text{if } (c-36) > z \geq (c-42) \\ 18 & \text{if } (c-42) \geq z \geq (c-48) \\ 0 & \text{otherwise} \end{cases}$$

(in)

For calculation with effects of the 12 in slab

$$Fcc(c) := \int_0^c b(c,z)\cdot fcs(c,z)\,dz$$ Force contribution from concrete

$$Mcc(c) := \int_0^c [z - [c - (h - RefCentY)]]\cdot b(c,z)\cdot fcs(c,z)\,dz$$ Moment contribution from concrete about the elastic centroid

PRESTRESS

Stress relieved steel

$A := 0.01091$ $B := 115.09$

Ramberg-Osgood Coefficients obtained from direct tensile tests of strands removed from test specimen 2.

$$\varepsilon pe := \frac{f_{pe}}{E_p} \qquad \varepsilon pe = 4.363636\times 10^{-3}$$

$$f(\varepsilon, c) := \text{if}\left[E_p\cdot\varepsilon(c)\cdot\left[A + \frac{1-A}{\left[1+(B\cdot\varepsilon(c))^{10}\right]^{0.1}}\right] < 250,\ E_p\cdot\varepsilon(c)\cdot\left[A + \frac{1-A}{\left[1+(B\cdot\varepsilon(c))^{10}\right]^{0.1}}\right],\ 250\right]$$

$$\varepsilon 1(c) := (d1-c)\cdot\left(\frac{d1-c}{c}\right) \qquad \varepsilon 2(c) := (d2-c)\cdot\left(\frac{d2-c}{c}\right) \qquad \varepsilon 3(c) := (d3-c)\cdot\left(\frac{d3-c}{c}\right)$$

$$\varepsilon_{p1}(c) := \varepsilon pe + \varepsilon 1(c) \qquad \varepsilon_{p2}(c) := \varepsilon pe + \varepsilon 2(c) \qquad \varepsilon_{p3}(c) := \varepsilon pe + \varepsilon 3(c)$$

$$F_{p1}(c) := Ap1\cdot\left(f\left(\varepsilon_{p1}, c\right)\right) \qquad F_{p2}(c) := Ap2\cdot f\left(\varepsilon_{p2}, c\right) \qquad F_{p3}(c) := Ap3\cdot f\left(\varepsilon_{p3}, c\right)$$

$$F_{ptotal}(c) := F_{p1}(c) + F_{p2}(c) + F_{p3}(c)$$

$M_{p1}(c) := F_{p1}(c)\cdot[d1 - (h - RefCentY)]$

$M_{p2}(c) := F_{p2}(c)\cdot[d2 - (h - RefCentY)]$

$M_{p3}(c) := F_{p3}(c)\cdot[d3 - (h - RefCentY)]$

$M_{ptotal}(c) := M_{p1}(c) + M_{p2}(c) + M_{p3}(c)$

$Ftotal(c) := Fcc(c) - F_{ptotal}(c) - F_{fiber}$

$Mtotal_{440}(c) := Mcc(c) + M_{ptotal}(c) + M_{fiber}$

$cc := root(Ftotal(c), c, 0, 15)$ $cc = 7.801$ Neutral axis distance from the top of the section

$Fcc(cc) = 611.11$

$Mtotal_{440}(cc) = 26473.61$ (kip-in) Ultimate moment capacity

$\frac{Mtotal_{440}(cc)}{12} = 2206.13$ (kip-ft) Ultimate moment capacity

UF Repair Design-As Built

The UF repair design as presented previous is shown below to demonstrate the capacity of the repair with the as built properties with a fiber length of 1.25" and a thickness of 0.50".

$h := 48$ (in) height of section

$width := 18$ (in) width of flange that the FRP will be applied to, to assist in carrying moment

$f'_c := 4.5$ (ksi)

Input thickness $t_f := 0.50$ (in)

$$RefCentY := \frac{13599 + 48\cdot width\cdot t_f + \frac{width}{2}\cdot t_f^2}{657 + width\cdot t_f}$$

$RefCentY = 21.071$ (in) Elastic Centroid

STEEL

$Ap1 := 6 \cdot 0.108$ (in^2) 1st layer of steel from the bottom

$Ap2 := 6 \cdot 0.108$ (in^2) 2nd layer of steel from the bottom

$Ap3 := 6 \cdot 0.108$ (in^2) 3rd layer of steel from the bottom

$d1 := 46$ (in) distance of first layer of steel from the top of section

$d2 := 44$ (in) distance of second layer of steel from the top of section

$d3 := 42$ (in) distance of third layer of steel from the top of section

$E_p := 27500$ (ksi) Modulus of elasticity of prestressing steel typical for 250 ksi steel

$f_{pe} := 120$ (ksi) Inputted value from calculation of prestress losses

FRP

$E_f := 1522$ (ksi) Modulus of FRP for spray-up from Boyd's thesis of 1.25 in fiber length

$\varepsilon_{fu} := 0.0143$ Material failure strain for spray-up from Boyd's thesis of 1.25 in fiber length

$\varepsilon_{fiber} := 0.0143$

$f_{fiber} := \varepsilon_{fiber} \cdot E_f$

$F_{fiber} := width \cdot t_f \cdot f_{fiber}$

$$M_{fiber} := F_{fiber} \cdot \left[\left(h + \frac{t_f}{2} \right) - RefCentY \right]$$

CONCRETE

$$\varepsilon top(c) := \frac{\varepsilon_{fu} \cdot c}{h - c}$$ Concrete compressive strain at the top of the section in terms of strain in FRP being at ultimate

$$\varepsilon_c(c, z) := \frac{\varepsilon top(c)}{c} \cdot z$$

$$\text{fcs}(c, z) := \left| \begin{array}{l} nf \leftarrow \frac{1}{2.5} \cdot f'_c + 0.8 \\ \varepsilon fc \leftarrow \frac{f'_c}{1265 \cdot \sqrt{f'_c} + 1000} \cdot \left[\frac{\left(\frac{f'_c}{2.5} + 0.8 \right)}{\left(\frac{f'_c}{2.5} + 0.8 \right) - 1} \right] \\ k \leftarrow \frac{f'_c}{9} + 0.67 \\ \varepsilon peak \leftarrow \exp\left[\frac{\ln\left[\frac{(nf - 1)}{(-1 + nf \cdot k)} \right]}{(nf \cdot k)} \right] \cdot \varepsilon fc \\ f_{.c\_peak} \leftarrow \frac{nf \cdot \left(\frac{\varepsilon peak}{\varepsilon fc} \right)}{nf - 1 + \left(\frac{\varepsilon peak}{\varepsilon fc} \right)^{nf \cdot k}} \cdot f'_c \\ adjust \leftarrow \frac{f'_c}{f_{.c\_peak}} \\ fcs\_actual \leftarrow \frac{nf \cdot \left(\frac{\varepsilon_c(c, z)}{\varepsilon fc} \right)}{nf - 1 + \left(\frac{\varepsilon_c(c, z)}{\varepsilon fc} \right)^{nf \cdot k}} \cdot f'_c \cdot adjust \\ fcs\_actual \end{array} \right.$$

Width of Section: z is the distance from the neutral axis; c is the neutral axis position from the top fiber of concrete

$$b(c, z) := \left| \begin{array}{l} 24 \quad \text{if} \quad c \geq z \geq (c - 12) \\ 12 \quad \text{if} \quad (c - 12) > z \geq (c - 18) \\ 6 + 2 \cdot [-(c - z) + 21] \quad \text{if} \quad (c - 18) > z \geq (c - 21) \\ 6 \quad \text{if} \quad (c - 21) > z \geq (c - 36) \\ [\, 6 - 2 \cdot [36 - (c - z)] \,] \quad \text{if} \quad (c - 36) > z \geq (c - 42) \\ 18 \quad \text{if} \quad (c - 42) \geq z \geq (c - 48) \\ 0 \quad \text{otherwise} \end{array} \right. \qquad \text{(in)}$$

For calculation with effects of the 12 in slab

$$Fcc(c) := \int_0^c b(c,z)\cdot fcs(c,z)\,dz$$ Force contribution from concrete

$$Mcc(c) := \int_0^c [\,z - [c - (h - RefCentY)]\,]\cdot b(c,z)\cdot fcs(c,z)\,dz$$ Moment contribution from concrete about the elastic centroid

PRESTRESS

Stress relieved steel

$A := 0.01091$

$B := 115.09$

Ramberg-Osgood Coefficients obtained from direct tensile tests of strands removed from test specimen 2

$$\varepsilon pe := \frac{f_{pe}}{E_p} \qquad \varepsilon pe = 4.363636\times 10^{-3}$$

$$f(\varepsilon,c) := \text{if}\left[E_p\cdot\varepsilon(c)\cdot\left[A + \frac{1-A}{\left[1+\left(B\cdot\varepsilon(c)\right)^{10}\right]^{0.1}}\right] < 250, E_p\cdot\varepsilon(c)\cdot\left[A + \frac{1-A}{\left[1+\left(B\cdot\varepsilon(c)\right)^{10}\right]^{0.1}}\right], 250\right]$$

$$\varepsilon 1(c) := (d1 - c)\cdot\left(\frac{\varepsilon_{fu}}{h-c}\right) \qquad \varepsilon 2(c) := (d2 - c)\cdot\left(\frac{\varepsilon_{fu}}{h-c}\right) \qquad \varepsilon 3(c) := (d3 - c)\cdot\left(\frac{\varepsilon_{fu}}{h-c}\right)$$

$$\varepsilon_{p1}(c) := \varepsilon pe + \varepsilon 1(c) \qquad \varepsilon_{p2}(c) := \varepsilon pe + \varepsilon 2(c) \qquad \varepsilon_{p3}(c) := \varepsilon pe + \varepsilon 3(c)$$

$$F_{p1}(c) := Ap1\cdot\left(f\left(\varepsilon_{p1},c\right)\right) \qquad F_{p2}(c) := Ap2\cdot f\left(\varepsilon_{p2},c\right) \qquad F_{p3}(c) := Ap3\cdot f\left(\varepsilon_{p3},c\right)$$

$$F_{ptotal}(c) := F_{p1}(c) + F_{p2}(c) + F_{p3}(c)$$

$$M_{p1}(c) := F_{p1}(c)\cdot[d1 - (h - RefCentY)]$$

$$M_{p2}(c) := F_{p2}(c)\cdot[d2 - (h - RefCentY)]$$

$$M_{p3}(c) := F_{p3}(c)\cdot[d3 - (h - RefCentY)]$$

$$M_{ptotal}(c) := M_{p1}(c) + M_{p2}(c) + M_{p3}(c)$$

$$Ftotal(c) := Fcc(c) - F_{ptotal}(c) - F_{fiber}$$

$$Mtotal_{440}(c) := Mcc(c) + M_{ptotal}(c) + M_{fiber}$$

$cc := root(Ftotal(c), c, 0, 15)$ $cc = 8.327$ Neutral axis distance from the top of the section

$Fcc(cc) = 665.312$

$Mtotal_{440}(cc) = 28950.94$ (kip-in) Ultimate moment capacity

$\frac{Mtotal_{440}(cc)}{12} = 2412.58$ (kip-ft) Ultimate moment capacity

APPENDIX B
THEORETICAL EVALUATION TOOLS

This appendix contains the MathCAD sheets used for calculating theoretical values that were referenced in Chapter 5.

Effective prestress

The following demonstrates how the effective prestress of the prestressing strands was calculated.

$kip := 1000lbf$ $ksi := 1000psi$

$f_{pu} := 250ksi$ $E_{ps} := 27500ksi$ $I_g := 50979in^4$ $A_g := 369in^2$

$A_{ps} := 22 \cdot (0.108in^2)$ $A_{ps} = 2.376in^2$

$f'_c := 4500psi$ $l := 40ft$ $y_{bar} := 20.17in$

$E_c := 57000\sqrt{f'_c \cdot psi}^{0.5}$ $E_c = 3.824 \times 10^3 ksi$

$n := \frac{E_{ps}}{E_c}$ $n = 7.192$

$K_{ci} := 0.9$ prestensioned

$e := 32in - y_{bar}$ $e = 11.83in$

$r := \sqrt{\frac{I_g}{A_g}}$ $r = 11.754in$

$f_{pi} := 0.7 \cdot f_{pu}$ $f_{pi} = 175ksi$

$P_i := f_{pi} \cdot A_{ps}$ $P_i = 415.8kip$

$V_c := A_g \cdot l$ $V_c = 177120in^3$

$\gamma_{conc} := 0.15\frac{kip}{ft^3}$

$W_{sw} := \gamma_{conc} \cdot V_c$ $W_{sw} = 15.375\text{kip}$

$w_{sw} := \frac{W_{sw}}{l}$ $w_{sw} = 0.384\frac{\text{kip}}{\text{ft}}$

$M_D := \frac{w_{sw} \cdot l^2}{8}$ $M_D = 76.875\text{kip}\cdot\text{ft}$

$f_{cs} := \left[K_{ci} \cdot \frac{P_i}{A_g} \cdot \left(1 + \frac{e^2}{r^2} \right) \right] - \frac{M_D \cdot e}{I_g}$ $f_{cs} = 1.827\text{ksi}$

$K_{es} := 1.0$ pretensioned

$\Delta f_{es} := n \cdot f_{cs} \cdot K_{es}$ $\Delta f_{es} = 13.143\text{ksi}$ Losses due to elastic shortening

$K_{cr} := 2.0$ normal weight concrete

$A_{dead} := 24\text{in} \cdot 12\text{in}$

$V_{dead} := A_{dead} \cdot l$ $V_{dead} = 80\text{ft}^3$

$W_{dead} := \gamma_{conc} \cdot V_{dead}$ $W_{dead} = 12\text{kip}$

$w_{dead} := \frac{W_{dead}}{l}$ $w_{dead} = 0.3\frac{\text{kip}}{\text{ft}}$

$M_{dead} := \frac{w_{dead} \cdot l^2}{8}$ $M_{dead} = 60\text{kip}\cdot\text{ft}$

$f_{cds} := \frac{M_{dead} \cdot e}{I_g}$ $f_{cds} = 0.167\text{ksi}$

$\Delta f_{cr} := K_{cr} \cdot n \cdot (f_{cs} - f_{cds})$ $\Delta f_{cr} = 23.882\text{ksi}$ Losses due to creep

$K_{sh} := 1.0$ pretensioned

$RH := 75$

$\text{perimeter} := 2 \cdot (6\text{in} + 6\text{in} + 15\text{in} + 6\text{in} + 9\text{in} + \sqrt{18}\text{in} + \sqrt{72}\text{in})$ $\text{perimeter} = 109.456\text{in}$

$VtoS := \frac{A_g}{\text{perimeter}}$ $VtoS = 3.371\text{in}$

$\Delta f_{sh} := 8.2 \cdot 10^{-6} \frac{\text{in}}{\text{in}} \cdot K_{sh} \cdot E_{ps} \cdot \left(1 - \frac{0.06}{\text{in}} \cdot VtoS \right) \cdot (100 - RH)$ $\Delta f_{sh} = 4.497\text{ksi}$ Losses due to shrinkage

$K_{re} := 18.5\text{ksi}$

$J := 0.14$

$\frac{f_{pi}}{f_{pu}} = 0.7$

$C := 1 + 9 \cdot \left(\frac{f_{pi}}{f_{pu}} - 0.7 \right)$ $C = 1$

$\Delta f_{re} := \left[K_{re} - J \cdot \left(\Delta f_{es} + \Delta f_{cr} + \Delta f_{sh} \right) \right] \cdot C$ $\Delta f_{re} = 12.687 ksi$ Losses due to relaxation of the prestressing strands

$\Delta f_{total} := \Delta f_{es} + \Delta f_{cr} + \Delta f_{sh} + \Delta f_{re}$ $\Delta f_{total} = 54.209 ksi$

$f_{pe} := f_{pi} - \Delta f_{total}$ $f_{pe} = 120.791 ksi$ Effective prestress

Cracking Capacity for Test Specimens in Undamaged and Damaged State

The following demonstrates how the theoretical capacity at cracking was calculated for the test specimens in the undamaged and damaged state.

$kip := 1000 lbf$ $ksi := 1000 psi$

$I_{girder} := 50979 in^4$

$A_{girder} := 369 in^2$ given values

$Y_{Tgirder} := 20.17 in$

$Y_{Bgirder} := 36 in - Y_{Tgirder}$ $Y_{Bgirder} = 15.83 in$

$A_{slab} := 24in \cdot 12in + 12in \cdot 6in + 6in \cdot 3in + 2 \cdot (.5 \cdot 3in \cdot 3in) + 6in \cdot 15in + 6in \cdot 6in + 2 \cdot (.5 \cdot 6in \cdot 6in) + 18in \cdot 6in$

$A_{slab} = 657 in^2$

$Ay_{bar} := (24in \cdot 12in) \cdot 6in + (12in \cdot 6in) \cdot 15in + (6in \cdot 3in) \cdot 19.5in + 2 \cdot (.5 \cdot 3in \cdot 3in) \cdot 19in + (6in \cdot 15in) \cdot 28.5in \ldots$
$+ (6in \cdot 6in) \cdot 39in + 2 \cdot (.5 \cdot 6in \cdot 6in) \cdot 40in + 18in \cdot 6in \cdot 45in$

$Ay_{bar} = 13599 in^3$

$Y_{NA} := \frac{Ay_{bar}}{A_{slab}}$ $Y_{NA} = 20.7 in$ $Y_T := Y_{NA}$ $Y_{Bslab} := 48in - Y_T$ $Y_{Bslab} = 27.3 in$

$$I_{slab} := \frac{1}{12}\cdot 24\,in\cdot(12\,in)^3 + 24\,in\cdot 12\,in\cdot\left(Y_{NA} - 6\,in\right)^2 + \frac{1}{12}\cdot 12\,in\cdot(6\,in)^3 + 12\,in\cdot 6\,in\cdot\left(Y_{NA} - 15\,in\right)^2 \ldots$$
$$+\frac{1}{12}\cdot 6\,in\cdot(3\,in)^3 + 6\,in\cdot 3\,in\cdot\left(Y_{NA} - 19.5\,in\right)^2 + 2\cdot\left[\frac{1}{36}\cdot 3\,in\cdot(3\,in)^3 + \frac{1}{2}\cdot 3\,in\cdot 3\,in\cdot\left(Y_{NA} - 19\,in\right)^2\right] \ldots$$
$$+\frac{1}{12}\cdot 6\,in\cdot(15\,in)^3 + 6\,in\cdot 15\,in\cdot\left(Y_{NA} - 28.5\,in\right)^2 + \frac{1}{12}\cdot 6\,in\cdot(6\,in)^3 + 6\,in\cdot 6\,in\cdot\left(Y_{NA} - 39\,in\right)^2 \ldots$$
$$+2\cdot\left[\frac{1}{36}\cdot 6\,in\cdot(6\,in)^3 + \frac{1}{2}\cdot(6\,in)^2\cdot\left(Y_{NA} - 40\,in\right)^2\right] + \frac{1}{12}\cdot 18\,in\cdot(6\,in)^3 + 18\,in\cdot 6\,in\cdot\left(Y_{NA} - 45\,in\right)^2$$

$I_{slab} = 165220.83\,in^4$

$r := \sqrt{\frac{I_{girder}}{A_{girder}}}$ $r = 11.75\,in$

$e := 36\,in - 4\,in - Y_{Tgirder}$ $e = 11.83\,in$

$c_b := Y_{Bgirder}$ $c_b = 15.83\,in$

$\lambda := 1.0$ normal wt concrete

Cracking Moment Equation from Nawy Prestressed Concrete text 3rd edition Page 403 Eqn 7.2b

$f'c := 4500$

$l := 40\,ft$

$V_{slab} := A_{slab}\cdot l$

$\gamma := 0.15\frac{kip}{ft^3}$

$w := \frac{V_{slab}\cdot\gamma}{l}$ $w = 0.68\frac{kip}{ft}$

$M_d := \frac{w\cdot l^2}{8}$ $M_d = 136.87\,kip\cdot ft$

UNDAMAGED $P_{exp} := 131.253\,kip$

$f_{pe} := 120\,ksi$ $A_{ps} := 22\cdot 0.108\,in^2$

$P_e := f_{pe}\cdot A_{ps}$ $P_e = 285.12\,kip$

$$M_{cr} := \frac{I_{slab}}{Y_{Bslab}}\cdot\left[\left[\left(\frac{P_e}{A_{girder}}\right)\cdot\left(1 + \frac{e\cdot c_b}{r^2}\right)\right] + \left(\frac{7.5\cdot\lambda\cdot\sqrt{f'c}}{1000}\cdot\frac{kip}{in^2}\right)\right] - M_d \qquad M_{cr} = 1034.728\,kip\cdot ft$$

$P_{cr} := \frac{M_{cr}}{15\,ft}\cdot 2$ $P_{cr} = 137.96\,kip$ load at cracking for both load cells

DAMAGED $P_{exp} := 107.88kip$

$f_{pe} := 120ksi$ $A_{ps} := 18 \cdot 0.108in^2$

$P_e := f_{pe} \cdot A_{ps}$ $P_e = 233.28kip$

$$M_{cr} := \frac{I_{slab}}{Y_{Bslab}} \cdot \left[\left(\frac{P_e}{A_{girder}} \right) \cdot \left(1 + \frac{e \cdot c_b}{r^2} \right) + \frac{7.5 \cdot \lambda \cdot \sqrt{f'c}}{1000} \cdot \frac{kip}{in^2} \right] - M_d \qquad M_{cr} = 867.84kip \cdot ft$$

$P_{cr} := \frac{M_{cr}}{15ft} \cdot 2$ $P_{cr} = 115.71kip$ load at cracking for both load cells

Ultimate Capacity for Test Specimens in Undamaged and Damaged State

The following demonstrates how the theoretical capacity at ultimate was calculated for the test specimens in the undamaged state. This method can be used to calculate the theoretical capacity at ultimate for test specimens in the undamaged state by reducing the area of the second and third layers of prestressing steel.

$h := 48$ (in) height of section

$f'_c := 4.5$ (ksi)

$RefCentY := \frac{13599}{657}$ Elastic Centroid

$RefCentY = 20.699$ (in)

STEEL

$Ap1 := 8 \cdot 0.108$ (in^2) 1st layer of steel from the bottom

$Ap2 := 8 \cdot 0.108$ (in^2) 2nd layer of steel from the bottom

$Ap3 := 6 \cdot 0.108$ (in^2) 3rd layer of steel from the bottom

$d1 := 46$ (in) distance of first layer of steel from the top of section

$d2 := 44$ (in) distance of second layer of steel from the top of section

$d3 := 42$ (in) distance of third layer of steel from the top of section

$E_p := 27500$ (ksi) Modulus of elasticity of prestressing steel typical for 250 ksi steel

$f_{pe} := 120$ (ksi) Inputted value from calculation of prestress losses

CONCRETE

$\varepsilon top(c) := 0.003$ Concrete compressive strain at the top of the section

$$\varepsilon_c(c,z) := \frac{\varepsilon top(c)}{c} \cdot z$$

$$fcs(c,z) := \left| \begin{array}{l} nf \leftarrow \frac{1}{2.5} \cdot f'_c + 0.8 \\ \varepsilon fc \leftarrow \frac{f'_c}{1265 \cdot \sqrt{f'_c} + 1000} \cdot \left[\frac{\left(\frac{f'_c}{2.5} + 0.8 \right)}{\left(\frac{f'_c}{2.5} + 0.8 \right) - 1} \right] \\ k \leftarrow \frac{f'_c}{9} + 0.67 \\ \varepsilon peak \leftarrow \exp\left[\frac{\ln\left[\frac{(nf-1)}{(-1+nf \cdot k)} \right]}{(nf \cdot k)} \right] \cdot \varepsilon fc \\ f_{.c\_peak} \leftarrow \frac{nf \cdot \left(\frac{\varepsilon peak}{\varepsilon fc} \right)}{nf - 1 + \left(\frac{\varepsilon peak}{\varepsilon fc} \right)^{nf \cdot k}} \cdot f'_c \\ adjust \leftarrow \frac{f'_c}{f_{.c\_peak}} \\ fcs\_actual \leftarrow \frac{nf \cdot \left(\frac{\varepsilon_c(c,z)}{\varepsilon fc} \right)}{nf - 1 + \left(\frac{\varepsilon_c(c,z)}{\varepsilon fc} \right)^{nf \cdot k}} \cdot f'_c \cdot adjust \\ fcs\_actual \end{array} \right.$$

Width of Section: z is the distance from the neutral axis; c is the neutral axis position from the top fiber of concrete

$$b(c,z) := \begin{cases} 24 & \text{if } c \geq z \geq (c-12) \\ 12 & \text{if } (c-12) > z \geq (c-18) \\ 6 + 2\cdot[-(c-z)+21] & \text{if } (c-18) > z \geq (c-21) \\ 6 & \text{if } (c-21) > z \geq (c-36) \\ [\,6 - 2\cdot[36-(c-z)]\,] & \text{if } (c-36) > z \geq (c-42) \\ 18 & \text{if } (c-42) \geq z \geq (c-48) \\ 0 & \text{otherwise} \end{cases}$$

(in)

For calculation with effects of the 12 in slab

$$Fcc(c) := \int_0^c b(c,z)\cdot fcs(c,z)\,dz$$ Force contribution from concrete

$$Mcc(c) := \int_0^c [\,z - [c-(h-RefCentY)]\,]\cdot b(c,z)\cdot fcs(c,z)\,dz$$ Moment contribution from concrete about the elastic centroid

PRESTRESS

Stress relieved steel

$A := 0.01091$ $B := 115.09$

Ramberg-Osgood Coefficients obtained from direct tensile tests of strands removed from test specimen 2.

$$\varepsilon pe := \frac{f_{pe}}{E_p} \qquad \varepsilon pe = 4.363636\times 10^{-3}$$

$$f(\varepsilon,c) := \text{if}\left[E_p\cdot\varepsilon(c)\cdot\left[A + \frac{1-A}{\left[1+(B\cdot\varepsilon(c))^{10}\right]^{0.1}}\right] < 250,\ E_p\cdot\varepsilon(c)\cdot\left[A + \frac{1-A}{\left[1+(B\cdot\varepsilon(c))^{10}\right]^{0.1}}\right],\ 250\right]$$

$$\varepsilon 1(c) := (d1-c)\cdot\left(\frac{d1-c}{c}\right) \qquad \varepsilon 2(c) := (d2-c)\cdot\left(\frac{d2-c}{c}\right) \qquad \varepsilon 3(c) := (d3-c)\cdot\left(\frac{d3-c}{c}\right)$$

$$\varepsilon_{p1}(c) := \varepsilon pe + \varepsilon 1(c) \qquad \varepsilon_{p2}(c) := \varepsilon pe + \varepsilon 2(c) \qquad \varepsilon_{p3}(c) := \varepsilon pe + \varepsilon 3(c)$$

$$F_{p1}(c) := Ap1 \cdot \left(f\left(\varepsilon_{p1}, c\right)\right)$$

$$F_{p2}(c) := Ap2 \cdot f\left(\varepsilon_{p2}, c\right)$$

$$F_{p3}(c) := Ap3 \cdot f\left(\varepsilon_{p3}, c\right)$$

$$F_{ptotal}(c) := F_{p1}(c) + F_{p2}(c) + F_{p3}(c)$$

$$M_{p1}(c) := F_{p1}(c) \cdot [d1 - (h - RefCentY)]$$

$$M_{p2}(c) := F_{p2}(c) \cdot [d2 - (h - RefCentY)]$$

$$M_{p3}(c) := F_{p3}(c) \cdot [d3 - (h - RefCentY)]$$

$$M_{ptotal}(c) := M_{p1}(c) + M_{p2}(c) + M_{p3}(c)$$

$$Ftotal(c) := Fcc(c) - F_{ptotal}(c)$$

$$Mtotal_{440}(c) := Mcc(c) + M_{ptotal}(c)$$

$cc := root(Ftotal(c), c, 1, 48)$ $cc = 7.435$ Neutral axis distance from the top of the section

$Fcc(cc) = 594$

$Mtotal_{440}(cc) = 24408.253$ (kip-in) Ultimate moment capacity

$\frac{Mtotal_{440}(cc)}{12} = 2034.021$ (kip-ft) Ultimate moment capacity

Ultimate Capacity for Repaired Test Specimens 3, 4, 5, and 6

The following demonstrates how the theoretical capacity at ultimate was calculated for Test Specimen 3. This method can be used to calculate the theoretical capacity for Test Specimens 4, 5, and 6 by making the necessary changes of fiber properties, laminate thickness, and laminate width.

$h := 48$ (in) height of section

$width := 16$ (in) width of flange that the FRP will be applied to, to assist in carrying moment

$f'_c := 4.5$ (ksi)

Input thickness $t_f := 0.16$ (in)

$$RefCentY := \frac{13599 + 48 \cdot width \cdot t_f + \frac{width}{2} \cdot t_f^{\,2}}{657 + width \cdot t_f}$$

$RefCentY = 20.805$ (in) Elastic Centroid

STEEL

$Ap1 := 6 \cdot 0.108$ (in^2) 1st layer of steel from the bottom

$Ap2 := 6 \cdot 0.108$ (in^2) 2nd layer of steel from the bottom

$Ap3 := 6 \cdot 0.108$ (in^2) 3rd layer of steel from the bottom

$d1 := 46$ (in) distance of first layer of steel from the top of section

$d2 := 44$ (in) distance of second layer of steel from the top of section

$d3 := 42$ (in) distance of third layer of steel from the top of section

$E_p := 27500$ (ksi) Modulus of elasticity of prestressing steel typical for 250 ksi steel

$f_{pe} := 120$ (ksi) Inputted value from calculation of prestress losses

FRP

$E_f := 10500$ (ksi) Modulus of FRP provided by manufacturer

$\varepsilon_{fu} := 0.0121$ Material failure strain provided by manufacturer

$\varepsilon_{fiber} := 0.0121$

$f_{fiber} := \varepsilon_{fiber} \cdot E_f$

$F_{fiber} := width \cdot t_f \cdot f_{fiber}$

$$M_{fiber} := F_{fiber} \cdot \left[\left(h + \frac{t_f}{2} \right) - RefCentY \right]$$

CONCRETE

$$\varepsilon top(c) := \frac{\varepsilon_{fu} \cdot c}{h - c}$$

Concrete compressive strain at the top of the section in terms of strain in FRP being at ultimate

$$\varepsilon_c(c,z) := \frac{\varepsilon top(c)}{c} \cdot z$$

$$fcs(c,z) := \left| \begin{array}{l} nf \leftarrow \frac{1}{2.5} \cdot f'_c + 0.8 \\ \varepsilon fc \leftarrow \frac{f'_c}{1265 \cdot \sqrt{f'_c} + 1000} \cdot \left[\frac{\left(\frac{f'_c}{2.5} + 0.8 \right)}{\left(\frac{f'_c}{2.5} + 0.8 \right) - 1} \right] \\ k \leftarrow \frac{f'_c}{9} + 0.67 \\ \varepsilon peak \leftarrow \exp\left[\frac{\ln\left[\frac{(nf-1)}{(-1+nf \cdot k)} \right]}{(nf \cdot k)} \right] \cdot \varepsilon fc \\ f_{.c\_peak} \leftarrow \frac{nf \cdot \left(\frac{\varepsilon peak}{\varepsilon fc} \right)}{nf - 1 + \left(\frac{\varepsilon peak}{\varepsilon fc} \right)^{nf \cdot k}} \cdot f'_c \\ adjust \leftarrow \frac{f'_c}{f_{.c\_peak}} \\ fcs\_actual \leftarrow \frac{nf \cdot \left(\frac{\varepsilon_c(c,z)}{\varepsilon fc} \right)}{nf - 1 + \left(\frac{\varepsilon_c(c,z)}{\varepsilon fc} \right)^{nf \cdot k}} \cdot f'_c \cdot adjust \\ fcs\_actual \end{array} \right.$$

Width of Section: z is the distance from the neutral axis; c is the neutral axis position from the top fiber of concrete

$$b(c,z) := \left| \begin{array}{l} 24 \quad \text{if} \quad c \geq z \geq (c-12) \\ 12 \quad \text{if} \quad (c-12) > z \geq (c-18) \\ 6 + 2 \cdot [-(c-z) + 21] \quad \text{if} \quad (c-18) > z \geq (c-21) \\ 6 \quad \text{if} \quad (c-21) > z \geq (c-36) \\ [\,6 - 2 \cdot [36 - (c-z)]\,] \quad \text{if} \quad (c-36) > z \geq (c-42) \\ 18 \quad \text{if} \quad (c-42) \geq z \geq (c-48) \\ 0 \quad \text{otherwise} \end{array} \right. \qquad \text{(in)}$$

For calculation with effects of the 12 in slab

$$Fcc(c) := \int_0^c b(c,z)\cdot fcs(c,z)\,dz$$ Force contribution from concrete

$$Mcc(c) := \int_0^c [\,z - [c - (h - RefCentY)]\,]\cdot b(c,z)\cdot fcs(c,z)\,dz$$ Moment contribution from concrete about the elastic centroid

PRESTRESS

Stress relieved steel

$A := 0.01091$

$B := 115.09$

Ramberg-Osgood Coefficients obtained from direct tensile tests of strands removed from test specimen 2

$$\varepsilon pe := \frac{f_{pe}}{E_p} \qquad \varepsilon pe = 4.363636\times 10^{-3}$$

$$f(\varepsilon,c) := if\left[E_p\cdot\varepsilon(c)\cdot\left[A + \frac{1-A}{\left[1+\left(B\cdot\varepsilon(c)\right)^{10}\right]^{0.1}}\right] < 250, E_p\cdot\varepsilon(c)\cdot\left[A + \frac{1-A}{\left[1+\left(B\cdot\varepsilon(c)\right)^{10}\right]^{0.1}}\right], 250\right]$$

$$\varepsilon 1(c) := (d1 - c)\cdot\left(\frac{\varepsilon_{fu}}{h-c}\right) \qquad \varepsilon 2(c) := (d2 - c)\cdot\left(\frac{\varepsilon_{fu}}{h-c}\right) \qquad \varepsilon 3(c) := (d3 - c)\cdot\left(\frac{\varepsilon_{fu}}{h-c}\right)$$

$$\varepsilon_{p1}(c) := \varepsilon pe + \varepsilon 1(c) \qquad \varepsilon_{p2}(c) := \varepsilon pe + \varepsilon 2(c) \qquad \varepsilon_{p3}(c) := \varepsilon pe + \varepsilon 3(c)$$

$$F_{p1}(c) := Ap1\cdot\left(f\left(\varepsilon_{p1},c\right)\right) \qquad F_{p2}(c) := Ap2\cdot f\left(\varepsilon_{p2},c\right) \qquad F_{p3}(c) := Ap3\cdot f\left(\varepsilon_{p3},c\right)$$

$$F_{ptotal}(c) := F_{p1}(c) + F_{p2}(c) + F_{p3}(c)$$

$$M_{p1}(c) := F_{p1}(c)\cdot[d1 - (h - RefCentY)]$$

$$M_{p2}(c) := F_{p2}(c)\cdot[d2 - (h - RefCentY)]$$

$$M_{p3}(c) := F_{p3}(c)\cdot[d3 - (h - RefCentY)]$$

$$M_{ptotal}(c) := M_{p1}(c) + M_{p2}(c) + M_{p3}(c)$$

$$Ftotal(c) := Fcc(c) - F_{ptotal}(c) - F_{fiber}$$

$$Mtotal_{440}(c) := Mcc(c) + M_{ptotal}(c) + M_{fiber}$$

$cc := root(Ftotal(c), c, 0, 15)$ $cc = 9.928$ Neutral axis distance from the top of the section

$Fcc(cc) = 793.364$

$Mtotal_{440}(cc) = 34976.31$ (kip-in) Ultimate moment capacity

$\frac{Mtotal_{440}(cc)}{12} = 2914.69$ (kip-ft) Ultimate moment capacity

Support Conditions

The following demonstrates how the support conditions were determined for Test Specimen 1.

$kip := 1000lbf$ $ksi := 1000psi$

Worksheet to determine the support conditions based on deflection behavior for the undamaged girder

$I_g := 165220.83in^4$

$\Delta_{exp} := .34895in$ total centerline deflection before the cracking load

$P := 98.4153kip$ Load at above given deflection before cracking

$l := 40ft$

$f'c := 4500psi$

$E := 57000\sqrt{f'c}\cdot\left(psi^{0.5}\right)$ $E = 3823.68ksi$

For pinned supports

$a := 15ft$

$$\Delta := \frac{\frac{P}{2}\cdot a}{24\cdot E\cdot I_g}\cdot\left(3\cdot l^2 - 4\cdot a^2\right) \qquad \boxed{\Delta = 0.328in}$$

For fixed supports

$b := 25ft$

$x := 20ft$

$$\Delta := 2\cdot\left[\frac{\frac{P}{2}\cdot b^2\cdot x^2}{6\cdot E\cdot I_g\cdot l^3}\cdot[(3\cdot a\cdot l) - (3\cdot a\cdot x) - b\cdot x]\right] \qquad \boxed{\Delta = 0.0701in}$$

Deflection at Ultimate for Test Specimen 1

The following demonstrates how the theoretical deflection at ultimate was determined for Test Specimen 1.

$kip := 1000lbf$ $ksi := 1000psi$

Worksheet to determine the theoretical ultimate deflection based on pinned supports and the theoretcial ultimate capacity determined for the undamaged girder

$M_{theoret} := 2034.02kip \cdot ft$

$P_{theoret} := \frac{M_{theoret}}{15ft}$ $P_{theoret} = 135.601kip$

$E_s := 27500ksi$

$f'c := 4500psi$

$E_c := 57000\sqrt{f'c} \cdot \left(psi^{0.5}\right)$ $E_c = 3823.676ksi$

$n := \frac{E_s}{E_c}$

$d_p := 44in$

$A_{ps} := 22 \cdot 0.108in^2$

$b := 24in$

$\rho_p := \frac{A_{ps}}{b \cdot d_p}$

$I_{cr} := n \cdot A_{ps} \cdot d_p^2 \cdot \left[1 - \left(1.6\sqrt{n \cdot \rho_p}\right)\right]$ $I_{cr} = 26349.392in^4$

$l := 40ft$

$a := 15ft$

$\Delta := \frac{P_{theoret} \cdot a}{24 \cdot E_c \cdot I_{cr}} \cdot \left(3 \cdot l^2 - 4 \cdot a^2\right)$ $\Delta = 5.669in$

REFERENCES

American Association of State Highway and Transportation Officials (AASHTO) (1990). *A policy of geometric design of highways and streets*, Washington D.C.: AASHTO.

American Concrete Institute (ACI) Committee 440 (2002). "Guide for the design and construction of externally bonded FRP systems for strengthening concrete structures." American Concrete Institute, ACI 440.2R-02, Farmington Hills, Michigan.

American Concrete Institute (ACI) Committee 440 (1996). "State-of-the-art report on fiber reinforced plastic reinforcement for concrete structures." American Concrete Institute, ACI 440R-96, Farmington Hills, Michigan.

American Institute of Steel Construction (AISC) (2001). *Manual of steel construction, load & resistance factor design*, Third Edition, American Institute of Steel Construction, Chicago: AISC.

American Society for Testing and Materials (ASTM) (2000). "Standard test method for tensile properties of polymer matrix composite materials." *D 3039-00*, West Conshohocken, Pennsylvania.

Arockiasamy, M. (1995). "Experimental studies on the feasibility of use of carbon fiber reinforced plastics in repair of concrete bridges." Center for Infrastructure and Constructed Facilities, Department of Ocean Engineering, Florida Atlantic University, Boca Raton, Florida.

Arockiasamy, M. and Barbosa, M. (2000). "Evaluation of conventional repair techniques for concrete bridges." Center for Infrastructure and Constructed Facilities, Department of Ocean Engineering, Florida Atlantic University, Boca Raton, Florida.

Bridge Engineering Software and Technology (BEST) Center (2001). "Maryland study, vehicle collisions with highway bridges." Department of Civil and Coastal Engineering, University of Maryland, College Park, Maryland.

Boyd, A.J. and Banthia, N. (2001). "Strengthening of full-scale bridge channel beams with sprayed FRP." *Proceedings of the Ninth International Conference on Structural Faults and Repair*, edited by M.C. Forde, London, UK, 11 pages [CD-ROM].

Boyd, A.J. (2000). "Rehabilitation of reinforced concrete beams with sprayed glass fiber reinforced polymers." PhD thesis, Department of Civil Engineering, University of British Columbia, Vancouver, Canada.

Collins, M. and Mitchell, D. (1991). *Prestressed concrete structures*, Prentice-Hall, Englewood Cliffs, New Jersey.

Consolazio, G.R., Fung, J., and Ansley, M. (in press). "M-phi-P diagrams for concrete sections under biaxial flexure and axial compression." American Concrete Institute (ACI) Structural Journal.

International Federation for Structural Concrete (FIB) (2001). "Technical Report on the design and use of externally bonded fibre reinforced polymer reinforcement (FRP EBR) for reinforced concrete structures." Bulletin 14, International Federation for Structural Concrete (FIB), Lausanne, Switzerland.

Florida Department of Transportation (FDOT) (1998). *Trucking manual,* Office of Motor Carrier Compliance, Fifth edition, Tallahassee, Florida.

Florida Department of Transportation (FDOT) (1999 revised 2002). *Traffic engineering manual,* Topic Number 750-000-005, Tallahassee, Florida.

Fung, J. (2002). "M-P-ϕ diagrams for prestressed concrete sections with surface bonded FRP composites." Master's thesis, Department of Civil and Coastal Engineering, University of Florida, Gainesville, Florida.

Klaiber, F.W., Wipf, T.J., Russo, F.M., Paradis, R.R., and Mateega, R.E. (1999). "Field/laboratory testing of damaged prestressed concrete girder bridges." *Iowa Department of Transportation Report HR-397*, Department of Civil and Construction Engineering, Iowa State University, Ames, Iowa.

Labossieere, P., Neale, K.W., Rochette, P., Demers, M., Lamothe, P., Lapierre, P., and Desgagne, G. (2000). "Fibre reinforced polymer strengthening of the Sainte-Emelie-de-l'Energie Bridge: design, instrumentation, and field testing." *Canadian Journal of Civil Engineering,* Vol. 27, 916-927.

Mayo, R., Nanni, A., Watkins, S., Barker, M., and Boothby, T. (1999). "Strengthening of bridge G-270 with externally bonded CFRP sheets." *Research Investigation Number 98-012, Center for Infrastructure Engineering Studies*, University of Missouri-Rolla, Rolla, Missouri.

Meier, U. and Winistorfer, A. (1995). "Retrofitting of structures through external bonding of CFRP sheets." *Non-Metallic (FRP) Reinforcement for Concrete Structures, Proceedings of the Second International RILEM Symposium*, E & FN Spon, London, UK, 509-516.

Nawy, E.G. (2000). *Prestressed concrete,* Prentice Hall, Englewood Cliffs, New Jersey.

Precast/Prestressed Concrete Institute (1999). *PCI design handbook*, Fifth Edition., Chicago, Illinois.

Scheibel, S., Parretti, R., and Nanni, A. (2001). "Repair and strengthening of impacted PC girders on bridge A4845." Missouri Department of Transportation (MoDOT) Report RDT01-017/RI01-016, Jefferson City, Missouri.

Sen, R. and Liby, L. (1994). "Repair of steel composite bridge sections using carbon fiber reinforced plastic laminates." *Report Number 0510616*, Department of Civil Engineering and Mechanics, University of South Florida, Tampa, Florida.

Shahawy, M. and Beitelman (1999). "Static and fatigue performance of RC beams strengthened with CFRP laminates." *Journal of Structural Engineering*, ASCE, 125(6), 613-621.

Shanafelt, G.O., and Horn, W.B. (1980). "Damage evaluation and repair methods for prestressed concrete bridge members." *NCHRP Report 226*, Transportation Research Board, National Research Council, Washington D.C.

Shanafelt, G.O., and Horn, W.B. (1985). "Guidelines for evaluation and repair of prestressed concrete bridge members." *NCHRP Report 280*, Transportation Research Board, National Research Council, Washington D.C.

Spadea, G., Swamy, R.N., and Bencardino, F. (2001). "Strength and ductility of RC beams repaired with bonded CFRP laminates." *Journal of Bridge Engineering*, ASCE, 6(5), 349-355.

Tedesco, J.W., Stallings, J.M., and EL-Mihilmy, M. (1998). "Rehabilitation of a reinforced concrete bridge using FRP laminates." *Highway Research Center Report Number 930-341, Harbert Engineering Center*, Auburn University, Auburn, Alabama.

Teng, J.G., Smith, S.T., Lam, L., and Chen, J.F. (2001). "Behaviour and strength of RC structures strengthened with FRP composites." *Proceedings of the Ninth International Conference on Structural Faults and Repair*, edited by M.C. Forde, London, UK, 15 pages [CD-ROM].

Teng, J.G., Chen, J.F., Smith, S.T., and Lam, L. (2002). *FRP strengthened RC structures*, John Wiley & Sons, LTD, Chicester, West Sussex, England.

Tumialan, J.G., Huang, P-C, and Nanni, A. (2001). "Strengthening of an impacted PC girder on bridge A10062, St. Louis County, Missouri." *Research, Development and Technology Report Number 01-013, Center for Infrastructure Engineering Studies*, University of Missouri-Rolla, Rolla, Missouri.

Zobel, R.S., Jirsa, J.O., Fowler, D.W., and Carrasquillo, R.L. (1996, revised 1997). "Evaluation and repair of impact-damaged prestressed concrete bridge girders." *Center for Transportation Research Report 1370-3F*, Bureau of Engineering Research, University of Texas at Austin, Austin, Texas.